PTEN regulates glutamine flux to pyrimidine synthesis and sensitivity to dihydroorotate dehydrogenase inhibition

Deepti Mathur

Submitted in partial fulfillment of the requirements for the degree of
Doctor of Philosophy
under the Executive Committee of the Graduate School of Arts and Sciences

COLUMBIA UNIVERSITY

2017

ABSTRACT

PTEN regulates glutamine flux to pyrimidine synthesis and sensitivity to dihydroorotate dehydrogenase inhibition

Deepti Mathur

The importance of metabolism in tumor initiation and progression is becoming increasingly clear. Metabolic changes induced by oncogenic drivers of cancer contribute to tumor growth and are attractive targets for cancer treatment. Phosphatase and Tensin homolog deleted from chromosome ten (PTEN) is one of the most commonly mutated tumor suppressors in cancer and operates in multiple roles, rendering it a hub for understanding cancer biology and for developing targeted therapy. PTEN's canonical function is its ability to antagonize the phosphoinositide 3-kinase (PI3K) pathway by dephosphorylating the lipid second messenger phosphatidylinositol (3,4,5) tri-phosphate (PIP3). This thesis focuses on the effects of PTEN loss on cellular metabolism, and the therapeutic vulnerability that stems from metabolic alterations.

First, we discovered that loss of Pten in mouse embryonic fibroblasts (MEFs) increases cellular proliferation and the number of replication forks per cell, launching our investigation into metabolic pathways that may be altered to support increased growth. Indeed, we found that *Pten*$^{-/-}$ cells exhibited a dependence on glutamine for their faster rate of growth, and that glutamine was channeled into the *de novo* synthesis of pyrimidines.

The next chapter examined dihydroorotate dehydrogenase (DHODH), a rate limiting enzyme for pyrimidine ring synthesis in the *de novo* pyrimidine synthesis pathway. We found that PTEN-deficient primary cells and cancer cell lines were more sensitive to inhibition of DHODH than PTEN WT cells were, and that the growth inhibition could be rescued by metabolites downstream of DHODH. Furthermore, we found that xenografted human triple negative breast cancer tumors in mice could be diminished by treatment with leflunomide, a DHODH inhibitor.

In the following chapter, we aimed to identify the mechanisms leading to cell death in PTEN mutant cells upon DHODH inhibition. We found that inherent defects in checkpoint regulation in PTEN-deficient cells were exacerbated by the stress of obstructed *de novo* pyrimidine synthesis, leading to a buildup of DNA damage at replication forks and ultimately chromosomal breaks. This was instigated by AKT-mediated phosphorylation of TOPBP1 that caused inadequate ATR activation, as well as AKT-mediated phosphorylation and inactivation of CHK1.

In sum, the findings of this thesis indicate that enhanced glutamine flux to *de novo* pyrimidine synthesis in PTEN mutant cells generates vulnerability to DHODH inhibition. The integration of altered glutamine regulation with PTEN's effect on replication, DNA damage, and the checkpoint response manifests as synthetic lethality upon DHODH inhibition in cells with PTEN inactivation. Inhibition of DHODH could thus be a promising therapy for patients with PTEN mutant cancers.

TABLE OF CONTENTS

LIST OF FIGURES

CHAPTER 4: MECHANISM OF DEATH

ACKNOWLEDGEMENTS

The completion of this thesis has been the joint effort of many people, both professionally and personally.

First and foremost, I'd like to thank my mentor, Dr. Ramon Parsons. I joined Columbia University as a graduate student primarily so that I could work in his lab, and it has been a wonderful experience learning from him. His enthusiasm for science and encouragement at every step of the way has allowed me to get to where I am today, and I am sincerely grateful for his guidance and mentorship.

Our lab has a wonderfully friendly and collaborative environment, and I want to thank all current and former lab members for your friendship and support. In particular, I want to thank Drs. Elias Stratikopoulos and Sait Ozturk for their work on mouse studies that were invaluable to the project, and Nicole Steinbach and Sarah Pegno for assistance with the project and for being great bay-mates. I also greatly appreciate everyone's feedback and editing help during the preparation of our manuscript. I inherited the metabolism project from Dr. Sarah Schoenfeld, and want to thank her for her guidance during the initiation of the project.

I've also been fortunate to have several collaborators. I would like to thank Dr. Lewis Cantley for his guidance on our project. I also want to thank Dr. John Asara and Min Yuan and Susanne Breitkopf for mass spectrometry work, and Dr. Vundavalli V. Murty for his karyotyping analysis. I also thank Dr.

Gerard Karsenty for use of his Seahorse XF and Dr. Grzegorz Sumara for training me to use it, and Dr. Raymund Yong for supplying us with glioblastoma tumor spheres.

This project could not have been developed without my thesis committee members, Drs. Andrea Califano, Eric Schon, and Bin Zheng. They have provided feedback and helped shape the project over the past few years, and I am happy to have been able to learn from them. I also want to thank Dr. Richard Baer for agreeing to be my additional thesis reader. Thank you to Dr. Califano and Dr. Baer for allowing me to rotate in your labs as well. I also want to thank Dr. Ron Liem, Dr. Donna Farber, and Zaia Sivo for their mentorship in the Integrated Program, and Dr. Matt Maurer and the directors of Med Into Grad for granting me a unique and valuable opportunity.

To all of my friends – thank you for being wonderful people!

I owe a special thank you to my fiancé, Sanchit, whose love and support has motivated me throughout graduate school. Thank you for always being there for me and for making me so happy! I couldn't have done this without you.

Finally, I owe the biggest gratitude to my family. Thank you Aarti for being the best sister and for always being able to make me laugh with your entertaining stories. Most of all, thank you to my parents. Words cannot describe how much I have treasured your love, encouragement, and support during graduate school and my whole life. Thank you for always believing that I could do anything – none of this would have been possible without you.

For my parents, for making me the woman I am today.

Chapter 1: Introduction

Cancer is an ancient disease. Tumors in other species occurred well before the evolution of humans, and even among people cancer was medically recognized early in civilization. The first written record of cancer is from Egypt in 2500 BCE, in which a papyrus scroll thought to be the notes of the physician Imhotep described a hard mass bulging from the breast of a patient — the first known documentation of what was likely breast cancer. While we cannot be certain that this was indeed the first case report for cancer, further early proof of human cancer came from archeologists who found evidence of a preserved abdominal cancer from 400 CE as well as a 2000-year-old mummy with what looks like bone cancer. Archeologists have also found a 2 million-year-old bone with markings that appear to have been caused by lymphoma (Mukherjee 2010).

A modern history of cancer

In the present day, cancer is now the 2nd leading cause of death in the United States (as concluded by the CDC, Centers for Disease Control and Prevention). We have come a long way since 4500 years ago in our understanding of the disease, and new research in the field is growing at a remarkable pace. However, much remains to be learned about this deadly foe. The introduction to this thesis will give a brief overview of cancer, discuss the field of cancer metabolism, and describe an important gene in tumor suppression called *PTEN*.

Cancer is primarily characterized by abnormal growth. This can be due to a genetic mutation either in 1) a proto-oncogene, which when mutated is an oncogene, or 2) a tumor suppressor gene. Oncogene

changes are usually gain-of-function, creating either a constitutively active protein or enhancing expression or activity, ultimately causing excessive pro-growth signaling in the cell. Tumor suppressor changes have the same ultimate effect but are typically loss-of-function, thereby removing the brakes on cellular growth (Lodish, Berk et al. 2000).

Such mutations are the root of the "hallmarks of cancer," a phrase coined by Drs. Hanahan and Weinberg in 2000. They organized known facets of cancer into a set of defining characteristics which they argued collectively create tumors in most cases. In their review, the authors described the following capabilities that define a tumor: to begin with, a cancer cell must exhibit sustained proliferative signaling due to oncogenic alterations described above. This leads to the deregulation of signaling pathways so that a tumor cell can maintain growth even in the absence of growth signals. Coupled to this is the ability to ignore growth suppressive signals and avoid cell death. Cancer cells must also be immortal and able to replicate indefinitely. In order to do so, the tumor must undergo angiogenesis to facilitate adequate avenues for nutrients. Lastly, most tumors metastasize to other parts of the body distinct from the site of the primary tumor (Hanahan and Weinberg 2000).

11 years later, the authors revised the original list to include newly found characteristics that may also be essential for tumor development. The first of these traits is the ability of a tumor cell to evade attack by the immune system; while immune cell inflammation can actually enable a tumor-promoting microenvironment, immune cells also target cancer cells for elimination. The second trait exhibited by cancer cells is the reprogramming of cellular energetics and metabolism (Hanahan and Weinberg 2011). Altered metabolism in a tumor cell will be a major topic of discussion in this thesis.

PTEN

One of the most commonly mutated tumor suppressors is PTEN: Phosphatase and Tensin homolog deleted from chromosome ten (Keniry and Parsons 2008). It was first discovered in 1997 by two independent groups: Li et al mapped a region on chromosome 10 that they found to be frequently mutated (Li, Yen et al. 1997), and Steck et al scanned the region deleted in gliomas and isolated a gene they termed MMAC1 (mutated in multiple advanced cancers 1) (Steck, Pershouse et al. 1997). We now know that MMAC1 is PTEN.

Germline mutations of PTEN can cause autosomal dominant disorders such as Cowden syndrome, characterized by benign growths called hamartomas; patients with Cowden syndrome do have a higher risk of getting cancer (Liaw, Marsh et al. 1997). Recently, an analysis of over 4700 tumors revealed PTEN to be among the top three genes significantly mutated both within a tumor type as well as in a pan-cancer cohort, validating the importance of PTEN as a hub for our understanding of cancer (Lawrence, Stojanov et al. 2014).

As a tumor suppressor, PTEN has an interesting property: it is haploinsufficient, meaning that just one mutated copy of the gene is enough to cause a phenotype. *Pten* heterozygous mice had neoplasms in the liver, GI tract, endometrium, and prostate, among others, and homozygous loss of *Pten* was actually found to be embryonic lethal in mice (Podsypanina, Ellenson et al. 1999). Intermittent levels of *Pten* in shRNA engineered mice led to hyperplasia in lymph nodes and prostate, as well as sebaceous adenomas, corroborating that partial reduction of Pten is sufficient for a tumorigenic phenotype (Shen-Li, Koujak et al. 2010). A series of mice with incremental *Pten* also revealed dose-dependency for prostate cancer progression (Trotman, Niki et al. 2003). This is an interesting feature because tumor

suppressors have previously been thought to behave recessively; that is, if one intact copy of the gene is present, the cell is protected from adverse effects. Haploinsufficency in a tumor suppressive setting can be due to interactions with other tumor suppressors or oncogenes. For example, either heterozygous or homozygous loss of PTEN hastened the progression of HER2+ breast cancer in mice, leading to an increase in HER2 protein levels without increasing HER2 transcript levels and ultimately causing a more basal-like and aggressive tumor (Dourdin, Schade et al. 2008). Additionally, while the genetic disruption of *PTEN* may be heterozygous, the intact copy of *PTEN* may not be well expressed. Both the liver and thymus of *Pten* heterozygous mice were found to have downregulated the wild-type (WT) copy of *Pten* (Podsypanina, Ellenson et al. 1999). This downregulation would cause the effective expression of *Pten* to be (potentially much) less than 50%, initiating cellular effects similar to those produced by homozygous mutations. As a corollary, "Super-PTEN" mice with elevated PTEN had anti-tumorigenic properties, and the cells were resistant to oncogenic transformation (Garcia-Cao, Song et al. 2012). Overall, the sum of these studies demonstrates the importance of PTEN levels in cancer progression.

PTEN is a fulcrum of multiple cellular functions. Its canonical role is that of a lipid phosphatase; in fact, its lipid phosphatase activity has been shown to be critical for tumor suppression. PTEN dephosphorylates the lipid second messenger phosphatidylinositol (3,4,5) tri-phosphate (PIP3) on the D3 phosphate site, resulting in phosphatidylinositol (4,5) bi-phosphate (PIP2) (Maehama and Dixon 1998, Myers, Pass et al. 1998). Through this, PTEN directly reverses the action of phosphoinositide 3-kinase (PI3K). To fully appreciate the implications of this action, we need to understand the PI3K pathway.

The PI3K pathway

PI3K can be activated by receptor tyrosine kinases (RTKs) on the cell surface, which dimerize and are activated upon binding to a ligand (Vanhaesebroeck and Waterfield 1999). For example, the PDGF (platelet-derived growth factor) receptor is autophosphorylated when it is bound by PDGF. This subsequently actives PI3K, as long as RAS is also activated (Klinghoffer, Duckworth et al. 1996). Tyrosine phosphorylation of IRS-1 (Insulin receptor substrate 1) upon binding insulin also activates PI3K (Backer, Myers Jr et al. 1992). Interestingly, the PI3K-activating RTKs HER2 (human epidermal growth factor receptor 2) and EGFR (epidermal growth factor receptor) have been found to be amplified in cancer (Sauter, Maeda et al. 1996, Moasser 2007). G-protein-coupled receptors can also activate PI3K in certain cells (Vanhaesebroeck and Waterfield 1999). Activated PI3K then sets off a chain of pro-growth signaling effects. First, PI3K phosphorylates PIP2 to generate PIP3; PIP3 levels have been found to correlate with cellular growth and transformation (Serunian, Auger et al. 1990). This is in part due to a protein called AKT.

AKT, also called protein kinase B (PKB), is a serine/threonine protein kinase. At the plasma membrane, AKT binds PIP3 through its lipid-binding PH (pleckstrin homology) domain, thereby causing a conformational change and exposing its phosphorylation sites. This allows phosphoinositide-dependent kinase 1 (PDK1), which is also activated by PIP3, to phosphorylate AKT on its threonine 308 site (Alessi, James et al. 1997, Stephens, Anderson et al. 1998). The partially phosphorylated AKT is then able to phosphorylate and suppress TSC2 and PRAS40, suppressors of mTOR (mammalian target of rapamycin), thus indirectly activating mTOR (Inoki, Li et al. 2002, Manning, Tee et al. 2002, Haar, Lee et al. 2007). mTOR has the ability to form 2 complexes: rapamycin-sensitive mTORC1 with raptor, and mTORC2 with rictor (Hara, Maruki et al. 2002, Kim, Sarbassov et al. 2002, Loewith, Jacinto et al. 2002, Dos, Ali et al.

2004). AKT is further phosphorylated at its serine 473 site by mTORC2 and DNA-PK (DNA-dependent protein kinase) (Feng, Park et al. 2004, Sarbassov, Guertin et al. 2005). In fact, it was found that S473 phosphorylation by DNA-PK increased AKT activity 10 fold (Feng, Park et al. 2004).

An active mTORC1 phosphorylates its downstream effectors, including p70 S6 kinase and 4E-BP1. Phosphorylation of the latter allows release from a repressive complex and initiation of translation (Burnett, Barrow et al. 1998). S6 kinase further enhances translation by phosphorylating the ribosomal protein S6 as well as eukaryotic translation initiation factor 4B (eIF4B) (Raught, Peiretti et al. 2004).

Tumor cells from $Pten^{+/-}$ mice have been shown to have both elevated phospho-AKT and active S6 kinase. The latter was affected by an mTOR inhibitor while phospho-AKT was intact, and the observed reduction in tumor size indicates the importance of this downstream effector in neoplastic development (Podsypanina, Lee et al. 2001).

Fully-activated AKT with both T308 and S473 phosphorylated triggers increased proliferation as well as anti-apoptotic signals. This can be accomplished in multiple ways; for example, AKT phosphorylates the cell cycle regulator p21, localizing the protein to the cytoplasm to prevent its nuclear function (Zhou, Liao et al. 2001). GSK-3β phosphorylates cyclin D1, encouraging its export from the nucleus and subsequent degradation. AKT phosphorylates and inhibits GSK-3β, thus allowing cyclin D1 action and progression through G1 and S phases (Diehl, Cheng et al. 1998, Alt, Cleveland et al. 2000). Furthermore, AKT promotes cell survival by phosphorylating and inhibiting the pro-apoptotic protein BAD (Datta, Dudek et al. 1997, Peso, González-García et al. 1997, Datta, Katsov et al. 2000) as well as by

phosphorylating MDM2, allowing the latter's localization to the nucleus to inhibit pro-apoptotic p53 (Mayo and Donner 2001, Zhou, Liao et al. 2001). AKT also phosphorylates and inhibits FoxO (Forkhead box O) transcription factors, preventing their growth inhibitory effects (Zhang, Tang et al. 2011).

Consequently, unchecked AKT activation is oncogenic, and phosphatases of AKT as well as the action of PTEN upstream curb AKT activity. Loss of PTEN, therefore, could mimic constitutively active AKT that could otherwise occur from sustained growth factors or cytokine signaling (Stambolic, Suzuki et al. 1998). By limiting PI3K and hence AKT, PTEN acts as a brake on excessive cellular growth. Notably, mutations in *PIK3CA* (encoding the catalytic p110α subunit of PI3K) are also found in cancer, signifying the importance of this pathway overall. A schematic of the pathway is shown in Figure 1.1 (Samuels and Ericson 2006).

Manifold functions

PTEN has additional functions outside the PI3K pathway. It has the capability of dephosphorylating proteins on serine, threonine, and tyrosine residues, earning it the title of a dual-specificity phosphatase (Myers, Stolarov et al. 1997). While PTEN's protein phosphatase activity has not been as well characterized as its role as a lipid phosphatase, there is evidence that it is important in cell cycle regulation.

Furnari et al showed in 1998 that introducing PTEN in U87 cells (which are PTEN null) caused GI cell cycle arrest, as tested by a BrdU assay. This phenotype was detectable in 2% serum but not in 10% serum conditions, indicating that the effect was growth factor related. Based on a TUNEL assay which detects

DNA fragmentation, they also showed that PTEN expression in U87 cells did not cause apoptosis (Furnari, Huang et al. 1998). Building on these data, Weng et al created PTEN mutants which were either completely phosphatase dead (C124S) or lipid phosphatase dead but with its protein phosphatase activity retained (G129E). Both mutants restored growth in MCF-7 cells compared to WT PTEN which reduced growth, indicating that its protein phosphatase activity plays a role in growth suppression. Furthermore, WT PTEN caused G1 arrest, the G129E mutant restored the defect, and the C124S enhanced the cell cycle even more, suggesting a role for both protein and lipid phosphatase activities. The authors also found that PTEN lipid phosphatase activity upregulates p27 while its protein phosphatase activity down regulates cyclin D1, both having the effect of preventing cell cycle progression at G1 (Weng, Brown et al. 2001). We will discuss PTEN's role in the cell cycle in more detail in chapter 4.

Additionally, PTEN affects cell migration and invasion in a mechanism independent of the PI3K pathway. PTEN was found to bind PREX2 and inhibit its GEF activity, thereby preventing activation of RAC1, a protein that drives cell mobility. Interestingly, PREX2 is mutated in cancer and these mutants appear to lose the ability to be inhibited by PTEN (Mense, Barrows et al. 2015).

Nuclear PTEN

The cell membrane is the site of action for PTEN's role in the PI3K pathway, but PTEN has also been found in the nucleus of cells, including breast ducts and neurons. It is thought that the presence of PTEN in the nucleus is important for tumor suppression, since neoplastic cells exhibit more cytosolic localization of the protein (Planchon, Waite et al. 2008). It was also shown in a screen of 92 patients with primary melanoma that a majority of the tumors had decreased nuclear PTEN. In this study,

immunohistochemistry stains were scored on a 3-level scale of negative/low, decreased, and normal levels of PTEN levels; while 33% of samples had decreased cytoplasmic staining, 91% exhibited decreased nuclear staining, suggesting an association between melanoma and loss of nuclear localization (Whiteman, Zhou et al. 2002).

Exclusion of PTEN from the nucleus can be due to mutation. The lysine 289 site on PTEN is normally monoubiquitinated by the E3 ubiquitin ligase NEDD4, which allows PTEN to cross the nuclear membrane. Once inside the nucleus, the site is deubiquitinated so that PTEN can no longer permeate the membrane and remains localized in the nucleus. However, a naturally occurring mutation in Cowden syndrome, K289E, is unable to be ubiquitinated and cannot get into (or out of) the nucleus. An additional mutation that occurs in gliomas, K13E, confers a similar defect in nuclear import (Trotman, Wang et al. 2007).

Along the same lines, it has been shown that PTEN is SUMOylated (SUMO, small ubiquitin-like modifier) on lysine 254. A mutation of this site, K254R, renders PTEN no longer localized to nucleus. Addition of a nuclear export inhibitor revealed PTEN to still be found in the nucleus. Therefore, mutation of the SUMO site, unlike the ubiquitination site above, allows PTEN to enter the nucleus but not be retained there (Bassi, Ho et al. 2013).

Once inside the nucleus, the role of PTEN may involve chromatin stability and the cell cycle, as described above and further detailed in chapter 4.

PTEN regulation

Ubiquitination of PTEN can also affect its protein levels. While monoubiquitination led to nuclear transport, as described above, polyubiquitination by NEDD4 led to degradation by the proteasome. Knockdown of NEDD4 led to increased PTEN protein levels, showing that NEDD4 acts as a negative regulator of PTEN. Furthermore, in human bladder cancer samples the amount of PTEN protein was anticorrelated with NEDD4 mRNA (Wang, Trotman et al. 2007).

PTEN protein stability is also regulated by phosphorylation of its C-terminal tail domain. S380, T382, and T383 residues are phosphorylated by protein kinase CK2 (casein kinase II) (Torres and Pulido 2001). Vazquez et al found that mutating these sites from serine or threonine to alanine lowered the half-life of the protein but also increased its enzymatic activity. Removal of the tail domain resulted in less stability but not less function, because the resulting protein had a higher enzymatic capability. Phosphorylation of the tail domain thus appears to regulate PTEN in dual manner, by maintaining protein stability while keeping its function in check (Vazquez, Ramaswamy et al. 2000). Phosphorylation of the C-terminal region in this manner also protects PTEN from cleavage by caspase 3, thereby preventing further protein instability (Torres, Rodriguez et al. 2003). Dephosphorylation of PTEN, on the other hand, exposed cationic residues that can electrostatically interact with the lipid bilayer and allowed its targeting to the membrane. This can explain the increased activity of PTEN in a dephosphorylated state, since the membrane is the site of action for PTEN's role in the PI3K pathway (Das, Dixon et al. 2003).

In addition to regulation by phosphorylation, acetylation can alter the function of PTEN. It has been shown that PTEN and the histone acetyltransferase PCAF (p300/CBP-associated factor) can physically

interact, resulting in acetylation of lysines 125 and 128 on PTEN. This led to a reduction of PTEN activity and a consequent increase in AKT phosphorylation (Okumura, Mendoza et al. 2006).

PTEN can be regulated not only at the level of protein stability, but also transcriptional expression. Methylation of the *PTEN* promoter can induce loss of expression of the gene, as seen in secondary glioblastomas. Interestingly, this can occur independently of any genetic mutation of *PTEN* (Wiencke, Zheng et al. 2007). *PTEN* has also been found to be the target of several microRNAs (miRs), short non-coding RNAs that can repress translation of mRNAs (Meng, Henson et al. 2007, Mouw, Yui et al. 2014, Tokudome, Sasaki et al. 2015). These discoveries corroborate the findings of Podsypanina et al described above, in which WT *Pten* alleles were downregulated; in light of the successive research, epigenetic changes and post-transcriptional repression are likely contributing causes of such dysregulation.

As described above, PTEN can regulate the activity of PREX2. As an interesting complementarity, PREX2 can regulate PTEN as well. PREX2 was found to inhibit the lipid phosphatase function of PTEN, and the ability of PREX2 to activate PI3K was dependent on its inhibition of PTEN. Its expression positively correlated with human cancer cells with WT PTEN and mutant PIK3CA, and in the setting of a PIK3CA mutation PREX2 assisted oncogenic transformation and growth (Fine, Hodakoski et al. 2009).

p53 is an important tumor suppressor; in fact, it has been revealed to be the gene with the highest penetration within a tumor subtype as well as across all cancers (Lawrence, Stojanov et al. 2014). Interestingly, there is a p53 binding site on the *PTEN* promoter, and increased p53 protein has been

shown to lead to increased *PTEN* mRNA expression (Stambolic, MacPherson et al. 2001). As an ancillary finding, PTEN can also regulate p53. Freeman et al showed that adding either WT or phosphatase-dead PTEN to cells lacking PTEN increased the protein stability of p53, indicating that the enzymatic activity of PTEN is not required to stabilize p53. Additionally, PTEN increased the ability of p53 to bind DNA to carry out its transcriptional activity (Freeman, Li et al. 2003). Thus, PTEN positively affects p53 function in two ways, and p53 positively regulates *PTEN* in kind. These results demonstrate a thought-provoking way in which an inter-tumor suppressor network is mediated.

PTEN in cancer

Allow us to now pivot from the intracellular facets of PTEN to the part it plays in cancer as a whole. In this section we will cover brain, breast, and prostate cancer, as PTEN is frequently deregulated in these tumor types.

Glioblastoma multiform (GBM) is a subset of gliomas and the most common type of malignant brain tumor. The current available treatment options are surgical resection, radiation, and the adjuvant administration of the chemotherapeutic agent temozolomide (TMZ). TMZ is an oral medication and is a DNA-alkylating agent, which damages DNA and causes cell death. However, even with the above treatments, median survival for patients with GBM is only 12-18 months (Bush, Chang et al. 2016). 75% monoallelic loss and 30% biallelic loss of *PTEN* have been observed in gliomas (Keniry and Parsons 2008). Furthermore, *PTEN* loss has been correlated to a shorter average survival time in these patients (Yang, Shao et al. 2010).

Prostate cancer is the second most common type of cancer in men (Siegel, Miller et al. 2016). In addition to surgery and radiation therapy, prostate cancer patients are most commonly given androgen deprivation therapy. Testosterone is the primary androgen in the body, and many prostate tumors are at least partly androgen-dependent; i.e. circulating systemic androgens fuel the cancer. Castration-resistant disease is characterized by the progression of a prostate tumor despite lower systemic testosterone levels due to androgen deprivation therapy. Although a few other endocrine therapies or immunotherapies are options, patients with castration-resistant prostate cancer are typically given chemotherapy, usually docetaxel. The PI3K pathway is altered in some way in almost all cases of this disease, and the most common alteration in prostate cancer overall is *PTEN* loss: 42% exhibit monoallelic loss and 10% exhibit biallelic loss (Keniry and Parsons 2008, Statz, Patterson et al. 2016). Several mTOR and PI3K inhibitors have been in clinical trials, either alone or in combination with chemotherapy, but so far only modest effects have been observed (Statz, Patterson et al. 2016). *PTEN* loss also leads to resistance to chemotherapy in prostate cancer, perhaps due to upregulation of the anti-apoptotic protein Bcl-2 (Huang, Cheville et al. 2001).

Of the several subtypes of breast cancer, the most aggressive is triple negative breast cancer (TNBC), characterized by low expression of estrogen receptor (ER), progesterone receptor (PR), and human epidermal growth factor receptor 2 (HER2). There are currently no targeted therapies for this disease that have been approved, leaving only chemotherapy (usually paclitaxel or carboplatin) as the standard of care. Hence, 50% of women with TNBC choose mastectomies (Sharma 2016). TNBC also bears frequent *PTEN* alterations, with 40-50% of cases containing monoallelic loss, and 5% biallelic loss (Keniry and Parsons 2008).

It is important to note that the actual level of PTEN protein loss in these cancers may be even more pronounced than their respective mutational frequencies, due to epigenetic downregulation or other regulatory mechanisms described above which could further depress the amount of functional PTEN.

A common theme in the cancers we described here is a dependence on chemotherapy for treatment. Chemotherapy can fall under two major categories: Taxanes are compounds originally derived from yew trees (of the genus *Taxus*). These compounds disrupt microtubules by stabilizing their GDP-bound form and preventing their deploymerization. Microtubule function is dependent on its ability to dynamically polymerize and depolymerize, and disruption by taxanes leads to an inhibition of mitosis. Preventing cell division reduces tumor growth, but also leads to systemic toxicities including peripheral neuropathy. Patients may also exhibit neutropenia, described by an abnormally low count of neutrophils, a type of white blood cell, ultimately leading to an increased susceptibility to bacterial infection (Rowinsky 1997). Anthracyclines, on the other hand, intercalate DNA and thereby prevent its synthesis. These compounds inhibit topoisomerase, a protein which uncoils DNA to assist replication. In patients, anthracyclines can cause cardiotoxicity (Minotti, Menna et al. 2004).

These methods of chemotherapy usually affect any dividing cell, thus disturbing some healthy non-tumor cells in the body as well. Radiation also does not necessarily discriminate between tumor vs non-tumor tissue. Finding successful targeted therapies for cancer is a great challenge, but an important goal in the face of insufficient treatment options. Targeted therapies that are tumor-specific are much needed, and identifying changes based on specific tumor suppressor or oncogene alterations will facilitate this effort. In fact, targeted therapies for certain subtypes of breast cancer, among others,

have already been proven to be clinically successful. Due to the high mutation rate of PTEN in cancer, the effects of PTEN could be at the heart of targeted therapy.

Metabolism

Allow us to pivot to cancer metabolism, which could be the core of both developing new targeted therapies and indeed our understanding of cancer *en masse*. Cancer metabolism is presently a cutting-edge field, and there has been a storm of new research in the past 15 years or so.

To understand cancer metabolism we must first review some normal metabolic pathways, the corruption of which will be the topic of this section.

In brief:

Glucose is an important sugar for the cell, and is processed through glycolysis which produces NADH, minor amounts of ATP, and pyruvate. Intermediates of glycolysis are also used for biosynthesis, such as ribose 5-phosphate from the glucose 6-phosphate-derived pentose phosphate pathway (PPP). The PPP also generates reducing power in the form of NADPH, and the ratio of $NADP^+$ to NADPH helps determine the flux into the pathway.

In anaerobic conditions (such as highly active skeletal muscle), pyruvate is fermented to lactate for the regeneration of NAD^+. In aerobic conditions, pyruvate is transported into the mitochondrion and used for the tricarboxylic acid (TCA) cycle, which further produces NADH and $FADH_2$ as electron carriers for

respiration. As with glycolysis, intermediates of the TCA cycle such as aspartate and citrate can also be used for biosynthesis of macromolecules. The TCA cycle has multiple imports as well; glutamine and other amino acids can be oxidized by this circular pathway.

In the electron transport chain, the flow of electrons through various complexes pumps protons into the mitochondrial intermembrane space. The motion of the proton gradient through ATP synthase generates copious amounts of ATP, providing energy for various cellular reactions.

Glutamine is another critical metabolite for cellular function. As mentioned, it can join the TCA cycle and by doing so can maintain adequate levels of TCA intermediates. Nitrogen from glutamine is donated to nucleotide synthesis, a function that will be important in this thesis (Nelson, Lehninger et al. 2008).

In actuality, the metabolic processes in mammalian cells are far more complex and involve myriad other interacting players and pathways. Although drastically simplified, the above framework will help us compare normal metabolism to the distorted versions found in tumors.

It is somewhat surprising that the metabolic links to cancer were overlooked until fairly recently, because the targeting of metabolites was among the first developments in cancer therapy. The first antimetabolite was an antifolate, designed and produced by Yellapragada Subbarao (Hutchings, Mowat et al. 1947) and given to patients by Sydney Farber. At the time, folates were given to patients with anemia; but, when Farber administered folates to leukemia patients their condition worsened. He

reasoned that an antifolate would have the opposite effect, and Subbarao developed a compound that was similar to folate but with slight differences that would inhibit its activity. They found that of 16 patients given this experimental drug, 10 improved and several were in remission for a few months, a considerable amount of time for leukemia patients. Although the leukemia eventually relapsed, the antifolate was considered quite successful (Farber , Diamond et al. 1948).

Glucose metabolism

Even before the advent of a metabolic therapy, an abnormal metabolic state in tumors was observed by a man named Otto Warburg. In 1924, he discovered that rat liver carcinomas produced a heightened level of lactic acid but did not consume more oxygen, and published another paper the same year quantifying that the amount of lactate produced by tumor cells was actually double that of normal cells (Koppenol, Bounds et al. 2011). Warburg also discovered that tumor cells take up more glucose than normal cells: he measured the concentrations of glucose in blood vessels leading to and from the tumor, and found that while most normal cells take up 2-16mg glucose from 100cc blood, tumors take up 70mg glucose from the same volume. A key aspect here is his calculation that 66% of the glucose was converted to lactate *regardless* of oxygen availability, with the remainder left for respiration (Warburg, Wind et al. 1927). This phenomenon is called aerobic glycolysis.

The seminal papers by Warburg laid the groundwork for a plethora of research into altered metabolic pathways in cancer. In fact, the observation that most tumors consume high levels of glucose is what allows visualization of tumors in the clinic by FDG-PET: 18-fluoro-2-deoxyglucose positron emission tomography uses radio-labeled glucose which is taken up by tumors and visualized by sensors that can detect radioactivity. The use of FDG-PET has been in place for several decades.

There remained, however, an outstanding question: why do tumors take up extra glucose? Since it occurs even in the presence of sufficient oxygen for respiration and intact mitochondria, the tumors are not being forced to use glycolysis for energy. In fact, the use of glycolysis for ATP production is far less efficient than production via the electron transport chain, and Warburg's evidence showed that even after lactate production there was enough glucose left to be fully oxidized in the mitochondria. The current theory is that the increased glucose uptake is not for energy at all; rather, it is used as a precursor for synthesizing macromolecules required for cellular (and tumor) growth.

Normal adult tissues express the M1 isoform of pyruvate kinase, the enzyme that converts phosphoenolpyruvate to pyruvate in glycolysis. Christofk et al showed that tumor cells express the M2 isoform, which actually has less enzymatic activity than M1 does. This may instigate the switch to aerobic glycolysis since glucose is less efficiently brought to the mitochondria, and cause a backup of the pathway intermediates into anabolic channels that branch off of glycolysis. The authors also found that knockdown of the M2 isoform in lung cancer cells reduced glucose metabolism and slowed proliferation (Christofk, Vander Heiden et al. 2008).

The pentose phosphate pathway is one such offshoot from glycolysis that has multiple anabolic capabilities. The PPP generates NADPH for reductive biosynthesis reactions, ribose 5-phophate as a sugar for nucleotides, and erythrose 4-phosphate used in amino acids with ring structures. Glucose-6-phosphate dehydrogenase (G6PD) shunts glucose-6-phosphate from glycolysis into the first step of the PPP. Backup of pathway intermediates (e.g. by PKM2 described above) could increase the production of PPP metabolic building blocks. X-linked deficiency of G6PD, found in men, does not decrease their risk

of cancer and this finding has shed some doubt on the importance of the PPP in cancer development (Ward and Thompson 2012). However, it is difficult to associate risk factors with molecular mechanisms. It is possible that the PPP is more vital for cancer progression in certain tissues or under specific regulation; since these factors were not used to stratify the risk study, a meaningful association could be clouded. Other anabolic pathways may also be employed in the face of G6PD deficiency. This does not mean that the shunting of glucose into the pathway is irrelevant to cancer development.

Aerobic glycolysis can be triggered by oncogenic mutations as well. HIF-1 is a transcription factor, which during hypoxia is not degraded and increases the transcription of glucose transporters and lactose dehydrogenase A (LDH-A) which converts pyruvate to lactate. When faced with insufficient oxygen cells are forced to increase glucose uptake and produce energy from glycolysis, and HIF-1 mediates this transition. However, mutations in VHL, which usually targets HIF-1 for degradation, can constitutively activate HIF-1, leading to aerobic glycolysis. Mutations in fumarate hydratase (FH) or succinate dehydrogenase (SDH) can also cause constitutively active HIF-1 (DeBerardinis, Lum et al. 2008).

A surge in glucose uptake can initiate increased synthesis of lipids. Downstream of glycolysis, citrate is generated in the TCA cycle. Citrate can also be exported from mitochondria to be made into oxaloacetate and acetyl-CoA, the latter of which is used as a lipid precursor. In fact, citrate efflux from mitochondria correlated with proliferation rate in hepatomas, suggesting that the biosynthesis of lipids assisted tumor growth (Parlo and Coleman 1984).

Single-carbon metabolism

An additional branch off of glycolysis is initiated by 3-phosphoglycerate (3PG). Single-carbon metabolism is so named due to the donation of individual carbons from amino acids for nucleotide production. 3PG can be converted to the amino acid serine, which is then converted to glycine. This process concurrently converts tetrahydrofolate (THF) to methyl tetrahydrofolate (mTHF), facilitating the folate cycle that contributes to making purines. 2PG can also activate 3PG.

Phosphoglycerate dehydrogenase (PHGDH) is the enzyme responsible for committing 3PG into serine synthesis, and has been found to be upregulated in melanoma and some breast cancers. PHGDH expression correlated with cancer progression, and its knockdown led to reduced cellular growth (Locasale, Grassian et al. 2011). Furthermore, in the NCI-60 panel of human cancer cell lines, the Warburg effect itself was not correlated with cell proliferation rate, while glycine uptake was the metabolite most strongly correlated with growth (Locasale 2013). Glycine cleavage also contributes to the folate cycle, linking this piece of data to the importance of single-carbon metabolism in cancer growth. When mice with xenografted colon cancer cells were deprived of serine and glycine from their diet, their tumors exhibited reduced growth (Locasale 2013).

5-fluorouracil (5FU) is the standard of care for some cancers. This drug blocks the methylation of dUMP to dTMP and disrupts the folate cycle. Metformin, also being explored as a cancer treatment, can inhibit one-carbon metabolism (Locasale 2013). It appears that the investigation of folates in cancer has come full circle from Syndey Farber's experiments with antifolates in the 1940s. Actually, inhibition of nucleotides in general has been studied as a therapeutic approach. Gemcitabine, used for pancreatic cancer, interferes with cytidine production (Locasale 2013). Conversely, it has been shown that

expression of the HPV oncogene leads to a decrease in all nucleotides, and that adding exogenous nucleotides decreased DNA damage (Bester, Roniger et al. 2011). Interfering with nucleotide synthesis will be the major subject of chapter 3.

Glutamine metabolism

Glutamine is a biologically thought-provoking amino acid. Mammals are capable of synthesizing it in most settings, but rapidly proliferating cells have a requirement for glutamine greater than what is internally produced – making it a conditionally essential amino acid (DeBerardinis and Cheng 2010).

Human hepatoma cells have been shown to take up glutamine faster than normal hepatocytes (Bode 2002). Once inside the cell, glutamine is processed to glutamate by the enzyme glutaminase; interestingly, glutaminase activity was correlated with the growth rate of hepatic tumors in rats (Linder-Horowitz, Knox et al. 1969).

The association between glutamine uptake and cancer raises the question of its objective in a tumor cell. From the annals of literature, it appears that glutamine serves multiple purposes in different situations. A schematic of some of the functions of glutamine is depicted in figure 1.2 (DeBerardinis, Lum et al. 2008).

Glutamate is converted to alphaketoglutarate, an intermediate of the TCA cycle, which can then continue being processed through the TCA cycle. Using ^{14}C labeling, Coles and Johnstone found that Ehrlich ascites-carcinoma cells have greater glutamine usage than normal cells, and that it is used primarily for replenishing TCA cycle components (Coles 1962). It is possible that if the majority of intracellular glucose is being used for anabolic purposes rather than processing by the TCA cycle, glutamine is required to fill in the gaps.

However, glutamine can be more than just a stand-in for glucose. Even in cells with adequate glucose flux through the TCA cycle, glutamine was used for the majority of TCA cycle intermediates and energy — these transformed HeLa cells preferentially chose to use glutamine as a major source of cellular energetics (Reitzer, Wice et al. 1979). Glutamine is also used for the generation of reducing equivalents. One of the steps of glutaminolysis converts malate to pyruvate and NADPH, catalyzed by malic enzyme. In glioblastoma cells, glutamine produced enough NADPH in this manner to support a substantial amount of fatty acid synthesis that uses NADPH as an electron donor (DeBerardinis, Mancuso et al. 2007).

As discussed in the discourse about glucose metabolism, mutations in various genes can affect glucose utilization in different ways. A similar situation is paralleled in glutamine metabolism. One such important player in altering the fate of glutamine is the oncogene K-Ras, which alters the normal modus operandi of both glucose and glutamine metabolism. *KRAS* mutations led to an increase in glucose uptake, but the excess glucose was not used for the TCA cycle. Rather, glutamine was used to provide carbons for the TCA cycle, amino acid synthesis, and nucleotide production via aspartate, rendering glutamine just as (if not more) important as glucose in *KRAS* mutant cells (Gaglio, Metallo et al. 2011).

This might explain why depriving colorectal carcinoma cells of glucose increased selection for clones with mutant *KRAS* (or *BRAF*), since they can utilize glutamine for the majority of both energetics and macromolecular synthesis. These clones also had increased expression of GLUT1 for more efficient glucose uptake, thus giving cells the power vested by K-Ras to employ both glucose and glutamine for cell growth (Yun, Rago et al. 2009).

Cells with oncogenic Myc are also acutely sensitive to glutamine. In fact, Myc elicits glutamine dependency; apoptosis was triggered in cells with activated Myc upon glutamine deprivation. Replenishing TCA cycle intermediates rescued cell death, indicating that glutamine flux is largely required for the TCA cycle, perhaps due to the demand for reducing equivalents (Yuneva, Zamboni et al. 2007).

In a remarkable twist, it has been shown that Myc actually diverts glucose toward lactate production in order to render cells more dependent on glutamine for TCA cycle intermediates and phospholipid synthesis (Wise, DeBerardinis et al. 2008). This is facilitated by increased production of LDH-A in Myc transformed cells, which converts pyruvate to lactate and thereby increases lactate production from glucose (LDH-B catalyzes the reverse reaction) (Shim, Dolde et al. 1997). Furthermore, enhanced Myc expression leads to an increase in the levels of glutamine importers ASCT2 and SN2, thus directly affecting glutamine uptake (Wise, DeBerardinis et al. 2008). Intriguingly, LDH-A function is necessary for c-Myc to cause anchorage-independent growth in soft agar, indicating that the metabolic reprogramming to glutamine dependence is requisite for c-Myc to be tumorigenic (Shim, Dolde et al. 1997). The upregulatation of LDH-A renders c-Myc transformed cells sensitive to glucose as well: blocking glycolysis led to apoptosis, and ectopic expression of LDH-A in non-transformed cells induced

apoptosis when these cells were deprived of glucose, indicating that LDH-A expression is at least in part responsible for glucose dependence (Shim, Chun et al. 1998). It is curious that the ability of Myc to divert metabolic pathways towards increased glutamine usage for heightened tumorigenicity also (perhaps inadvertently) creates a point of vulnerability in another pathway as well. These results provide evidence that metabolic reprogramming is at the crux of cancer development.

As oncogenes can regulate glutamine metabolism, so too can glutamine affect oncogenes. The uptake of glutamine is a rate limiting step for mTOR activation, a protein that triggers cellular growth as mentioned above. Glutamine is taken up by cells, but then is quickly effluxed in exchange for essential amino acids which activate mTOR. The simultaneous efflux of glutamine and influx of amino acids is regulated by the transporter SLC7A5/SLC3A2, the inhibition of which led to growth arrest (Nicklin, Bergman et al. 2009).

A fascinating paper by Newsholme et al asserts that the influx of glucose or glutamine in tumor cells often exceeds the rate that either metabolite can be oxidized or used for precursors, and that the high rate of uptake serves an additional purpose: the capability to fine-tune regulation. High flux upstream means that the source of a nutrient is not a limiting factor, and that a cell can control how to direct the flux downstream with different oncogenic changes. For example, a cell can increase macromolecule synthesis without increasing or decreasing energy production, since the node for regulation is downstream of nutrient availability (Newsholme, Crabtree et al. 1985).

Mitochondrial metabolism in cancer

Mutations in mitochondrial components can also lead to metabolic reprogramming that is advantageous for a tumor (Zanssen and Schon 2005). Using ^{13}C glucose labeling, Mullen et al showed that in osteosarcoma cells with complex III mutations, glucose did not contribute any carbons to making citrate. This is unusual, since citrate is the first TCA cycle intermediate directly derived from acetyl-CoA, downstream of glycolysis. Additionally, citrate had 5 of its carbons derived from glutamine, while normal progression of glutamine supplementing TCA cycle intermediates would contribute 4 carbons to citrate. This suggested that citrate was being synthesized directly from glutamine-derived alphaketoglutarate into isocitrate, rather than going around the full TCA cycle. The authors discovered that isocitrate dehydrogenase 1 and 2 (IDH1 and 2) were working in a reverse direction, converting alphaketoglutarate to isocitrate and then generating citrate. The reverse TCA cycle continued with oxaloacetate succeeding citrate, followed by malate, fumarate, and succinate. (Succinate, actually, was formed in both forward and reverse directions of the TCA cycle.) This reversal caused citrate to produce acetyl-CoA in another reverse reaction, which was then used as a precursor for fatty acid synthesis. The phenomenon was named reductive carboxylation, and was also observed in a renal tumor line. In addition to its anabolic function, is possible that reductive carboxylation is used to rescue the NAD^+/NADH ratio that is disturbed by mitochondrial mutation (Mullen, Wheaton et al. 2012).

Mitochondrial abnormalities can also lead to a vicious cycle of tumorigenicity. Hypoxia and glucose deprivation, which can occur in the poorly vascularized tumor core, leads to the generation of reactive oxygen species (ROS) in mitochondria. These stabilize HIF-1 alpha, which in the short term leads to cell cycle arrest. However, prolonged hypoxia can stabilize HIF-2 alpha which activates c-MYC transcription. Extended hypoxia also causes DNA damage and potentially more pro-tumorigenic mutations.

Conversely, stimulating ROS production excessively will overwhelm the cell and cause cell death. While non-cancer cells have a lower threshold for ROS toxicity, a sufficiently high amount of ROS will ultimately kill tumor cells as well (Ralph, Rodríguez-Enríquez et al. 2010). We will discuss the root of ROS further in chapter 2.

Cancer cells may depend on mitochondrial DNA as well, since cells without mtDNA proliferated more slowly. An intriguing study found that mtDNA-deficient tumor cells actually facilitated horizontal transfer of mitochondrial DNA from host cells to tumor cells. The restoration of mtDNA reinstated respiratory function and tumorigenicity (Tan, Baty et al. 2015).

Cause and effect

Altered metabolism isn't necessarily only a byproduct of oncogenic change, but a cause in and of itself. It was found that 80% of high-grade gliomas have a specific IDH1 mutation: R132H. This mutation causes loss of function for the dephosphorylation of isocitrate, but also gains the unique capability to reduce alphaketoglutarate using NADPH. This results in the production of the metabolite 2-hydroxyglutarate (2HG) (Dang, White et al. 2009). A similar mutation in IDH2 also produces 2HG, which has been labeled an "oncometabolite" due to its ability to cause promoter hypermethylation and inhibit TET2 and DNA demethylation. 2HG also has been shown to impair myeloid differentiation and thereby contribute to acute myeloid leukemia (AML) (Figueroa, Abdel-Wahab et al. 2010).

Independently of the generation of oncometabolites, mutations in metabolic genes can have direct effects on cancer. Fumarate hydratase (FH) is a tumor suppressor, and loss of FH alleles have been found in renal cancer (Tomlinson 2002). Mutations in succinate dehydrogenase (SDH) have also been linked to hereditary paraganglioma (Baysal, Ferrell et al. 2000).

The dialogue of cause and effect is an important one – while it was previously thought that metabolic alterations were secondary to oncogenic signaling, it may well be the opposite. Rationally, even if a cell has proliferation-driving oncogenic changes, unless the cell can produce enough macromolecules to sustain growth proliferation can't occur and the oncogenic changes are moot. Altered metabolism can therefore be considered crucial for tumorigenesis and tumor maintenance. Metabolic pathways are not reprogrammed as a pawn for oncogenic signaling, but a knight – a driving force for cancer.

Systemic metabolism

Metabolism affects cancer not only at a cellular level but on the organismal scale. For example, data show that consumption of animal fat increases colorectal cancer risk, while dietary fiber reduces it. Colorectal cancer is particularly susceptible to changes in the diet, likely due to the sensitivity of gut microbiota. In fact, switching from a high fiber/low fat and sugar diet to a diet rich in animal fat and processed sugar changes the composition of the microbiome within a day. This is due in part to the ability of digested molecules to alter the inflammatory environment of the gut. For example, some plants when digested produce butyrate which is an HDAC inhibitor and is anti-carcinogenic. On the other

hand, hydrogen sulfide is a byproduct from the digestion of some animal fats and can have a pro-inflammatory effect (Bultman 2016).

Non-gastrointestinal cancers are also susceptible to dietary modulation. Obesity is associated with an increased risk of gall bladder, ovarian, pancreatic, kidney, liver, and endometrial cancers. Each additional BMI point also directly correlates with metastasis in breast cancer. However, the implications of obesity rather than body weight itself might be the actual contributors to tumor development (Klil-Drori, Azoulay et al. 2016). For example, obesity and diabetes can lead to insulin resistance. Hyperinsulinemia is associated with breast cancer risk, and it has been shown that insulin resistance leads to cancer (Goodwin, Pritchard et al. 2008). In addition, insulin receptor levels have been observed to be 6 times higher in breast cancer cells compared to normal breast tissue (Papa, Pezzino et al. 1990). Metformin reduces the amount of insulin in blood and increases insulin sensitivity and uptake by tissues. It is used to treat diabetes, and appears to have anti-cancer properties as well; administration of metformin improved insulin resistance in breast cancer patients, even those without diabetes (Goodwin, Pritchard et al. 2008).

PTEN pathway and metabolism

Our discussion of insulin is the perfect transition into describing the known interactions between the PTEN pathway and metabolic pathways. Insulin binds the insulin receptor on cells, which phosphorylates insulin receptor substrate 1 (IRS-1) which binds PI3K (Lee and Pilch 1994). Increased circulating insulin therefore promotes PI3K signaling; it is possible that the relationship between insulin and breast cancer coalesces at PI3K. Interestingly, *Pten* heterozygous mice exhibited enhanced insulin sensitivity and glucose uptake in skeletal muscle, suggesting that Pten negatively regulates insulin-

stimulated glucose uptake. In fact, following a glucose challenge, blood glucose levels returned to normal twice as quickly in *Pten*$^{+/-}$ mice compared to WT (Wong, Kim et al. 2007). Patients with Cowden syndrome (germline PTEN mutation) also exhibited increased insulin sensitivity and higher body weight (Pal, Barber et al. 2012). Insulin receptor substrate 2 (Irs2) deficiency caused insulin resistance and β–cell failure; heterozygous deletion of *Pten* in *Irs2*$^{-/-}$ mice restored insulin sensitivity and glucose tolerance, and improved β–cell function (Kushner, Simpson et al. 2005). As one may expect from the above data, mice with increased Pten expression have been shown to have lower body weight and fat, and their cells exhibited less glucose uptake (Garcia-Cao, Song et al. 2012, Ortega-Molina, Efeyan et al. 2012). Deletion of the Pten inhibitor Prex2 in MEFs reduced glucose uptake, and it was found that insulin-resistant patients exhibited decreased PREX2 and increased PTEN activity in adipose tissue (Hodakoski, Hopkins et al. 2014).

Insulin also stimulates fatty acid synthase (FAS). Inhibitors of PI3K prevented activation of the FAS promoter, while transfecting AKT into cells stimulated FAS independently of insulin. This indicated that FAS activation is mediated by insulin through PI3K and AKT (Sul, Latasa et al. 2000). As a complementary finding, PTEN null cells overexpress FAS, and reintroduction of PTEN in LNCAP cells reversed the FAS increase. FAS is found to be elevated in cancer (Van de Sande, De Schrijver et al. 2002).

We have already described the importance of fatty acid synthesis in tumor progression. The PI3K pathway also contributes to lipid metabolism through an alternate mechanism. Constitutively active AKT increases GLUT4 translocation to the membrane and increases expression of GLUT1, both of which bring glucose into the cell. This has been shown to lead to constitutive lipogenesis (Kohn, Summers et

al. 1996). AKT also phosphorylates and activates ATP citrate lyase (ACL) on S454, such that it can convert cytosolic citrate to acetyl-CoA as a precursor for lipids (Berwick, Hers et al. 2002).

Studies in prostate cancer cells have also shown that loss of PTEN leads to an increase in the uptake of LDL (low-density lipoprotein), which is hydrolyzed to free fatty acids and free cholesterol that is then esterified. This process was found to be dependent on PI3K and AKT. The authors showed that blocking cholesterol esterification reduced prostate tumor growth *in vitro* and *in vivo*. Moreover, the cholesterol found in lipid droplets in prostate cancer was not synthesized *de novo* but was in fact derived from the uptake of exogenous lipids. These data argue for the use of cholesterol-reducing drugs for cancer, and there is evidence that statins have had an effect on decreasing the risk of prostate cancer (Yue, Li et al. 2014).

Bringing our metabolic conversation full-circle, it has been shown that AKT stimulates aerobic glycolysis. While not all tumors were detected by FDG-PET, AKT-induced cells were visible on the scans, indicating their higher glucose uptake. These cells also increased glycolysis: NADH levels were elevated in spite of the presence of an electron transport chain inhibitor, ascertaining that the NADH was glycolysis-derived and not from mitochondria. Lactate production was increased while oxygen consumption was not, indicating that oxidative phosphorylation was not going up. A PI3K inhibitor prevented glucose uptake and lactate production, and glucose depletion led to apoptosis. AKT-induced cells therefore appear to be dependent on high levels of glucose (Elstrom, Bauer et al. 2004). PI3K also appears to upregulate glycolysis in an AKT-independent manner. Fructose-bisphosphate aldolase catalyzes the splitting of fructose 1,6-bisphosphate into dihydroxyacetone phosphate (DHAP) and glyceraldehyde 3-phosphate (G3P). Aldolase can be inhibited by its binding to actin; Rac-mediated actin remodeling, stimulated by

PI3K, releases aldolase from actin and allows its function in glycolysis (Hu, Juvekar et al. 2016). Super-PTEN mice with elevated Pten expression displayed increased energy expenditure and mitochondrial respiration accompanied by a reduction in lactate and the glycolysis regulator PFKFB3 (6-phosphofructo-2-kinase/ fructose-2,6-biphosphatase isoform 3), suggestive of an anti-Warburg phenotype (Garcia-Cao, Song et al. 2012). Glucose-derived lipids were also decreased in Super-PTEN cells, indicative of reduced anabolism. Interestingly, these mice also had lower levels of glutaminase and concomitant diminished glutamine uptake, possibly regulated by APC/C-Cdh1 (anaphase-promoting complex/cyclosome-Cdh1)-mediated ubiquitination (Garcia-Cao, Song et al. 2012). Further evidence suggests that PTEN positively regulates energy expenditure by increasing the activity of brown adipose tissue (BAT), which uncouples the electron transport chain and ATP production. PI3K inhibition also stimulated BAT and uncoupling protein 1, although in their model BAT had increased glucose uptake in the presence of increased Pten (Ortega-Molina, Efeyan et al. 2012).

Overall, the current body of literature illustrates that metabolic changes induced by oncogenic drivers of cancer are important contributors to tumor growth and are therefore attractive targets for cancer treatment. PTEN has a multifaceted function in the cell, including a role in metabolism. However, we do not as of yet have the complete picture of the part it plays in metabolic regulation. This thesis focuses on the metabolic consequences of PTEN inactivation, the therapeutic vulnerability thus exposed, and the mechanism of synthetic lethality distinctive to PTEN deficiency.

CHAPTER 1 FIGURE LEGENDS AND FIGURES

Figure 1.1. Schematic of PTEN pathway. A diagram of components of the PTEN/PI3K pathway, including PI3K and AKT activation and downstream effectors (Samuels and Ericson 2006). While new research has shown that the pathway has additional complexity, this schematic provides a framework for our understanding. Key: GFs = growth factors; RTKs = receptor tyrosine kinases; IRS2 = insulin receptor substrate 2; PIK3CA = catalytic p110α subunit of PI3K; PIP2 = phosphatidylinositol (4,5) bi-phosphate; PIP3 = phosphatidylinositol (3,4,5) tri-phosphate; PTEN = Phosphatase and Tensin homolog deleted from chromosome ten; PDK-1 = phosphoinositide-dependent kinase 1; PHLPP = PH domain and Leucine rich repeat Protein Phosphatases; FKHR = FOXO1; FKHRL1 = FOXO3; AFX = IKK = IκB kinase; NF-κB = nuclear factor kappa-light-chain-enhancer of activated B cells; Tuberin = Tuberous Sclerosis Complex 2; GSK3β = Glycogen Synthase Kinase 3 Beta; Rheb = Ras homolog enriched in brain; mTOR = mammalian target of rapamycin; eIF4G = Eukaryotic translation initiation factor 4 G; p70 S6K = Ribosomal protein S6 kinase beta-1; 4E-BP1 = 4E-binding protein 1.

Figure 1.2. Contributions of glutamine. In this schematic, glutamine is shown to contribute to nucleotides and TCA cycle anaplerosis (DeBerardinis, Lum et al. 2008). The details of these pathways and their interaction with other metabolic pathways will be discussed further in our text.

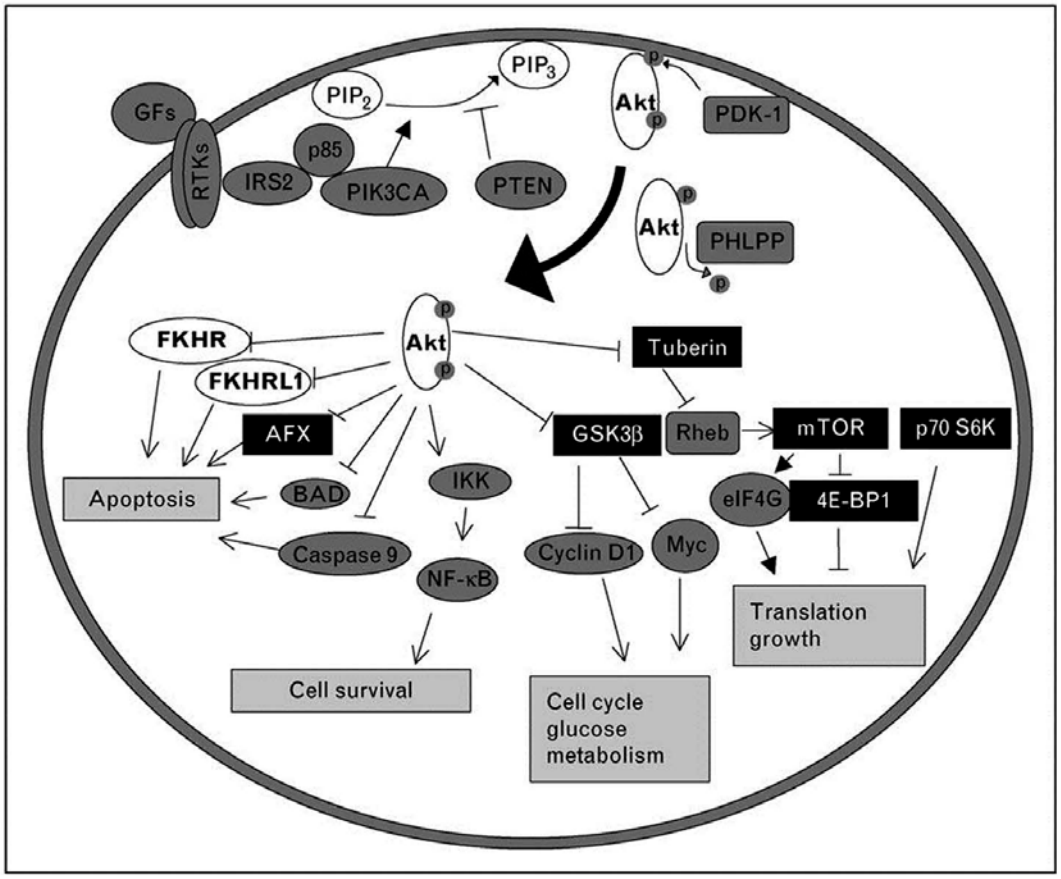

Figure by Samuels and Ericson, Current Opinion in Oncology 2006

Figure 1.1

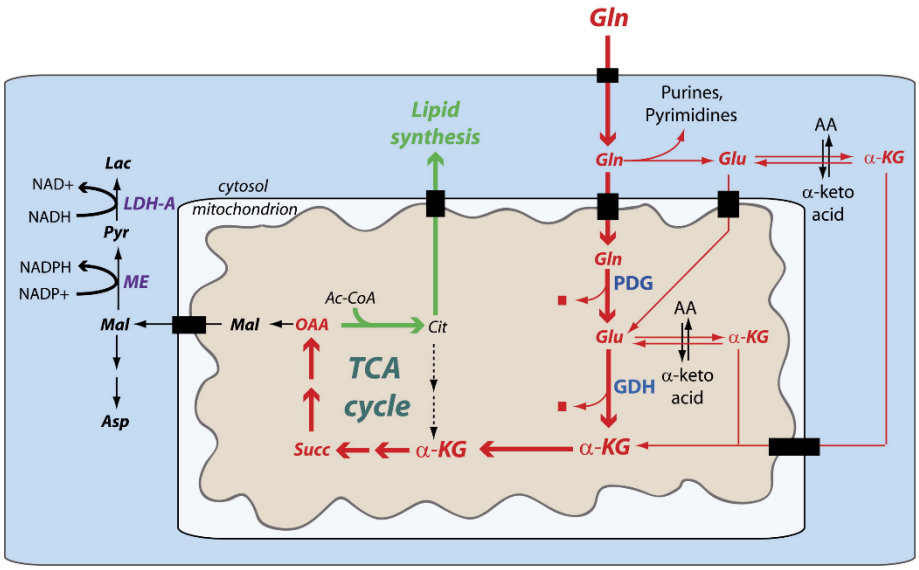

Figure by DeBerardinis et al, Cell Metabolism 2008

Figure 1.2

Chapter 2: Characterization of PTEN loss

As described in the introductory chapter, loss of PTEN to varying degrees has been implicated in processes as diverse as lipid second messenger signaling, metabolism, regulation of other proteins, and, of course, tumorigenesis. It is for this reason that fully understanding the implications of PTEN deficiency is central to our grasp of cancer itself, in a symphysis of intracellular and systemic knowledge. We therefore begin our study of PTEN by observing the changes in cellular function upon its deletion, with an emphasis on metabolic alterations.

Results

MEFs as a model system

An important decision in any biological project is choosing an appropriate model system. Since we wished to determine the effects of PTEN loss, we started the project using isogenic cell lines: pairs of cell lines derived from the same parental line but differing in their PTEN genotype. In our early studies, we used MCF10A (untransformed human breast epithelial), HEC1A (human endometrial cancer), HCT116 (human colorectal carcinoma), and DLD1 (human colorectal carcinoma) cells, each with $PTEN^{+/+}$ and $PTEN^{-/-}$ genotypes. To complement these human lines, we also studied isogenic pairs of dominant-negative p53-immortalized mouse embryonic fibroblasts (p53dn MEFs), also with $PTEN^{+/+}$ and $PTEN^{-/-}$ genotypes.

We soon realized, however, that using these isogenic lines was not an ideal approach. While one would expect the $PTEN^{-/-}$ lines to have similar phenotypes to each other, there were few consistencies across

lines, including little similarity in gene signatures among PTEN$^{-/-}$ lines (Fig. 2.1). Although within each pair there were transcript differences between the PTEN$^{-/-}$ and WT settings, overall the signature changes did not highly correlate across cell lines. It appeared that PTEN loss in each isogenic line altered the gene signatures in dissimilar ways rather than eliciting a consistent transcriptional response. While it is possible that more pairs of immortalized MEFs would yield higher power and statistical significance, our results indicated that a better model system may be warranted.

Additionally, we applied the eigenvector-based Principal Components Analysis (PCA) to four pairs of p53dn MEFs. An eigenvector of matrix T is a vector that does not change direction when linearly transformed by T, although it may change in terms of scale. PCA calculates the covariance of each gene across samples, and calculates the eigenvectors of the resulting matrix. A best-fit ellipsoid (3-dimensional ellipse) is then fit to the vectors, with each vector corresponding to an axis of the ellipsoid. When normalized, the longest vector is the primary axis, second longest is the secondary axis, and so on. The clustering of the samples based on the primary axis reveals the main distinguisher of the samples. Using PCA, we found that rather than the PTEN$^{-/-}$ cells clustering together, each line only clustered with its isogenic partner (Fig. 2.2A). This may be in part because some of the PTEN$^{+/+}$ lines began to lose PTEN expression (Fig. 2.2B).

The above results suggested to us the following: first, the isogenic cell lines we used have been cultured and passaged for so long that p53dn MEFs which originally started out genetically similar have likely diverged over time, accumulating changes in gene expression that distinguish each pair from the others (including deregulation of PTEN itself). Second, it is possible that the human cell lines have amassed so

many genetic mutations (which can interact differently with the loss of PTEN) that the single PTEN genetic change didn't make enough of a consistent difference in this setting.

What we needed was a cleaner system, in which PTEN loss was the only genetic change such that we can say with certainty the effects of PTEN *per se*. We therefore decided to use primary mouse embryonic fibroblasts (MEFs), non-immortalized and passaged fewer than 8 times to ensure viability. The MEFs were generated from mice which had LoxP sites (short sequences derived from a bacteriophage) surrounding exon 5 of *Pten* (Li, Robinson et al. 2002)(Fig. 2.3A). After extracting embryos from pregnant mice, we isolated fibroblasts and grew them as adherent cells. Infection with an adenovirus containing the Cre Recombinase enzyme recombined the LoxP sites, thereby deleting the *Pten* exon and preventing Pten expression (Fig. 2.3A-B). An adenovirus not containing Cre was used as a control. (To generate the p53dn MEFs used above, pairs of these otherwise genetically identical MEFs were immortalized with dnp53.)

PCA on 4 pairs of wild-type (WT) and Pten knockout (KO) MEFs revealed the KO cells clustering together and the WT cells clustering together, showing that Pten status is the principal defining factor in these MEFs (Fig. 2.3C). It is important to note that while the overall WT cluster and KO cluster are fairly close together, each pair (MEF 1, 2, etc.) has considerable separation between the WT and KO, indicating that Pten is the primary difference between the cells. We therefore use primary MEFs in this thesis to establish the effects of Pten loss, and use other cell lines (both human and mouse) to determine universality and applicability in further studies.

Growth and Proliferation

Since PTEN is a *bona fide* tumor suppressor and negatively regulates the PI3K/AKT pathway described above, we reasonably hypothesized that loss of PTEN would increase the rate of cellular growth. To ascertain the role of PTEN in growth, we plated an equal number of WT and KO primary MEFs and measured the increase in cellular confluence over time using phase-confluence images. *Pten*$^{-/-}$ MEFs[1] consistently grew faster over time (Fig. 2.4A-B). These results were also reproduced using a crystal violet assay (Fig. 2.4C).

By infecting MEFs containing no LoxP sites with Cre adenovirus, we confirmed that the Cre virus alone was not affecting growth (Fig. 2.4D). We further observed that *Pten*$^{-/-}$ MEFs grew faster than those which were not infected at all, confirming that the virus is not toxic and the effect on growth is veritable and biologically meaningful (Fig. 2.4E).

Associated with the increased growth rate of *Pten*$^{-/-}$ MEFs were a greater number of replication forks per cell, as measured by EdU. EdU (5-ethynyl-2'-deoxyuridine) is an analog of thymidine and is incorporated into DNA during DNA synthesis. A click chemistry reaction allowed us to attach a fluorescent dye to EdU in order to detect its levels. We visualized EdU foci using confocal microscopy, and quantified the number of foci per cell (Fig. 2.5A-B). Since this method quantifies a limited number of cells, we also performed flow cytometry on 5000 cells per sample; the shift to the right in EdU intensity in *Pten*$^{-/-}$ compared to WT cells indicates more replication per cell in the *Pten*$^{-/-}$ population (Fig. 2.5C).

[1] We henceforth refer to Pten genotypes as WT and Pten$^{-/-}$. However, we still use "WT" and "KO" in figures for brevity.

The faster growth of *Pten*$^{-/-}$ cells opened a two-pronged question: are *Pten*$^{-/-}$ cells growing more because they are dying less than WT cells, or because they are truly proliferating faster? To address this, we measured cell death using Annexin V and 7-Aminoactinomycin D (7-AAD). In healthy cells, phosphatidylserine is restricted to the inner leaflet of the plasma membrane by flippase; however, in early-stage apoptosis scramblase translocates some phosphatidylserine to the outer leaflet where it can be recognized and bound by the protein Annexin V. Late-stage apoptosis is associated with loss of membrane integrity. While the fluorescent chemical 7-AAD is not cell permeable, it can easily enter cells during late-stage apoptosis and bind to DNA. Using these indicators in combination shows the population of cells which are alive (no staining for either marker), in early-stage (Annexin V-positive only) or late-stage apoptosis (Annexin V and 7-AAD positive), or dead via necrosis or an alternate death mechanism (7-AAD positive only). As a positive control we used the RNA polymerase blocker actinomycin D to induce cell death. By using these markers and detecting fluorescent readings by flow cytometry, we did not observe a difference in the percentage of live cells between Pten$^{-/-}$ and WT populations (Fig. 2.6A).

To address proliferation, we performed a cell cycle assay using bromodeoxyuridine (BrdU) and propidium iodide (PI). BrdU, like EdU, is a synthetic nucleoside analog of thymidine. The BrdU we employed was conjugated to Anti-BrdU Alexa Fluor® 488 which emits green when excited by a blue laser. Propidium iodide intercalates DNA and fluoresces yellow/orange when bound to nucleotides. Using these two in combination, we can determine the population of cells in G1 (low PI and low BrdU signal), S-phase (intermediate PI and high BrdU) and G2 (high PI and low BrdU) stages of the cell cycle. We found an increased proportion of cells within S-phase in Pten$^{-/-}$ cells, suggesting that they may be synthesizing more DNA in order to proliferate at a higher rate (Fig 2.10B). While a greater percentage of cells in S-phase can in principle also indicate S-phase arrest, in this case the S-phase data coupled with

the greater number of replication forks and increased rate of growth indicate that the Pten$^{-/-}$ cells are in fact progressing through the cell cycle and proliferating faster than their WT counterparts. At any given time, the Pten$^{-/-}$ population has a greater proportion of cells in S-phase and increased replication forks per cell in order to achieve faster proliferation.

We also decided to investigate senescence in our MEFs using β-galactosidase (β-gal), a standard assay for senescence. β–gal is an enzyme that cleaves galactosides, and is expressed in senescent fibroblasts (Dimri 1995). By first staining cells with X-gal, a galactose that is blue upon cleavage, we could quantify the percentage of blue/senescent cells in the Pten$^{-/-}$ and WT populations. We did not, however, observe a significant difference in cellular senescence between Pten$^{-/-}$ and WT MEFs (Fig. 2.7).

Growth and metabolism are inexorably linked. In order to sustain a higher growth rate, it stands to reason that PTEN mutant cells have adjusted their metabolism to produce more of the cellular entities required for growth. In the next sections we identify metabolic changes induced upon Pten loss.

Mitochondrial Activity

It would be remiss to have a discussion on metabolism without investigating the mitochondrion, the home of the Citric Acid Cycle, electron transport chain, and multiple redox reactions.

Oxygen is the final electron acceptor in the electron transport chain, and different rates of respiration could be indicative of changes in mitochondrial function. Additionally, a decrease in pH outside of the

cell can be indicative of metabolic changes just upstream of the mitochondria, due to the conversion of pyruvate to lactic acid which releases free protons and causes extracellular acidification. This can occur either due to the inability of pyruvate to be properly processed in the mitochondria, or to aerobic glycolysis leading to a buildup of glycolytic intermediates (including pyruvate).

To assess these mitochondrial functions, we used an instrument called the Seahorse, which is capable of detecting the partial pressure of dissolved oxygen and the concentration of free protons. To achieve this, we plated cells in wells with a small surface area such that when the Seahorse probe was lowered into the well only 7μL of media remained between the cells and sensor, creating a small controlled volume for detection. There are two fluorophores at the bottom of the sensor, one detecting H^+ ions and the other quenched by O_2. Multiple measurements were taken over time, and the resulting slope corresponds to the rate of consumption or secretion of O_2 and protons, respectively.

To narrow down which part of mitochondrial function may be altered, we used inhibitors of various electron transport chain complexes. Oligomycin inhibits ATP synthase, creating a backup of the electron transport chain and resulting in less oxygen consumption by the cell but increased extracellular acidification, as pyruvate is converted to lactate when not used in the mitochondrion. FCCP (Carbonyl cyanide-4-(trifluoromethoxyphenylhydrazone) disrupts the proton gradient by allowing H^+ ions to pass through the inner mitochondrial membrane. This increases oxygen consumption, as the cells ramp up churning of the electron transport chain in a futile effort to generate ATP. Extracellular acidification can be reduced in this case, since pyruvate is demanded by mitochondria, but if the demand for glucose is increased the rate of acidification may rise. Finally, rotenone inhibits the transfer of electrons from complex I, blocking the electron transport chain and shutting down oxygen consumption. By

sequentially adding these poisons, we can determine the differences in ATP production, maximum respiratory capacity, and non-mitochondrial respiration (remaining O_2 consumption even after inhibition of electron transport chain O_2 consumption).

We tested primary MEFs as well as isogenic cell lines with the Seahorse. Primary WT and $Pten^{-/-}$ MEFs did not show a significant difference in mitochondrial function, and there was no consistent trend among the other cell lines (Fig. 2.8-2.10). Although one of the immortalized MEF pairs displayed a difference in uncoupled oxygen consumption rate, this did not repeat in other immortalized MEFs and therefore may not be due to PTEN *per se*.

Hand in hand with the above mitochondrial readouts is the level of reactive oxygen species (ROS), a byproduct of mitochondrial respiration. As mentioned above, oxygen is the final electron acceptor in the electron transport chain. In fact, electrons are frequently "donated" to oxygen in biological systems because it has a greater standard reduction potential — propensity to be reduced — than other common cellular atoms such as nitrogen, sulfur, carbon, and hydrogen (listed in decreasing order of potential). Hydrogen is often the source of electrons, as H_2 can split as two electrons and two H^+ ions. Complete reduction of molecular oxygen, O_2, results in H_2O. Partial reduction of oxygen, however, confers a reactive state to the molecule, earning it the name reactive oxygen species. The table below describes the possible states of reactivity of oxygen: (Hancock, Desikan et al. 2001, Nelson, Lehninger et al. 2008).

$O_2 + e^- \rightarrow O_2^{\cdot -}$	Superoxide
$O_2^{\cdot -} + e^- \rightarrow O_2^{2-} + 2H^+ \rightarrow H_2O_2$	Hydrogen peroxide
$H_2O_2 + e^- \rightarrow {}^{\cdot}OH + OH^-$	Hydroxyl radical and hydroxide ion

The most common way for ROS to be generated is in the mitochondrion itself: electrons that leak out between ubiquinone and complex III rather than getting passed along properly can prematurely be transferred to O_2, resulting in superoxide. It is important to note that a low level of ROS thus generated as a byproduct of respiration is normal, and about 2% of cellular oxygen is processed in this manner (Ames, Shigenaga et al. 1993). Superoxide can then be further reduced spontaneously or by superoxide dismutase or peroxisomal oxidases to form hydrogen peroxide and ultimately hydroxyl radicals. The latter is the most reactive form of ROS, and can damage lipids, proteins, and DNA, potentially leading to mutations (Novo and Parola 2008).

Fortunately, the cell has several built-in safeguards against excess ROS. Peroxisomes can be a defense against ROS as well a generator of them; the peroxisomal enzyme catalase eliminates H_2O_2 by converting it into water and molecular oxygen. Glutathione can similarly break down H_2O_2, and antioxidant compounds such as Vitamin E block the progression of radical chains, thereby preventing free radicals from damaging other molecules. The equilibrium between ROS and antioxidant mechanisms keep normal cells at a healthy level of oxidation. However, perturbation to any of these pathways can upset the redox balance and lead to levels of ROS which are higher than can be quenched by cellular antioxidants (Novo and Parola 2008).

The relationship between ROS and cancer is a complicated one. While hypoxic conditions and heightened metabolism often increases ROS in tumors, cancer cells have also been able to adapt to oxidative stress and can upregulate antioxidant enzymes, protecting the cancer from cytotoxic effects of excessive ROS buildup. It is therefore difficult to predict how a particular cancer cell will react to ROS inducing or extinguishing agents. PTEN's association with ROS is unclear as well; it has been shown both that loss of PTEN increases ROS due to AKT activation (Dolado and Nebreda 2008, Nogueira, Park et al. 2008), and that PTEN loss can prevent increases in ROS (Zhu, Hoell et al. 2007). This suggests that the role of PTEN in ROS production and elimination may be cancer- or tissue-specific and dependent on other signaling pathways with which the PTEN pathway interacts.

We decided to investigate ROS in our cells as well, using two different methods of measurement. 2,7-Dichlorodihydrofluorescein diacetate (DCF-DA) fluoresces green upon oxidation through interaction with ROS, and measures overall cellular ROS including what has diffused out of the mitochondria. MitoSOX™ Red, on the other hand, measures superoxide specifically as it is not efficiently oxidized by other forms of ROS.

Previous data from our lab found a lower level of total ROS in some PTEN mutant lines compared to their isogenic pair, but the trend did not hold true for all lines. Here, we found that primary WT and $Pten^{-/-}$ MEFs displayed no consistent difference in mitochondrial or total ROS, suggesting that Pten loss alone does not significantly affect ROS (Fig. 2.11A-B). There was also no difference in the protein level of TOM20, a marker of mitochondrial mass (Fig. 2.11C).

From these data as well as those from the Seahorse, we cannot conclude that there are significant mitochondrial alterations in the transport chain attributable to loss of Pten, although it is possible that there are other changes we did not measure. Additionally, the different patterns in mitochondrial metabolism in isogenic cancer lines (i.e. ROS and Seahorse data) furthered our confidence in using primary MEFs as a model system to study mechanistic changes upon PTEN loss.

Metabolomics and nutrient deprivation

To understand the intracellular metabolic changes induced by Pten loss, we used an unbiased approach and performed steady-state metabolomic profiling of 292 aqueous metabolites by mass spectrometry. A program called IMPaLA (Integrated Molecular Pathway Level Analysis) sorted the metabolites into pathways, and revealed that seven of the ten most upregulated pathways in *Pten*$^{-/-}$ MEFs involved nucleotide synthesis and DNA metabolism, including a higher concentration of pyrimidine 2-deoxyribonucleotides in *Pten*$^{-/-}$ MEFs (Fig. 2.12). Since glutamine contributes both nitrogen and carbon to making pyrimidines, we hypothesized that glutamine flux into pyrimidine synthesis was elevated in *Pten*$^{-/-}$ cells. To test this, we performed targeted metabolic flux analysis using heavy isotope labeling. In our environment, carbon exists predominately as ^{12}C, and nitrogen as ^{14}N. However, there are stable (non-radioactive) isotopes of these elements, ^{13}C and ^{15}N, each of which has an extra neutron in the atom's nucleus. We obtained glutamine which had either all carbons or the amide nitrogen (which gets directly incorporated into pyrimidines) exchanged for their heavy isotope versions, and replaced glutamine in media with either ^{13}C glutamine or ^{15}N glutamine. We incubated the cells for one hour in the labeled media prior to collecting metabolites, allowing us to monitor the flux of glutamine. Mass spectrometry showed increased synthesis of dihydroorotate, orotate, and other components of the *de novo* pyrimidine synthesis pathway in *Pten*$^{-/-}$ MEFs relative to WT (Fig. 2.13, 2.14A). In addition, the pyrimidine metabolism gene set was upregulated in mRNA from *Pten*$^{-/-}$ MEFs (Fig. 2.14B).

It has previously been shown by Brendan Manning's group that active S6 kinase due to mTORC1 activation phosphorylates and activates CAD, a *de novo* pyrimidine synthesis enzyme. This led to an increase in pathway intermediates that could be blocked by inhibition of mTORC1 (Ben-Sahra, Howell et

al. 2013). Consistent with this prior report, we found CAD phosphorylation to be increased in *Pten*$^{-/-}$ cells, likely contributing to the push of glutamine flux into the pyrimidine synthesis pathway (Fig. 2.14C).

Moreover, we found that the growth advantage of *Pten*$^{-/-}$ MEFs was dependent on glutamine: depletion of glutamine collapsed the growth difference between *Pten*$^{-/-}$ and WT MEFs, as did the addition of the glutaminase inhibitor CB-839 which blocks the conversion from glutamine to glutamate (Fig 2.15A-B). The requirement of glutamine for the growth advantage conferred by Pten loss therefore connects to the patterns of glutamine flux in Pten$^{-/-}$ MEFs. Nucleotide synthesis is a prerequisite for cellular growth, and *Pten*$^{-/-}$ MEFs appear to channel glutamine for this purpose.

Pten$^{-/-}$ MEFs had somewhat elevated steady-state glucose metabolism and glycolytic flux relative to WT MEFs, consistent with previous literature (Fig. 2.12A and 2.15C). Unlike many types of cancer cells which are highly sensitive to glucose deprivation due to the Warburg effect described above, depletion of glucose from the medium of MEFs did not rescue the differences in cell growth, suggesting that glutamine was more critical for the growth advantage of *Pten*$^{-/-}$ cells (Fig 2.15D). We must note, however, that there was still a trace amount of glucose present in the media's serum.

Discussion

In this chapter, we made the following overarching observations: 1) MEFs are a good model system for studying cellular changes caused by PTEN loss; 2) there are no notable differences in mitochondrial respiration or ROS production between WT and *Pten*$^{-/-}$ cells; 3) Pten loss increases the proliferation rate and the number of replication forks per cell; 4) this is supported by an increase in glutamine flux into the

de novo pyrimidine synthesis pathway; 5) *Pten*$^{-/-}$ cells are dependent on glutamine for their growth differential. Through these results, we have performed a general characterization of the consequences of Pten loss in terms of metabolic capacity and nutrient dependence.

Our result of a faster proliferative rate upon Pten loss is consistent with its general mechanism of tumor suppression as well as current literature about the pro-growth downstream effectors of the PI3K pathway (outlined in the introductory chapter). However, there is a small body of research that suggests that loss of Pten prompts cellular senescence instead.

Chen et al claim that while heterozygous loss of Pten in MEFs increases growth rate, complete loss decreases growth rate and induces senescence that can be rescued by additional loss of p53 (Chen, Trotman et al. 2005). However, this paper used a different negative control than our group did: while we infected matched paired *Pten*$^{fl/fl}$ MEFs with either Cre-containing virus or empty virus (separately controlling for effects of Cre itself), Chen et al used WT MEFs infected with Cre as a control. It is possible that the different embryos respond differently to the Cre virus due to differences in the mice themselves, not necessarily the genetic status of Pten, thus producing the different result. A subsequent paper by the same group did compare *Pten*$^{fl/fl}$ MEFs with Cre or Gfp infection and still found poorer growth in Cre-infected cells (Alimonti, Nardella et al.). It would be valuable to see the effects of their viruses on WT MEFs (like our controls in Fig. 2.4) to ensure accuracy of the results. Interestingly, they see increased senescence of Pten-deficient cells in the absence of DNA damage; our results as well as previous reports demonstrate an endogenous level of DNA damage in *Pten*$^{-/-}$ cells as described in chapter 4, and this could affect the senescence phenotype. It is also possible that subtle variations in mouse background can confound results. Additionally, Pten loss may induce a senescent sub-population

of cells that is overshadowed by the increased growth rate of the population as a whole. Authors of these papers do, however, acknowledge that complete loss of PTEN is commonly found in aggressive cancers (Trotman, Niki et al. 2003).

It is notable in our data that pyrimidine synthesis was upregulated more than other facets of glutamine metabolism such as the TCA cycle. This supports the principles justified by current literature that different oncogenic changes affect specific nutrient addictions for particular metabolic pathways, rather than indiscriminate nutrient uptake and processing. Newsholme's theory (discussed in the introductory chapter) also comes into play here (Newsholme, Crabtree et al. 1985): it is possible that all of glutamine metabolism is somewhat upregulated, but the change in pyrimidine flux is detectable as being magnified because it is under regulation by PTEN.

We also note that UMP is not significantly altered in PTEN-deficient cells, although the trend is towards upregulation. We think there are two possibilities as to why the UMP upregulation was not found to be significant. First, UMP and pseudouridine have been shown to be difficult to differentiate from each other using mass spectrometry. Pseudouridine was not measured in our panel, but it's possible that some of the signal from UMP was conflated with pseudouridine. Second, in addition to UDP, UMP is also directly converted to uridine which was not measured in our panel. Some of the orotate to UMP to UDP pathway may be sidetracked to uridine directly from UMP, thus seemingly "skipping" a step (Charette and Gray 2000, Quinn, Basanta-Sanchez et al. 2013). However, since the other measured metabolites in the pathway were consistently upregulated in ^{13}C, ^{15}N, and unlabeled metabolic extracts, and given the previous literature on the subject, we are confident that the pathway is in fact upregulated in *Pten*$^{-/-}$ cells.

As mentioned in the introductory chapter, Myc also induces glutamine dependency, albeit for TCA cycle intermediates and phospholipid precursors over nucleotides (Wise, DeBerardinis et al. 2008). While the paper showed that PI3K or AKT inhibition did not alter reliance on glutamine in a Myc-amplified glioma line, this is not necessarily inconsistent with our data. First, unless PTEN is lost and the PI3K pathway is actually upregulated, blocking the pathway may be moot. Second, Myc induction of glutamine dependency is likely independent of the PTEN/PI3K pathway and can therefore continue to increase glutamine uptake regardless of PI3K or AKT activity. In fact, independent modes of glutamine upregulation could help explain the different downstream pathways of glutamine that are augmented in Pten-deficient versus Myc-amplified cells.

Our data are also reminiscent of transformed HeLa cells, which use glutamine preferentially even in the presence of adequate glucose. It is not so strange, then for *Pten*$^{-/-}$ cells to be less sensitive to glucose deprivation, as there is precedent for it (Reitzer, Wice et al. 1979).

Our findings in this chapter are illuminating in several ways. First, it is common in our field for mechanistic studies to be performed on cancer cell lines, isogenic or otherwise. While this has the benefit of being a human system, we provide evidence that cell lines can confound the true nature of a genetic change and may be better suited for follow-up studies to show broad applicability rather than for initial observations in some cases. Second, we identify a greater number of replication forks per cell in *Pten*$^{-/-}$ cells. Confocal microscopy data allowed us to visualize the increased number of foci in the nucleus, and flow cytometry quantified the EdU signal in thousands of cells, a number that would be prohibitive in microscopy experiments alone. These data also support our finding of increased

proliferation in *Pten*$^{-/-}$ MEFs. Third, we have connected nutrient deprivation experiments with metabolomics and targeted flux mass spectrometry for a more complete picture of metabolic changes.

In the following chapter, we use this knowledge to expose a therapeutic vulnerability in PTEN mutant cells.

CHAPTER 2 FIGURE LEGENDS AND FIGURES

Figure 2.1. Genetic profiling of isogenic cell lines. RNA was collected from PTEN$^{-/-}$ and WT isogenic cell lines and microarray analysis was performed. Data were uploaded to and analyzed by the Broad Institute's Morpheus software. Expression levels are shown; rows correspond to different genes.

Figure 2.2. PCA analysis and Pten expression of immortalized MEFs. (A) PCA analysis of 3 pairs of isogenic immortalized MEFs. (B) Immunoblot of Pten protein expression of the same 3 pairs of isogenic immortalized MEFs with loading control.

Figure 2.3. PCA analysis of primary MEFs. (A) Diagram of mouse model with LoxP sites. (B) Diagram of how isogenic MEF pairs were produced from flox/flox mice. Ad-Cre = adenovirus containing Cre recombinase; Ad-null = empty adenovirus used as a control. (C) PCA analysis of 4 pairs of WT and *Pten*$^{-/-}$ primary MEFs.

Figure 2.4. Cellular growth rate is affected upon loss of Pten. (A) Pten$^{fl/fl}$ MEFs infected with an empty adenovirus (WT) or one containing Cre recombinase (KO) were plated in equal numbers in 96 well plates, and growth was measured over time using phase-contrast images from an Incucyte Zoom (two-way ANOVA, *p<.0001, n=3). (B) Immunoblot of Pten protein of Pten$^{fl/fl}$ MEFs derived from two independent embryos, infected with an empty adenovirus or one containing Cre recombinase, 2 passages after infection. (C) Pten WT and KO primary MEFs were plated in equal numbers in 48 well plates, and growth was measured over time using crystal violet staining (two-way ANOVA, *p<.05, n=3). (D) WT MEFs (with no LoxP sites) were infected with an empty adenovirus or one containing Cre recombinase to determine whether Cre alone affects growth (two-way ANOVA, p>.05, non-significant, n=3). (E) Pten $^{fl/fl}$ MEFs were infected with an empty virus (Ad-null) or one containing Cre Recombinase or GFP. Uninfected MEFs are also shown as a control. Cells were plated in equal numbers in 96 well

plates and growth was measured over time using crystal violet staining (two-way ANOVA, *p<.0001, n=3).

Figure 2.5. Pten loss increases replication forks. (A) MEFs were pulsed with EdU for 45min, and labeled with an EdU-binding fluorescent tag following fixation. Representative confocal microscopy images are shown. (B) Quantification of images represented in Fig.1A (Student's *t*-test, *p<.05, n=6). (C) MEFs were pulsed with EdU for 45min, and labeled with an EdU-binding fluorescent tag following fixation. Flow cytometry determined the mean fluorescence intensity (MFI) of EdU signal among cells positively stained, indicating the amount of EdU incorporation in replicating cells (Student's *t*-test, *p<.01, n=3).

Figure 2.6. Apoptosis and the cell cycle. (A) Cells were collected and labeled with annexin V and 7AAD, and flow cytometry was used to determine the percentage of positively or negatively stained cells in the population. Left: representative population distribution of a sample; right: quantification of replicates (Student's *t*-test, p>.05, n=3). (B) MEFs were pulsed with BrdU for 18h, fixed, and labeled with an anti-BrdU antibody and propidium iodide. Flow cytometry was used to determine the cells in each population corresponding to G1, S, and G2 phases of the cell cycle. Top: representative population distribution of a sample; bottom: quantification of replicates (Student's *t*-test, *p<.001, n=3).

Figure 2.7. Senescence assay in primary MEFs. Primary MEFs were stained with β-gal and DAPI, and the percent of senescent cells was quantified by counting positive cells and normalizing to total cell count (Student's *t*-test, p>.05, n=3).

Figure 2.8. Seahorse analysis of primary MEFs. (A) Oxygen consumption rate (OCR) and (B) extracellular acidification rate (ECAR) of WT and *Pten*$^{-/-}$ primary MEFs. Oligomycin, FCCP, and rotenone were added at points A, B, and C, respectively.

Figure 2.9. Seahorse analysis of immortalized MEFs. (A) Oxygen consumption rate (OCR) and (B) extracellular acidification rate (ECAR) of 2 pairs of isogenic immortalized MEFs. Oligomycin, FCCP, and rotenone were added at points A, B, and C, respectively.

Figure 2.10. Seahorse analysis of isogenic human cancer cell lines. (A) Oxygen consumption rate (OCR) and (B) extracellular acidification rate (ECAR) of isogenic human cancer cell lines. Oligomycin, FCCP, and rotenone were added at points A, B, and C, respectively.

Figure 2.11. Reactive oxygen species. (A) Intracellular ROS on two pairs of primary MEFs was measured by DCFDA. Flow cytometry determined the mean fluorescence intensity (MFI) of DCFDA signal (Student's *t*-test, p>.05, n=3). (B) Mitochondrial ROS on two pairs of primary MEFs was measured by MitoSox. Flow cytometry determined the mean fluorescence intensity (MFI) of MitoSox signal (Student's *t*-test, p>.05, non-significant, n=3). (C) Immunoblot of mitochondrial protein TOM20 in primary MEFs.

Figure 2.12. Global metabolic profiling. (A) Over 200 soluble metabolites were measured by LC-MS/MS from unlabeled MEFs. Data were analyzed with the Integrated Molecular Pathway Analysis program (IMPaLA) and the top 5 hits for pathways upregulated in *Pten*$^{-/-}$ MEFs are shown in green, all related to pyrimidine metabolism. As a comparison, 5 other pathways upregulated in *Pten*$^{-/-}$ MEFs are shown: purine metabolism, the TCA cycle, and glucose metabolism are farther down the list. (B) Relative metabolite concentrations of DNA nucleotide precursors (dGMP was unable to be measured so dGTP was used) show a significant increase in pyrimidine but not purine precursors (Student's *t*-test, *p<.05, n=3). (C) The relative levels of each metabolite listed in the "pyrimidine metabolism" and "nucleotide metabolism" pathways from (A) are shown (Student's *t*-test, *p<.05, n=3).

Figure 2.13. *De novo* pyrimidine synthesis. (A) Schematic of the *de novo* pyrimidine synthesis pathway. (B) MEFs were incubated with ^{13}C glutamine or ^{15}N glutamine for 1 hour and metabolites were measured by LC-MS/MS . Relative metabolite levels of glutamine-labeled *de novo* pyrimidine synthesis

intermediates are shown (Student's *t*-test, *p<.05, n=3). Data were also analyzed with IMPaLA: ^{13}C glutamine-derived pyrimidine metabolism enrichment in $PTEN^{-/-}$ MEFs q-value = $3.92x10^{-09}$.

Figure 2.14. Pyrimidine enrichment in $Pten^{-/-}$ MEFs. (A) Metabolites from Fig. 2.13B mapped out onto the *de novo* pyrimidine synthesis pathway. Graphs on the left side of the figure correspond to ^{15}N labeled glutamine, and on the right side to ^{13}C labeled glutamine. Some metabolites are missing either a ^{13}C or ^{15}N graph because not every metabolite was able to be measured in both panels (Student's *t*-test, *p<.05, n=3). (B) Gene set enrichment analysis of the pyrimidine synthesis gene set on microarray data from 4 pairs of primary MEFs (FDR q-value <.05). (C) Immunoblot of pCAD S1859 and total CAD in MEFs.

Figure 2.15. Nutrient dependency induced by Pten loss. (A) *Pten* WT and KO MEFs were plated in media containing full glutamine (6mM) or no glutamine, and growth was measured over time using phase-contrast images from an Incucyte Zoom (one-way ANOVA, *p<.0001, n=3). (B) MEFs were treated with 12.5nM CB-839 or DMSO, and growth was measured over time using phase-contrast images from an Incucyte Zoom (one-way ANOVA, *p<.0001, n=3). (C) MEFs were incubated with ^{13}C glucose and metabolites were measured by LC-MS/MS . Relative metabolite levels of glucose-labeled glycolysis intermediates are shown (Student's *t*-test, *p<.05, n=3). (D) MEFs were grown in the presence of full glucose or no added glucose, and growth was measured over time using phase-contrast images from an Incucyte Zoom.

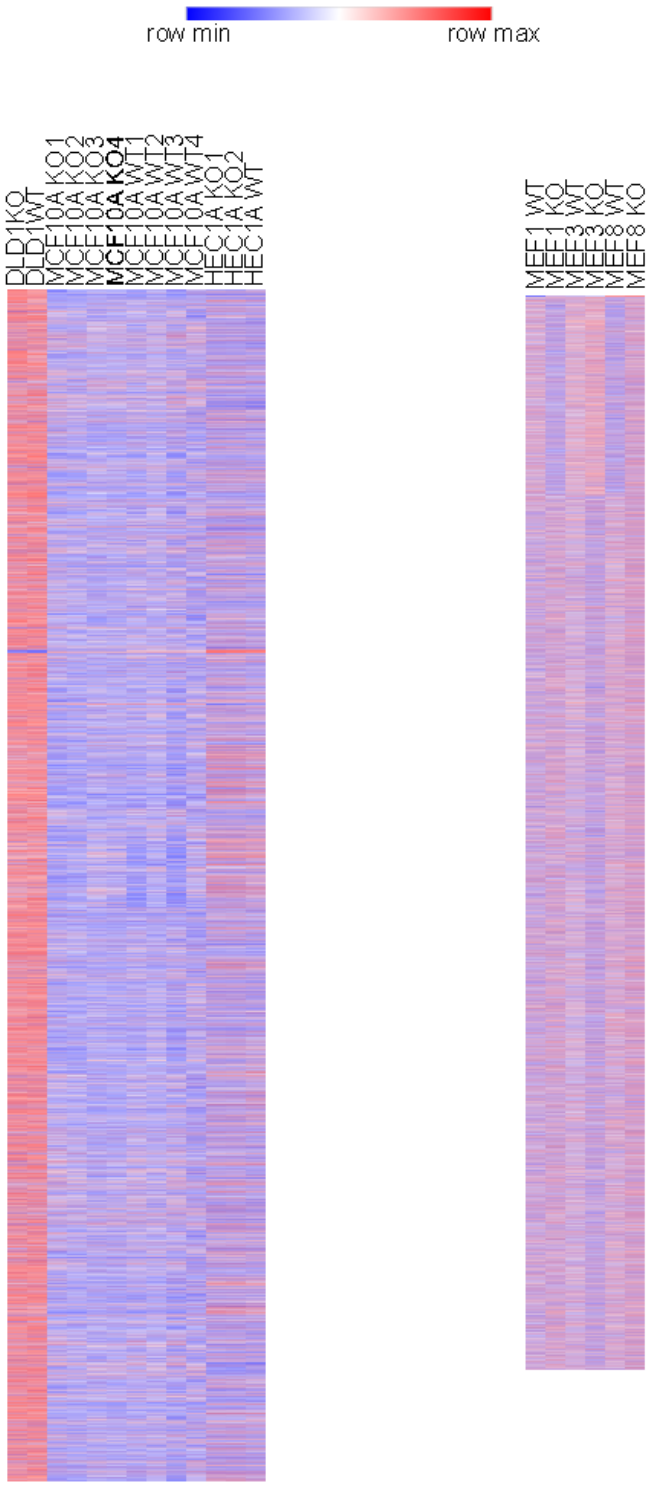
row min
row max
DLD1KO
DLD1WT
MCF10A KO1
MCF10A KO2
MCF10A KO3
MCF10A KO4
MCF10A WT1
MCF10A WT2
MCF10A WT3
MCF10A WT4
HEC1A KO1
HEC1A KO2
HEC1A WT
MEF1 WT
MEF1 KO
MEF3 WT
MEF3 KO
MEF8 WT
MEF8 KO

Figure 2.1

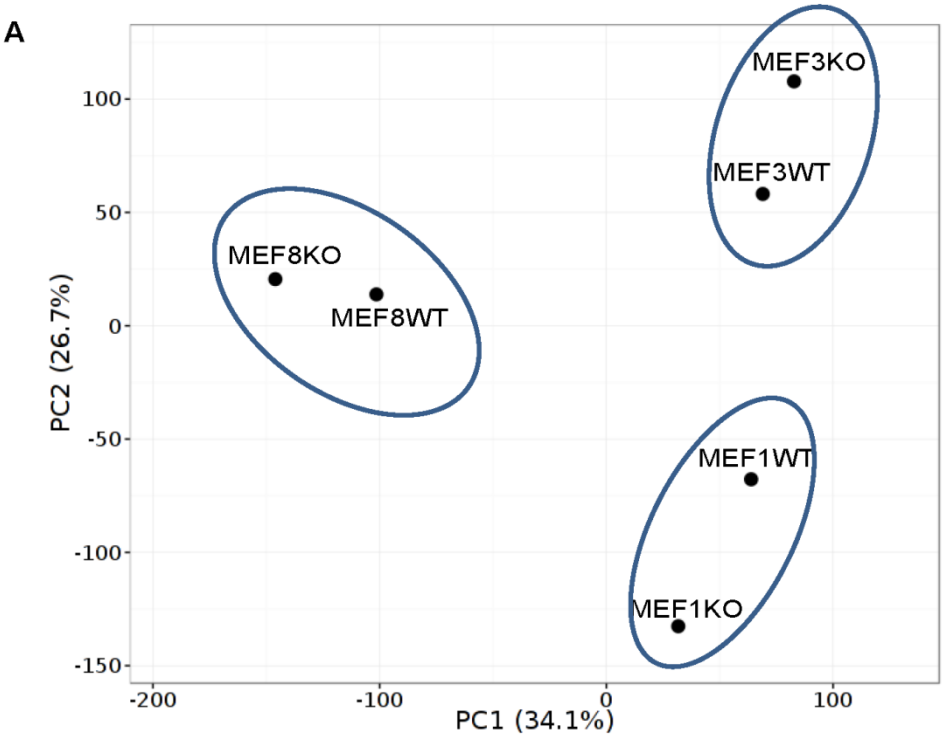
A
MEF3KO
MEF3WT
MEF8KO
MEF8WT
MEF1WT
MEF1KO
100
50
0
-50
-100
-150
-200
-100
0
100
PC2 (26.7%)
PC1 (34.1%)

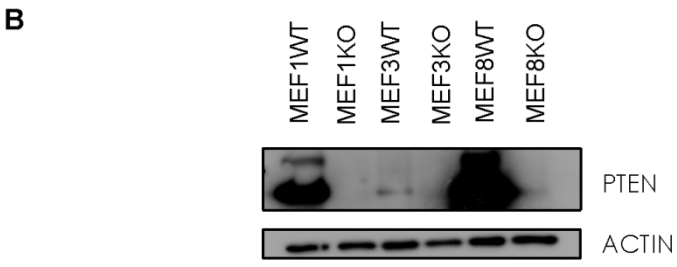
B
MEF1WT
MEF1KO
MEF3WT
MEF3KO
MEF8WT
MEF8KO
PTEN
ACTIN

Figure 2.2

A

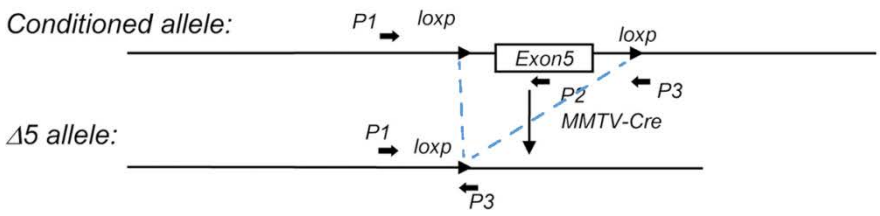

Figure adapted from Li et al, Development 2002

B

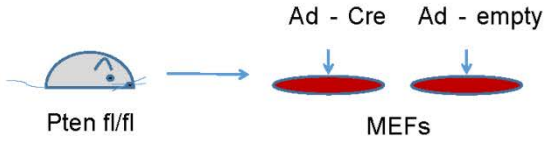

C

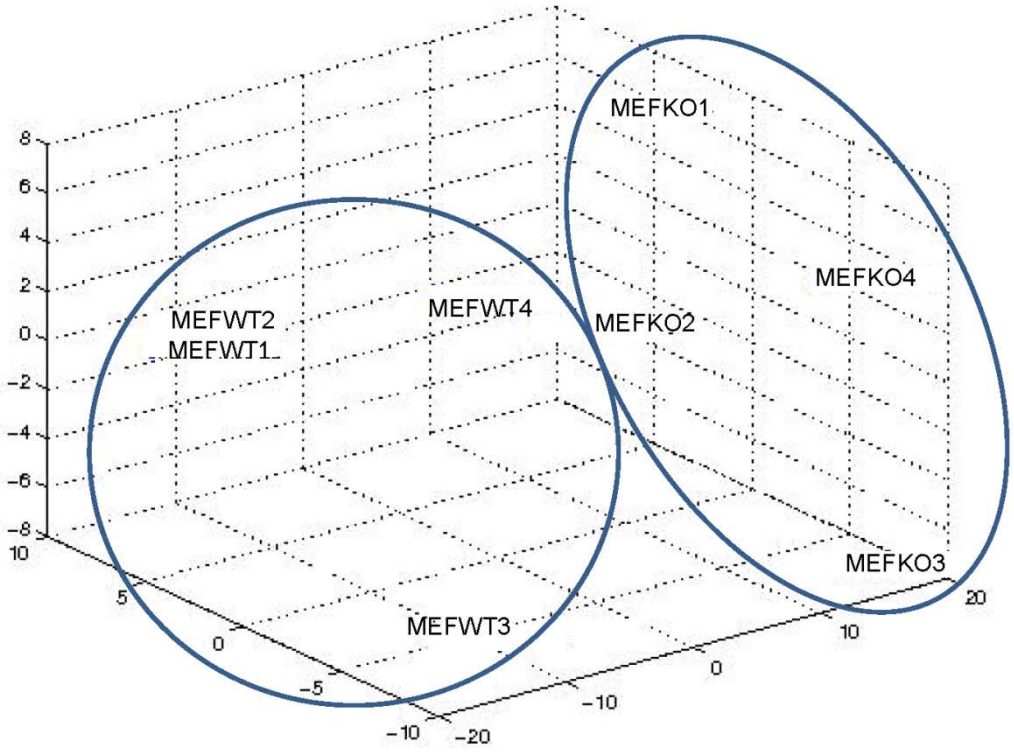

Figure 2.3

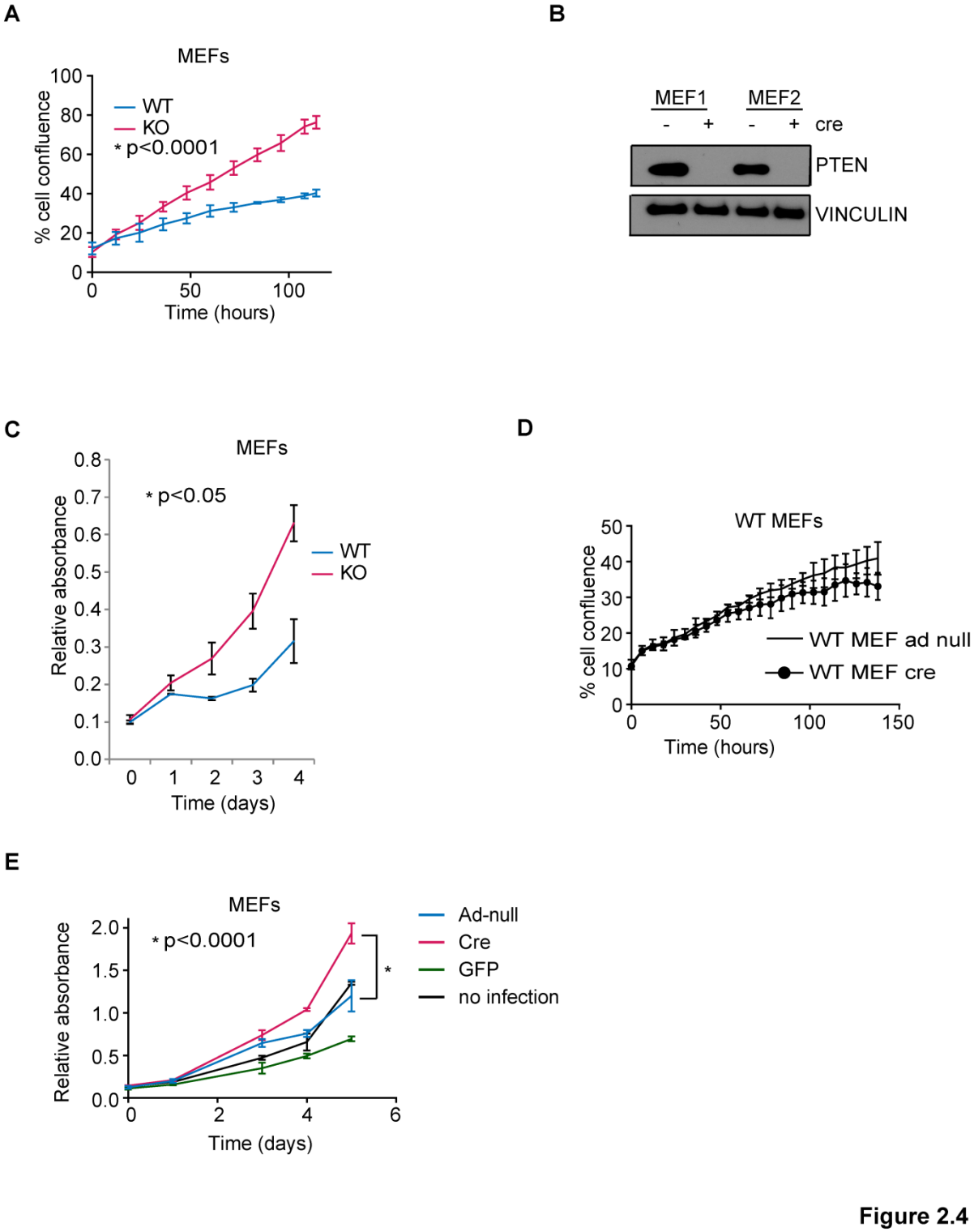
A
MEFs
% cell confluence
WT
KO
* p<0.0001
Time (hours)
B
MEF1
MEF2
- + - + cre
PTEN
VINCULIN
C
MEFs
* p<0.05
Relative absorbance
WT
KO
Time (days)
D
WT MEFs
% cell confluence
WT MEF ad null
WT MEF cre
Time (hours)
E
MEFs
* p<0.0001
Relative absorbance
Ad-null
Cre
GFP
no infection
Time (days)

Figure 2.4

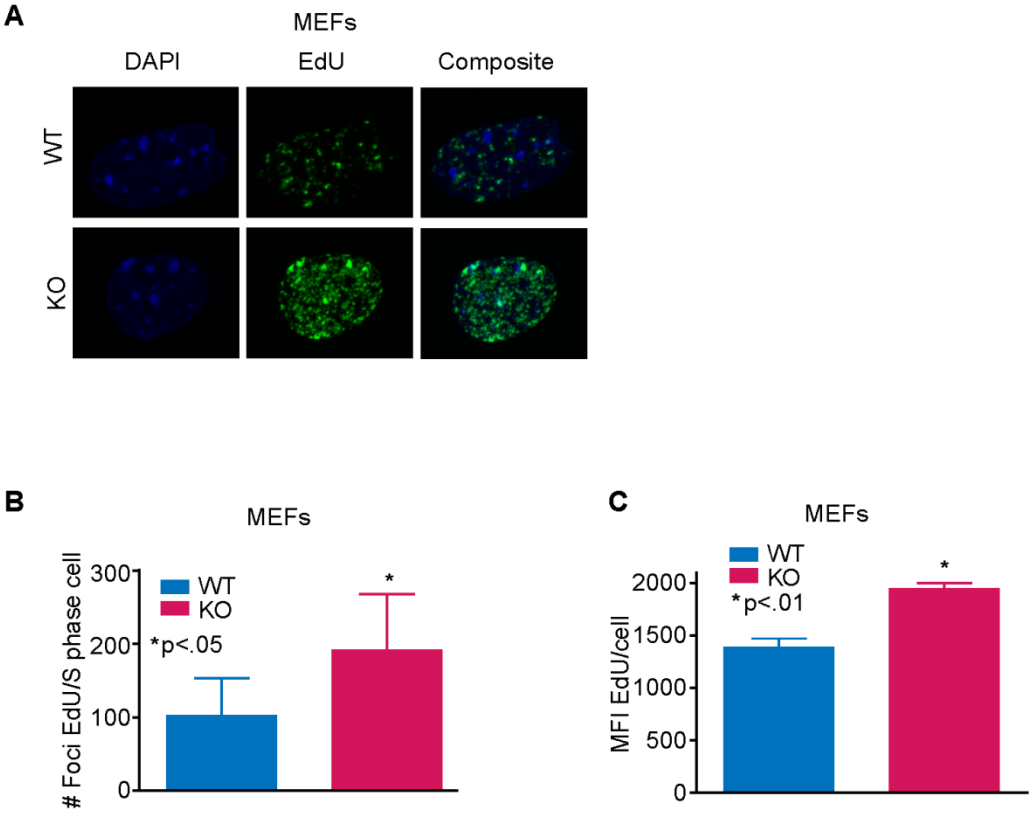
A
MEFs
DAPI
EdU
Composite
WT
KO
B
MEFs
Foci EdU/S phase cell
300
200
100
0
WT
KO
*p<.05
*
C
MEFs
MFI EdU/cell
2000
1500
1000
500
0
WT
KO
*p<.01
*

Figure 2.5

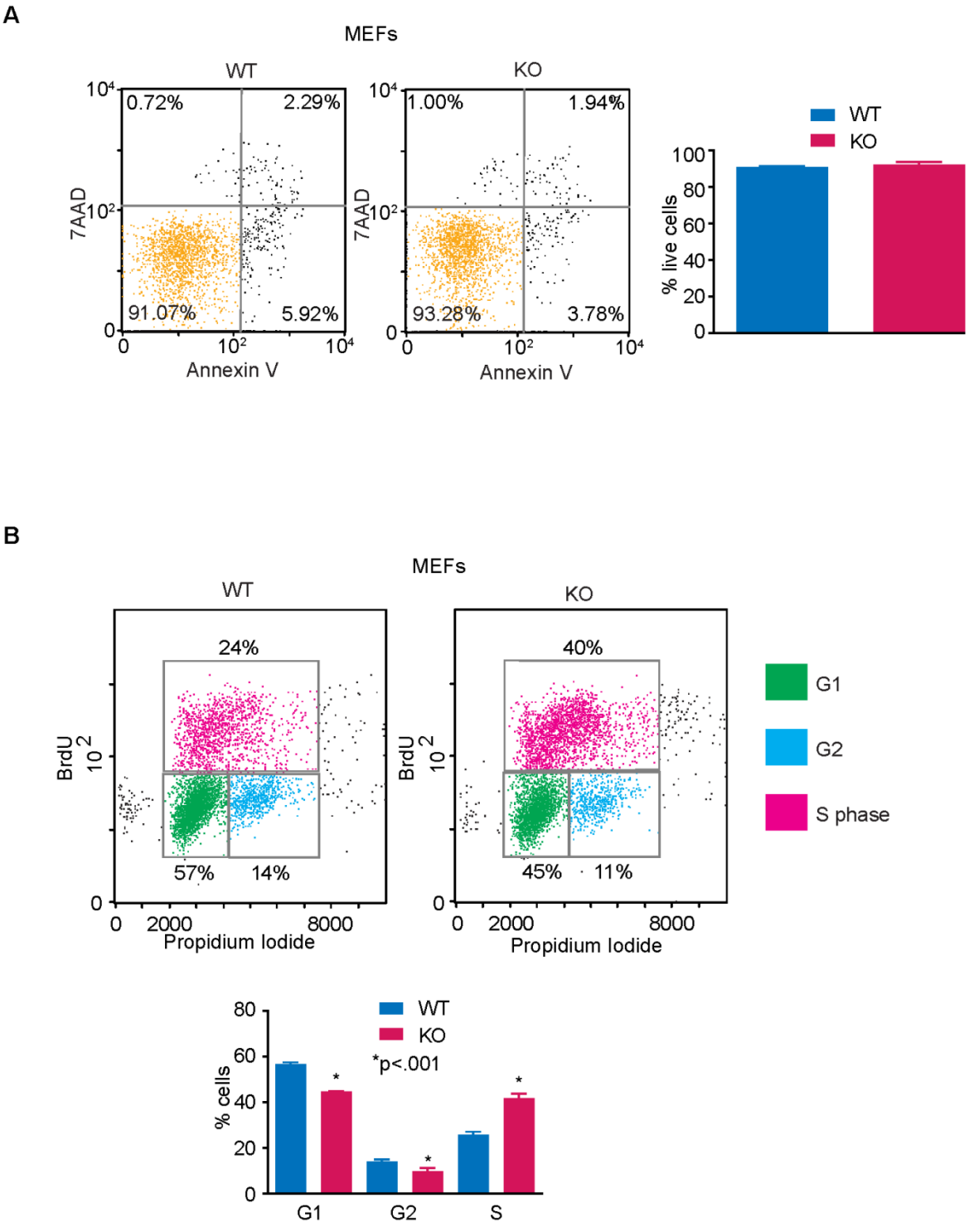
A
MEFs
WT
KO
0.72%
2.29%
91.07%
5.92%
1.00%
1.94%
93.28%
3.78%
7AAD
Annexin V
WT
KO
% live cells
B
MEFs
WT
KO
24%
57%
14%
40%
45%
11%
BrdU
Propidium Iodide
G1
G2
S phase
WT
KO
*p<.001
% cells
G1
G2
S

Figure 2.6

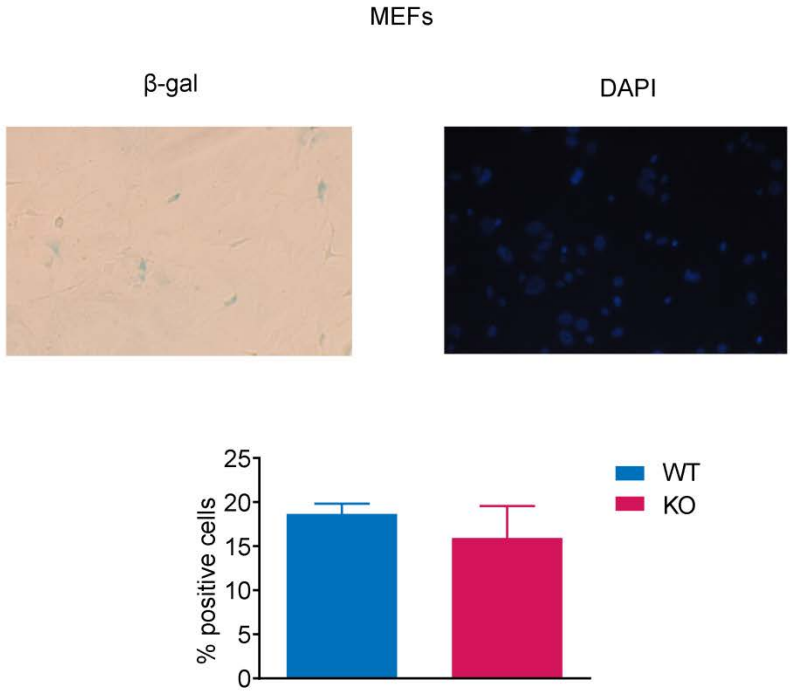

Figure 2.7

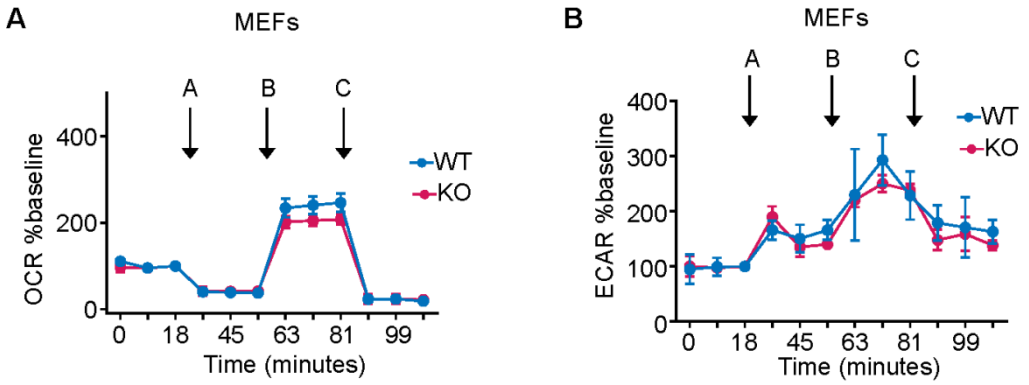
A
MEFs
A
B
C
OCR %baseline
400
200
0
WT
KO
0
18
45
63
81
99
Time (minutes)
B
MEFs
A
B
C
ECAR %baseline
400
300
200
100
0
WT
KO
0
18
45
63
81
99
Time (minutes)

Figure 2.8

A

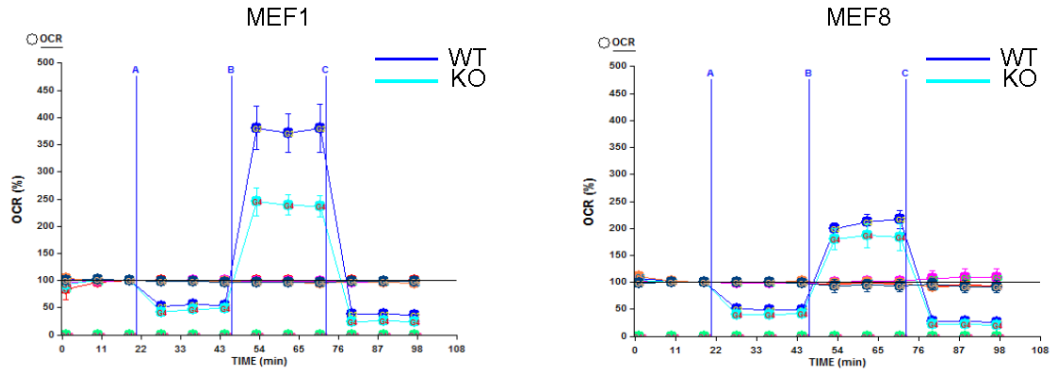
MEF1
OCR
WT
KO
OCR (%)
TIME (min)
MEF8
OCR
WT
KO
OCR (%)
TIME (min)

B

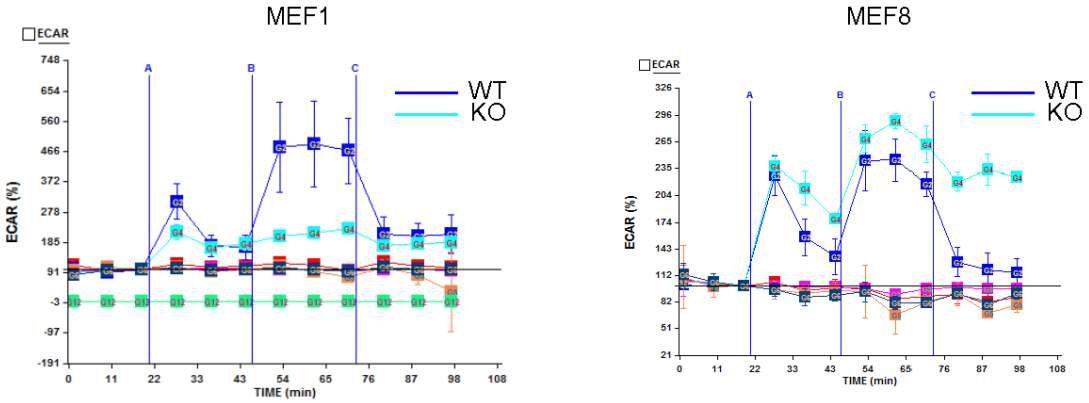
MEF1
ECAR
WT
KO
ECAR (%)
TIME (min)
MEF8
ECAR
WT
KO
ECAR (%)
TIME (min)

Figure 2.9

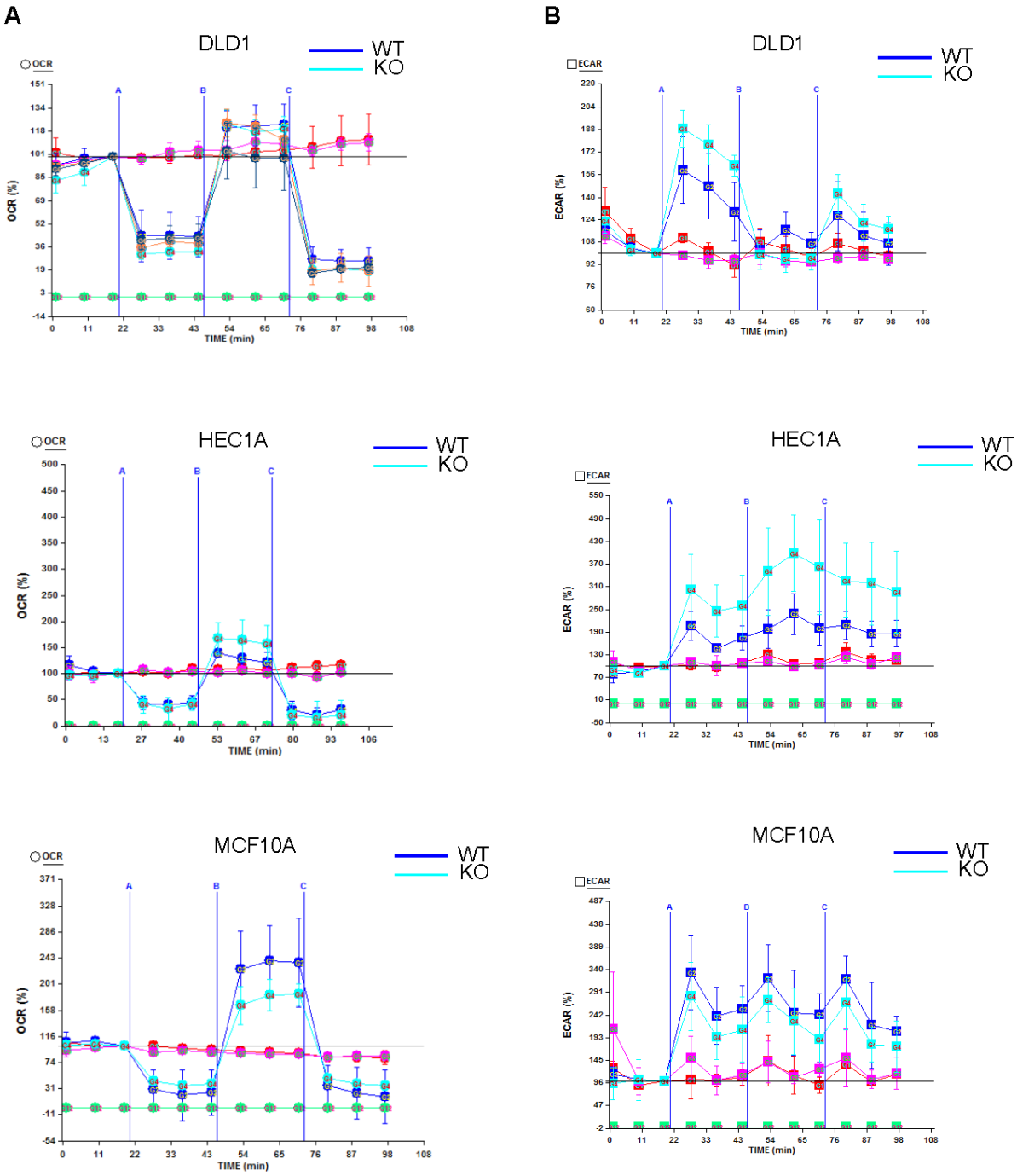
A
DLD1
WT
KO
OCR
OCR (%)
TIME (min)
B
DLD1
WT
KO
ECAR
ECAR (%)
TIME (min)
HEC1A
WT
KO
OCR
OCR (%)
TIME (min)
HEC1A
WT
KO
ECAR
ECAR (%)
TIME (min)
MCF10A
WT
KO
OCR
OCR (%)
TIME (min)
MCF10A
WT
KO
ECAR
ECAR (%)
TIME (min)

Figure 2.10

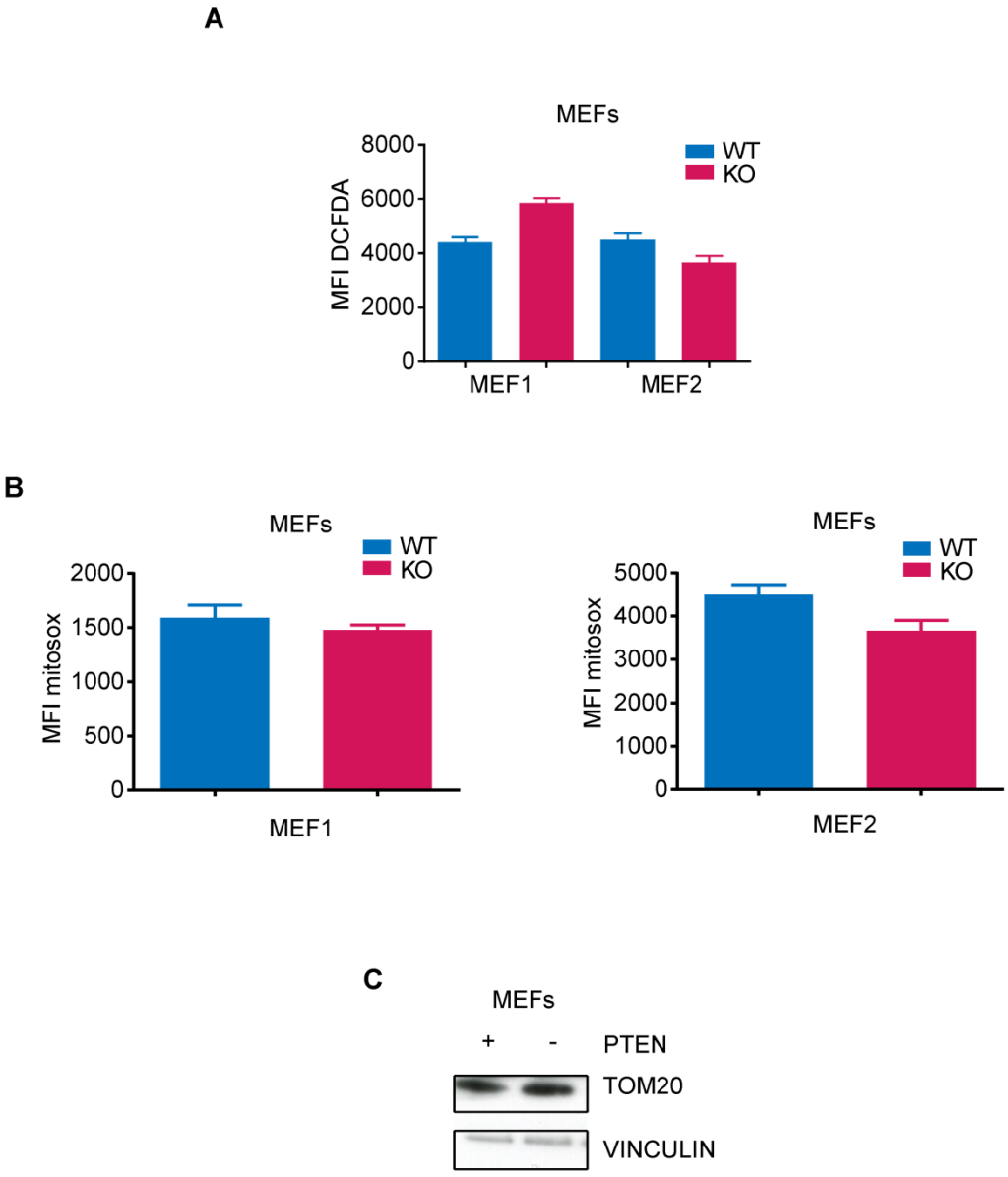
A
MEFs
WT
KO
MFI DCFDA
8000
6000
4000
2000
0
MEF1
MEF2
B
MEFs
WT
KO
MFI mitosox
2000
1500
1000
500
0
MEF1
MEFs
WT
KO
MFI mitosox
5000
4000
3000
2000
1000
0
MEF2
C
MEFs
+
-
PTEN
TOM20
VINCULIN

Figure 2.11

A

Upregulated metabolite pathways in *Pten*$^{-/-}$ MEFs

	Pathway	IMPaLA q-value	Source
1	Nucleotide metabolism	1.86×10^{-09}	Reactome
2	Metabolism	5.94×10^{-09}	Reactome
3	Pyrimidine metabolism	1.36×10^{-06}	KEGG
4	Pyrimidine metabolism	4.18×10^{-09}	EHMN
5	Metabolism of nucelotides	5.48×10^{-09}	Wikipathways
7	Purine metabolism	1.67×10^{-05}	EHMN
8	Purine catabolism	5.65×10^{-05}	Reactome
79	Glucose metabolism	0.014	Reactome
113	DNA strand elongation	0.026	Reactome
143	Citric acid cycle	0.049	SMPDB

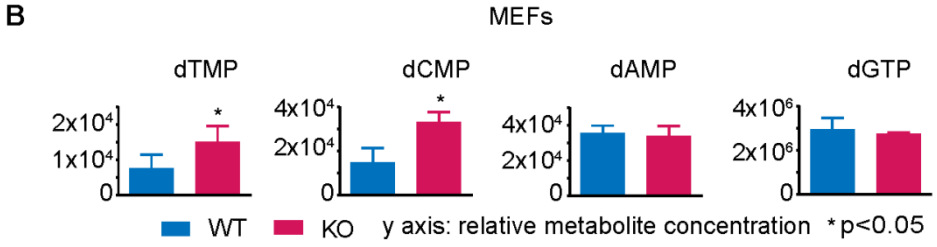

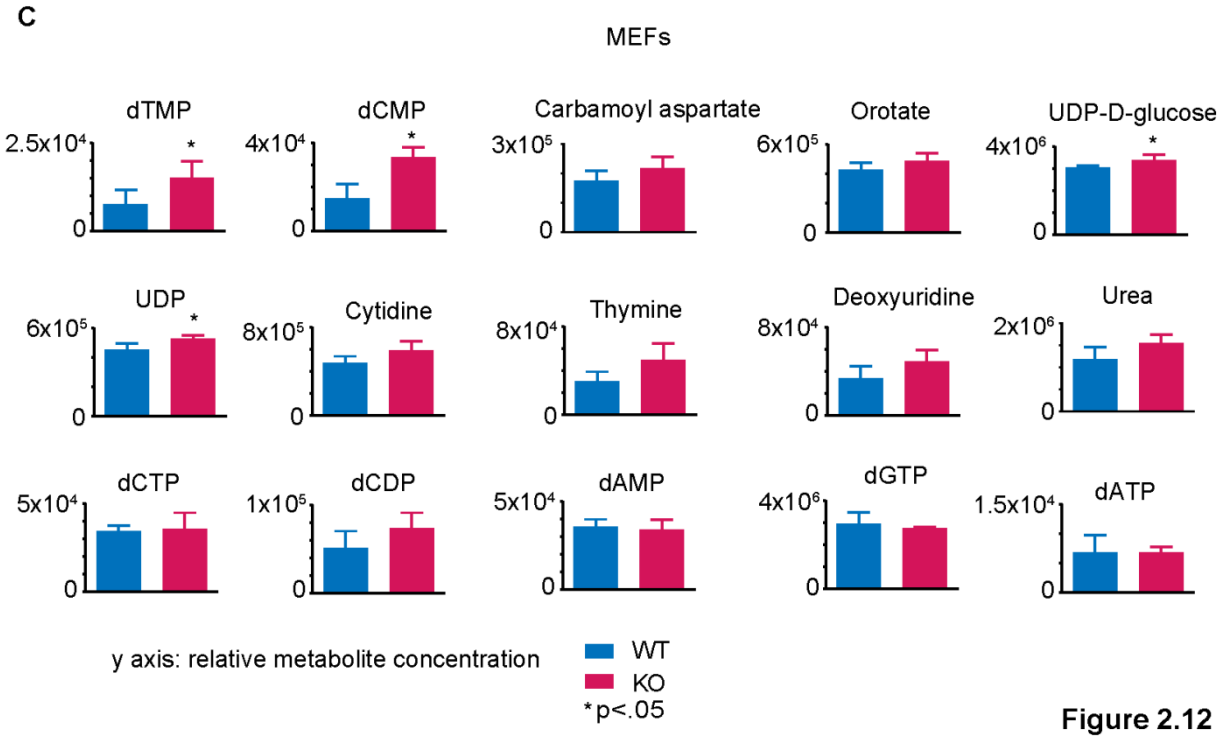

Figure 2.12

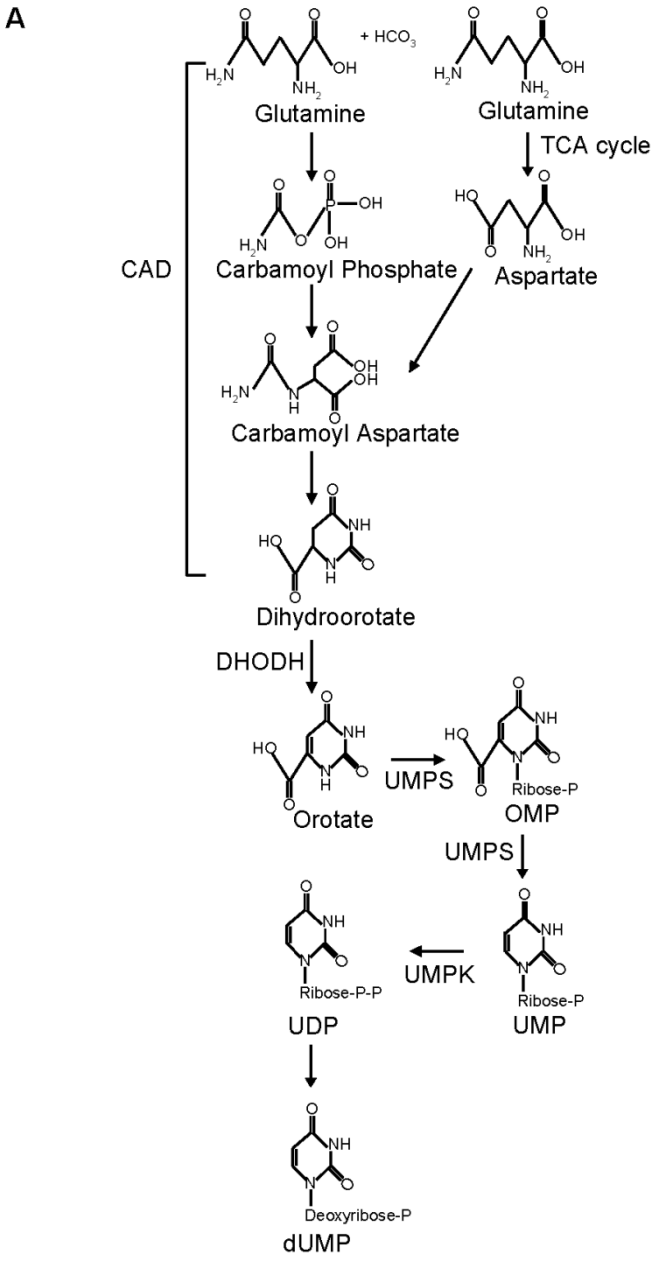
A
+ HCO3
Glutamine
Glutamine
TCA cycle
CAD
Carbamoyl Phosphate
Aspartate
Carbamoyl Aspartate
Dihydroorotate
DHODH
Orotate
UMPS
Ribose-P
OMP
UMPS
UMPK
Ribose-P-P
UDP
Ribose-P
UMP
Deoxyribose-P
dUMP

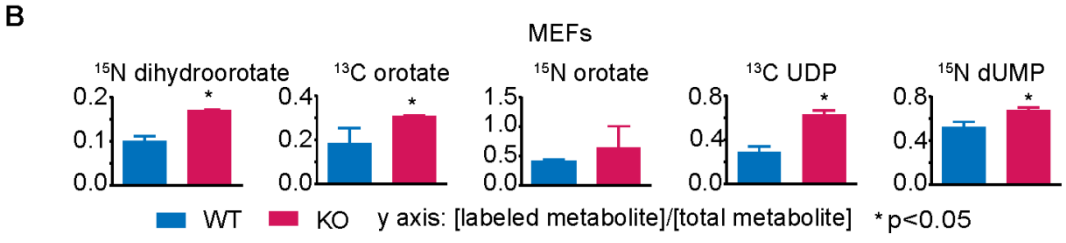
B
MEFs
15N dihydroorotate
13C orotate
15N orotate
13C UDP
15N dUMP
WT
KO
y axis: [labeled metabolite]/[total metabolite]
*p<0.05

Figure 2.13

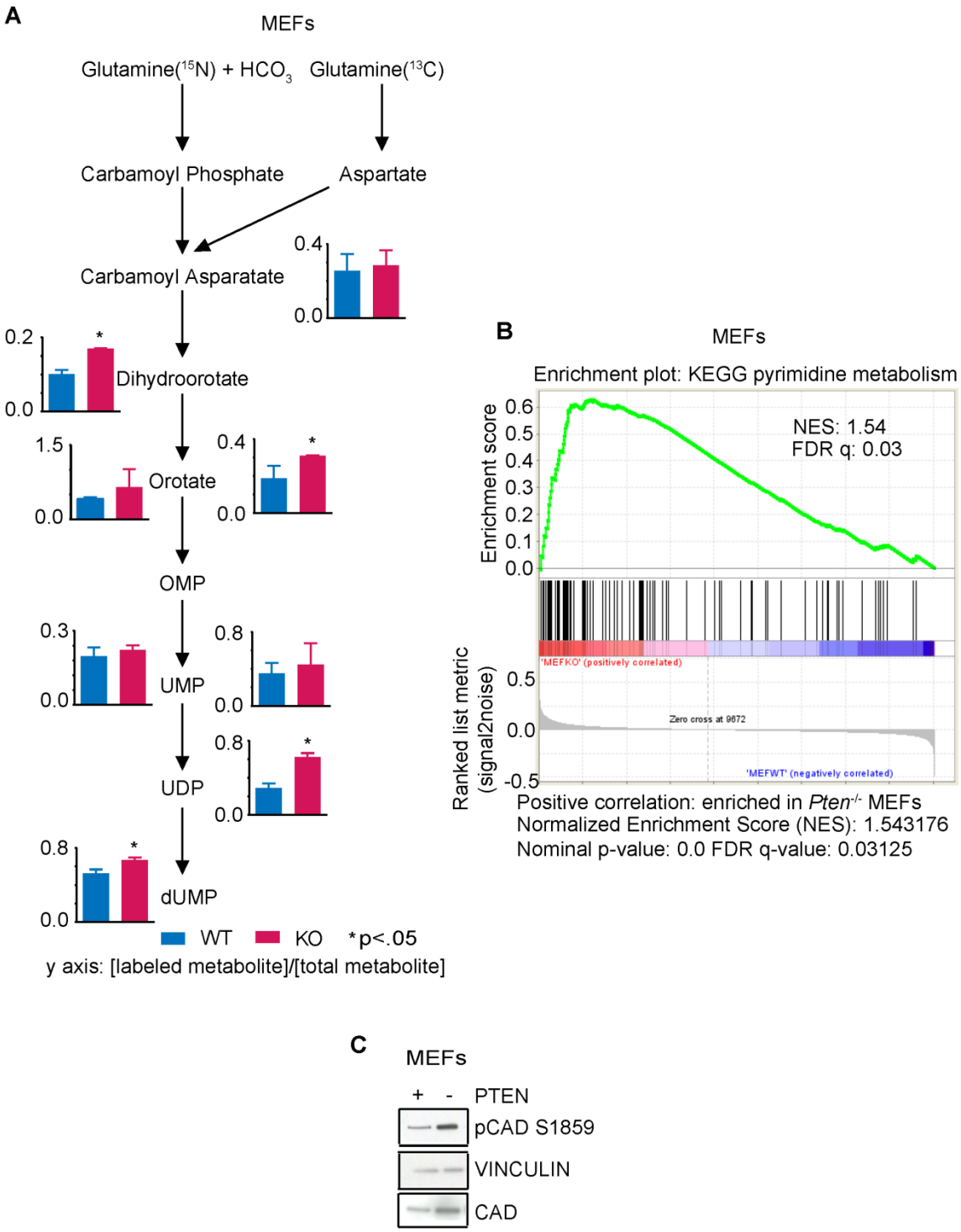
A
MEFs
Glutamine(15N) + HCO3
Glutamine(13C)
Carbamoyl Phosphate
Aspartate
Carbamoyl Asparatate
Dihydroorotate
Orotate
OMP
UMP
UDP
dUMP
WT
KO
*p<.05
y axis: [labeled metabolite]/[total metabolite]
B
MEFs
Enrichment plot: KEGG pyrimidine metabolism
Enrichment score
NES: 1.54
FDR q: 0.03
'MEFKO' (positively correlated)
Zero cross at 9872
'MEFWT' (negatively correlated)
Ranked list metric (signal2noise)
Positive correlation: enriched in Pten-/- MEFs
Normalized Enrichment Score (NES): 1.543176
Nominal p-value: 0.0 FDR q-value: 0.03125
C
MEFs
+ - PTEN
pCAD S1859
VINCULIN
CAD

Figure 2.14

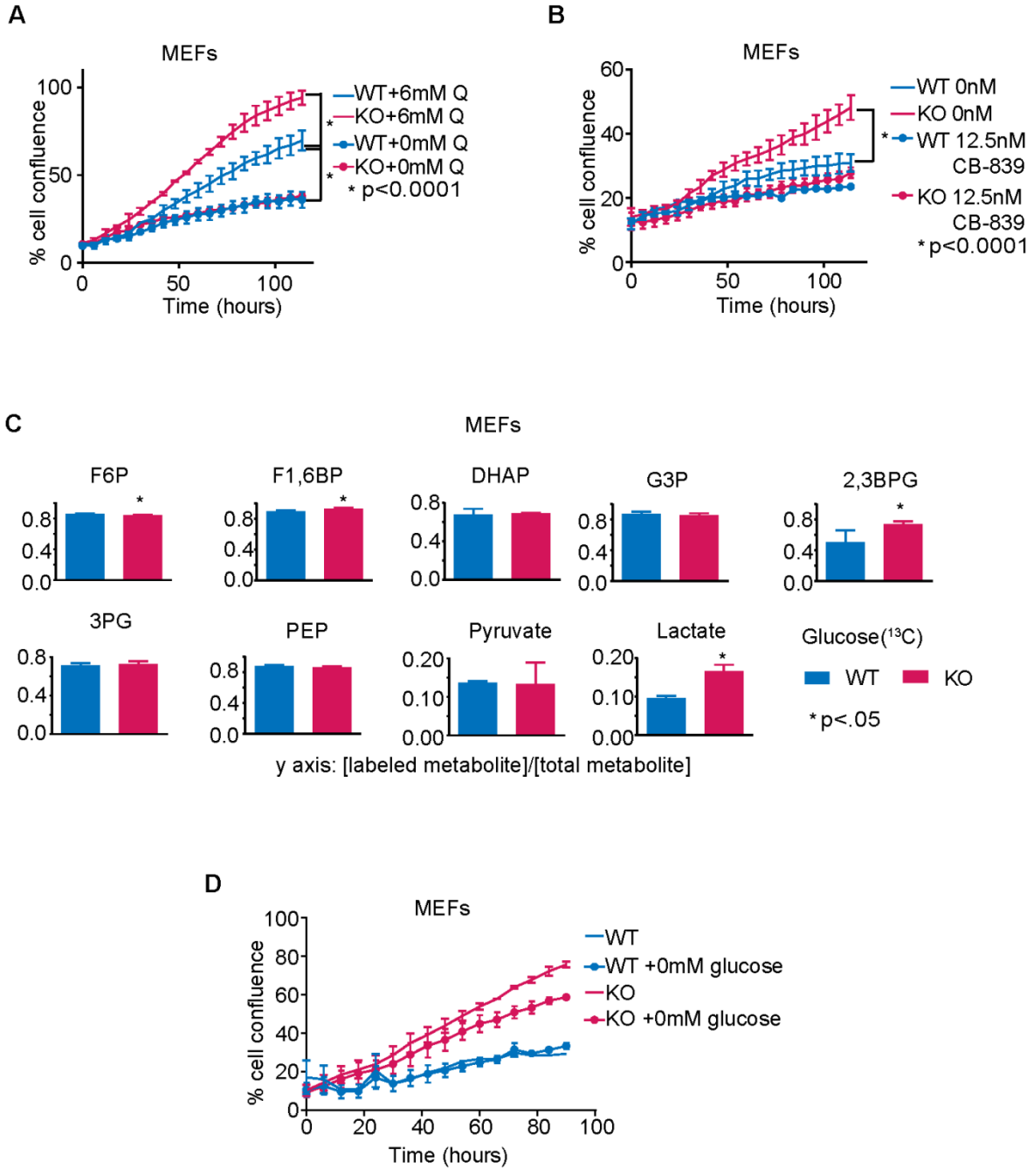
A
MEFs
% cell confluence
Time (hours)
WT+6mM Q
KO+6mM Q
WT+0mM Q
KO+0mM Q
* p<0.0001
B
MEFs
% cell confluence
Time (hours)
WT 0nM
KO 0nM
WT 12.5nM CB-839
KO 12.5nM CB-839
* p<0.0001
C
MEFs
F6P
F1,6BP
DHAP
G3P
2,3BPG
3PG
PEP
Pyruvate
Lactate
Glucose(13C)
WT
KO
* p<.05
y axis: [labeled metabolite]/[total metabolite]
D
MEFs
% cell confluence
Time (hours)
WT
WT +0mM glucose
KO
KO +0mM glucose

Figure 2.15

Chapter 3: Exploiting the metabolic vulnerability of PTEN mutant cells

In the previous chapter we observed an increase in DNA synthesis and number of replication forks in *Pten*$^{-/-}$ cells. We further identified the dependence of *Pten*$^{-/-}$ cells on glutamine, and believe that glutamine flux is upregulated in part to support the demands of increased replication via *de novo* pyrimidine synthesis. It will therefore be illuminating to delve into the *de novo* pyrimidine synthesis pathway; in this chapter we explore an enzyme in the pathway, dihydroorotate dehydrogenase (DHODH), and the vulnerability of PTEN mutant tumors to DHODH inhibition.

Introduction

A brief summary of nucleotide synthesis

Since we found an association between Pten loss and nucleotide metabolism, it will be helpful to understand more about the pathways involved. Nucleotides can be made via *de novo* synthesis or through what is termed the salvage pathway. *De novo* synthesis of purines involves production from glutamine, glycine, aspartate, and tetrahydrofolate derivatives, and pyrimidines from glutamine, bicarbonate, and aspartate (Cory and Cory 2006). (More details about one-carbon metabolism for purine synthesis were outlined in the introductory chapter.) Aspartate in turn can be made from oxaloacetate, which is derived from either glutamine or glucose in the TCA cycle; glucose contributes carbon while glutamate (from glutamine) contributes nitrogen and carbon. Salvage production of nucleotides, on the other hand, occurs from the recycling of downstream nucleotide intermediates from one another; in fact, purines and pyrimidines can indirectly be made from one another.

De novo pyrimidine synthesis

Since we found that *Pten*$^{-/-}$ cells appear to be dependent on glutamine and channel its flux into the manufacture of pyrimidines, we focus here on the *de novo* pyrimidine synthesis pathway in mammals. The first step of this pathway is the combination of glutamine with bicarbonate to create carbamoyl phosphate; through this, the amide nitrogen of glutamine is incorporated (Cory and Cory 2006). Carbamoyl phosphate is then fused to aspartate, creating carbamoyl aspartate, which is then converted to dihydroorotate. The above reactions are catalyzed by a tri-functional protein with activity as carbamoylphosphate synthetase (CPS II), aspartate transcarbamoylase, and dihydroorotase, all encoded by the gene *CAD* (Coleman, Suttle et al. 1977). The fourth step in the *de novo* pyrimidine synthesis pathway is the conversion of dihydroorotate to orotate, catalyzed by dihydroorotate dehydrogenase (DHODH) (Stamato and Patterson 1979). Orotate is converted to OMP then UMP by uridine monophosphate synthetase (UMPS), followed by UDP by uridine monophosphate kinase (UMPK), and finally to dUMP (Fig. 2.13A)

DHODH

DHODH is of particular interest because there are several inhibitors to this enzyme in existence that are in use clinically. Here, we first present some information about its biology. DHODH contains a flavin mononucleotide (FMN), which is an oxidizing agent that is part of several enzymes involved in redox reactions. By reducing FMN to $FMNH_2$, dihydroorotate is simultaneously oxidized to orotate. $FMNH_2$ is then restored to its original oxidized state through the reduction of coenzyme Q/ubiquinone, which also binds DHODH. Class 2 DHODH (present in humans) is a mitochondrial enzyme, residing in the inner mitochondrial membrane. Due to its binary function, DHODH can affect both pyrimidine synthesis and the electron transport chain (Munier-Lehmann, Vidalain et al. 2013).

DHODH may also have a function in transcriptional elongation. In melanoma cell lines, DHODH inhibition resulted in a decrease in elongation but not of initiation, as determined by Pol II occupancy (White, Cech et al. 2011). There has been considerable interest in DHODH for some time, and various inhibitors to the enzyme have been developed.

Leflunomide was discovered to be a DHODH inhibitor in 1995, and ^{14}C labeling experiments confirmed leflunomide's target a few years later (Greene, Watanabe et al. 1995, Rückemann, Fairbanks et al. 1998). Even before its mechanism was known, leflunomide (HWA 486) was recognized for its ability to reduce inflammation and prevent the advancement of rheumatoid arthritis (RA) (Bartlett and Schleyerbach 1985), a disease characterized by inflammation and degradation of synovial connective tissue in joints (Breedveld and Dayer 2000). More specifically, leflunomide was shown to inhibit B-cell and T-cell proliferation (ANITA, Finnegan et al. 1993, Siemasko, Chong et al. 1996). Its immunomodulatory effects were connected to its DHODH inhibitory mechanism; T-cells treated with leflunomide accumulated dihydroorotate, and uridine rescued proliferation (Cherwinski, Cohn et al. 1995). Leflunomide was eventually produced under the trade name Arava as a rheumatoid arthritis medication for human use.

As a drug, leflunomide has several interesting properties. It is tightly bound to the protein albumin in serum, and has a half-life of about two weeks in the body (quite long for a drug) (Breedveld and Dayer 2000). Because of this, to achieve steady-state levels in humans a loading dose of 100mg/kg for 3 days is first typically required, followed by a daily dose of 20-40mg/kg to maintain steady levels. Toxicity in

patients treated with leflunomide is relatively low – diarrhea and vomiting occurred upon the first few days of treatment, but the symptoms desisted after some time (Breedveld and Dayer 2000).

Leflunomide is actually a pro-drug, and its active metabolite which physically binds DHODH is called teriflunomide, or A771726. Leflunomide can be processed in either the GI tract or in plasma, and is converted to teriflunomide by nonenzymatic opening of its ring structure (Breedveld and Dayer 2000, Rozman 2002). Normal rheumatoid arthritis dosing achieved a steady-state plasma level of 200-250μM teriflunomide when leflunomide was administered orally (Mone and Byrd 2004). Teriflunomide is sold under the name Aubagio for use in multiple sclerosis (MS).

Leflunomide and A771726 are the only clinically available DHODH inhibitors, but there are other commercially available inhibitors for use in the laboratory. Brequinar is one such example. While the exact mechanism of DHODH inhibition is not completely known, there is evidence that A771726 and brequinar are both uncompetitive for the dihydroorotate binding site, while brequinar is competitive and A771726 is noncompetitive for the ubiquinone binding site (McLean, Neidhardt et al. 2001). It is possible that the different mode of action on DHODH of the various inhibitors influences their precise effects on DHODH modulation. Brequinar caused several side effects in patients, including severe lymphopenia, myelosuppression, and nausea, and the clinical trial was withdrawn (Peters, Schwartsmann et al. 1990, Rückemann, Fairbanks et al. 1998). Since DHODH is an important target for RA, MS, and perhaps malaria, additional inhibitors to the enzyme are being designed (Munier-Lehmann, Vidalain et al. 2013).

In the following section, we examine the effects of DHODH inhibition in the setting of PTEN deficiency.

Results

In vitro sensitivity

Given the upregulation of the *de novo* pyrimidine synthesis pathway in *Pten*$^{-/-}$ cells, we hypothesized that this could also be an Achilles' heel — and that PTEN mutant cells would be sensitive to inhibition of this pathway. Since DHODH has preexisting inhibitors (described above) readily available, we proceeded to test them *in vitro*.

Pten$^{-/-}$ MEFs were about 3-fold more sensitive to leflunomide than WT MEFs were, suggesting that orotate contributes to the growth effects we observe (Fig. 3.1A). In fact, increasing doses of leflunomide not only collapsed the growth difference between WT and null MEFs, but allowed the WT cells to overtake *Pten*$^{-/-}$ cells (Fig. 3.1B-C). *Pten*$^{-/-}$ MEFs were also more sensitive to A771726, the active metabolite of leflunomide, as well as brequinar, indicating that the observed effects were likely through DHODH (Fig. 3.1A). To determine whether PTEN genotype is predictive of susceptibility to DHODH inhibition in cancer cells, we tested human breast, glioblastoma, and prostate cell lines with DHODH inhibitors. Consistently, the GI50 of the PTEN mutant lines was lower than that of WT (Fig. 3.2A-B). Mouse breast cancer line MCCL-357 (*Myc, Pten*$^{-/-}$) was more sensitive than mouse breast cancer line MCCL-278 (*Myc, Pik3ca* H1047R) was, and mouse prostate cancer line CaP8 (*Pten*$^{-/-}$) was more sensitive than mouse prostate cancer line Myc-CaP (*Myc*) was (Fig. 3.2C-E) (Jiao, Wang et al. 2007, Stratikopoulos, Dendy et al. 2015). Moreover, *Pten*$^{-/-}$ MEFs, PTEN mutant human breast cancer cell lines, and *Pten*$^{-/-}$ mouse breast cancer cell lines displayed an increased accumulation of dead cells over time upon

treatment with leflunomide (Fig. 3.3). While we can't say with certainty that this sensitivity in PTEN mutant cells is universal, the many cell systems we do see this in is predictive of a strong correlation.

Data from 2-dimensional culture is very informative, but doesn't always accurately reflect how a drug would work on a 3-D tumor. To this end, we seeded HCC1419, MDA-MB 468, and ZR57-1 cells in conditions that induce growth as mammospheres in culture. Rather than adhering to the dish as a monolayer, the cells were packed into dense spherical clusters. We disrupted the formed tumor spheres into single cell suspensions and re-seeded them for secondary tumor sphere assessment. Formation of spheres is considered a marker of the ability to regenerate tumors, and hence tumorigenicity (Freedman and Shin , Shaw, Harrison et al. 2012). The suspended cells were treated with various concentrations of leflunomide, and the number of formed spheres was counted in each condition. We found that formation of tumor spheres was inhibited at lower concentrations of leflunomide in PTEN-deficient samples compared to WT; however, this experiment was only done once and added data would be required to draw a definitive conclusion (Fig. 3.4). We therefore address tumor spheres further in the following section with an additional model.

To independently test if DHODH inhibition is detrimental to PTEN deficient cells, we performed a rescue experiment with orotate, the metabolite directly downstream of DHODH, as well as with uridine, a metabolite further downstream. Increasing concentrations of orotate or uridine rescued growth inhibition by leflunomide, verifying that DHODH was the target of the small molecule inhibitors (Fig. 3.5). In addition, siRNA against DHODH preferentially killed PTEN mutant cells, corroborating the target of sensitivity (Fig. 3.6A-B).

Addition of a reducing agent, n-acetylcysteine, did not rescue growth inhibition, verifying that the dihydroorotate-orotate conversion by DHODH is more important for growth in this system than its function in reducing ubiquinone (Fig. 3.6C). Leflunomide also did not differentially affect mitochondrial ROS (Fig. 3.6D). Recall that in figure 2.8 we stressed cells with various fast-acting mitochondrial poisons and showed there was no difference in respiratory function between *PTEN*$^{-/-}$ and WT cells. One of the poisons used was rotenone, which inhibits the transfer of electrons from Complex 1 to ubiquinone, the carrier that is reduced in part by DHODH. Rotenone acts rapidly, and served as a proxy for leflunomide in this part of the electron transport chain. We therefore deem the blockade of *de novo* pyrimidine synthesis to be the primary cause of sensitivity in PTEN mutant cells.

It is also important to note that a faster growth rate is not the cause of — or a requirement for — sensitivity to DHODH inhibitors. While we believe that cells with PTEN loss use glutamine flux to sustain faster proliferation, we posit that other cancer mutations which affect the growth rate of a cell (and may overshadow PTEN's contribution) may not contribute to leflunomide sensitivity. *Myc, Pik3ca* H1047R cells grow at approximately the same rate as *Myc, Pten*$^{-/-}$ cells even though it is only the *Pten*$^{-/-}$ cells that are sensitive to leflunomide, and the resistant Myc-CaP cells grow somewhat faster than the sensitive CaP8 cells (Fig. 3.7A-B). Sensitivity to leflunomide was also not associated with the proliferation rates of human breast cancer cell lines (Fig. 3.7C). It therefore appears that PTEN status is a predictor of susceptibility while proliferation rate is not. This is noteworthy because association with growth rates would indicate that DHODH inhibitors are acting like a chemotherapeutic agent, while our data suggest it is a targeted therapy for PTEN mutant cells.

There was no endogenous difference in DHODH protein level between *Pten*$^{-/-}$ and WT MEFs, indicating that the source of pyrimidine flux is not from upregulation of DHODH and instead may well be via CAD phosphorylation as described above (Fig. 3.8A). It was previously shown that that re-expression of PTEN in the PTEN-null U87 cell line lowered the level of carbamoyl aspartate, indicating that PTEN may regulate CAD-mediated upregulation of *de novo* pyrimidine synthesis (Ben-Sahra, Howell et al. 2013). Phosphorylated CAD levels were increased in *Pten*$^{-/-}$ MEFs with or without the presence of leflunomide, as well as in *Pten*$^{-/-}$ mouse breast lines (Fig. 2.14C and Fig. 3.8B-C). Additionally, we found that A771726 did not affect PI3K signaling, signifying that the effects we saw were through DHODH and not inhibition of PI3K (Fig. 3.8D).

While brequinar was effective in PTEN deficient MEFs and mouse breast cancer cell lines, there was not a significantly different sensitivity in human breast cancer cell lines (Fig. 3.1A, 3.9). Since brequinar did not work well in our human cell systems, we chose to use leflunomide and A771726 for further studies.

Interestingly, human breast cancer cell lines with a *PIK3CA* mutation did not exhibit a significant sensitivity to leflunomide, although their collective GI50 trended lower than that of WT *PIK3CA*/WT *PTEN* (Fig. 3.10A). And, as described above, mouse cancer cell line MCCL-357 (*Myc, Pten*$^{-/-}$) was more sensitive than MCCL-278 (*Myc, Pik3ca* H1047R) in terms of both growth inhibition and cell death (Fig. 3.2D-E, 3.3B). While PTEN and PI3K are in the same pathway, loss of *PTEN* and activation of *PIK3CA* are not equivalent. This may be in part because, consistent with previous reports, we found that *Pten* homozygous deletion induced greater AKT phosphorylation than *Pik3ca* missense mutation did (Stemke-Hale, Gonzalez-Angulo et al. 2008). This was particularly prominent in the nuclear fractions, where AKT may phosphorylate nuclear substrates (Fig. 3.10B-D). Heightened active AKT leads to greater mTORC1

activation and consequently more phosphorylated CAD, likely contributing to the *de novo* pyrimidine synthesis dependency we describe. The difference in active AKT between *Pik3ca* mutant and *Pten*$^{-/-}$ cells will also be important in cell death mechanisms described in chapter 4.

We also wanted to ascertain whether *any* nucleotide inhibitor would be effective against PTEN mutant cells. 5-flurouracil inhibits thymidylate synthase upon conversion to fluorodeoxyuridine monophosphate, and is a nucleotide analog that is toxic to RNA when misincorporated in place of uridine (Yoshida, Hoshi et al. 1980). Mercaptopurine inhibits phosphoribosyl pyrophosphate amidotransferase in *de novo* purine synthesis as well as the IMP to AMP conversion in the purine salvage pathway (Salser, Hutchison et al. 1960, Tay, Lilley et al. 1969). However, treatment with either of these drugs did not show a differential sensitivity, demonstrating that *Pten*$^{-/-}$ MEFs are selectively vulnerable to inhibition of *de novo* pyrimidine synthesis in particular (Fig. 3.11A-B).

Myc activation is also known to cause glutamine addiction. CaP8 (*Pten*$^{-/-}$) cells were nearly as sensitive to glutamine deprivation as Myc-CaP (*Myc*) cells were, substantiating that a notable level of glutamine dependency is also elicited by PTEN loss (Fig. 3.11C). Since Myc-CaP cells were resistant to leflunomide, it seems it is not the entry alone of glutamine but its flux into pyrimidines that is important (Fig. 3.2C). While Myc is known to largely direct glutamine to the TCA cycle and phospholipid synthesis, our data show that PTEN loss in MEFs causes glutamine to cascade through the *de novo* pyrimidine synthesis pathway, creating the point of vulnerability to DHODH inhibition.

These data gave us confidence that PTEN mutant cells are indeed more vulnerable than PTEN WT cells to DHODH inhibition. To further the preclinical data, we tested additional models as described in the next section.

Table 3.1. Breast cancer cell lines used in this chapter:

Cell line	**Genotype**
MDAMB 231	PTEN and PIK3CA WT
HCC 1187	PTEN and PIK3CA WT
HCC 1806	PTEN and PIK3CA WT
HCC 1419	PTEN and PIK3CA WT
SKBR3	PTEN and PIK3CA WT
HCC 1937	PTEN mut
ZR75-1	PTEN mut
SUM 149	PTEN mut
BT549	PTEN mut
MDAMB 468	PTEN mut
T47D	PIK3CA mut
HCC 1954	PIK3CA mut
SUM 159	PIK3CA mut

In vivo models and patient samples

We next wanted to determine how clinically relevant leflunomide may be as a targeted cancer therapy. We focus here on two sets of models: breast cancer and glioblastoma.

We proceeded to test *in vivo* mouse models of triple negative breast cancer, a subset with particularly high *PTEN* mutation rates. We first tested SUM149, a human cancer cell line with PTEN deficiency that

was found to be sensitive to leflunomide *in vitro*. Cells were xenografted into mice, and once tumors were established the mice were treated orally as is done clinically. Due to the long half-life of leflunomide, we did not treat every day in order to prevent accumulation of the drug in the system beyond our intended dose. By measuring tumor volume using calipers, we found that treatment of mice carrying SUM149 tumors with 100mg/kg leflunomide significantly slowed down tumor growth (Fig. 3.12A).

To confirm this result, we tested an additional triple negative breast cancer model. Like SUM149, MDA-MB 468 cells have PTEN deficiency and were also highly sensitive to DHODH inhibition *in vitro*. We also expressed luciferase in these cells prior to injection into mice, allowing us to visualize tumor size by luminescence. (This was accomplished using the IVIS® Spectrum *In Vivo* Imaging System.) Similar to the model above, we treated mice orally with 100mg/kg leflunomide for four consecutive days per week. In the MDA-MB 468 model, tumor size was diminished upon leflunomide treatment, and in some cases the tumor disappeared altogether (Fig. 3.12B).

It is possible for a cancer therapy to be efficacious on small tumors, but fail to reduce or even stabilize large tumors. Since vascularization of a tumor increases drug delivery, poorly perfused large tumors will not properly access the given drug (Allen 2004). To test the efficacy of leflunomide in this setting, we allowed untreated MDA-MB 468 xenografts to grow for seven weeks until the size of the tumor was about 10 times larger than the starting size in figure 3.12B. We then treated daily with 100mg/kg leflunmomide; remarkably, even these large tumors ($4x10^7$ photons) regressed after only 1 week of treatment (Fig. 3.12C). We were also able to stabilize a large SUM149 tumor with leflunomide (Fig. 3.12D). Overall, our data show that leflunomide could have clinical success as a neoadjuvant therapy.

Furthermore, we obtained patient-derived xenograft (PDX) mice, in which tumor samples from a breast cancer patient with known PTEN deficiency were implanted. PDXs hold an advantage over established cell line xenografts: while cell lines also originated from human tumors, PDXs have been obtained more recently and have not been passaged over many years, and therefore are less likely to have evolved away from the original genetics of the patient's tumor. We treated a cohort of mice bearing a PTEN mutant PDX for four consecutive days each week, and found a significant but modest slowing of tumor growth compared to the control group (Fig. 3.13A). When we checked lysates made from tumor sections, however, we detected a considerable amount of PTEN – it is unclear whether this is coming from the stroma and not the actual tumor cells, or if there is truly PTEN expression in the tumor itself, explaining the modest effect we see with leflunomide (Fig. 3.13B).

To confirm that the Pten-specificity of leflunomide sensitivity we observed *in vitro* is upheld *in vivo*, we xenografted MCCL-357 and MCCL-278 cells into mice and measured the tumors' response. Treatment of the mice with leflunomide resulted in a 4-fold greater response in MCCL-357 xenografts than in MCCL-278 xenografts (Fig. 3.13C).

Based on the above in vivo experiments, we concluded that leflunomide could indeed have efficacy for patients with PTEN mutant breast cancers. We next proceeded to test models of glioblastoma.

From Dr. Raymund Yong, a neurosurgeon at Mt Sinai hospital, we obtained four patient glioblastoma samples which we were able to grow as 3-dimensional tumor spheres in culture. This model gave us the

advantage of testing leflunomide's efficacy in penetrating a 3-D tumor, more closely resembling a real-life scenario than 2-D adherent cells would. And, like PDXs, these samples held the advantage of being recent acquisitions from patients and therefore likely to maintain the original tumor genetics. Two of our samples expressed PTEN and two did not (Fig. 3.14A). We first disrupted the tumor spheres into single cell suspensions; as described above, formation of spheres is considered a marker of tumorigenicity (Grimshaw, Cooper et al. 2008, Shaw, Harrison et al. 2012). The suspended cells were treated with various concentrations of leflunomide, and the number of formed tumor spheres was counted in each condition. We found that formation of tumor spheres was inhibited at lower concentrations of leflunomide in PTEN-deficient samples compared to WT; in fact, one of the PTEN-expressing tumors was not inhibited by leflunomide even at the highest concentration used, while both of the PTEN-deficient tumors were inhibited at the lowest drug concentration used (Fig. 3.14B). We concluded that leflunomide can penetrate tightly-packed 3-D clusters of human cells and can inhibit at least some PTEN-deficient patient-derived glioblastomas.

Combination therapy

A common problem with cancer therapy is the eventual development of resistance. Combining multiple therapies may be a way to overcome acquired resistance or enhance the tumor-reducing ability of leflunomide in the first place in sensitive cells. We therefore performed numerous combination therapy experiments.

We first tried a few rational approaches: combining leflunomide with other drugs in the same pathway. The first was actually a double-hit on DHODH, with brequinar. Adding brequinar to MEFs reduced the GI50 of leflunomide for both WT and *Pten*$^{-/-}$ cells, but thereby removed the differential sensitivity

between the two (Fig. 3.15A). Adding brequinar on top of leflunomide to PTEN mutant human breast cancer cell lines did not have an effect (Fig. 3.15B).

We next tried various steps of the PI3K pathway. A PI3K inhibitor also reduced the GI50 of leflunomide for both WT and *Pten*$^{-/-}$ MEFs but eliminated the differential sensitivity between the two (Fig. 3.15C). Additionally, the PI3K-leflunomide combination seemed to work better in PTEN WT human breast cancer cell lines compared to PTEN mutant lines (Fig. 3.15D).

Rad001 is a rapamycin analog, acting on mTORC1. It has previously been shown that cells with Pten loss are more sensitive to rapamycin than WT cells, and our data were consistent with this finding (Neshat, Mellinghoff et al. 2001, Podsypanina, Lee et al. 2001). However, rad001 did not synergize with leflunomide in *Pten*$^{-/-}$ cells: in both MEFs and mouse breast cancer cells, addition of the GI25 of leflunomide did not decrease the GI50 of rad001. The GI25 of rad001 also did not decrease the GI50 of leflunomide in MEFs, and in mouse breast lines the addition of the GI25 of rad001 eliminated the leflunomide GI50 difference between MCCL-357 and MCCL-278 cells (Fig. 3.16).

Since leflunomide is a pyrimidine synthesis inhibitor, we questioned whether other nucleotide disruptors could crash the system, leading to enhanced cell death. Adding leflunomide to a 5FU titration lowered the GI50 of 5FU in MCCL-278 cells only, and yielded no difference in sensitivity between the genotypes. At a GI25 dose, 5FU lowered the GI50 of leflunomide in MCCL-278 but not MCCL-357 cells, thus again losing the difference between the two (Fig. 3.17A-B).

Methotrexate inhibits dihydrofolate reductase (DHFR) in the folate cycle for one-carbon metabolism involved in primarily purine synthesis. There was no difference in methotrexate GI50 at baseline between *Pten*$^{-/-}$ and WT cells, and addition of leflunomide lowered the GI50 to an approximately equal degree in both. The GI25 of methotrexate lowered the leflunomide GI50 to a greater degree in MCCL-278 compared to MCCL-357 cells, losing the difference in sensitivity between the two genotypes (Fig. 3.17C-D).

Our data show that our rational combinations thus far did not synergize. We therefore also tried combining leflunomide with various chemotherapies that are used as standard of care for cancer treatment.

Pten$^{-/-}$ and WT cells were neither differentially sensitive to carboplatin at baseline nor with the addition of leflunomide, although leflunomide lowered the carboplatin GI50 for both genotypes. The GI25 of carboplatin lowered the leflunomide GI50 to a greater degree in MCCL-278 compared to MCCL-357 cells, losing the difference in leflunomide sensitivity between the two (Fig. 3.18A-B).

Pten$^{-/-}$ and WT cells were also not differentially sensitive to doxorubicin at baseline. Interestingly, the combination with leflunomide enhanced WT sensitivity to doxorubicin, although there was still no significant difference between genotypes in the combination. Doxorubicin also decreased the GI50 of leflunomide for Pten WT cells, and there was no difference between the genotypes with the combination (Fig. 3.18C-D).

Lastly, we tried a combination therapy experiment with paclitaxel. Addition of the GI25 of paclitaxel did not affect the GI50 of leflunomide in the dose response experiment. However, despite no baseline difference in paclitaxel sensitivity, addition of leflunomide created a profound GI50 difference between *Pten*$^{-/-}$ and WT cells (Fig. 3.19A-B). This interesting *in vitro* result prompted an *in vi*vo experiment:

We treated MDA-MB 468 xenografts with vehicle or 100mg/kg leflunomide. After 4 weeks, half of the vehicle-treated and half of the leflunomide-treated cohorts were then treated with 20mg/kg paclitaxel, creating 4 arms of the experiment: vehicle, leflunomide alone, paclitaxel alone, and combination treatment. However, there were no significant differences between leflunomide alone, paclitaxel alone, or combination-treated mice in terms of tumor size (Fig. 3.19C). It appears that leflunomide and paclitaxel are fairly equivalent for tumor reduction, and combining the two at these doses was not efficacious.

While our attempts at an effective combination therapy have so far been unsuccessful, these data do not close the door on finding a good combination option in the future.

Discussion

We find the results of this chapter to be quite exciting. Our evidence that DHODH inhibition is effective against PTEN mutant cancers could have terrific impact in the clinic; in fact, we are currently working to initiate a clinical trial in patients with TNBC. Further experiments will show the validity of the model in other tumor types, and if successful could launch clinical trials in glioblastoma and prostate cancer patients. For example, we found *in vitro* that the PTEN mutant human glioblastoma cell line DBTRG was

sensitive to leflunomide. We therefore plan to use this line for a xenograft experiment in collaboration with Drs. Hadjipanayis and Boras at Mt. Sinai, as a model for invasive brain tumors.

Our results are also satisfying at a conceptual level. Through DHODH inhibition we prove that *de novo* pyrimidine synthesis is in fact as important for PTEN deficient cells as we conjectured from our results in chapter 2. These data also provide proof of principle that studying metabolic consequences of oncogene or tumor suppressor alterations and interfering with the deregulated pathways could be effective treatments. We also show the specificity of *de novo* pyrimidine synthesis inhibition over other nucleotide inhibition in *Pten*$^{-/-}$ cells, demonstrating that metabolic data can be predictive of drug response.

An interesting paper by Hail et al found cytostatic effects of A771726 in prostate cancer cells in the short term, and some cytotoxicity with prolonged treatment. Notably, the DU-145 cell line they used is *PTEN* heterozygous. The partial loss of PTEN function could explain the inhibitory effects of A771726, but could also explain why toxicity was only seen at high doses since PTEN was not fully inactivated. Excess uridine did not rescue the effects of A771726 in the cells, and the authors claim that in some cases the salvage pathway for pyrimidines is not sufficient to compensate for blocking *de novo* synthesis. It would be informative to see whether orotate would rescue the inhibition, then, since the *de novo* pathway could resume just after the inhibited enzyme. Interestingly, they observed that short-term exposure to A771726 decreased ROS production, and only a very high dose for extended time caused mitochondrial dysfunction in their study (Hail, Chen et al. 2010). This could explain why we do not observe mitochondrial defects or rescue by antioxidants in our system.

There is some controversy about whether leflunomide/A771726 has effects other than on DHODH. Some literature suggests it can inhibit tyrosine kinases in T- and B-cells, in particular p56, Jak1, and Jak3, or indirectly AKT (Breedveld and Dayer 2000, Sawamukai, Saito et al. 2007). Conversely, other studies claim it can activate tyrosine kinases such as ERK and AKT, and thereby protect cells from apoptosis and DNA fragmentation (Leger, Liagre et al. 2006). Our ability to rescue leflunomide-induced growth defects with orotate and uridine gives us confidence that DHODH is the target of the effects we see. Furthermore, siRNA to DHODH recapitulated cell death in PTEN mutant cells, and we did not see differences in phospho-AKT upon teriflunomide treatment of MEFs. We therefore believe that at least in our system, leflunomide is acting primarily on DHODH and not tyrosine kinases to exact its effects on PTEN mutant cells.

It is also important to note discrepancies between enzymatic IC50s and intracellular GI50s. Since leflunomide binds tightly to serum proteins, the amount of leflunomide added to cells in culture may exceed the level getting into the cells, which further exceeds that which actually interacts with and inhibits DHODH. The concentration required to achieve growth inhibition of 50% is therefore likely greater than the enzymatic IC50, and relatively high concentrations are required for inhibitory effects as demonstrated by us and previous studies; these concentrations are also normally maintained in RA patients (Hail, Chen et al. 2010, White, Cech et al. 2011). Our experiments with glioblastoma tumor spheres were performed in serum-free media, but are not directly comparable to adherent cell experiments since the amount of leflunomide required to penetrate 3-dimensional spheres could be greater. It would be illuminating to try adherent cell leflunomide experiments in a serum gradient, although even those results could be confounded by the detrimental effect of serum starvation on cells.

In the current literature, there is some evidence of DHODH inhibition being effective against cancer cells. A771726 was cytostatic in a human T-lymphoblastoma cell line, which could be rescued by uridine (Greene, Watanabe et al. 1995). Brequinar was also shown to be efficacious in acute myeloid leukemia (AML) models by triggering myeloid differentiation (Sykes, Kfoury et al.), perhaps unsurprisingly due to the known ability of leflunomide to affect B-cell and T-cell proliferation. Treatment of $BRAF^{V600E}$ mutant melanomas with a DHODH inhibitor in combination with a $BRAF^{V600E}$ inhibitor slowed down tumor growth *in vitro* and *in vivo* (White, Cech et al. 2011). To our knowledge, our data are the first to claim that leflunomide could be used as a single agent therapy for patients with PTEN mutant cancers. However, even good targeted therapies incur a problem: that of tumor resistance, in which alterations in additional pathways are selected for in order to bypass the block of a targeted therapy. Combination therapies may avert or delay resistance, and in the final chapter of this thesis we discuss in more detail the combination therapies we have tried and have yet to try.

CHAPTER 3 FIGURE LEGENDS AND FIGURES

Figure 3.1. Pten$^{-/-}$ MEFs are sensitive to DHODH inhibitors. (A) *Pten* WT and KO cells were treated with dose titrations of leflunomide, A771726, or brequinar to determine GI50s (Student's *t*-test, p*<.05, n=3). (B) MEFs were treated with 25μM leflunomide or DMSO, and growth was measured over time using phase-contrast images from an Incucyte Zoom. (C) MEFs were treated with 100μM leflunomide and growth was measured over time using phase-contrast images from an Incucyte Zoom (one-way ANOVA, *p<.001, n=3).

Figure 3.2. PTEN mutant cancer cells are sensitive to DHODH inhibitors. (A) Cells were treated with dose titrations of leflunomide to determine GI50s (Student's *t*-test, p*<.05, n=3). (B-E) Cells were treated with dose titrations of DHODH inhibitors as indicated to determine GI50s (Student's *t*-test, *p-values as reported on the figures, n=3).

Figure 3.3. DHODH inhibitors kill PTEN mutant cells. (A-B) Cells were treated with 100μM leflunomide and DRAQ7. Live cell imaging of phase confluence and red fluorescence over time was used to determine accumulation of cell death (two-way ANOVA, *p<.01). (C) Cells were treated with 100μM leflunomide and DRAQ7. Live cell imaging of phase confluence and red fluorescence over time was used to determine accumulation of cell death (two-way ANOVA between PTEN WT and mut, *p<.0001).

Figure 3.4. Human breast cancer cell line tumor spheres. PTEN WT and mutant breast cancer cell lines were grown as tumor spheres in untreated media, DMSO, or 50, 100, or 200μM leflunomide. After 5 days, the number of tumor spheres in each condition was counted.

Figure 3.5. Rescue of growth inhibition. (A) Cells were treated with 50μM leflunomide in combination with 0 or 640μM orotate. Confluence of cells after 5 days of treatment was measured (Student's *t*-test, *p<.05, n=3). (B) Cells were treated with 100μM leflunomide in combination with 0 or 3.125mM

uridine. Confluence of cells after 5 days of treatment was measured (Student's *t*-test, *p<.05, n=3). (C) Cells were treated with 50μM leflunomide in combination with 0, 31.25, 62.5 or 125μM orotate. Confluence of cells after 5 days was measured (Student's *t*-test, *p<.05, n=3). (D) Cells were treated with 25μM leflunomide in combination with 0, 312.5, or 625μM orotate. Confluence of cells after 5 days was measured (Student's *t*-test, *p<.05, n=3). Note that here as well as in A-C a large amount of DMSO was used in each condition to match the amount of orotate needed, narrowing the growth differential we normally observe between leflunomide treated and untreated cells in the PTEN mutant setting. (E) Cells were treated with 100μM leflunomide in combination with 0, 3.125, or 6.25mM uridine. Confluence of cells after 5 days was measured (Student's *t*-test, *p<.05, n=3). (F) Cells were treated with 100μM leflunomide in combination with 0, 3.125, or 6.25mM uridine. Confluence of cells after 5 days of treatment was measured (Student's *t*-test, *p<.05, n=3). (G) Cells were treated with 25μM leflunomide in combination with 0, 6.25, or 12.5mM uridine. Confluence of cells after 5 days was measured (Student's *t*-test, *p<.05, n=3).

Figure 3.6. The role of DHODH. (A) Cells were transfected with siRNA against DHODH or control (scrambled) siRNA; cell viability was measured using Annexin V and 7AAD via flow cytometry and the percentage of live cells in each condition was normalized to control. 0.5μg/mL actinomycin D was a positive control for cell death (Student's *t*-test, *p<.05, n=3). (B) Immunoblot of DHODH after knockdown with one of 2 DHODH siRNAs or with control siRNA. (C) Cells were treated with 50μM leflunomide in combination with DMSO or 10mM n-acetylcysteine. Confluence of cells after 5 days of treatment was measured. (D) Cells were incubated with 100μM leflunomide or DMSO and stained with MitoSox Red. Flow cytometry was used to determine the mean fluorescence intensity (MFI), indicating the relative level of mitochondrial superoxide (Student's *t*-test, p>.05, n=3).

Figure 3.7. Growth rate does not predict sensitivity to DHODH inhibition. (A) MCCL-278 and MCCL-357 growth rates, measured over time using phase-contrast images from an Incucyte Zoom. (B) Myc-

CaP and CaP8 growth rates, measured over time using phase-contrast images from an Incucyte Zoom. (C) Human breast cancer cell line growth rates, measured over time using phase-contrast images from an Incucyte Zoom.

Figure 3.8. The source of pyrimidine flux. (A) Immunoblot of DHODH in MEFs. (B) Immunoblot of pCAD before and after treatment with 100μM leflunomide in MEFs. (C) Immunoblot of pCAD S1859 in mouse breast cancer cell lines. (D) Immunoblot of pAKT T308 before and after treatment with 50μM A771726.

Figure 3.9. Sensitivity to brequinar. (A) MEFs were incubated with 12.5μM brequinar or DMSO and growth was measured over time using phase-contrast images from an Incucyte Zoom. (B) Cells were treated with dose titrations of brequinar to determine the GI50s (Student's *t*-test, *p<.05, n=3). (C) Cells were treated with dose titrations of brequinar to determine the GI50s (Student's *t*-test, p>.05, n=3). 5 WT, 5 PTEN mutant and 3 PIK3CA mutant cell lines were used, listed in table 3.1.

Figure 3.10. Differential AKT signaling. (A) Cells were treated with dose titrations of leflunomide to determine the GI50s (Student's *t*-test, *p<.05, n=3). 5 WT, 5 PTEN mutant and 3 PIK3CA mutant cell lines were used, listed in table 3.1. (B) Immunoblots of pAKT and total AKT in nuclear fractions of *Pten*$^{-/-}$ and *Pik3ca* mutant MEFs. (C) Immunoblot of pAKT and total AKT in whole cell lysate of *Pten*$^{-/-}$ and *Pik3ca* mouse cancer cell lines. (D) Immunoblot of pAKT and total AKT in nuclear fractions of *Pten*$^{-/-}$ and *Pik3ca* mutant mouse cancer cell lines.

Figure 3.11. Specificity of nucleotide inhibition sensitivity. (A-B) Cells were treated with dose titrations of 5-fluorouracil or mercaptopurine, respectively, to determine GI50s (Student's *t*-test, p>.05, n=3). (C) Cells were grown in media containing full glutamine (4mM) or no glutamine.

Figure 3.12. *In vivo* treatment with leflunomide of triple negative breast cancer models. (A) SUM149 xenografts. Mice were treated with 100mg/kg leflunomide or vehicle on days indicated with arrows and

tumor size was measured by calipers (two-way ANOVA with multiple *t*-tests, corrected for multiple comparisons, *p<.01 for ANOVA and *t*-tests, n=6). (B) MDA-MB 468 xenografts expressing luciferase. Treatment was started on day 7, with 100mg/kg leflunomide or vehicle for four consecutive days each week. Tumor size was measured by assessing luminescence, quantified by photons/second/cm^2/steradian and normalized to control (one-way ANOVA with multiple *t*-tests, corrected for multiple comparisons, *p<.05 for ANOVA and *t*-tests, n=5). Right panel: luminescence of treated and control mice after 2 weeks of treatment. (C) MDA-MB 468 xenografts which were never treated and allowed to grow for seven weeks were then treated with 100mg/kg leflunomide for 7 days. Tumor size was measured by assessing luminescence, quantified by photons/second/cm^2/steradian (multiple *t*-tests, corrected for multiple comparisons, *p<.05, n=2). (D) SUM149 xenografts which were never treated and allowed to grow for four weeks were then treated with 100mg/kg leflunomide on days indicated by arrows. Tumor size was measured by calipers (n=4).

Figure 3.13. *In vivo* treatments with leflunomide of additional models. (A) PDX xenografts. Mice were treated with 100mg/kg leflunomide or vehicle 4 consecutive days per week on days indicated with arrows and tumor size was measured by calipers (two-way ANOVA with multiple *t*-tests, corrected for multiple comparisons, *p<.01 for ANOVA and *t*-tests, n=6). (B) Immunoblots of PTEN protein in PDX samples and MCCL-278 as a positive control for Pten expression. (C) Xenografts of MCCL-278 (Myc, Pik3ca HR) and MCCL-357 (Myc, $Pten^{-/-}$) cell lines. Mice were treated with 100mg/kg leflunomide or vehicle for four consecutive days each week on days indicated by arrows and tumor volume was measured by calipers. Growth rate of the tumors was determined by calculating the slope of the tumor growth. (Student's *t*-test, *p<.01, n=8).

Figure 3.14. Leflunomide treatment of patient-derived glioblastomas. (A) Immunoblot of PTEN of four patient-derived glioblastomas. (B) Dispersed (single cell suspension) glioblastomas were treated with

DMSO or 50, 100, or 200μM leflunomide for 5 days. At the endpoint, the number of 3-dimensional tumor spheres was quantified and normalized to untreated samples. (Student's *t*-test, *p<.05, n=3).

Figure 3.15. Combination of leflunomide with brequinar or GDC0941. (A-B) Cells were treated with dose titrations of leflunomide in the presence or absence of brequinar to determine GI50s (Student's *t*-test, *p-values on figures, ns not significant, n=3). (C) Cells were treated with dose titrations of leflunomide in the presence or absence of 20 or 100nM GDC0941 to determine GI50s (Student's *t*-test, *p-values on figure, n=3). (D) Cells were treated with dose titrations of leflunomide in the presence or absence of GDC0941 to determine GI50s (Student's *t*-test, *p-values on figure, n=3).

Figure 3.16. Combination of leflunomide with rad001. (A) Cells were treated with dose titrations of rad001 in the presence or absence of leflunomide to determine GI50s (Student's *t*-test, p>.05, n=3). (B) Cells were treated with dose titrations of leflunomide in the presence or absence of rad001 to determine GI50s (Student's *t*-test, *p-values on figures, n=3). (C) Cells were treated with dose titrations of rad001 in the presence or absence of leflunomide to determine GI50s (Student's *t*-test, p>.05, n=3). (D) Cells were treated with dose titrations of leflunomide in the presence or absence of rad001 to determine GI50s (Student's *t*-test, *p-values on figures, n=3). (D) Immunoblot of pS6 to ensure potency of rad001; less signal in the treated samples indicated that rad001 was effective.

Figure 3.17. Nucleotide inhibitor combinations. (A) Cells were treated with dose titrations of 5FU in the presence or absence of leflunomide to determine GI50s (Student's *t*-test, p>.05, n=3). (B) Cells were treated with dose titrations of leflunomide in the presence or absence of 5FU to determine GI50s (Student's *t*-test, *p-values on figures, n=3). (C) Cells were treated with dose titrations of methotrexate in the presence or absence of leflunomide to determine GI50s (Student's *t*-test, p>.05, n=3). (D) Cells were treated with dose titrations of leflunomide in the presence or absence of methotrexate to determine GI50s (Student's *t*-test, *p-values on figures, n=3).

Figure 3.18. Chemotherapy combinations. (A) Cells were treated with dose titrations of carboplatin in the presence or absence of leflunomide to determine GI50s (Student's *t*-test, *p-values on figures, n=3). (B) Cells were treated with dose titrations of leflunomide in the presence or absence of carboplatin to determine GI50s (Student's *t*-test, *p-values on figures, n=3). (C) Cells were treated with dose titrations of doxorubicin in the presence or absence of leflunomide to determine GI50s (Student's *t*-test, *p-values on figures, n=3). (D) Cells were treated with dose titrations of leflunomide in the presence or absence of doxorubicin to determine GI50s (Student's *t*-test, *p-values on figures, n=3).

Figure 3.19. Combination treatment of leflunomide and paclitaxel. (A) Cells were treated with dose titrations of leflunomide in the presence or absence of paclitaxel to determine GI50s (Student's *t*-test, *p-values on figures, n=3). (B) Cells were treated with dose titrations of paclitaxel in the presence or absence of leflunomide to determine GI50s (Student's *t*-test, *p-values on figures, n=3). (C) Mice xenografted with MDA-MB 468 cells were treated with 100mg/kg leflunomide or vehicle for 4 weeks, 4 times per week. About half of the vehicle treated mice were then treated with 20mg/kg paclitaxel alone, and half of the leflunomide treated mice were treated with paclitaxel + leflunomide. Arrows correspond to paclitaxel treatments which were given once a week while leflunomide was still administered 4 times per week. Tumor size was measured by assessing luminescence, quantified by photons/second/cm^2/steradian (two-way ANOVA, *p<.0001, n>5).

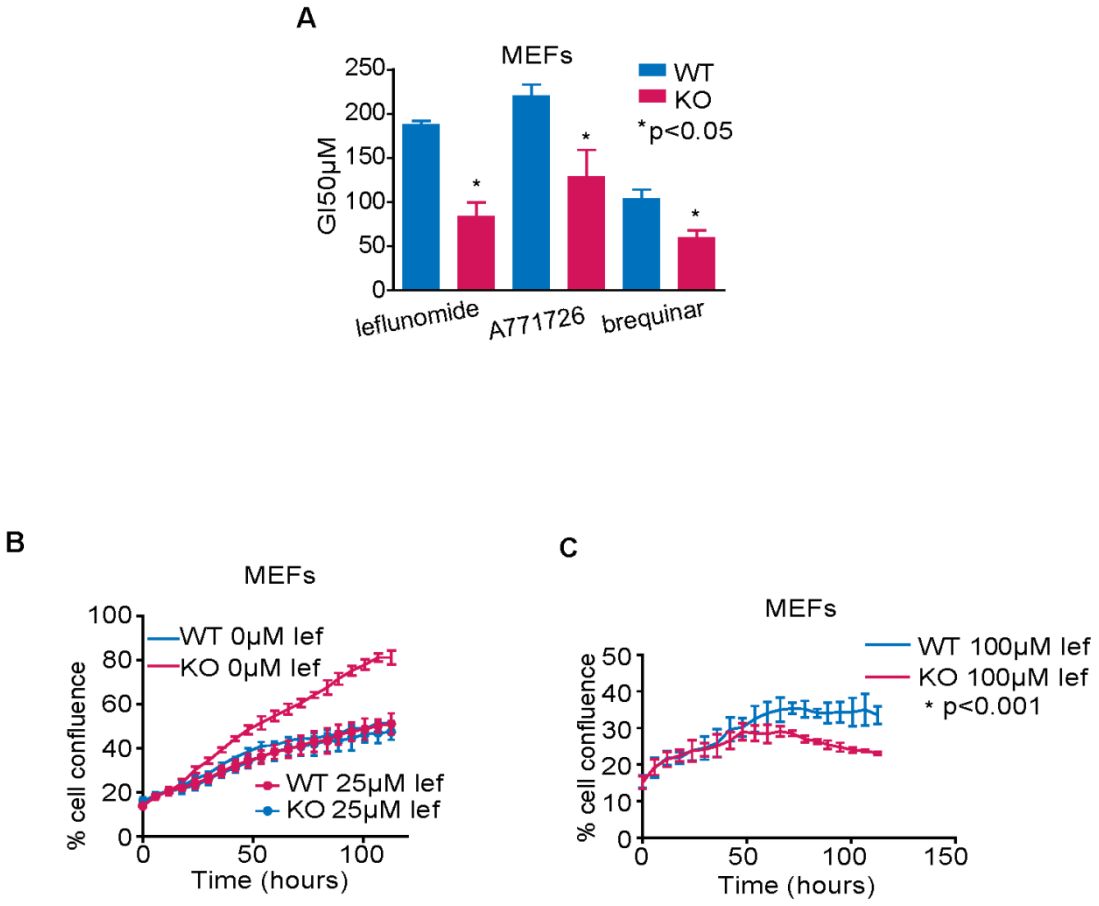
A
MEFs
WT
KO
*p<0.05
GI50μM
250
200
150
100
50
0
leflunomide
A771726
brequinar
B
MEFs
WT 0μM lef
KO 0μM lef
WT 25μM lef
KO 25μM lef
% cell confluence
Time (hours)
C
MEFs
WT 100μM lef
KO 100μM lef
* p<0.001
% cell confluence
Time (hours)

Figure 3.1

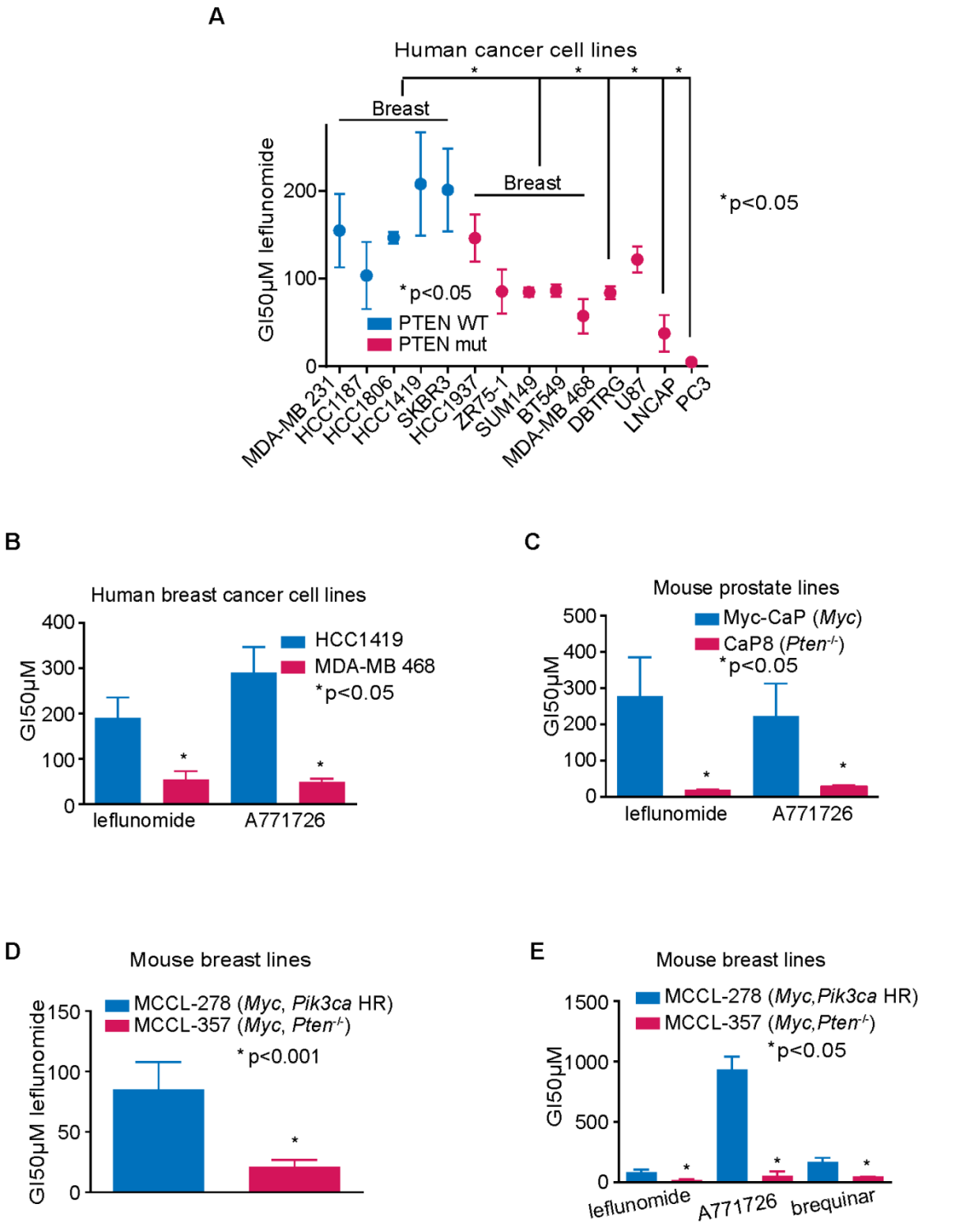
A
Human cancer cell lines
Breast
Breast
*p<0.05
GI50μM leflunomide
200
100
0
*p<0.05
PTEN WT
PTEN mut
MDA-MB 231
HCC1187
HCC1806
HCC1419
SKBR3
HCC1937
ZR75-1
SUM149
BT549
MDA-MB 468
DBTRG
U87
LNCAP
PC3
B
Human breast cancer cell lines
GI50μM
400
300
200
100
0
HCC1419
MDA-MB 468
*p<0.05
leflunomide
A771726
C
Mouse prostate lines
GI50μM
500
400
300
200
100
0
Myc-CaP (Myc)
CaP8 (Pten-/-)
*p<0.05
leflunomide
A771726
D
Mouse breast lines
GI50μM leflunomide
150
100
50
0
MCCL-278 (Myc, Pik3ca HR)
MCCL-357 (Myc, Pten-/-)
*p<0.001
E
Mouse breast lines
GI50μM
1500
1000
500
0
MCCL-278 (Myc,Pik3ca HR)
MCCL-357 (Myc,Pten-/-)
*p<0.05
leflunomide
A771726
brequinar

Figure 3.2

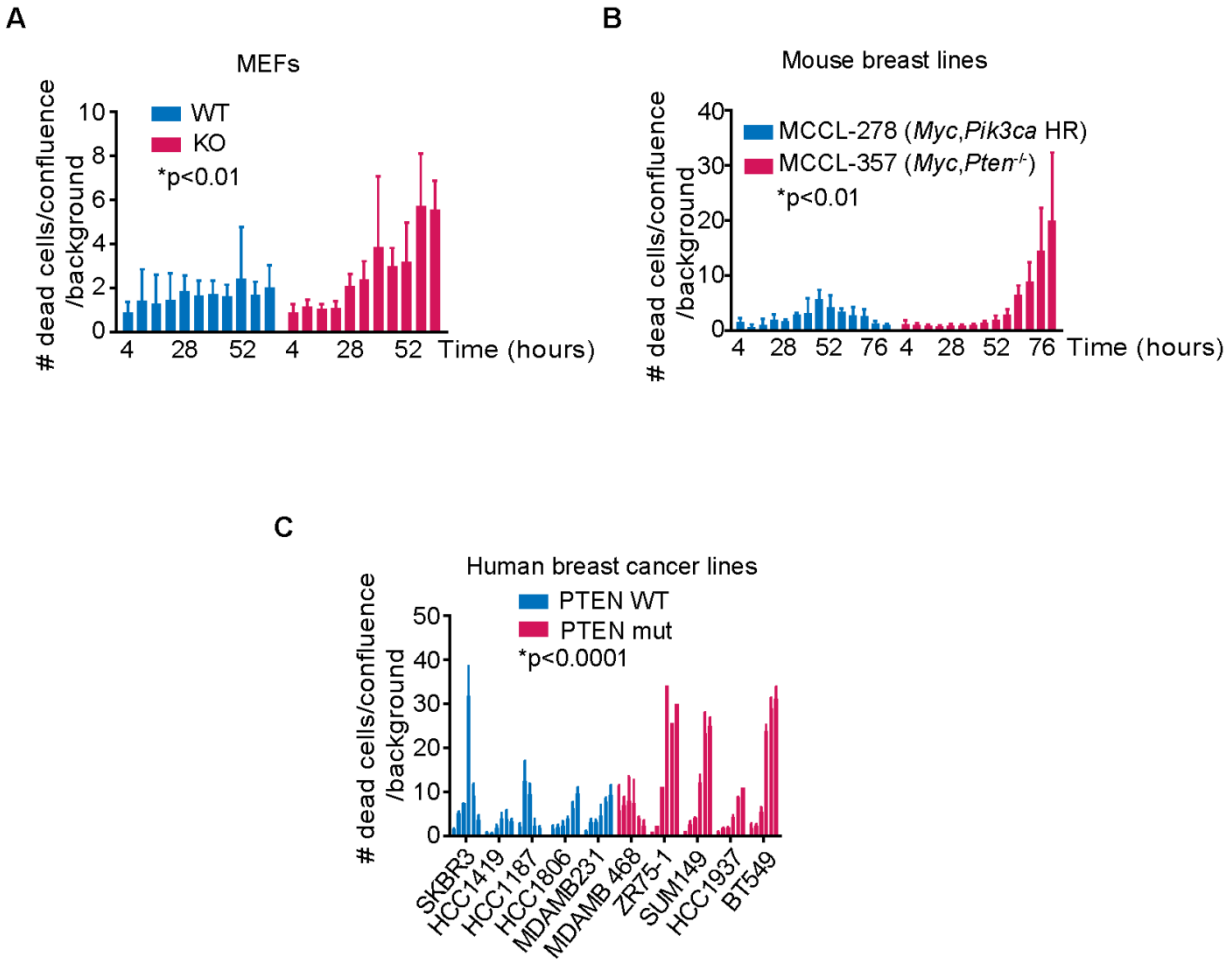
A
MEFs
dead cells/confluence /background
WT
KO
*p<0.01
Time (hours)
B
Mouse breast lines
MCCL-278 (Myc,Pik3ca HR)
MCCL-357 (Myc,Pten-/-)
*p<0.01
Time (hours)
C
Human breast cancer lines
PTEN WT
PTEN mut
*p<0.0001
SKBR3
HCC1419
HCC1187
HCC1806
MDAMB231
MDAMB 468
ZR75-1
SUM149
HCC1937
BT549

Figure 3.3

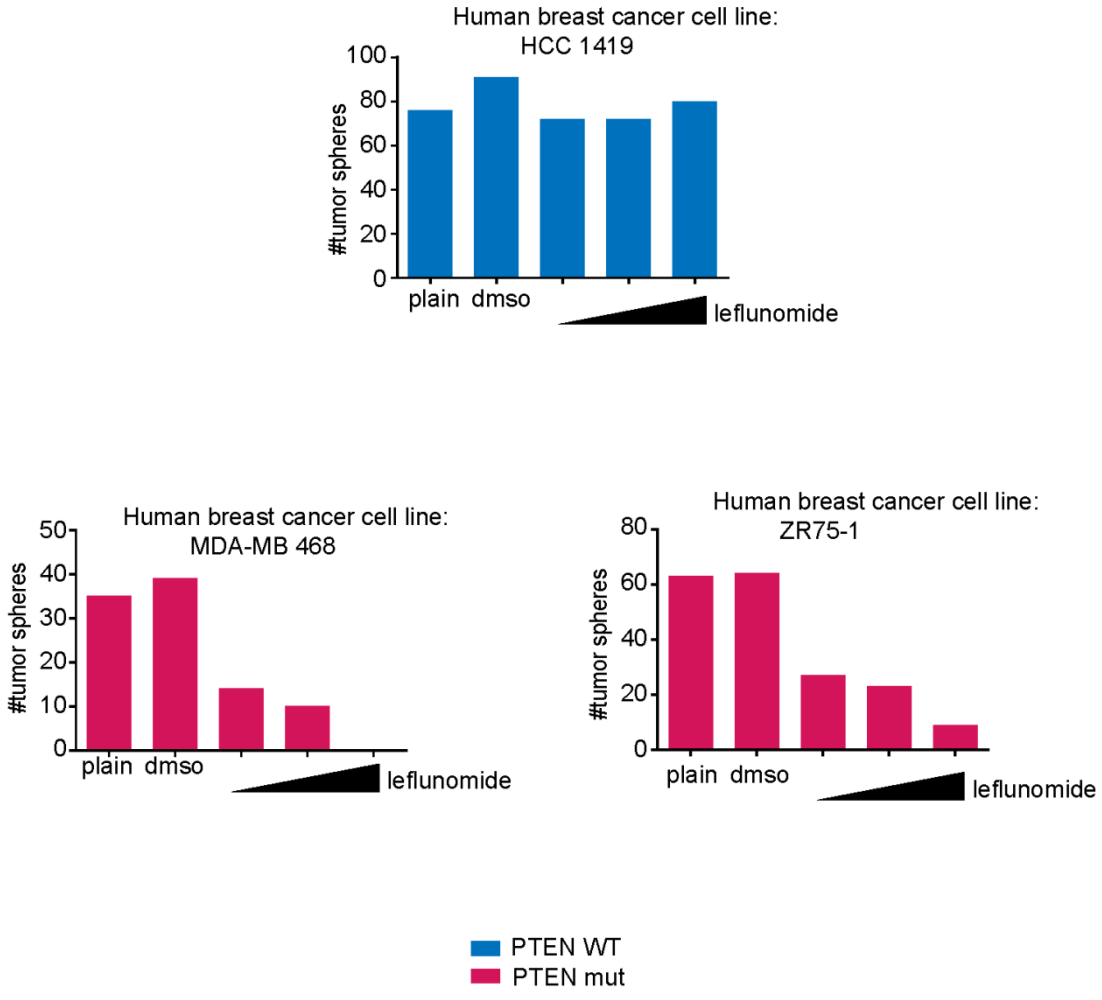
Human breast cancer cell line:
HCC 1419
#tumor spheres
100
80
60
40
20
0
plain
dmso
leflunomide
Human breast cancer cell line:
MDA-MB 468
#tumor spheres
50
40
30
20
10
0
plain
dmso
leflunomide
Human breast cancer cell line:
ZR75-1
#tumor spheres
80
60
40
20
0
plain
dmso
leflunomide
PTEN WT
PTEN mut

Figure 3.4

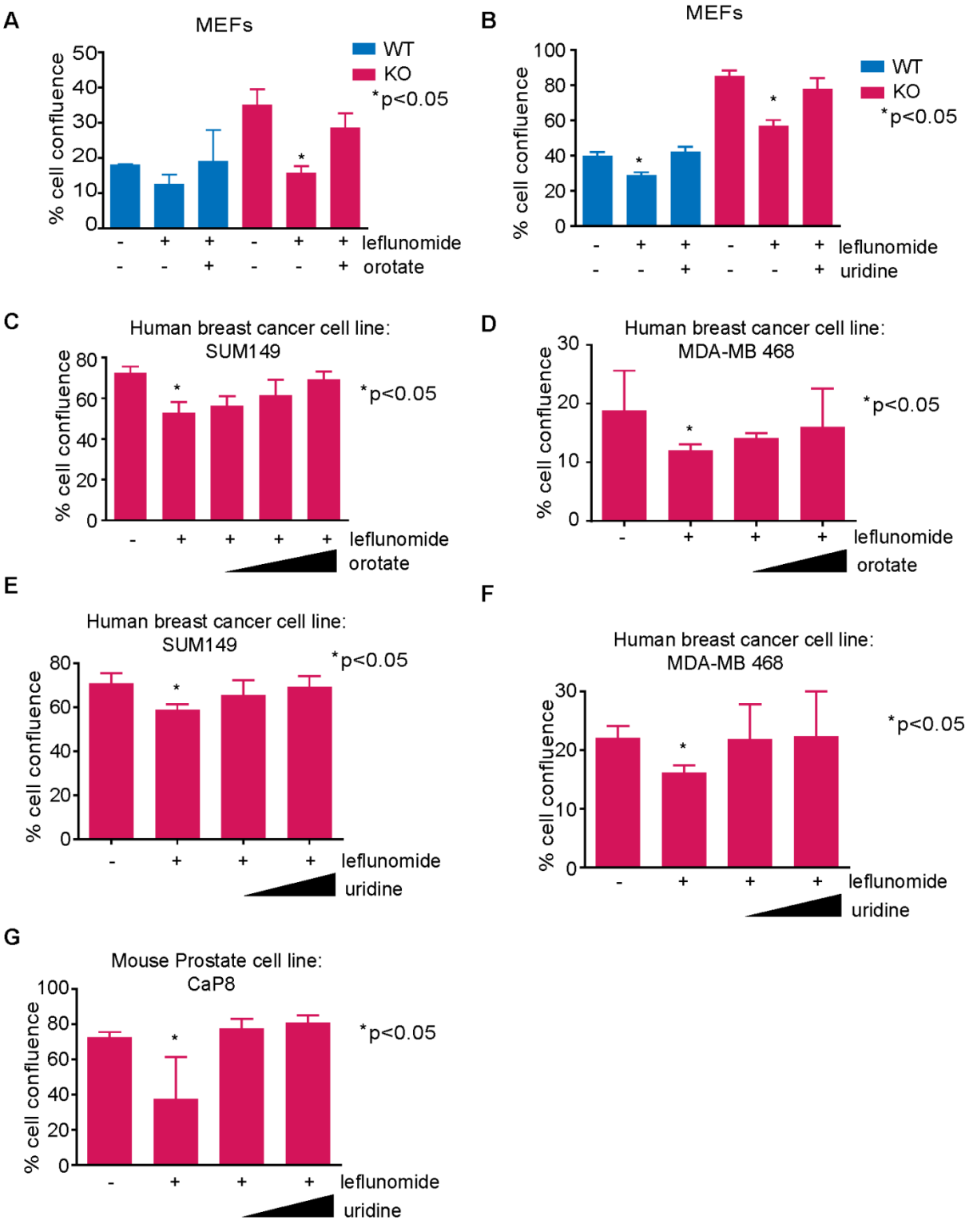
A
MEFs
WT
KO
*p<0.05
% cell confluence
leflunomide
orotate
B
MEFs
WT
KO
*p<0.05
% cell confluence
leflunomide
uridine
C
Human breast cancer cell line:
SUM149
*p<0.05
% cell confluence
leflunomide
orotate
D
Human breast cancer cell line:
MDA-MB 468
*p<0.05
% cell confluence
leflunomide
orotate
E
Human breast cancer cell line:
SUM149
*p<0.05
% cell confluence
leflunomide
uridine
F
Human breast cancer cell line:
MDA-MB 468
*p<0.05
% cell confluence
leflunomide
uridine
G
Mouse Prostate cell line:
CaP8
*p<0.05
% cell confluence
leflunomide
uridine

Figure 3.5

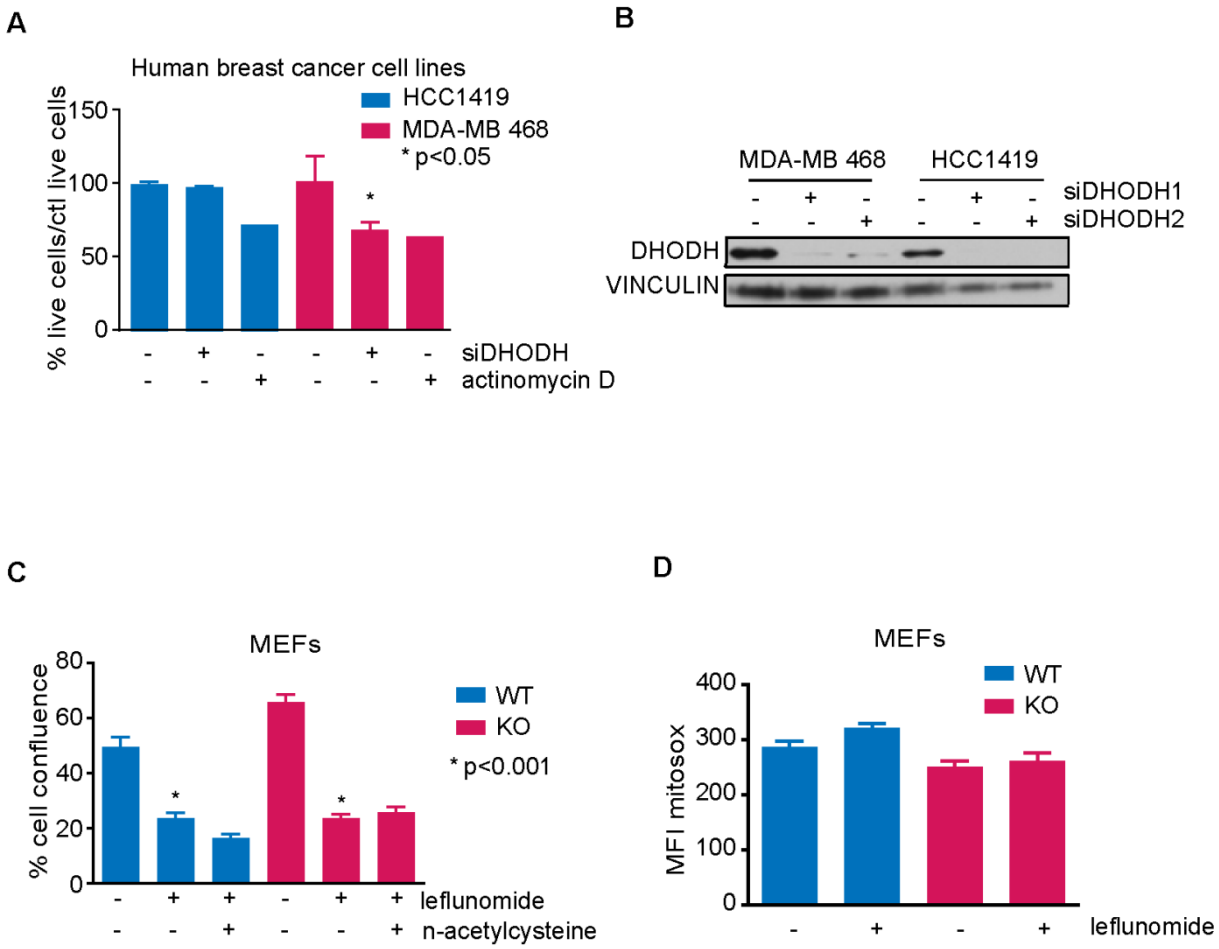
A
Human breast cancer cell lines
HCC1419
MDA-MB 468
* p<0.05
% live cells/ctl live cells
150
100
50
0
siDHODH
actinomycin D
B
MDA-MB 468
HCC1419
siDHODH1
siDHODH2
DHODH
VINCULIN
C
MEFs
WT
KO
* p<0.001
% cell confluence
80
60
40
20
0
leflunomide
n-acetylcysteine
D
MEFs
WT
KO
MFI mitosox
400
300
200
100
0
leflunomide

Figure 3.6

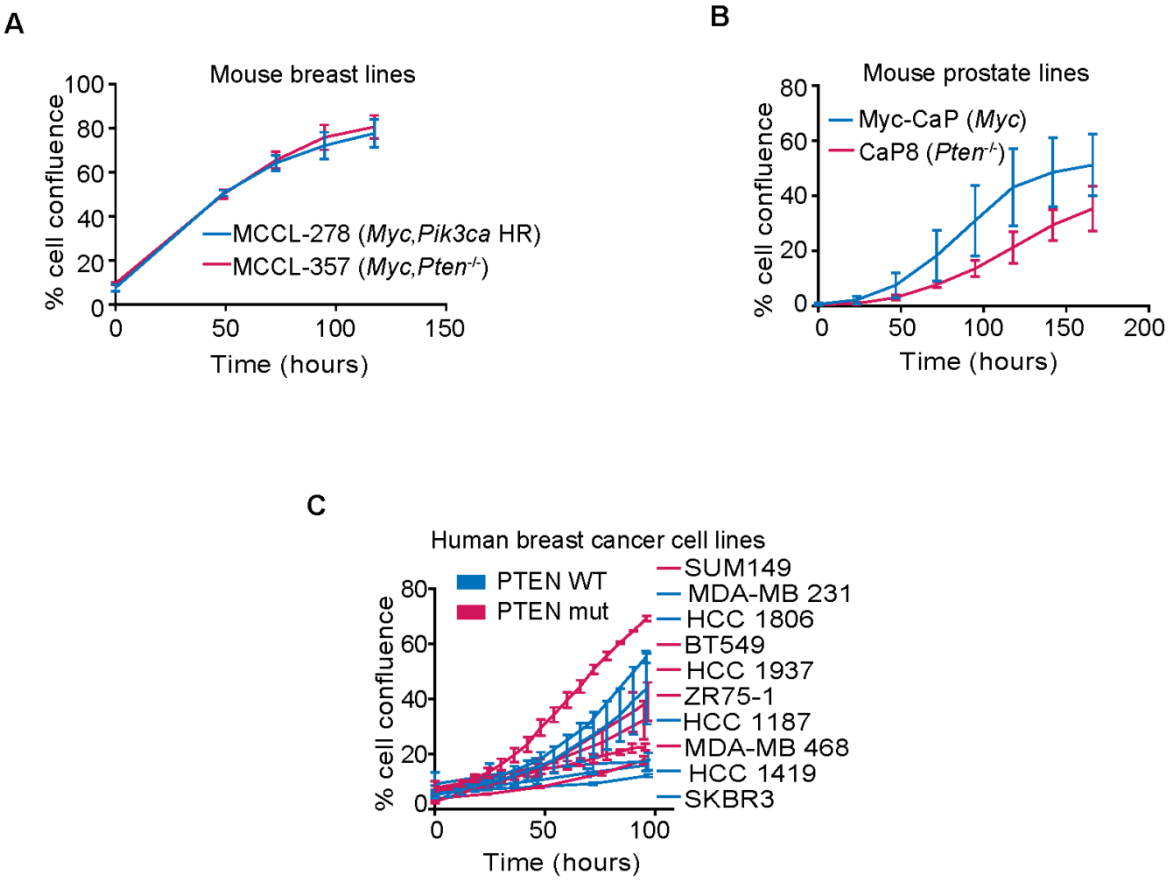
A
Mouse breast lines
% cell confluence
Time (hours)
MCCL-278 (Myc,Pik3ca HR)
MCCL-357 (Myc,Pten-/-)
B
Mouse prostate lines
Myc-CaP (Myc)
CaP8 (Pten-/-)
C
Human breast cancer cell lines
PTEN WT
PTEN mut
SUM149
MDA-MB 231
HCC 1806
BT549
HCC 1937
ZR75-1
HCC 1187
MDA-MB 468
HCC 1419
SKBR3

Figure 3.7

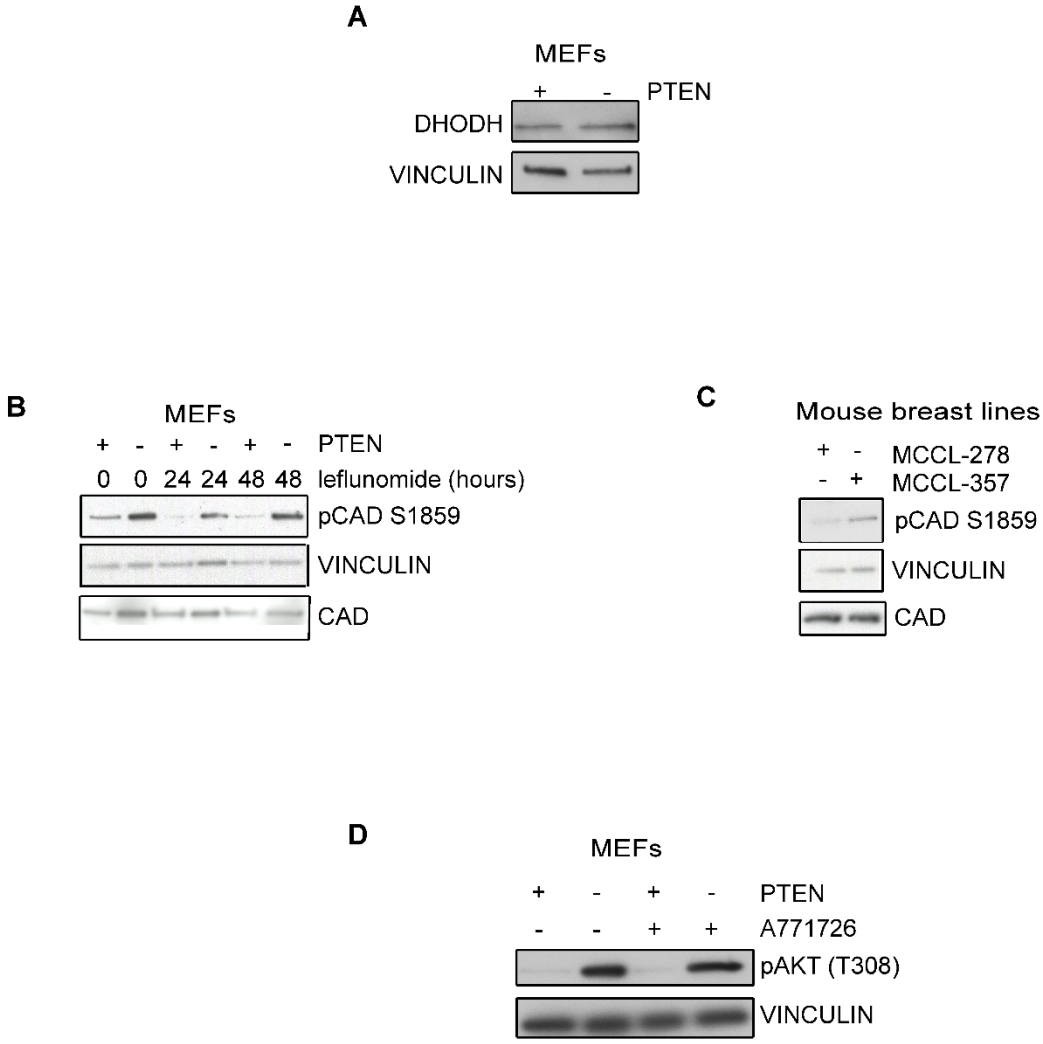
A
MEFs
+ - PTEN
DHODH
VINCULIN
B
MEFs
+ - + - + - PTEN
0 0 24 24 48 48 leflunomide (hours)
pCAD S1859
VINCULIN
CAD
C
Mouse breast lines
+ - MCCL-278
- + MCCL-357
pCAD S1859
VINCULIN
CAD
D
MEFs
+ - + - PTEN
- - + + A771726
pAKT (T308)
VINCULIN

Figure 3.8

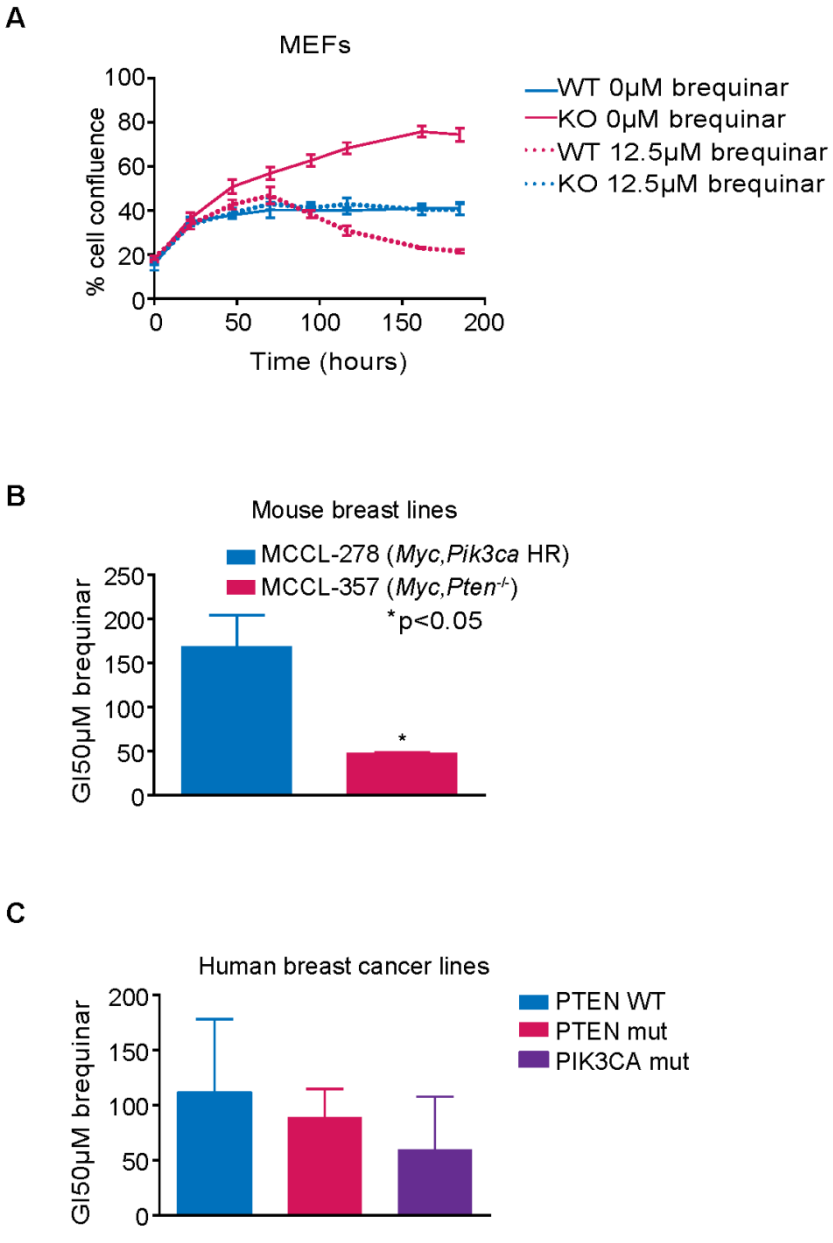
A
MEFs
% cell confluence
Time (hours)
WT 0μM brequinar
KO 0μM brequinar
WT 12.5μM brequinar
KO 12.5μM brequinar
B
Mouse breast lines
GI50μM brequinar
MCCL-278 (Myc,Pik3ca HR)
MCCL-357 (Myc,Pten-/-)
*p<0.05
C
Human breast cancer lines
GI50μM brequinar
PTEN WT
PTEN mut
PIK3CA mut

Figure 3.9

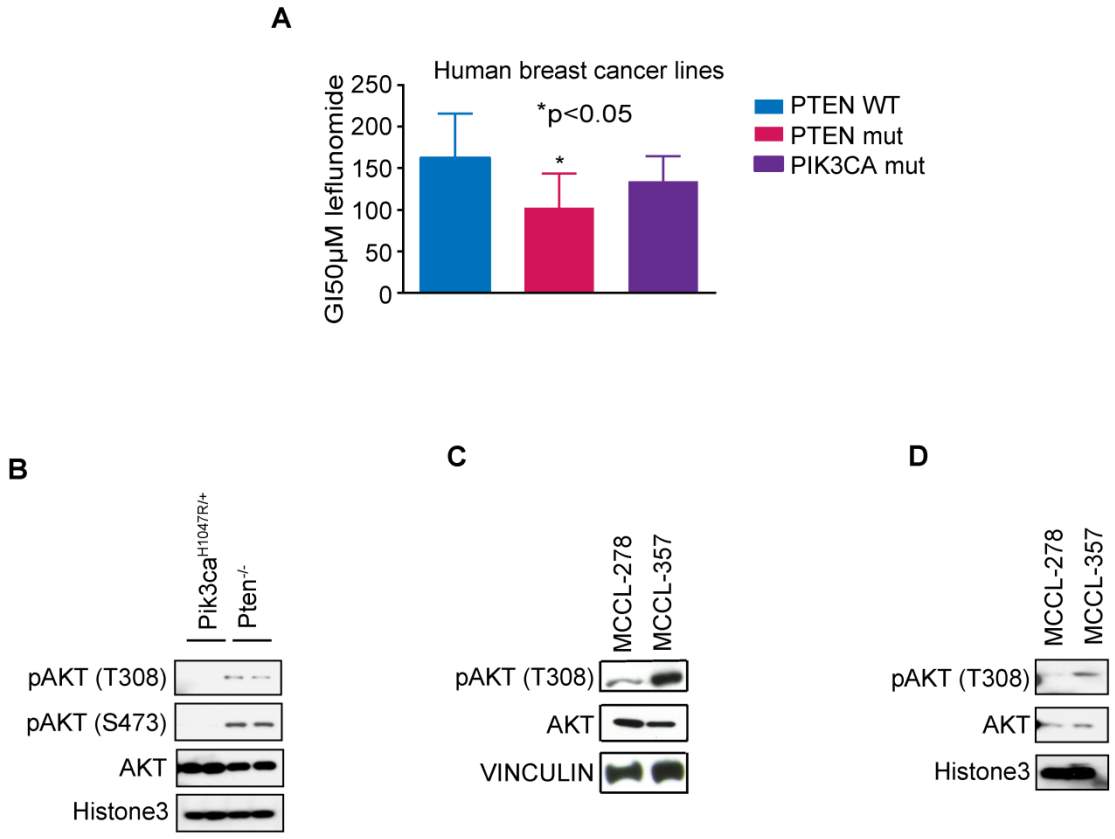
A
Human breast cancer lines
*p<0.05
GI50μM leflunomide
250
200
150
100
50
0
PTEN WT
PTEN mut
PIK3CA mut
B
Pik3ca H1047R/+
Pten -/-
pAKT (T308)
pAKT (S473)
AKT
Histone3
C
MCCL-278
MCCL-357
pAKT (T308)
AKT
VINCULIN
D
MCCL-278
MCCL-357
pAKT (T308)
AKT
Histone3

Figure 3.10

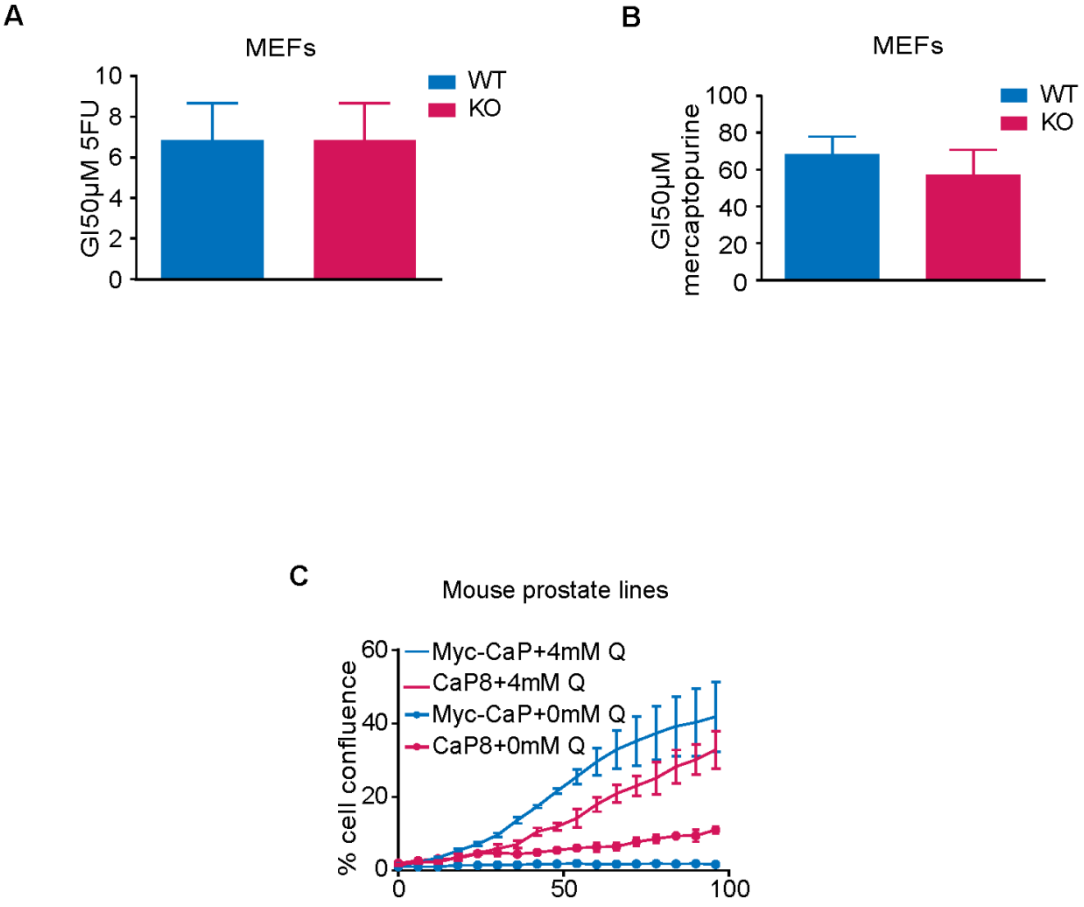
A
MEFs
GI50μM 5FU
10
8
6
4
2
0
WT
KO
B
MEFs
GI50μM mercaptopurine
100
80
60
40
20
0
WT
KO
C
Mouse prostate lines
% cell confluence
60
40
20
0
0
50
100
Myc-CaP+4mM Q
CaP8+4mM Q
Myc-CaP+0mM Q
CaP8+0mM Q

Figure 3.11

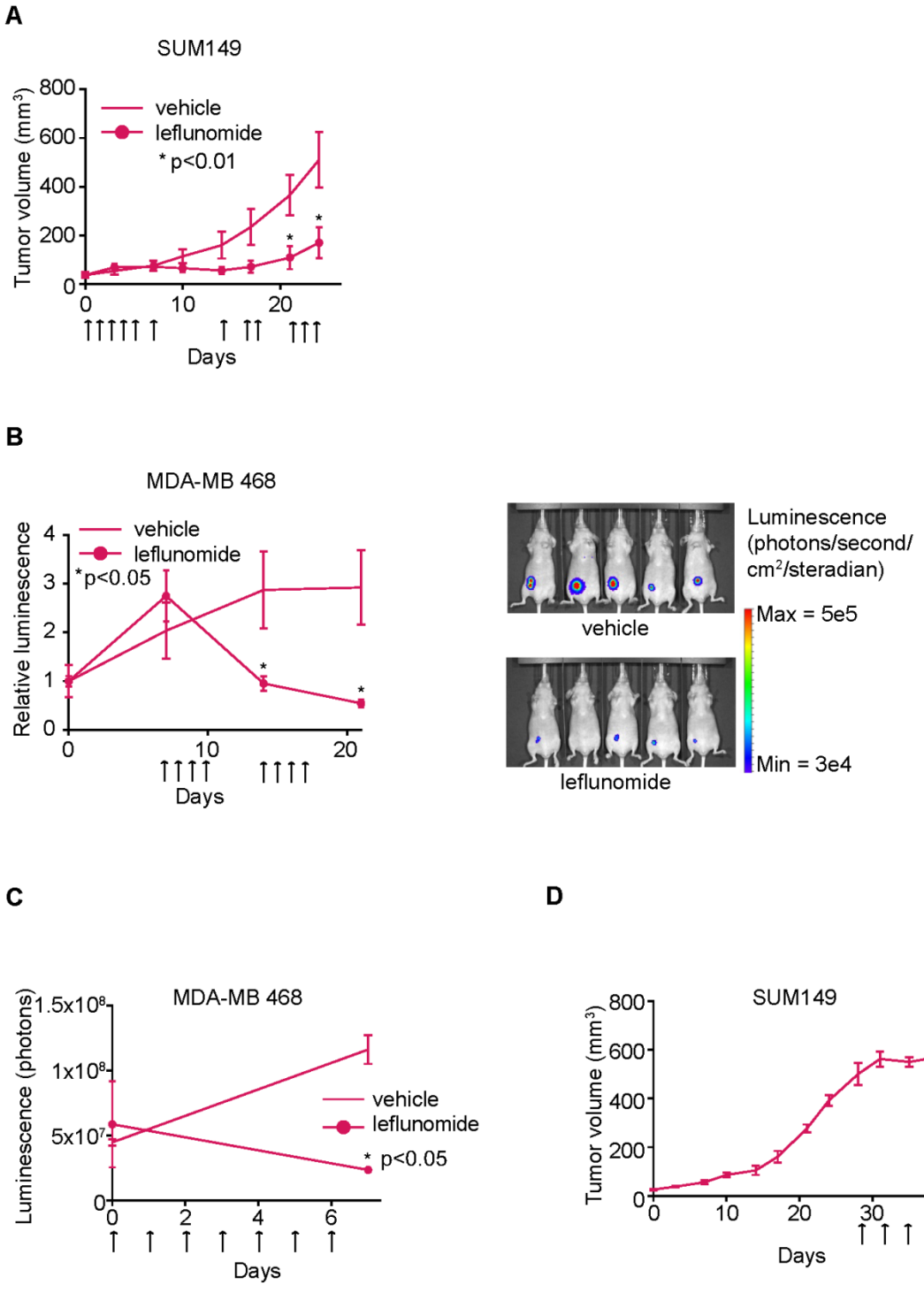
A
SUM149
Tumor volume (mm3)
800
600
400
200
0
vehicle
leflunomide
* p<0.01
0
10
20
Days
B
MDA-MB 468
Relative luminescence
4
3
2
1
0
vehicle
leflunomide
*p<0.05
0
10
20
Days
Luminescence (photons/second/ cm2/steradian)
Max = 5e5
Min = 3e4
vehicle
leflunomide
C
MDA-MB 468
Luminescence (photons)
1.5x10^8
1x10^8
5x10^7
0
vehicle
leflunomide
* p<0.05
0
2
4
6
Days
D
SUM149
Tumor volume (mm3)
800
600
400
200
0
0
10
20
30
40
Days

Figure 3.12

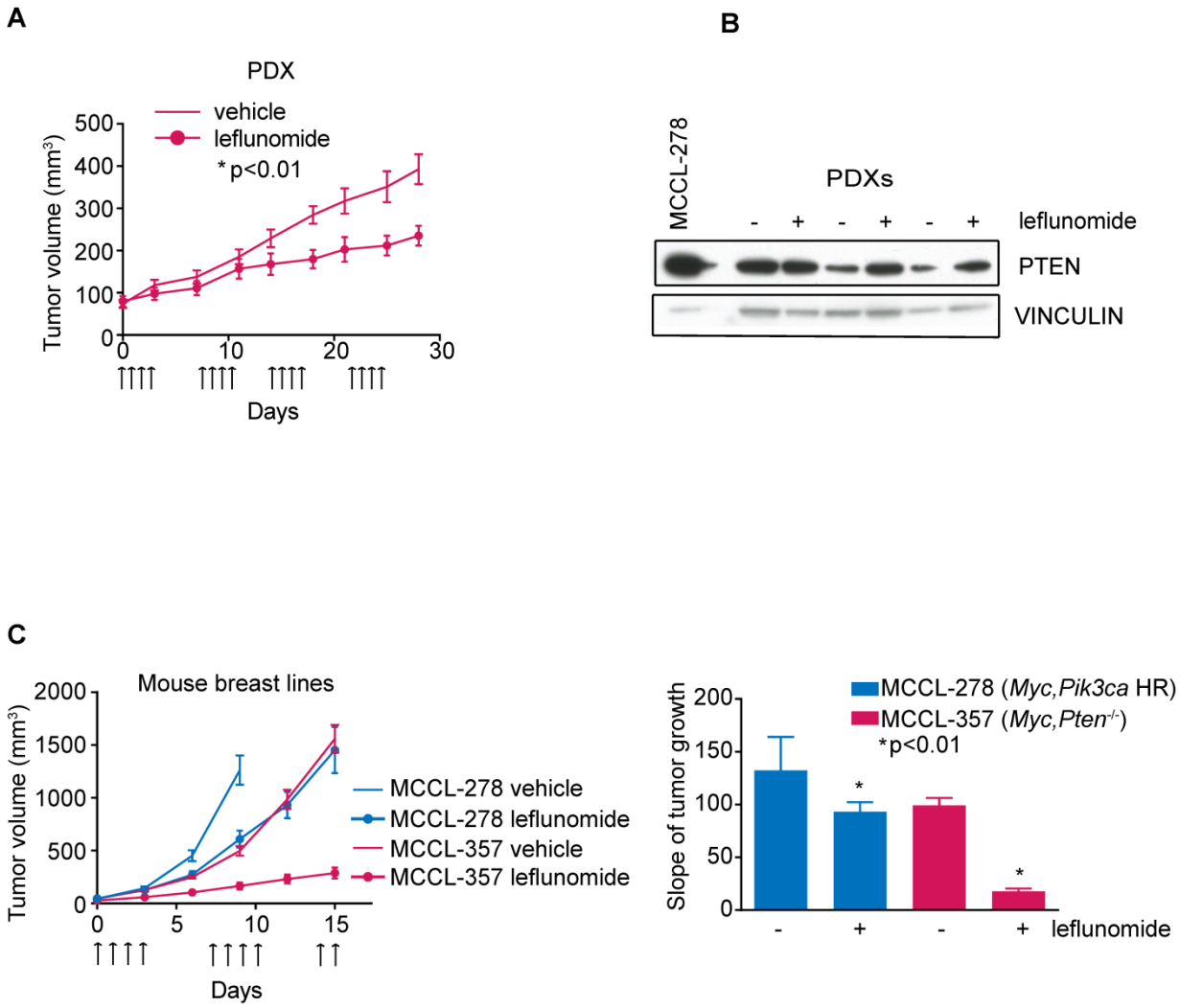
A
PDX
vehicle
leflunomide
* p<0.01
Tumor volume (mm3)
Days
B
MCCL-278
PDXs
leflunomide
PTEN
VINCULIN
C
Mouse breast lines
Tumor volume (mm3)
MCCL-278 vehicle
MCCL-278 leflunomide
MCCL-357 vehicle
MCCL-357 leflunomide
Days
MCCL-278 (Myc,Pik3ca HR)
MCCL-357 (Myc,Pten-/-)
*p<0.01
Slope of tumor growth
leflunomide

Figure 3.13

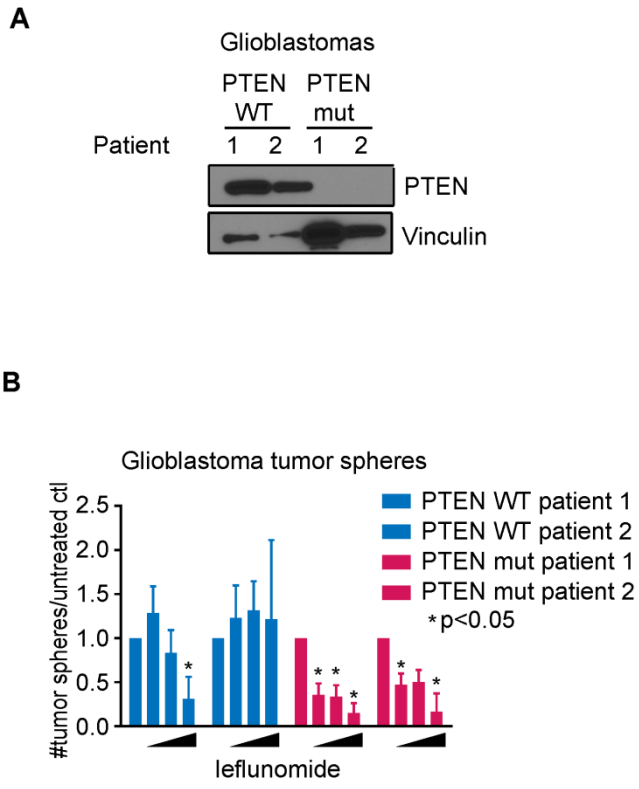
A
Glioblastomas
PTEN WT
PTEN mut
Patient
1 2 1 2
PTEN
Vinculin
B
Glioblastoma tumor spheres
#tumor spheres/untreated ctl
2.5
2.0
1.5
1.0
0.5
0.0
PTEN WT patient 1
PTEN WT patient 2
PTEN mut patient 1
PTEN mut patient 2
*p<0.05
leflunomide

Figure 3.14

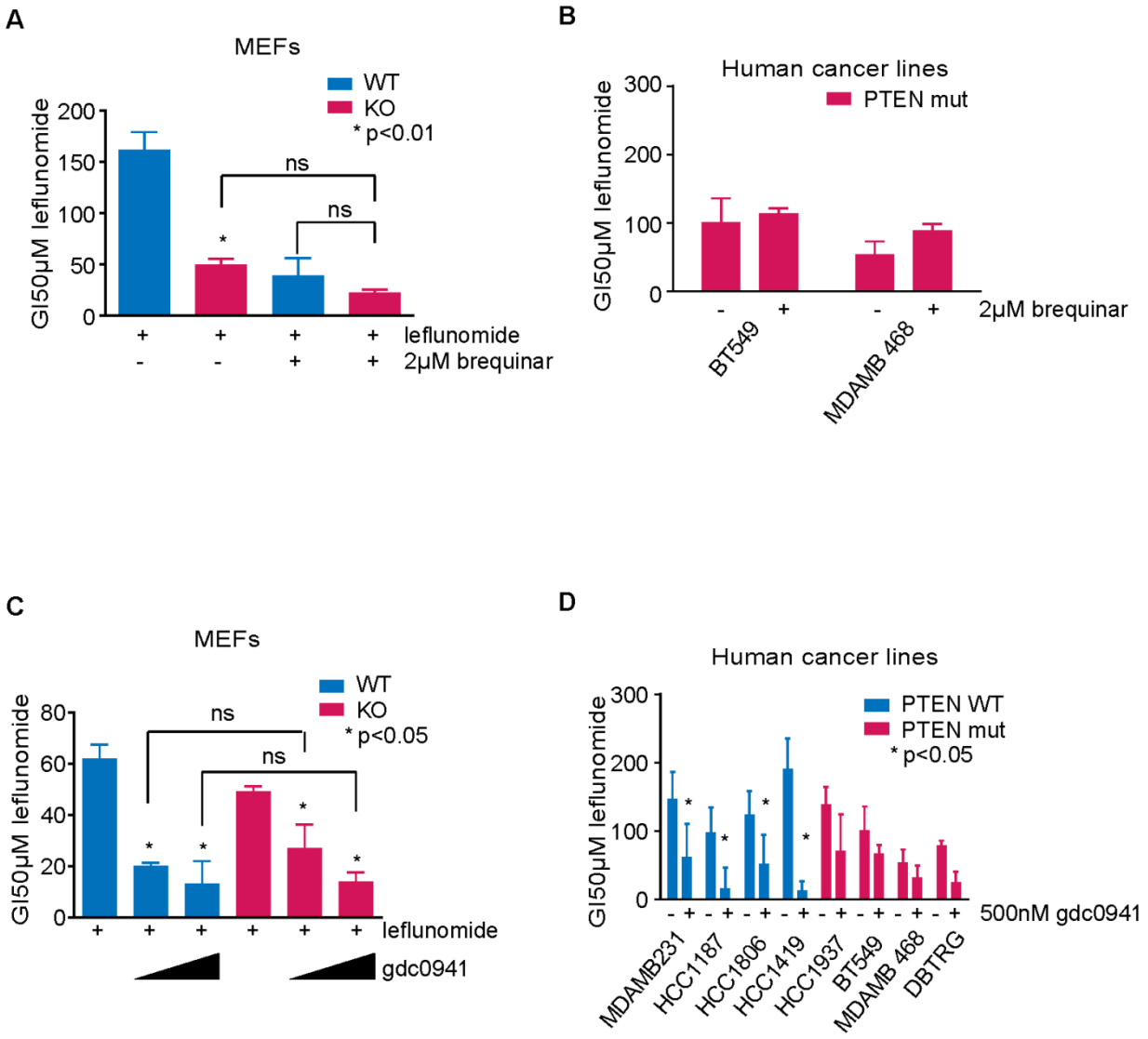
A
MEFs
WT
KO
* p<0.01
GI50μM leflunomide
200
150
100
50
0
ns
ns
*
+ + + + leflunomide
- - + + 2μM brequinar
B
Human cancer lines
PTEN mut
GI50μM leflunomide
300
200
100
0
- + - + 2μM brequinar
BT549
MDAMB 468
C
MEFs
WT
KO
* p<0.05
GI50μM leflunomide
80
60
40
20
0
ns
ns
+ + + + + + leflunomide
gdc0941
D
Human cancer lines
PTEN WT
PTEN mut
* p<0.05
GI50μM leflunomide
300
200
100
0
- + - + - + - + - + - + - + - + 500nM gdc0941
MDAMB231
HCC1187
HCC1806
HCC1419
HCC1937
BT549
MDAMB 468
DBTRG

Figure 3.15

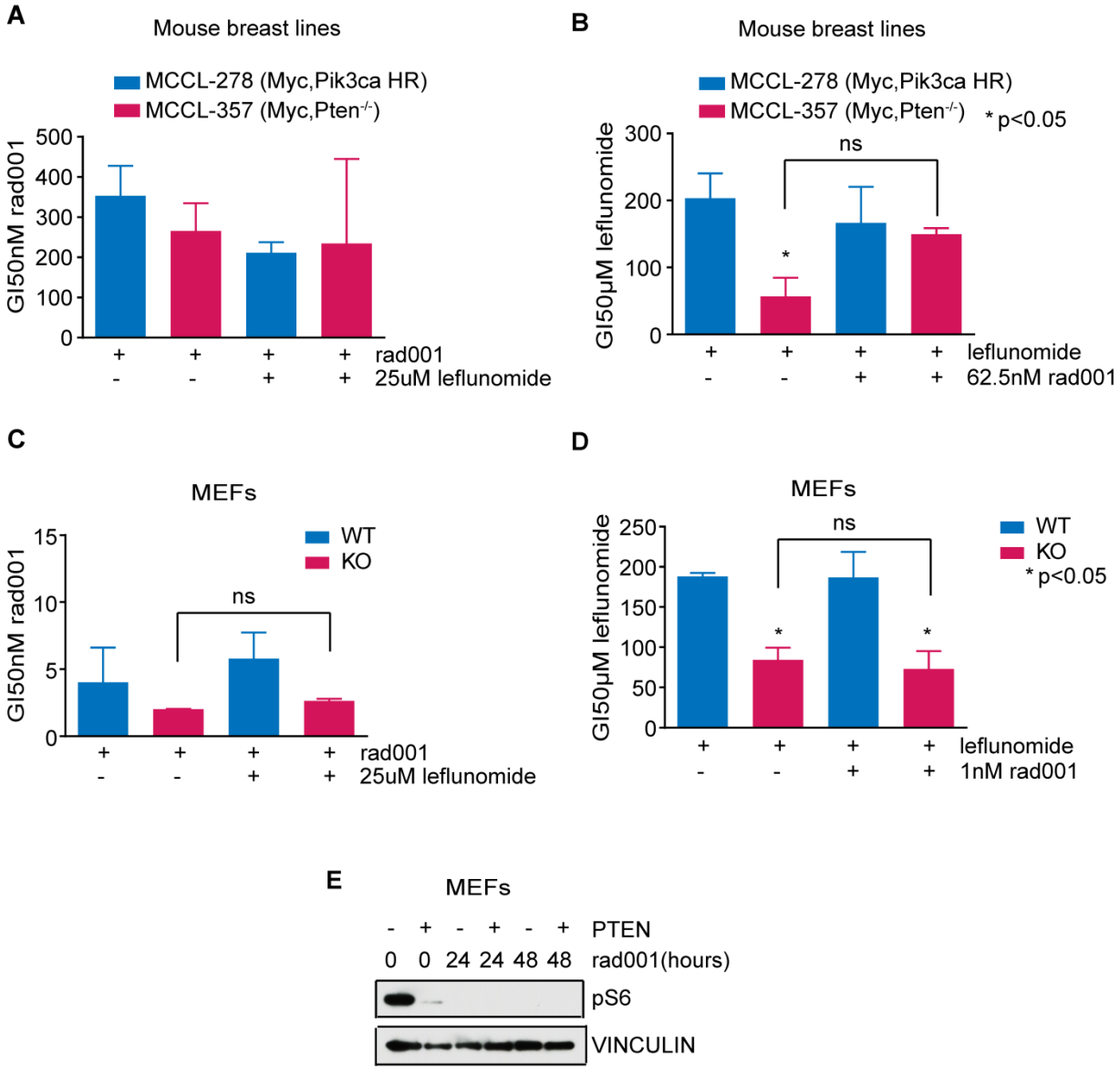
A
Mouse breast lines
MCCL-278 (Myc,Pik3ca HR)
MCCL-357 (Myc,Pten-/-)
GI50nM rad001
500
400
300
200
100
0
+ + + + rad001
- - + + 25uM leflunomide
B
Mouse breast lines
MCCL-278 (Myc,Pik3ca HR)
MCCL-357 (Myc,Pten-/-)
* p<0.05
GI50μM leflunomide
300
200
100
0
ns
*
+ + + + leflunomide
- - + + 62.5nM rad001
C
MEFs
WT
KO
GI50nM rad001
15
10
5
0
ns
+ + + + rad001
- - + + 25uM leflunomide
D
MEFs
WT
KO
* p<0.05
GI50μM leflunomide
250
200
150
100
50
0
ns
*
*
+ + + + leflunomide
- - + + 1nM rad001
E
MEFs
- + - + - + PTEN
0 0 24 24 48 48 rad001(hours)
pS6
VINCULIN

Figure 3.16

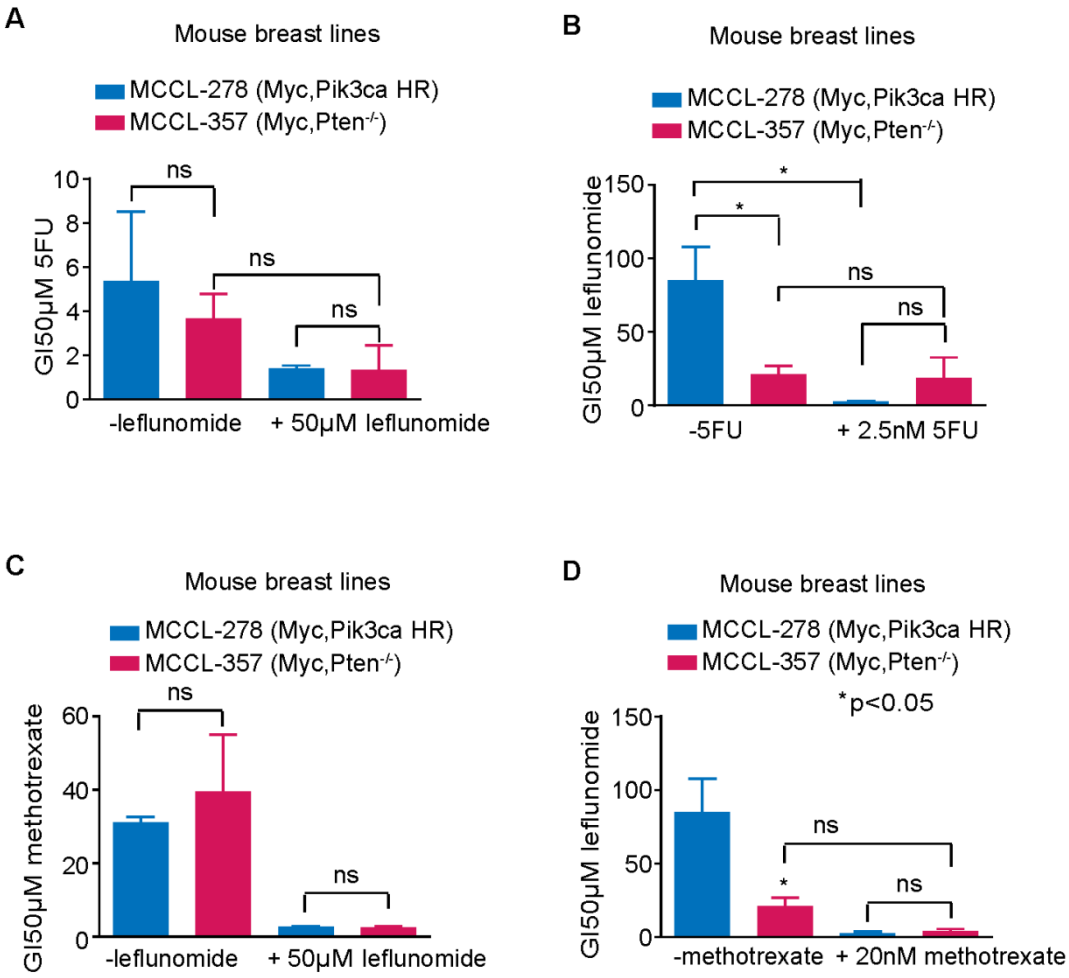
A
Mouse breast lines
MCCL-278 (Myc,Pik3ca HR)
MCCL-357 (Myc,Pten-/-)
GI50μM 5FU
10
8
6
4
2
0
ns
ns
ns
-leflunomide
+ 50μM leflunomide
B
Mouse breast lines
MCCL-278 (Myc,Pik3ca HR)
MCCL-357 (Myc,Pten-/-)
GI50μM leflunomide
150
100
50
0
*
*
ns
ns
-5FU
+ 2.5nM 5FU
C
Mouse breast lines
MCCL-278 (Myc,Pik3ca HR)
MCCL-357 (Myc,Pten-/-)
GI50μM methotrexate
60
40
20
0
ns
ns
-leflunomide
+ 50μM leflunomide
D
Mouse breast lines
MCCL-278 (Myc,Pik3ca HR)
MCCL-357 (Myc,Pten-/-)
*p<0.05
GI50μM leflunomide
150
100
50
0
ns
*
ns
-methotrexate
+ 20nM methotrexate

Figure 3.17

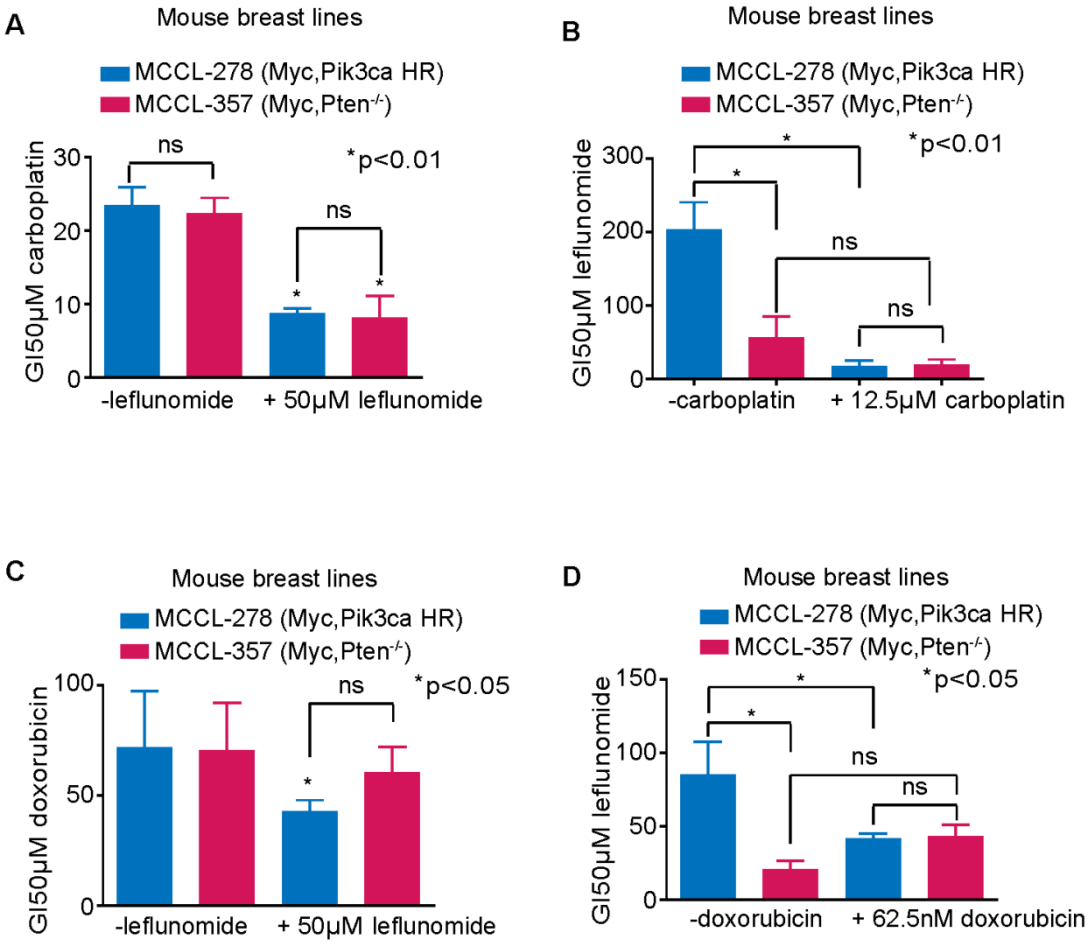
A
Mouse breast lines
MCCL-278 (Myc,Pik3ca HR)
MCCL-357 (Myc,Pten-/-)
GI50μM carboplatin
30
20
10
0
ns
*p<0.01
ns
*
*
-leflunomide
+ 50μM leflunomide
B
Mouse breast lines
MCCL-278 (Myc,Pik3ca HR)
MCCL-357 (Myc,Pten-/-)
GI50μM leflunomide
300
200
100
0
*
*
*p<0.01
ns
ns
-carboplatin
+ 12.5μM carboplatin
C
Mouse breast lines
MCCL-278 (Myc,Pik3ca HR)
MCCL-357 (Myc,Pten-/-)
GI50μM doxorubicin
100
50
0
ns
*p<0.05
*
-leflunomide
+ 50μM leflunomide
D
Mouse breast lines
MCCL-278 (Myc,Pik3ca HR)
MCCL-357 (Myc,Pten-/-)
GI50μM leflunomide
150
100
50
0
*
*
*p<0.05
ns
ns
-doxorubicin
+ 62.5nM doxorubicin

Figure 3.18

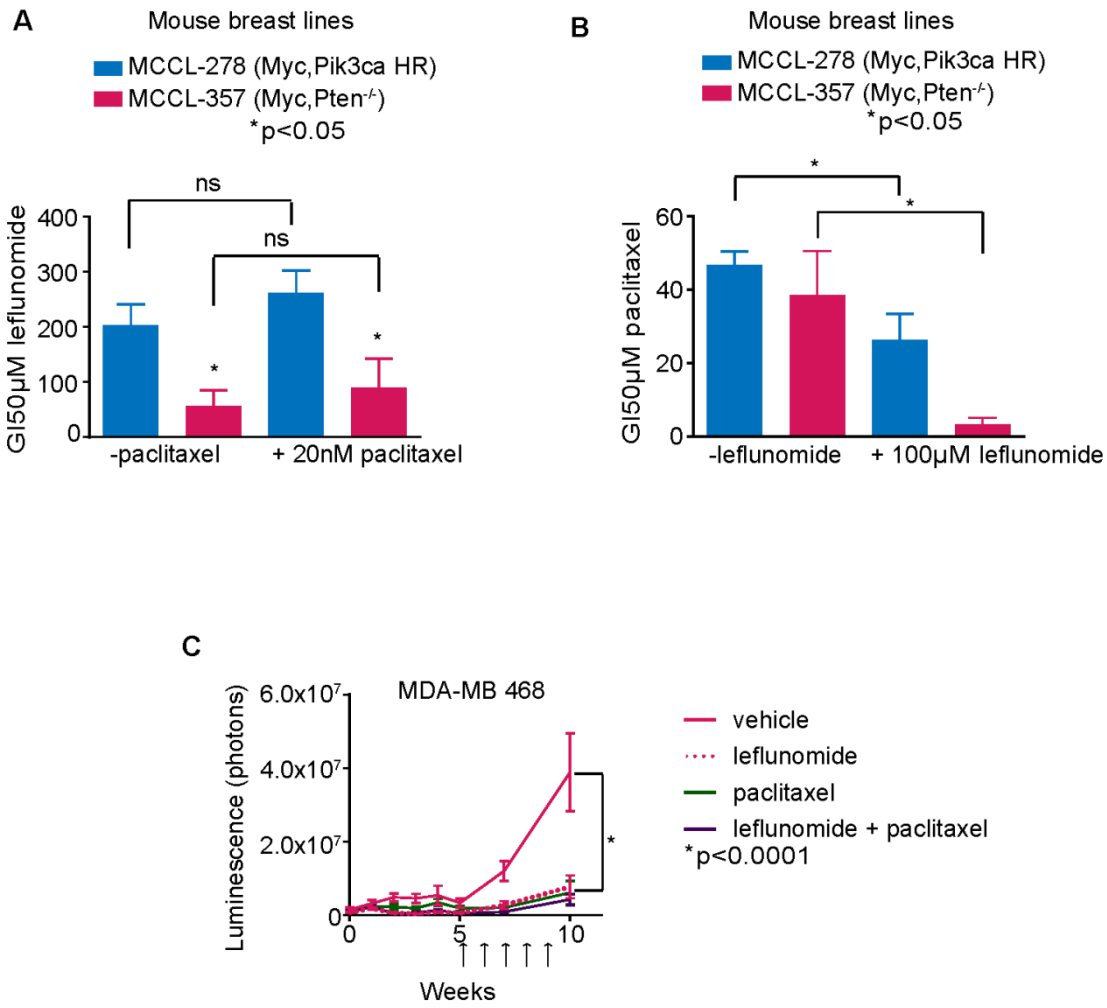
A
Mouse breast lines
MCCL-278 (Myc,Pik3ca HR)
MCCL-357 (Myc,Pten-/-)
*p<0.05
ns
ns
*
*
GI50μM leflunomide
400
300
200
100
0
-paclitaxel
+ 20nM paclitaxel
B
Mouse breast lines
MCCL-278 (Myc,Pik3ca HR)
MCCL-357 (Myc,Pten-/-)
*p<0.05
*
*
GI50μM paclitaxel
60
40
20
0
-leflunomide
+ 100μM leflunomide
C
MDA-MB 468
Luminescence (photons)
6.0x10^7
4.0x10^7
2.0x10^7
0
0
5
10
Weeks
*
vehicle
leflunomide
paclitaxel
leflunomide + paclitaxel
*p<0.0001

Figure 3.19

Chapter 4: Mechanism of Death

In the previous chapter we discovered the vulnerability of PTEN-deficient cells to DHODH inhibition due to dependence on the *de novo* pyrimidine synthesis pathway. These data raised the following question: upon DHODH inhibition, what is occurring downstream to drive cell death? As mentioned in the introductory chapter, the PTEN pathway can affect cell cycle regulation and DNA damage. The majority of this chapter will expand upon these concepts, and will pertain to how DNA damage and a deficient checkpoint response induces synthetic lethality upon DHODH inhibition.

Introduction

Cell cycle checkpoints

It is important for a cell to ensure that DNA integrity is intact prior to cell division, including checking for errors in replication and chromosome segregation. Cell cycle checkpoint pathways assess the level of DNA damage, and regulate cell cycle progression (Elledge 1996). The G0 phase consists of non-replicating cells; interphase consists of the G1, S, and G2 phases and is followed by mitosis and cytokinesis.

Injury to a cell's DNA through ionizing radiation, DNA-intercalating agents, or induction of stalled replication such as by ultraviolet light normally instigates checkpoints. Checkpoint activation can be through the kinases ATM (ataxia telangiectasia mutated) or ATR (ataxia telangiectasia and Rad3-related protein). It is generally considered that ATM is activated by double strand breaks (such as those caused

by ionizing radiation) and ATR by stalled replication or chemotherapeutics, but there can be overlap in the signaling pathways between the two (Bartek and Lukas 2003).

Since nucleotide inhibition can cause stalled replication, we focus here primarily on ATR, the activation of which is dependent on two signals. The first signal is replication protein A (RPA), which coats single stranded DNA and recruits ATRIP (ATR interacting protein). ATR-ATRIP binding allows ATR to associate with DNA (Zou and Elledge 2003). The second signal is via TOPBP1 (DNA Topoisomerase II-Binding Protein 1), which is involved in normal DNA replication and binds to DNA gaps and breaks. TOPBP1 also induces the kinase activity of ATR, and is required for the ability of ATR to phosphorylate its downstream effectors (Kumagai, Lee et al. 2006). Thus, the integration of RPA and TOPBP1 signals yields recruitment and activation of ATR.

Downstream of operational ATR is the activation of the checkpoint protein CHK1; phosphorylation on S317 by ATM and S345 by ATR activates the protein to carry out its function in halting cell cycle progression (Liu, Guntuku et al. 2000, Zhao and Piwnica-Worms 2001, Gatei, Sloper et al. 2003), allowing proper DNA repair (which itself is mediated by numerous proteins). Cells without CHK1 have been shown to have defects in the S and G2 checkpoints after insult with ionizing radiation (Zhao, Watkins et al. 2002).

Hydroxyurea is an inhibitor of ribonucleotide reductase, an enzyme that converts ribonucleotides to deoxyribonucleotides for synthesis of DNA; this drug can therefore cause stalled replication (Yarbro 1992). Depletion of nucleotide pools by hydroxyurea activates the ATR checkpoint at replication forks in

S-phase cells, and treatment with hydroxyurea in cells with CHK1 knockdown increased DNA damage and cell death (Tibbetts, Cortez et al. 2000, Cho, Toouli et al. 2005). Toledo et al showed that ATR normally restrains origin firing to preserve adequate amounts of RPA, and that cells treated with hydroxyurea and an ATR inhibitor had an excess of single-stranded DNA due to unrestrained origin firing and stalled forks. This exhausted the RPA pool, leading to a conversion of stalled forks to double strand breaks and triggering replication catastrophe (Toledo, Altmeyer et al. 2013).

The PTEN pathway and checkpoint regulation

While there is considerable literature about the role of PTEN in DNA damage and checkpoint signaling, some of it is conflicted. Shen et al proposed that Pten is localized at centromeres in order to contribute to DNA stability. The authors showed that mutants of the C-terminal of Pten caused loss of robustness of centromeres in MEFs, and that *Pten*$^{-/-}$ MEFs had more DNA breaks and less RAD51, an important protein in double strand break repair (Shen, Balajee et al. 2007). However, a contradictory paper by Gupta et al did not find any compelling DNA-Pten interaction in WT MEFs or difference in ATM activation, RAD51 expression, or homologous repair, even when the cells were treated with ionizing radiation. The authors of this paper claim that the increase in DNA damage in Pten deficient cells is not due to defects in repair but rather due to aberrant cell cycle checkpoints. They found that a CHK1 inhibitor only affected WT cells in terms of chromosomal abnormalities, suggesting that *Pten*$^{-/-}$ cells were already deficient in functional CHK1. To further support their hypothesis, the authors found that *Pten*$^{-/-}$ cells bypassed taxol-induced mitotic arrest, indicating that the real crisis may be that these cells do not have enough time for proper repair before cell division (Gupta, Yang et al. 2009). Additional evidence showed a lack of differential RAD51 expression or homologous recombination between PTEN WT and mutant prostate cancer lines (Fraser, Zhao et al. 2012).

A paper by Bassi et al may help resolve the conflict. The authors found that RAD51 is still expressed in in PTEN mutant cells, but is not recruited to sites of damage as well as in PTEN WT cells. The authors also demonstrate that SUMO-PTEN (localized to the nucleus) is needed for homologous recombination repair of double stranded breaks. Furthermore, it was shown that PTEN is phosphorylated by ATM and that mutation of this phosphorylation site prevented nuclear exclusion of SUMO-PTEN. There was both less nuclear PTEN in cells exposed to genotoxic stress due to ATM activation, and cells were more sensitive to this stress when PTEN was consequently absent from the nucleus (Bassi, Ho et al. 2013).

PTEN has also been shown to interact with RPA in isogenic HCT116 cell lines. PTEN may stabilize RPA by binding both RPA and a deubiquitinase to prevent proteasomal degradation of RPA; stabilization of RPA would then protect DNA. RPA and PTEN are often co-lost in colorectal carcinoma, and tumors were more poorly differentiated in in RPA heterozygous mice compared to WT in a colon cancer mouse model (Wang, Li et al. 2015).

Interestingly, AKT has been shown to phosphorylate TOPBP1 on its S1159 site, allowing TOPBP1 to oligomerize and suppress E2F1 (E2F Transcription Factor 1)-mediated apoptosis (Liu, Paik et al. 2006). This process simultaneously inhibits the ability of TOPBP1 to activate ATR in the checkpoint response, by preventing its recruitment to chromatin in favor of its other function. The phosphorylation and ensuing oligomerization state of TOPBP1 is therefore a regulatory switch for its roles in transcriptional regulation and response to replication stress (Liu, Graves et al. 2013).

PTEN and the PI3K pathway have also been directly linked to CHK1. Literature shows that *Pten*$^{-/-}$ cells have a partially defective checkpoint upon exposure to ionizing radiation, and that AKT phosphorylates CHK1 on its S280 site causing it to be ubiquitinated and localized to the cytoplasm (King, Skeen et al. 2004, Puc, Keniry et al. 2005). This led to increased aneuploidy in PTEN mutant primary breast carcinomas (Puc, Keniry et al. 2005). A subsequent paper by Puc et al found that K274 is the ubiquitination site on CHK1 that follows S280 phosphorylation, and mutation to K274R eliminated ubiquitination of CHK1 and increased its nuclear localization. The authors further concluded that inhibition of CHK1 function due to PTEN loss causes double stranded breaks (Puc and Parsons 2005).

Results

Using the above information as a framework for our studies, we can further our understanding of the cell death mechanisms in play in PTEN mutant cells upon inhibition of DHODH.

DNA damage

It is logical that a blockade of pyrimidine synthesis would stop cells from dividing, as the cells would no longer have the requisite nucleotides for DNA replication. As discussed in chapter 3, leflunomide has in fact been previously established as a cytostatic drug (Greene, Watanabe et al. 1995, Rückemann, Fairbanks et al. 1998). What is more enigmatic, however, is why DHODH inhibition would cause *PTEN*$^{-/-}$ cells to die. What is inducing cytotoxicity, and why is this specific to PTEN-deficient cells?

Based on the literature discussed above, we hypothesized that the answer may lie within checkpoint pathway defects. To solve this mystery, we had a couple of clues. First, we observed that *Pten*$^{-/-}$ MEFs

had a higher level of the DNA-damage indicator gamma-H2AX, consistent with prior reports (Fig. 4.1A). (DNA damage is followed by phosphorylation of the histone H2AX, which in its phosphorylated form is called gamma-H2AX.) We hypothesized that the dearth of pyrimidine deoxynucleotides caused by DHODH inhibition would exacerbate this defect, and indeed discovered that leflunomide (or A771726) augmented DNA damage to a significantly greater degree in PTEN-deficient cells compared to PTEN WT (Fig. 4.1B-F). Furthermore, gamma-H2AX co-localized with replication forks labeled with EdU, indicating that the source of damage was originating at (or very close to) sites of DNA replication (Fig. 4.2A). Leflunomide-induced DNA damage was rescued by uridine, demonstrating that damage is likely instigated by pyrimidine depletion (Fig. 4.2B).

Our second clue concerned the number of replication forks per cell. Recall from chapter 2 that *Pten*$^{-/-}$ MEFs had a greater number of replication forks per cell compared to WT MEFs as measured by EdU (Fig. 2.5). We also see a greater EdU signal in MCCL-357 (Myc, Pten$^{-/-}$) than in MCCL-278 (Myc, Pik3ca H1047R) cells (Fig. 4.3A). Interestingly, the greater number of replication forks in Pten$^{-/-}$ cells remained intact after 24h of treatment with leflunomide, showing that the cells continue to replicate despite the presence of DNA damage (Fig. 4.3B-D). We initially expected the number of replication forks to decrease upon leflunomide treatment, since we are blocking nucleotide synthesis. However, while initially counterintuitive, these data demonstrate that *Pten*$^{-/-}$ cells are not properly sensing the blockade of pyrimidines, and attempting to continue growth as usual; it reasonably follows that this will lead to problems.

ATR pathway defects

Since depletion of nucleotide pools normally activates the ATR checkpoint, we next examined whether there could be defects in ATR signaling leading to inappropriate growth signals.

As discussed above, ATR checkpoint activation at stalled forks requires both RPA interaction with single-strand DNA to recruit the ATRIP-ATR complex, and TOPBP1 interaction with the ATR activation domain so that ATR is functional and can activate CHK1. We investigated each part of this pathway.

First, we inspected the interaction of RPA and gamma-H2AX by flow cytometry. This dual-staining created a quadrant of possible outcomes: cells with low RPA and low gamma-H2AX, low RPA and high gamma-H2AX, high RPA and low gamma-h2AX, or high RPA and high gamma-H2AX. We found that at early time points an increase in RPA signal was achieved in the presence of A771726 treatment regardless of *PTEN* genotype. In this setting, the population of cells shifted from low RPA and low gamma-H2AX in the untreated condition to high RPA and low gamma-H2AX in the short-term treated condition. At later time points, this was followed by a shift toward both high RPA and high gamma-H2AX-positive cells in *Pten*$^{-/-}$ MCCL-357 but not in *Pten* WT MCCL-278 cells. The RPA signal in *Pten* WT cells declined after sustained treatment, while *Pten*$^{-/-}$ cells maintained the RPA signal and gained the high gamma-H2AX signal (Fig. 4.4A). Moreover, gamma-H2AX appeared almost exclusively in RPA-positive MCCL-357 cells treated with A771726; there were negligible cells in the low RPA high gamma-H2AX quadrant at any time point (Fig. 4.4B).

From these data, we learned that 1) DHODH inhibition initially triggers RPA loading regardless of *Pten* status, 2) *Pten* WT cells lose RPA signal despite sustained treatment while 3) *Pten*$^{-/-}$ cells continue loading RPA and start presenting gamma-H2AX, and 4) gamma-H2AX only occurs after RPA loading in this setting. We surmise that nucleotide depletion triggers RPA in any cell, but only *Pten*$^{-/-}$ cells compared to PTEN WT cells exhibit significant damage. It is likely that a defect in ATR signaling is downstream of RPA.

We next investigated the second signal required to activate ATR: TOPBP1. As mentioned above, AKT phosphorylation of TOPBP1 on serine 1159 inhibits its ATR-activating function by preventing its recruitment to DNA. We indeed found greater TOPBP1 S1159 phosphorylation and concomitantly less TOPBP1 localization to replication forks in *Pten*$^{-/-}$ cells compared to *Pten* WT cells (Fig. 4.5A-C). Interestingly, TOPBP1 localization in WT cells increased initially upon leflunomide treatment but then declined, similar to its RPA pattern. Diminished AKT activity through PI3K inhibition reduced both phospho-TOPBP1 levels and leflunomide-induced DNA damage (Fig. 4.5D-E). It is likely that *Pten*$^{-/-}$ cells cannot properly activate ATR due to a lack of TOPBP1 signal. Therefore, when faced with DHODH inhibition, the ATR pathway activated in *Pten* WT cells is abruptly halted in *Pten*$^{-/-}$ cells.

If phosphorylated TOPBP1 leads to deficient ATR activation in PTEN mutant cells, CHK1 would not be properly activated due to insufficient functional ATR. Additionally, as mentioned above, AKT phosphorylation of CHK1 on serine 280 is inhibitory, and prior work from our lab showed increased CHK1 serine 280 phosphorylation and consequent reduced CHK1 activity in PTEN$^{-/-}$ cells compared to WT cells. We measured the active CHK1 signal in our cells and found that A771726 triggered ATR phosphorylation of CHK1 at serine 345 at early time points in *Pten* WT cells, and this activation of CHK1 declined as RPA declined suggesting that *Pten* WT cells eventually recovered from DHODH inhibition.

(The recruitment and then decline of TOPBP1 localization to replication forks also suggests recovery in WT cells.) Conversely, *Pten*$^{-/-}$ cells activated CHK1 to a much lesser extent upon A771726 treatment (Fig. 4.6A-B). Thus, *Pten*$^{-/-}$ cells appear to be incapable of generating an appropriate activation of the ATR-CHK1 checkpoint at replication forks, and instead accumulated damage at 18h.

By 48h this genomic stress manifested in a greater number of chromosome gaps, breaks, and multiradial formations in MCCL-357 cells treated with A771726 compared to MCCL-278 cells (Fig. 4.6C-F). These findings are reminiscent of the sensitivity to hydroxyurea that occurs in the setting of an ATR inhibitor (Toledo, Altmeyer et al. 2013).

To test that our proposed mechanism is indeed the method by which cell death is induced, we transfected PTEN mutant cells with TOPBP1 and CHK1 mutants incapable of being phosphorylated by AKT (S1159A and S280A, respectively). These mutants rescued DNA damage and cell death in leflunomide-treated PTEN mutant cells, demonstrating that the synthetic lethality between pyrimidine depletion and mutation of PTEN is due to the AKT-mediated defects in the ATR pathway (Fig. 4.7A-B). The AKT-dependence of this mechanism of toxicity explains why *Pten*$^{-/-}$ cells were more sensitive to DHODH inhibition than *Pik3ca* mutant cells — as shown in chapter 3, phosphorylated AKT is higher in *Pten*$^{-/-}$ cells compared to *Pik3ca* mutant cells, especially in the nucleus.

The actual induction of death could be mediated by multiple known cell death mechanisms downstream of DNA damage, such as mitotic catastrophe or apoptosis. Mitotic catastrophe is defined by a cell's premature entry into mitosis without proper DNA repair, consistent with our hypothesis. It is also

characterized by abnormal nuclei, polyploidy, and mitotic abnormalities, all of which were observed in *Pten*$^{-/-}$ cells (but not Pten WT cells) upon A771726 treatment. Mitotic catastrophe can be followed by apoptosis or can be an independent cell death mechanism. We did observe apoptosis in *Pten*$^{-/-}$ MEFs upon treatment with leflunomide, as detected by cleaved caspase 3 (Fig. 4.7C). Interestingly, DNA damage triggered by the same event can elicit completely different modes of death in different cells, and it is not clear why one method will be used over another in a given cell (Surova and Zhivotovsky 2013). We suspect that more than one operation of death occurs in our model.

Based on our data, we propose that inhibition of DHODH in PTEN deficient cells first causes stalled forks due to inadequate nucleotide pools required to support increased replication, and that sustained treatment leads to insufficient ATR activation due to AKT phosphorylation of TOPBP1 and CHK1, leading to a buildup of DNA damage and cell death. PTEN WT cells do not exhibit this dependency on pyrimidine synthesis and have fewer replication forks per cell. In PTEN WT cells, treatment initially increased the RPA signal and triggered transient phosphorylation of CHK1, while longer treatment led to abated RPA with little concurrent increase in gamma-H2AX, explaining the largely unaffected WT population upon DHODH inhibition. While Pik3ca mutant cells also exhibit AKT signaling, their relative resistance to DHODH inhibitors suggests that a PI3K signaling dosage-effect due to their lower level of AKT activation as compared to PTEN mutant cells may be important (Fig. 4.8).

Alternate hypotheses

In an effort to be thorough, we also investigated potential alternate explanations beyond the hypothesis described above for the specific toxicity to DHODH inhibition in PTEN deficient cells. The first possibility is death by UPR (unfolded protein response).

The unfolded protein response (Chang, Kamata et al.) is a built-in stress response in cells. Stress to the endoplasmic reticulum (ER) in the form of accumulated misfolded proteins initiates the UPR, including activation of signaling protein IRE1 (inositol-requiring enzyme 1). IRE1 splices an intron from *XBP-1*, generating active XBP-1 which transcribes genes involved in the transport and degradation of misfolded proteins (Xu 2005). However, prolonged ER stress leads to apoptosis by several proposed mechanisms (Sano and Reed 2013). There is evidence that the PTEN pathway affects the UPR: cells with active AKT have increased levels of ENTPD5 (Ectonucleoside Triphosphate Diphosphohydrolase 5), an endoplasmic reticulum protein. ENTPD5 hydrolyzes UMP to UDP, causing increased N-glycosylation and proper protein folding in the ER. Knockdown of ENTPD5 in PTEN-deficient cells has been shown to cause ER stress, triggering the UPR and apoptosis (Shen, Huang et al. 2011). We hypothesized that if DHODH inhibition depletes the pool of UDP, it could have the same effect as an ENTPD5 knockdown.

We therefore measured levels of CHOP10 (GADD153) and ATF4 (CREB2), proteins that are upregulated upon ER stress and are involved in its apoptotic response (Xu, Bailly-Maitre et al. 2005). There was no difference between $Pten^{-/-}$ or WT cells in the levels of either of these proteins at baseline nor upon treatment with leflunomide. However, treatment with Brefeldin A, a known inducer of ER stress that was used as a positive control (Oslowski and Urano 2011) increased ER stress to a greater degree in $Pten^{-/-}$ cells (Fig. 4.9A).

The second possibility we explored is PARP-mediated cell death. Poly ADP-ribosylation (PARylation) of proteins by poly(ADP-ribose) polymerases (PARPs) can occur after DNA damage. PARP can bind to both single and double stranded DNA breaks, and may help recruit DNA repair proteins. Somewhat

paradoxically, while low levels of DNA damage causes PARP to initiate repair, high levels of DNA damage can cause PARP to promote cell death (Kim, Zhang et al. 2005). We hypothesized that high levels of DNA damage caused by leflunomide could lead to PARP-mediated cell death. The PARP inhibitor AZD2218 did partially rescue leflunomide-induced cell death in MCC-357 cells, but did not in another $Pten^{-/-}$ cell line (Fig. 4.9B-C). Therefore, our data do not support PARP-mediated cell death as a key mechanism of death in the setting of DHODH inhibition in PTEN deficient cells.

Discussion

In this section, we discovered that DHODH inhibition kills PTEN-deficient cells in a synthetically lethal manner. First, DHODH inhibition obstructs a pathway that PTEN mutant cells are dependent on for growth and sufficient support of DNA replication. Second, the inherent ATR and CHK1 defects in PTEN-deficient cells are exploited, crashing the system and causing cell death. To our knowledge, this is the first time specific nutrient dependency induced by PTEN loss has been mechanistically linked to DNA damage and checkpoint defects, intersecting at the inhibition of a metabolic pathway.

There are a few points in regards to our data that should be noted.

The rescue of DNA damage by TOPBP1 and CHK1 mutants in leflunomide-treated PTEN mutant cells was not 100%, and this is likely because the WT TOPBP1 and CHK1 proteins were still present in the cells. It is also of course possible that the checkpoint defect mechanism is the primary but not only source of toxicity in pyrimidine-depleted PTEN mutant cells.

While our data seem largely consistent with prior knowledge in the field, there are a few points of contention. There is evidence in the literature that PTEN mutant cells have less RAD51 expression and recruitment, leading to a deficiency in homologous recombination repair and a resulting sensitivity to PARP inhibitors (Mendes-Pereira, Martin et al. 2009). Our results do not reflect this sensitivity; we see either no effect or a protective effect of PARP inhibition in leflunomide-treated PTEN mutant cells (although we have not tried PARP inhibition alone). Since there was variability in response among our cell lines, perhaps the effects of PARP on PTEN mutant cells is context- and cell line-dependent. Additionally, the sensitivity to PARP inhibition was observed in isogenic HCT116 and HEC1A lines, which — as we described in chapter 2 — may not always be reliable for mechanistic studies.

There are also a couple of papers that may not be fully consistent with our findings. One paper reports that loss of PTEN leads to an inability to continue the cell cycle after replication stress (Martin and Ouchi 2008). Contrary to other reports, the authors show that loss of CHK1 prevents cell cycle progression, while other literature shows that loss of CHK1 leads to progression through S/G2 (Zhao, Watkins et al. 2002). Martin et al further state that activation of CHK1 on S317 after stalled replication induces phosphorylation of PTEN on T383 to promote cellular reentry into G2/M, and that WT PTEN but not a T383A mutation leads to cell cycle recovery (Martin and Ouchi 2008). It is unclear whether this could be consistent with our data: S317 is the ATM activation site, which we did not explore, and replication stress in the paper was induced by hydroxyurea which we also did not use. However, we show that loss of PTEN without replication stress increases proliferation, and that adding DHODH inhibitors does not affect the number of replication forks. This paper could possibly be reconciled with our results if the effects of different replication stressors causes PTEN to switch functions between promotion and hindrance of the cell cycle.

An additional report found that *PTEN* deletion led to impairment of both replication fork progression and recovery from stalled forks. However, the authors also report that PTEN loss causes a premature exit from S phase and increased anaphase bridges and endogenous replication stress. The authors claim that PTEN is needed to restart replication after a stalled fork (He, Kang et al. 2015). We see a higher number of replication forks in PTEN deficient cells; while it is possible that progression at these forks is impaired, this is not likely due to the faster growth rate of *Pten*$^{-/-}$ cells. Our data is consistent, however, with their findings of premature S-phase exit which may contribute to cellular death after DHODH inhibition.

Consistent with our findings are reports that show high AKT activity in G2/M, which can be caused by PTEN loss, and accumulation of mutations instead of apoptosis in mutagen-exposed cells with activated AKT (Kandel, Skeen et al. 2002, Shtivelman, Sussman et al. 2002). The studies further show that inhibition of PI3K induced apoptosis at this cell cycle transition and activated CHK1 (Shtivelman, Sussman et al. 2002). An additional report discussed in the introductory chapter also showed that WT PTEN induces G1 arrest (Weng, Brown et al. 2001). It is clear that the role of PTEN in replication and the cell cycle is not completely agreed upon, and we hope that our findings shed some light on PTEN's effect on growth at baseline and on checkpoint activation under stress from DHODH inhibition.

We did not uncover any effects on UPR with DHODH inhibition. However, our data with Brefeldin A suggest that PTEN may be protective against ER stress, and there could therefore be a non-DHODH mediated mechanism of inducing UPR-mediated death in PTEN mutant cells. Understanding the effects of ER stress inducers on cancer cell lines with PTEN mutations would reveal whether there could be

another potential cancer therapy option in this regard. There is, however, the danger of increasing ER stress in normal cells and having a detrimental effect in patients.

It would be interesting to see the effects of DHODH inhibition on cells with BRCA1 mutations, which are commonly found in breast cancer. BRCA1 is also downstream of ATR and is recruited as a DNA repair protein (Tibbetts, Cortez et al. 2000). It is possible that cells with both PTEN and BRCA1 mutations would be more sensitive to DHODH inhibition, since the ATR pathway would be even more disrupted. On the other hand, it is possible that there will be no effect if there is redundancy in the defect.

Even without DNA damage, ATM and ATR control origin firing. Shechter et al found that inhibition of ATM and ATR with caffeine or antibodies led to a rapid increase in the number of origins, perhaps due to the regulation of S-phase-promoting kinase (SPK) (Shechter, Costanzo et al. 2004). The inherent ATR defects in PTEN mutant cells due to AKT-mediated phosphorylation of TOPBP1 could therefore explain why we see a naturally higher number of replication forks in PTEN deficient cells. Bringing our data full circle, our exploration of the events leading to cell death following DHODH inhibition in PTEN mutant cells may have uncovered the fundamental cause of increased replication in these cells. We explore this concept further in the next and final chapter of the thesis.

CHAPTER 4 FIGURE LEGENDS AND FIGURES

Figure 4.1. DNA damage is exacerbated by DHODH inhibition. (A) Cells were labeled with a gamma-H2AX antibody. Flow cytometry determined the mean fluorescence intensity (MFI) of gamma-H2AX signal, indicating the level of gamma-H2AX in the cells (Student's *t*-test, *p<.05, n=3). (B-F) Cells treated with 100μM leflunomide or A771726 overnight were labeled with a gamma-H2AX antibody. Flow cytometry determined the mean fluorescence intensity (MFI) of gamma-H2AX signal in each condition (Student's *t*-test, *p-values on figures, n=3).

Figure 4.2. The source of DNA damage. (A) MEFs were treated with 150μM A771726 for 24h, and labeled with an EdU-binding fluorescent tag and gamma-H2AX antibody following a 45min EdU pulse. Left: representative confocal microscopy images. Right: quantified EdU and gamma-H2AX colocalized foci per cell (Student's *t*-test, *p<.05, n=3). (B) Cells were treated with 100μM leflunomide with or without uridine and labeled with a gamma-H2AX antibody. Flow cytometry determined the mean fluorescence intensity (MFI) of gamma-H2AX signal in each condition (Student's *t*-test, *p-values on figures, n=3).

Figure 4.3. The status of replication forks upon DHODH inhibition. (A) Cells were pulsed with EdU for 45min, and labeled with an EdU-binding fluorescent tag following fixation. Flow cytometry determined the mean fluorescence intensity (MFI) of EdU signal, indicating the amount of EdU incorporation in cells (Student's *t*-test, *p<.05, n=3). (B) MEFs were treated with 100μM leflunomide or control for 48h, pulsed with EdU for 45min prior to fixation, and were labeled with an EdU-binding fluorescent tag. Left: representative confocal microscopy images. Right: quantification of the number of EdU foci per cell (Student's *t*-test, p>.05, n=6). (C) Images in Fig. 4F were used to quantify the percent of cell area covered by EdU staining, a metric used to normalize foci to cell size to ensure that cell size is not a confounding factor (Student's *t*-test, p>.05, ns not significant, n=6). (D) MEFs were treated with 100μM

leflunomide or control for 48 hours, pulsed with EdU for 45min prior to fixation, and were labeled with an EdU-binding fluorescent tag. Flow cytometry determined the MFI of EdU signal among cells positively stained for EdU, to measure the difference in EdU incorporation in replicating cells in each condition (Student's *t*-test, p>.05, n=3).

Figure 4.4. RPA and DNA damage. Cells were treated with 150μM A771726 for times indicated and labeled with antibodies to RPA and gamma-H2AX. Flow cytometry determined the percentage of the cell population positively-stained for (A) RPA alone ("high RPA") or both RPA and gamma-H2AX ("high RPA + high gamma-H2AX"), or (B) the percentage of cells positively-stained for gamma-H2AX and negatively-stained for RPA ("low RPA + high gamma-H2AX"). (Student's *t*-test, *p-values on figures, n=4).

Figure 4.5. Localization and phosphorylation of TOPBP1. (A) Cells were labeled with a pTOPBP1 S1159 antibody. Flow cytometry determined the mean fluorescence intensity (MFI) of pTOPBP1 signal (Student's *t*-test, *p<.01, n=3). (B) MEFs were treated with 100μM leflunomide for times indicated, pulsed with EdU for 45min, and labeled with an EdU-binding fluorescent tag and TOPBP1 antibody following fixation. Representative confocal microscopy images are shown. (C) Quantified EdU and TOPBP1 colocalized foci per cell (Student's *t*-test, *p<.05, n=3). (D) Cells were treated with 100nM PI3K inhibitor GDC0941 or control and labeled with a pTOPBP1 antibody. Flow cytometry determined the mean fluorescence intensity (MFI) of pTOPBP1 signal in each condition (Student's *t*-test, *p<.05, n=3). (E) Cells were treated with 100μM leflunomide with or without the presence of 100nM GDC0941 overnight and labeled with a gamma-H2AX antibody. Flow cytometry determined the mean fluorescence intensity (MFI) of gamma-H2AX signal in each condition (Student's *t*-test, *p<.05, n=3).

Figure 4.6. Deterioration of the checkpoint response. (A) pCHK1 S345 immunoblot after cells were treated with 150μM A771726 for times indicated. (B) pCHK1 S345 immunoblot after cells were treated

with 200μM leflunomide for 24 hours. (C) MCCL-357 cells were treated with 50μM A771726 for 48 hours. Representative images of types of DNA damage accrued. (D-F) Cells were treated with 50 or 100μM A771726 for 48 hours. Quantified chromosomal breaks and multiradial formations per haploid genome (Student's *t*-test, *p-values on figure, cells scored/replicate>100). Pulverized chromosomes could not be quantified due to the very high number of fragments.

Figure 4.7. Rescue of DNA damage and cell death. (A) PTEN mutant cells were transfected with either WT TOPBP1 and CHK1, or mutants incapable of being phosphorylated by AKT, and labeled with a gamma-H2AX antibody following 100μM leflunomide treatment overnight. Flow cytometry determined the mean fluorescence intensity (MFI) of gamma-H2AX signal (Student's t-test, *p<.05, n=3). (B) PTEN mutant cells were transfected with either WT TOPBP1 and CHK1, or mutants incapable of being phosphorylated by AKT. Live imaging of phase confluence and DRAQ7 staining (red fluorescence) over time was used to determine accumulation of cell death (two-way ANOVA, *p<.05, n=3). (C) Cleaved caspase 3 immunoblot after MEFs were treated with 200μM leflunomide for 24 hours.

Figure 4.8. Model. Model of WT (left) and $Pten^{-/-}$ cells (right) before and after DHODH inhibition. After glutamine enters $Pten^{-/-}$ cells, it is largely channeled into pyrimidine synthesis to help sustain the greater number of replication forks relative to WT cells. DHODH inhibition blocks pyrimidine synthesis leading to stalled forks and RPA loading. In the setting of PTEN deficiency, AKT phosphorylates CHK1 and TOPBP1, releasing TOPBP1 from chromatin and preventing checkpoint activation in a dual manner. Cells continue to attempt division while DNA damage accumulates, leading to cell death. WT cells do not have the same dependency on glutamine flux into pyrimidine synthesis, high number of replication forks, nor inherent checkpoint pathway defects, and therefore do not exhibit the same downstream consequences of DHODH inhibition.

Figure 4.9. Assessment of UPR and PARP inhibition. (A) Immunoblot of UPR pathway proteins after cells were treated for 18h with 100µM leflunomide, 18µM brefeldin A, or DMSO. (B-C) Cells were treated with 100µM leflunomide with or without the presence of 5µM AZD2281. Live imaging of phase confluence and DRAQ7 staining (red fluorescence) over time was used to determine accumulation of cell death.

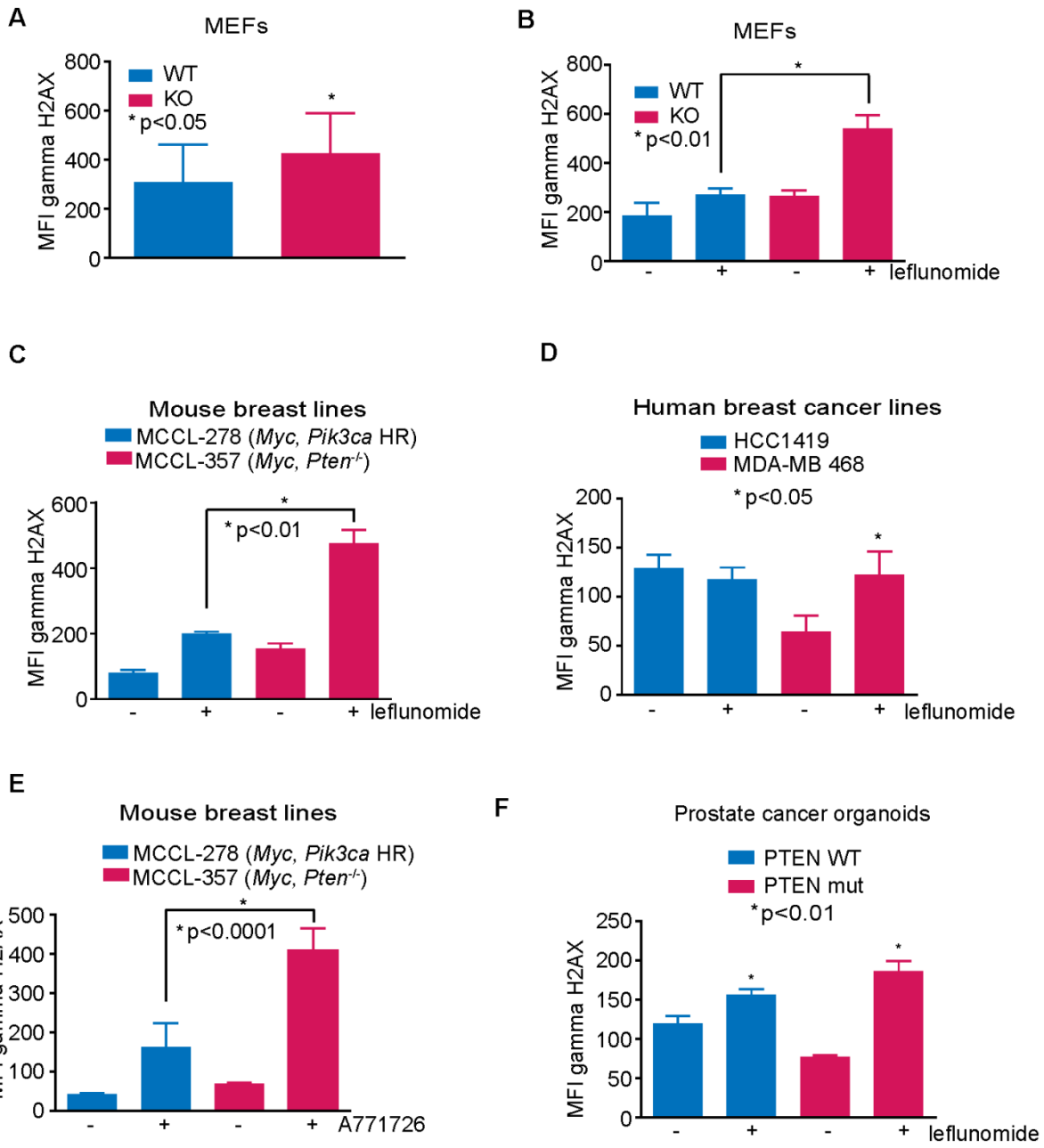
A
MEFs
MFI gamma H2AX
800
600
400
200
0
WT
KO
*p<0.05
*
B
MEFs
MFI gamma H2AX
800
600
400
200
0
WT
KO
*p<0.01
*
- + - + leflunomide
C
Mouse breast lines
MCCL-278 (Myc, Pik3ca HR)
MCCL-357 (Myc, Pten-/-)
MFI gamma H2AX
600
400
200
0
*p<0.01
*
- + - + leflunomide
D
Human breast cancer lines
HCC1419
MDA-MB 468
*p<0.05
MFI gamma H2AX
200
150
100
50
0
*
*
- + - + leflunomide
E
Mouse breast lines
MCCL-278 (Myc, Pik3ca HR)
MCCL-357 (Myc, Pten-/-)
MFI gamma H2AX
500
400
300
200
100
0
*p<0.0001
*
- + - + A771726
F
Prostate cancer organoids
PTEN WT
PTEN mut
*p<0.01
MFI gamma H2AX
250
200
150
100
50
0
*
*
- + - + leflunomide

Figure 4.1

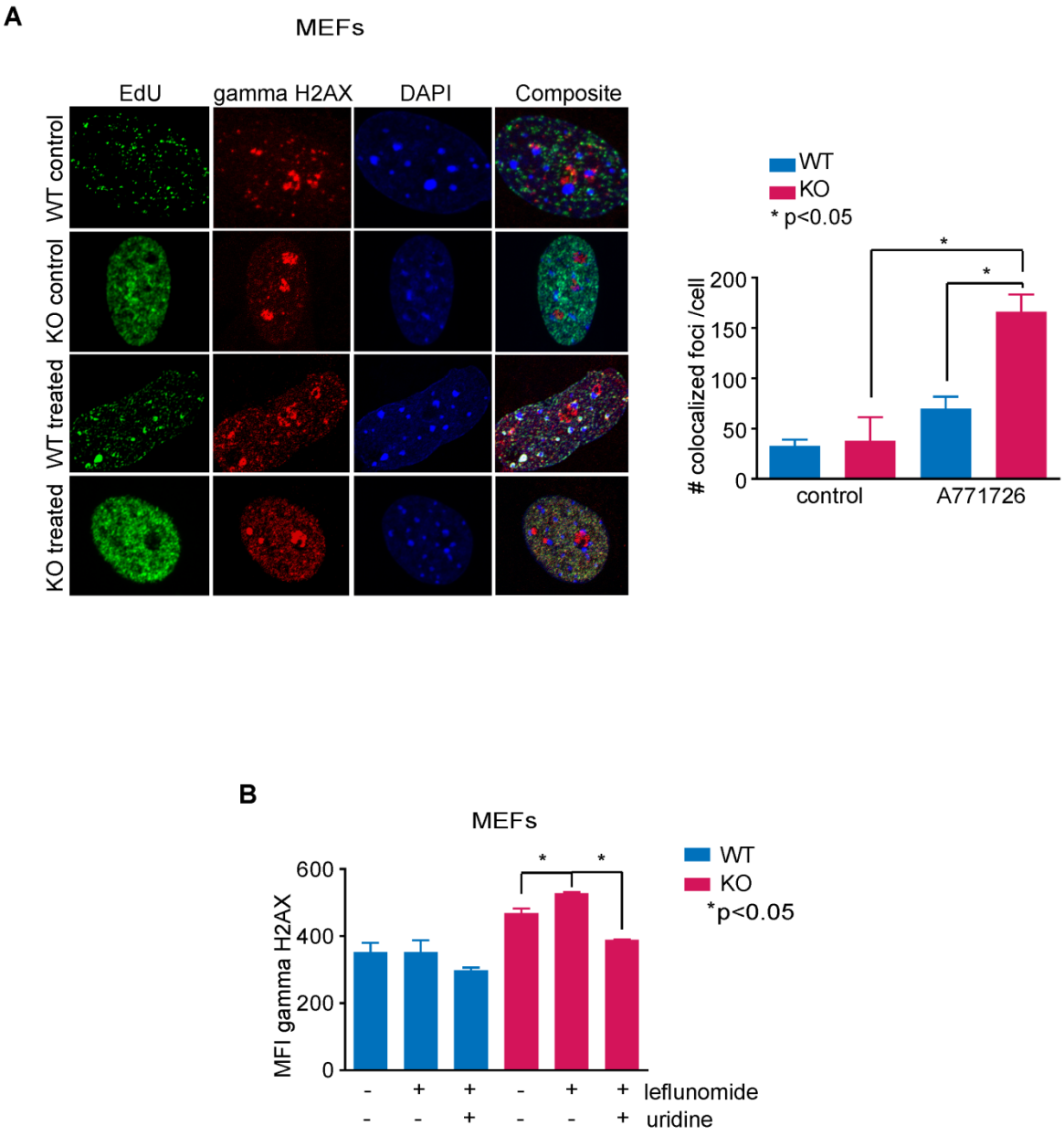
A
MEFs
EdU
gamma H2AX
DAPI
Composite
WT control
KO control
WT treated
KO treated
WT
KO
* p<0.05
# colocalized foci /cell
200
150
100
50
0
control
A771726
B
MEFs
MFI gamma H2AX
600
400
200
0
WT
KO
*p<0.05
leflunomide
uridine

Figure 4.2

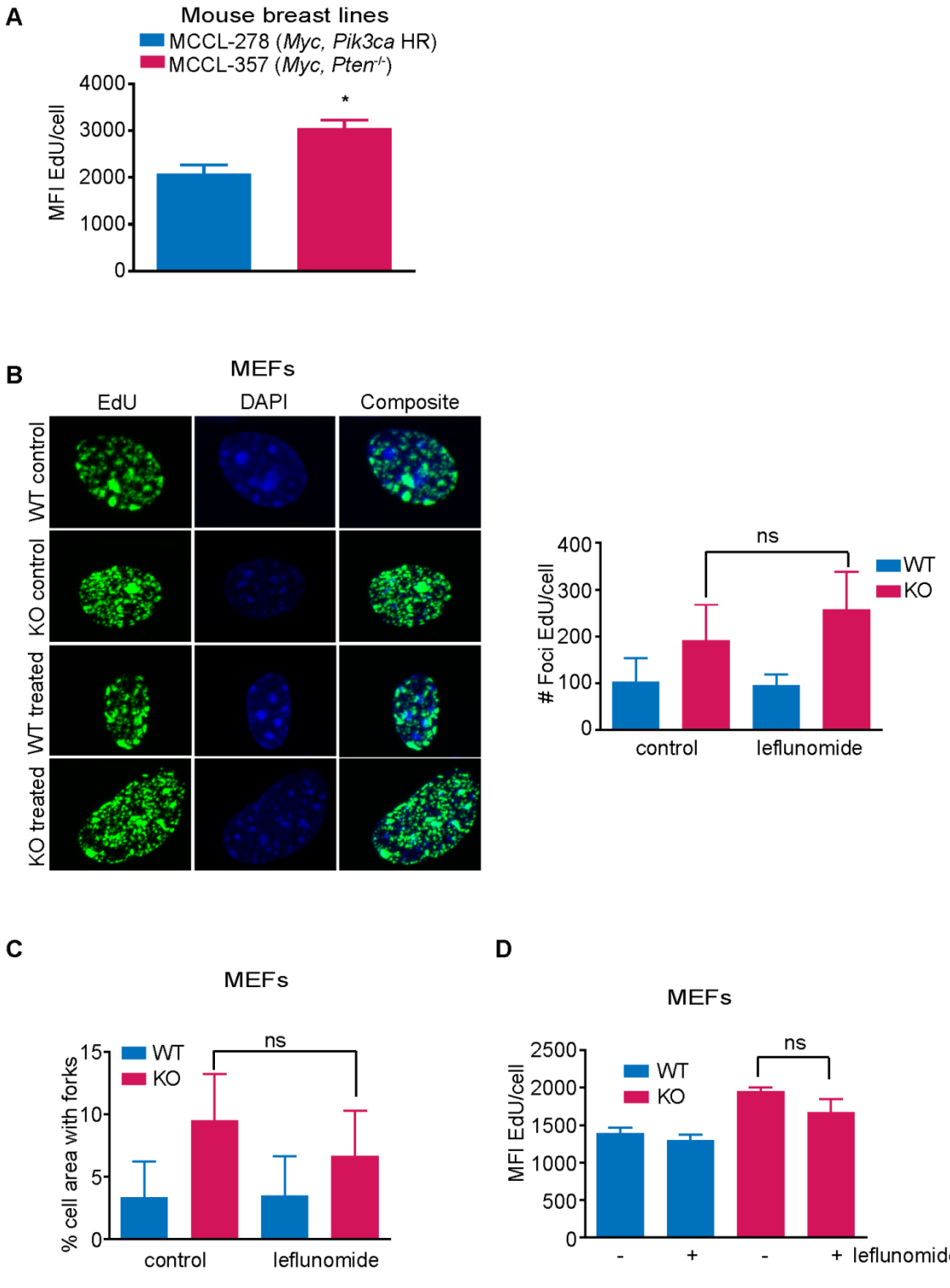
A
Mouse breast lines
MCCL-278 (Myc, Pik3ca HR)
MCCL-357 (Myc, Pten-/-)
MFI EdU/cell
4000
3000
2000
1000
0
*
B
MEFs
EdU
DAPI
Composite
WT control
KO control
WT treated
KO treated
Foci EdU/cell
400
300
200
100
0
ns
WT
KO
control
leflunomide
C
MEFs
% cell area with forks
15
10
5
0
WT
KO
ns
control
leflunomide
D
MEFs
MFI EdU/cell
2500
2000
1500
1000
500
0
WT
KO
ns
-
+
-
+ leflunomide

Figure 4.3

A

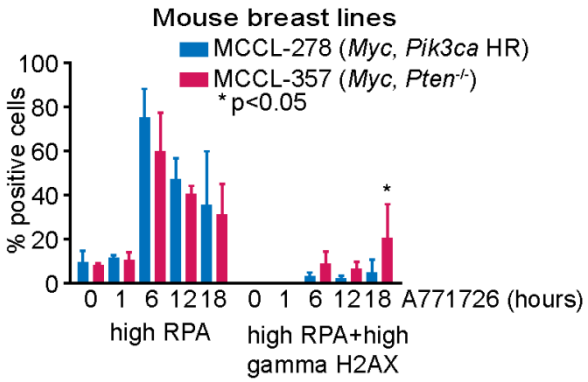
Mouse breast lines
MCCL-278 (Myc, Pik3ca HR)
MCCL-357 (Myc, Pten-/-)
* p<0.05
% positive cells
100
80
60
40
20
0
*
0 1 6 12 18 0 1 6 12 18 A771726 (hours)
high RPA
high RPA+high gamma H2AX

B

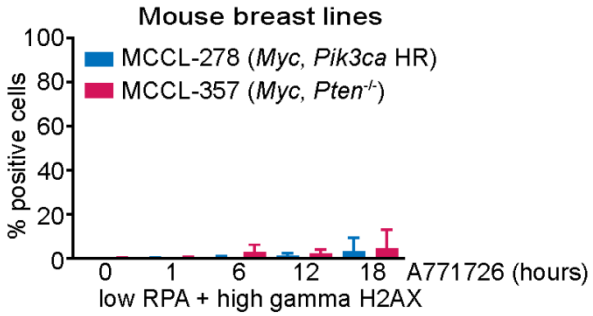
Mouse breast lines
MCCL-278 (Myc, Pik3ca HR)
MCCL-357 (Myc, Pten-/-)
% positive cells
100
80
60
40
20
0
0 1 6 12 18 A771726 (hours)
low RPA + high gamma H2AX

Figure 4.4

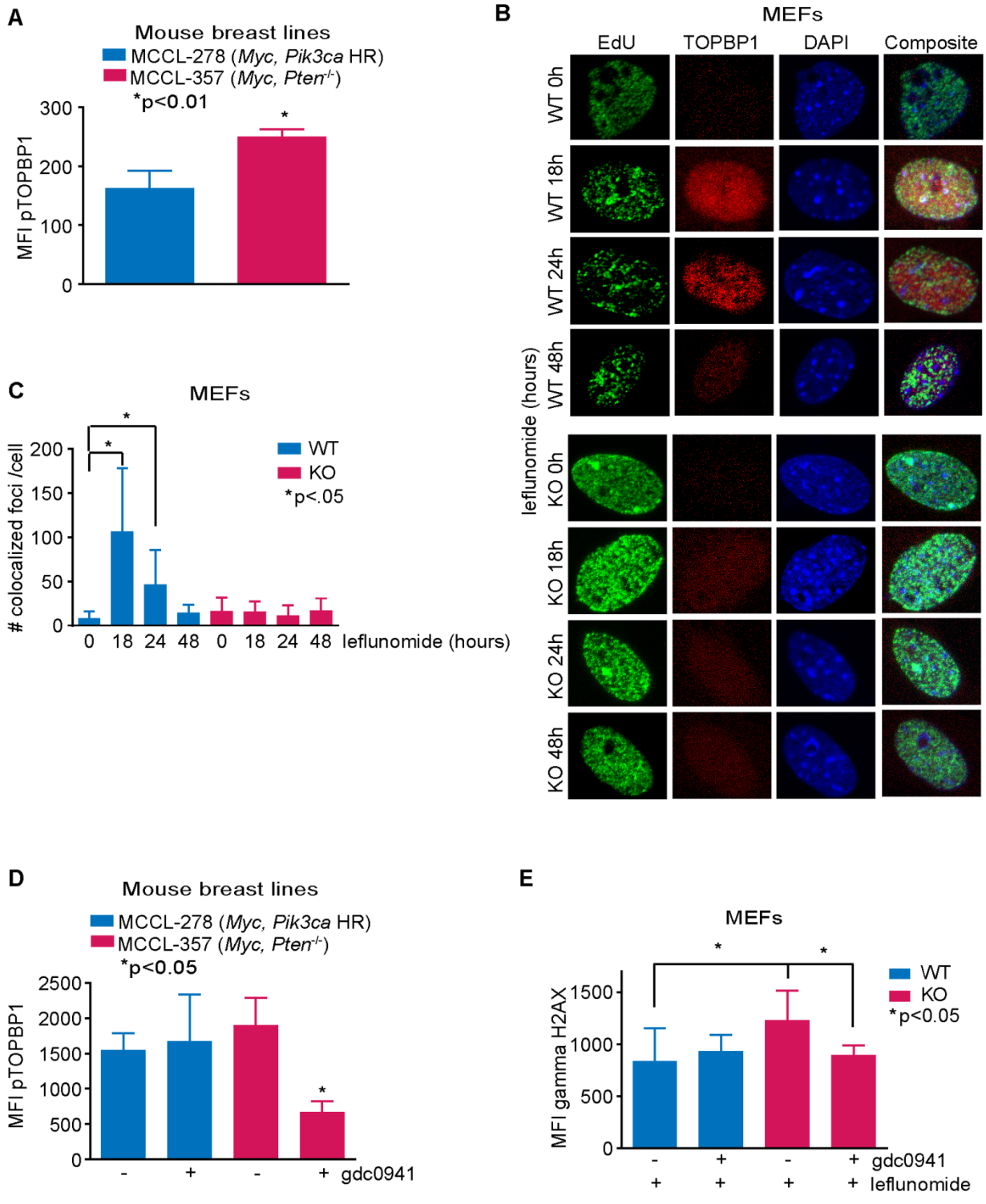
A
Mouse breast lines
MCCL-278 (Myc, Pik3ca HR)
MCCL-357 (Myc, Pten-/-)
*p<0.01
MFI pTOPBP1
300
200
100
0
*
B
MEFs
EdU
TOPBP1
DAPI
Composite
WT 0h
WT 18h
WT 24h
WT 48h
KO 0h
KO 18h
KO 24h
KO 48h
leflunomide (hours)
C
MEFs
colocalized foci /cell
200
150
100
50
0
*
*
WT
KO
*p<.05
0 18 24 48 0 18 24 48 leflunomide (hours)
D
Mouse breast lines
MCCL-278 (Myc, Pik3ca HR)
MCCL-357 (Myc, Pten-/-)
*p<0.05
MFI pTOPBP1
2500
2000
1500
1000
500
0
*
- + - + gdc0941
E
MEFs
*
*
WT
KO
*p<0.05
MFI gamma H2AX
1500
1000
500
0
- + - + gdc0941
+ + + + leflunomide

Figure 4.5

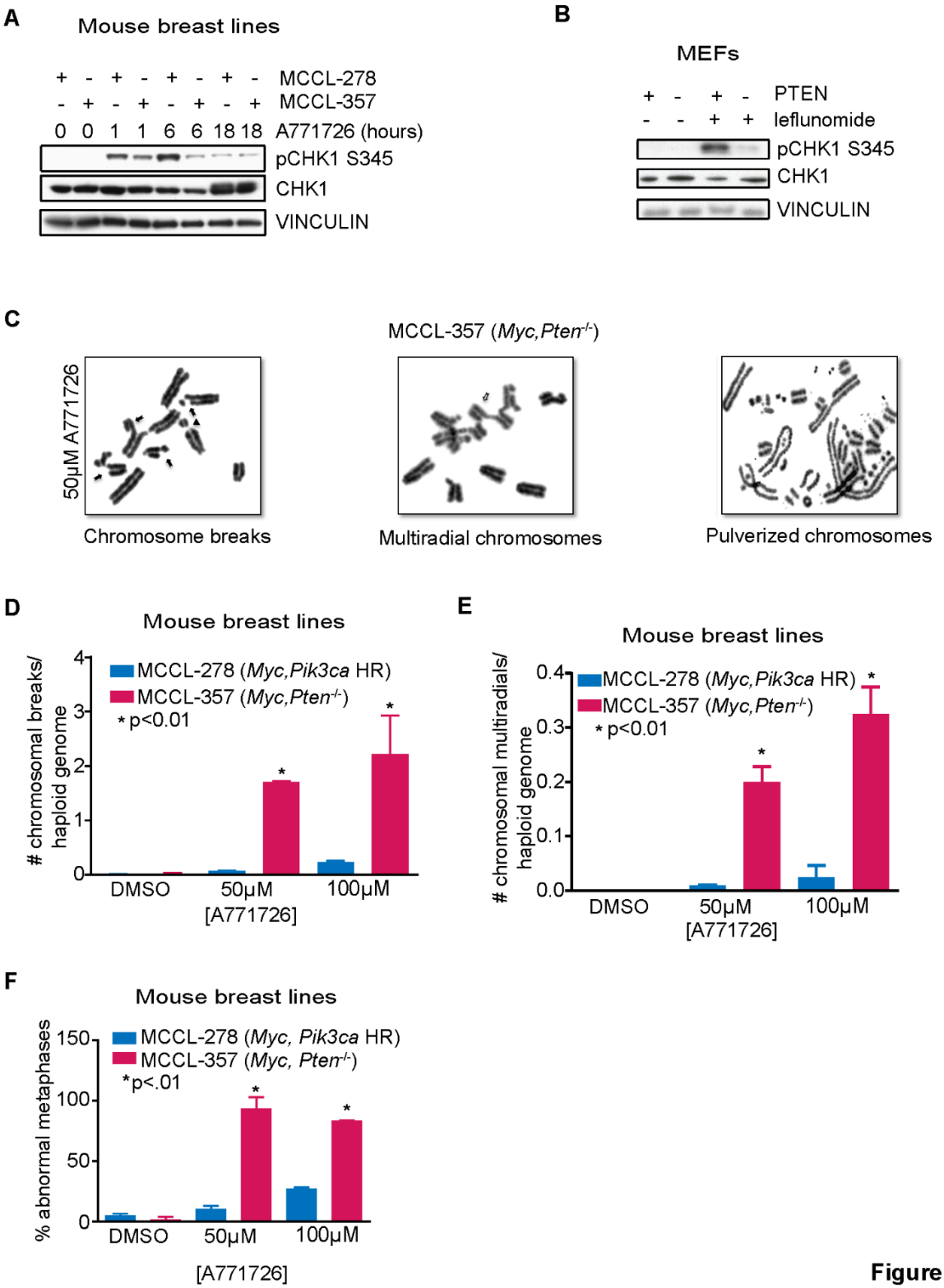
A
Mouse breast lines
+ - + - + - + - MCCL-278
- + - + - + - + MCCL-357
0 0 1 1 6 6 18 18 A771726 (hours)
pCHK1 S345
CHK1
VINCULIN
B
MEFs
+ - + - PTEN
- - + + leflunomide
pCHK1 S345
CHK1
VINCULIN
C
MCCL-357 (Myc,Pten-/-)
50μM A771726
Chromosome breaks
Multiradial chromosomes
Pulverized chromosomes
D
Mouse breast lines
chromosomal breaks/ haploid genome
MCCL-278 (Myc,Pik3ca HR)
MCCL-357 (Myc,Pten-/-)
* p<0.01
DMSO
50μM
100μM
[A771726]
E
Mouse breast lines
chromosomal multiradials/ haploid genome
MCCL-278 (Myc,Pik3ca HR)
MCCL-357 (Myc,Pten-/-)
* p<0.01
DMSO
50μM
100μM
[A771726]
F
Mouse breast lines
% abnormal metaphases
MCCL-278 (Myc, Pik3ca HR)
MCCL-357 (Myc, Pten-/-)
*p<.01
DMSO
50μM
100μM
[A771726]

Figure 4.6

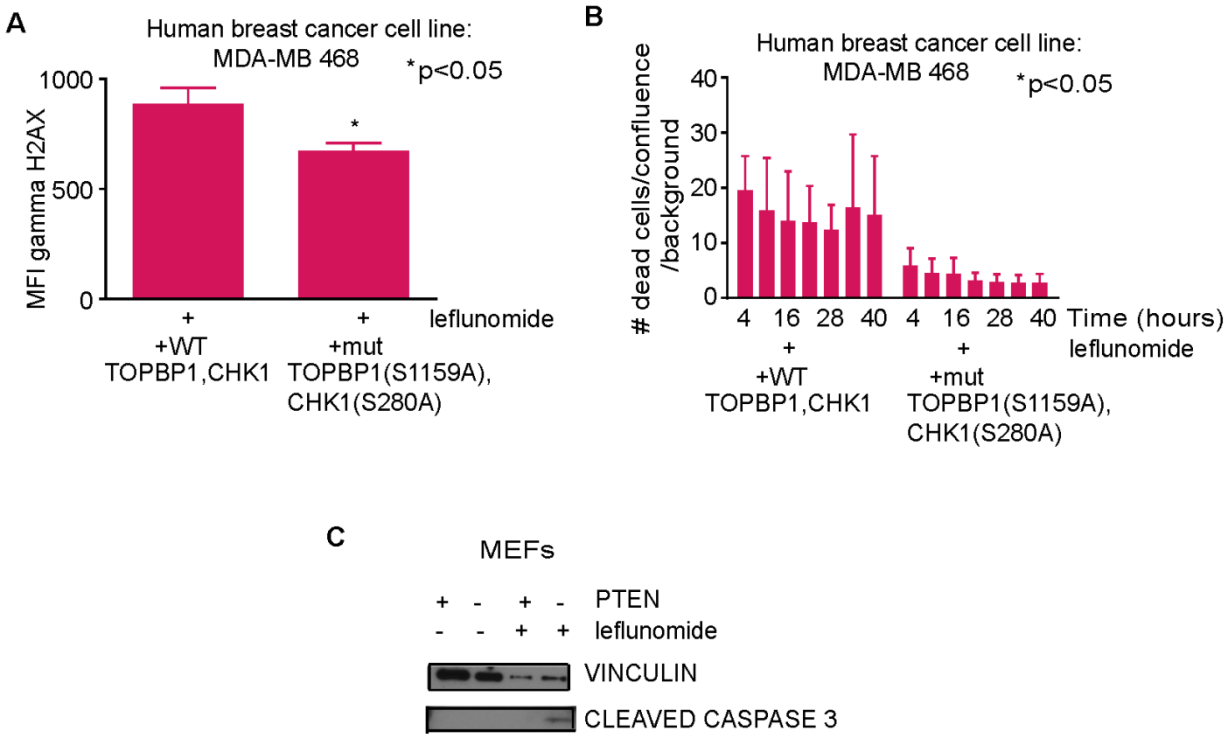
A
Human breast cancer cell line:
MDA-MB 468
*p<0.05
MFI gamma H2AX
1000
500
0
*
+
+WT
TOPBP1,CHK1
+
+mut
TOPBP1(S1159A),
CHK1(S280A)
leflunomide
B
Human breast cancer cell line:
MDA-MB 468
*p<0.05
dead cells/confluence
/background
40
30
20
10
0
4 16 28 40 4 16 28 40 Time (hours)
+
+WT
TOPBP1,CHK1
+
+mut
TOPBP1(S1159A),
CHK1(S280A)
leflunomide
C
MEFs
+ - + - PTEN
- - + + leflunomide
VINCULIN
CLEAVED CASPASE 3

Figure 4.7

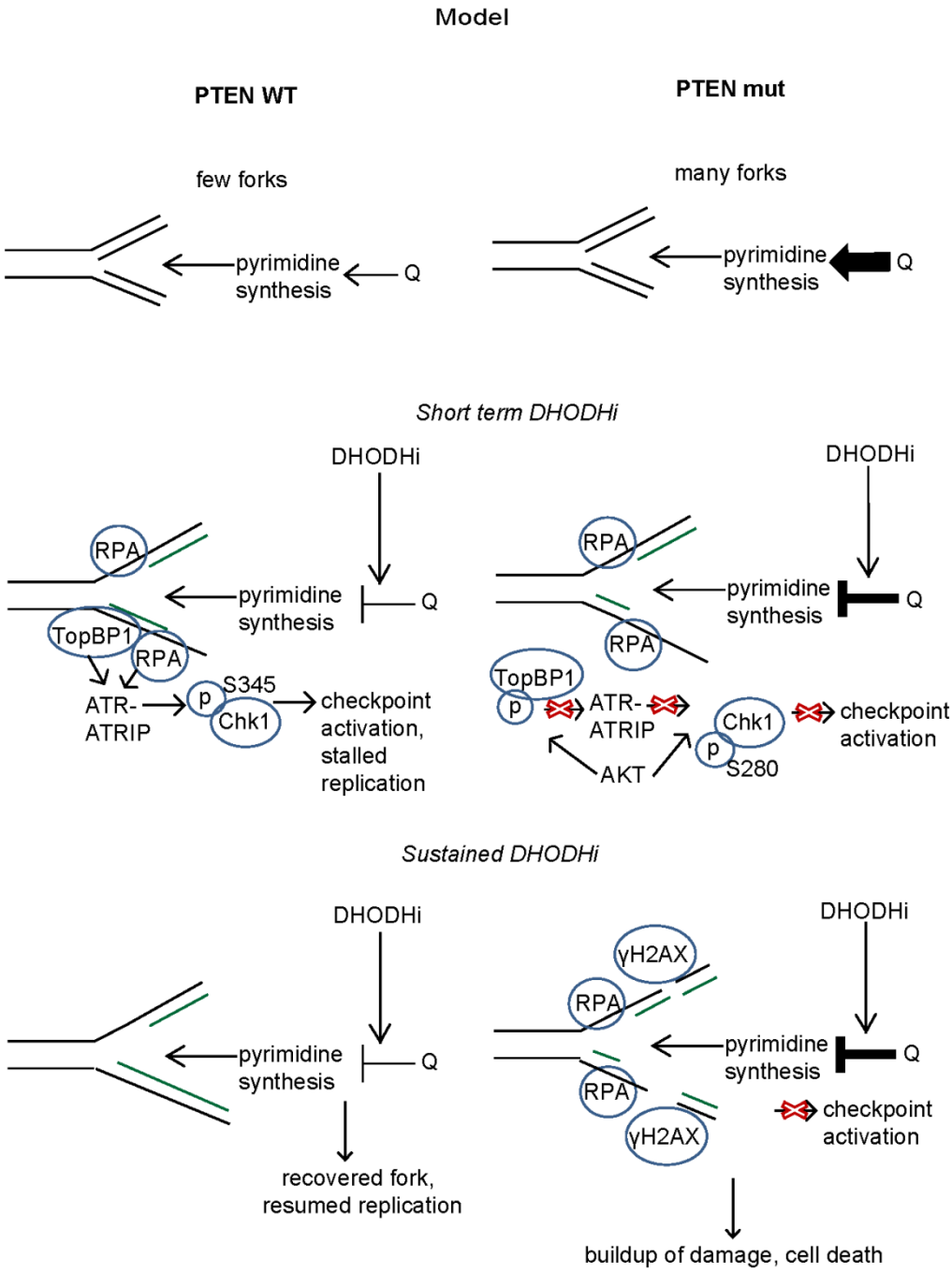
Model
PTEN WT
PTEN mut
few forks
many forks
pyrimidine synthesis
Q
Short term DHODHi
DHODHi
RPA
TopBP1
ATR-ATRIP
p
S345
Chk1
checkpoint activation, stalled replication
AKT
S280
checkpoint activation
Sustained DHODHi
γH2AX
recovered fork, resumed replication
buildup of damage, cell death

Figure 4.8

A

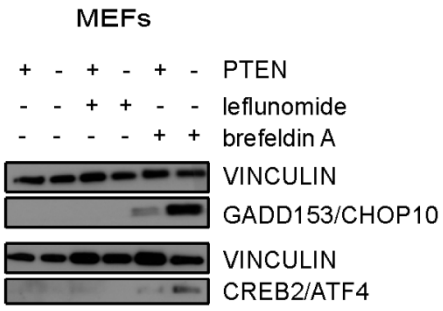

B

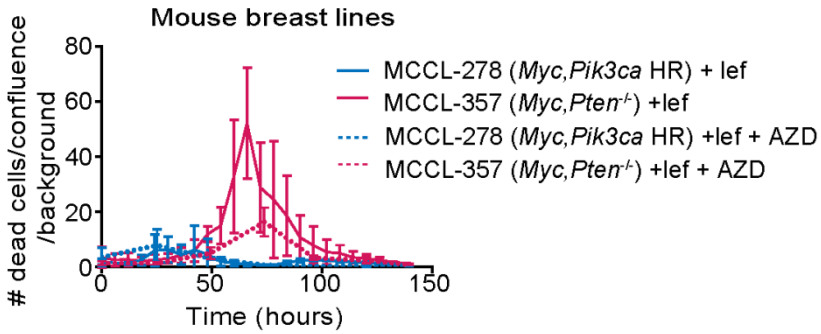

C

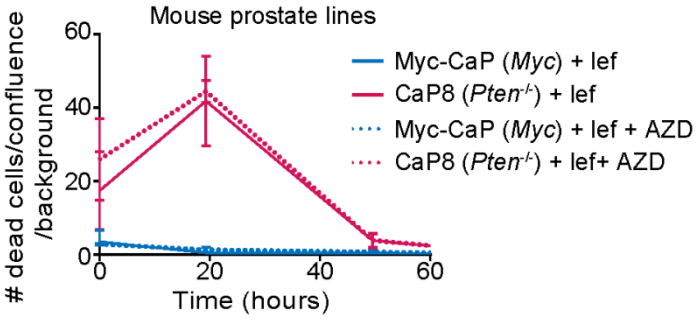

Figure 4.9

Chapter 5: Summary and Perspectives

The findings of this thesis have unveiled metabolic consequences of PTEN loss and the role they play in proliferation. This created a double-edged sword for tumor cells, exposing a therapeutic vulnerability we were able to exploit by inhibiting the *de novo* pyrimidine synthesis enzyme DHODH. Furthermore, we identified DNA damage and checkpoint defects induced by PTEN deficiency as the basis of synthetic lethality upon DHODH inhibition. In this final chapter, we present a summary of our work and offer perspectives for future advancements in the field.

Summary

In the introductory chapter of this thesis we ventured into the world of cancer metabolism, describing old and new findings in the field. We also focused on the tumor suppressor PTEN and its pathway, a hub of scientific inquiry for our understanding of cell biology as well as for development of cancer therapeutics. Linking these ideas, we presented the current literature investigating how various components of the pathway affect metabolism, and summarize the questions that have yet to be answered. The remainder of the thesis endeavored to answer some of these questions.

In chapter 2, we found that loss of Pten causes an increase in the rate of growth, associated with an increased number of replication forks per cell. The enhanced proliferation did not appear to be associated with changes in mitochondrial respiration, but rather with the induction of glutamine dependency. Historically, an increased uptake and addiction to glucose has been defined as a characteristic of tumor cells, but the relative importance of glutamine for tumors is coming to light through our research as well as others'.

We also realized that the use of isogenic lines can be misleading. This is an interesting finding, because the cell lines in question are often used in our field, and the inconsistencies we have uncovered may help explain some of the lack of reproducibility of results across the world. We decided that the use of primary cells for mechanistic studies and cancer cell lines for applicability and follow-up studies was a good strategy for achieving accurate results.

In primary *Pten*$^{-/-}$ MEFs, we further found that glutamine was being directed to *de novo* synthesis of pyrimidines. In chapter 3, we discovered that this created a point of vulnerability for PTEN-deficient cells. Inhibition of DHODH, a key enzyme in the *de novo* pyrimidine synthesis pathway, preferentially killed cells with PTEN loss. Remarkably, we were also able to diminish tumor growth *in vivo* with the DHODH inhibitor leflunomide, giving us hope that this will be useful for cancer patients with PTEN mutations.

Although several attempts at identifying a valuable combination therapy with leflunomide were unsuccessful (including with chemotherapeutic agents, PI3K pathway inhibitors, and other metabolic disruptors), leflunomide was an effective single-agent therapy. We do plan to continue the search for a viable combination strategy as well.

Chapter 4 uncovered a mode of synthetic lethality. Inherent defects in the checkpoint signaling pathway are exacerbated by the upstream block of *de novo* pyrimidine synthesis, thus exemplifying a duality of sensitivity to DHODH inhibitors. This illustrates a fascinating circular concept: PTEN loss drives ATR

signaling defects and subsequent replication fork increases, which encourages glutamine dependency and pyrimidine flux to sustain growth while simultaneously being the cause of cell death upon inhibition of the metabolic pathway.

Perspectives

In the introductory chapter we discussed the role of altered metabolism in cancer development in a broad sense: are deregulated metabolic pathways a byproduct of oncogenic signaling changes, or is altered metabolism actually the ultimate goal in order to produce sufficient cellular components for growth, with oncogenic changes simply the means to an end? A survey of the literature indicates a combination of the two, with neither stark viewpoint completely encompassing the true nature of the interaction between oncogenic signaling, metabolism, and tumor development.

In PTEN mutant cells, for example, glutamine flux into *de novo* pyrimidine synthesis helps support increased replication, but other downstream signaling effects in the cell cycle, etc. also contribute to proliferation and may even be the cause of increased replication forks in the first place. The integration of enhanced metabolism with signaling alterations not only encourages tumorigenicity, but in this case also exposed a therapeutic vulnerability. We present a model of specific nutrient dependency mechanistically linked to DNA damage and checkpoint defects, converging at a tumor suppressor-driven metabolic pathway and its inhibition.

This brings to light an important question: within this system, what is the cause of glutamine flux and what is the effect? Is the push of glutamine into the *de novo* pyrimidine synthesis pathway by CAD

responsible for creating the flux, or are increased replication forks downstream pulling glutamine into the pathway to sustain themselves and merely using CAD phosphorylation to facilitate this? It is probable that both are true – that it is a supply as well as a demand, a push as well as a pull – coalescing on the *de novo* pyrimidine synthesis pathway. This is particularly likely because evidence suggests that enzyme alterations alone could be buffered, so to speak, leading to homeostasis of metabolites rather than chronic increases in a pathway. An outlet for the pathway, on the other hand, could maintain the upregulation (Fendt, Buescher et al. 2010). This dual-dependence may also be why the synthetic lethality is so effective.

Pathway specificity

We can wonder, then, whether DHODH inhibition *per se* is required to take advantage of this sensitivity in PTEN mutant cells, or whether other inhibitors in the same pathway will achieve the same goal. Our experiments with DHODH inhibitors began because of the availability of FDA-approved drugs against this enzyme, but it's possible that targeting other components of the *de novo* pyrimidine pathway will have the same effect.

This has launched a series of experiments we are currently conducting in the lab to tackle the question of specificity. To address this, we will determine the effects of PALA, an inhibitor of CAD, and move upstream to mTORC1 inhibition and then glutaminase inhibition. If our hypothesized mechanism is correct, it is likely that PALA will phenocopy leflunomide or A771726, although we do not yet know if PALA has off-target effects and is not as "clean" of a drug, confounding results. A CRISPR mutant of CAD that cannot be phosphorylated could also help determine the necessity of pCAD in our mechanism. Moving up the funnel of glutamine flux, it becomes more difficult to predict the outcomes.

We do have some preliminary data to assist us: we found, consistent with prior reports, that PTEN mutant cells are more sensitive to the rapamycin analog rad001. What we don't know is whether this is in actuality due to its effects on CAD. Inhibiting mTORC1 will indeed effect CAD (Ben-Sahra, Howell et al. 2013), but will also affect the myriad other downstream effectors we discussed in the introductory chapter. Since these components of the pathway are also more upregulated in PTEN deficient cells it is tenable that only PTEN deficient cells will be targeted, as we and others have seen. The ability of orotate or uridine to rescue rad001 inhibition will answer this question — if the rescue is successful, CAD is likely responsible for rad001 sensitivity; if not, other components of the mTORC1 signaling pathway are likely mediating the sensitivity. Interestingly, additional literature suggests that mTORC1 increases expression of glutamate dehydrogenase, which is downstream of the glutaminase activity but could affect the TCA cycle pathway for pyrimidines from glutamine (Csibi, Fendt et al. 2013). Blocking this could have an effect on the amount of aspartate available for pyrimidine synthesis, unless glucose is able to compensate for the deficiency. However, inhibitors of mTORC1 have had limited efficacy in the clinic, and leflunomide or A771726 may be better in that regard (Statz, Patterson et al. 2016).

We also know that the glutaminase inhibitor CB-839 collapsed the growth difference between WT and *Pten*$^{-/-}$ MEFs, but as of yet do not know whether the effects were primarily through growth arrest or cell death, or of its applicability to PTEN human cancer cell lines. CB-839 has been shown to have efficacy in triple negative breast xenografts (Gross, Demo et al. 2014), and given the frequency of PTEN mutations in this disease it is possible that glutaminase inhibition will be efficacious. However, DHODH inhibition has the advantage of affecting a specific pathway of glutamine flux downstream of glutaminase, thus

preserving glutamine's other important functions in the cell such as the TCA cycle. This increases the specificity of DHODH inhibitors to those cells which are dependent on glutamine's role in pyrimidine synthesis *per se*, and is perhaps why their toxicity is low enough to be taken as a daily medication by rheumatoid arthritis and multiple sclerosis patients (Munier-Lehmann, Vidalain et al. 2013). Furthermore, the escalated effect of shutting down other glutamate-derived substrates could have the counterproductive outcome of narrowing the differential sensitivity between the two genotypes, since other components of glutamine metabolism were less upregulated than *de novo* pyrimidine synthesis in $Pten^{-/-}$ cells.

As described above, our current plans include determining whether inhibition of proteins upstream of DHODH phenocopy our results with leflunomide/A771726. This will not only give us insight into the mechanistic underpinnings of the synthetic lethality in PTEN deficient cells, but could open possibilities for combination therapies.

Further affirmation of the hypothesis

While we are quite confident in the results of this thesis, there are additional experiments which could further solidify our hypothesis.

Genes are highly interconnected in complex networks. It is possible, therefore, that loss of *PTEN* could lead to transcriptional changes in other genes or epigenetic changes in the genome. Reintroduction of PTEN into PTEN-deficient cell lines and subsequent rescue of leflunomide sensitivity and DNA damage would confirm that it is the loss of PTEN in particular that is causing our observed phenotypes, rather

than a downstream rewiring that may not be reversed by the addition of PTEN. Specific reintroduction of a lipid phosphatase-dead mutant PTEN which cannot dephosphorylate PIP3 would also be illuminating; theoretically, it should not rescue PTEN null cells while a protein phosphatase-dead PTEN mutant would.

This idea of phenotype reversal brings up another interesting speculation: if AKT is responsible for the phosphorylation of TOPBP1, could PTEN be a phosphatase for TOPBP1? A phosphatase assay in the presence of PTEN protein would be revealing, and if found to be a phosphatase for TOPBP1 would add a function to the role of PTEN in the nucleus.

ρ0 cells are cells in which the mitochondria have no mitochondrial DNA. These can be generated by treatment with ethidium bromide or ditercalinium (Segal-Bendirdjian, Coulaud et al. 1988). With oxidative phosphorylation thus disrupted, electron transfer in the respiratory chain is also disrupted, affecting the ability of DHODH to utilize ubiquinone. Theoretically, then, addition of leflunomide should not affect the cells, since DHODH is already disrupted. This would complement our rescue data to further prove that the effects we see are due to targeting of DHODH; if cells are further affected by leflunomide, it's possible that off target effects are in play.

Relatedly, it would be interesting to determine the levels of pCAD in the human cancer cell lines we used. Because PIK3CA mutant breast cancer cell lines had an intermediate level of leflunomide sensitivity, it is possible that they also exhibit intermediate flux into the pyrimidine pathway. A moderate level of pCAD would be consistent with this, since PIK3CA mutations elicit mTORC1 activation

via AKT but to a lesser extent than PTEN mutation does. In fact, it would be interesting if our cell lines exhibited a gradient of pCAD (as well as pTOPBP1) protein levels, correlated to leflunomide sensitivity. If so, it would add further credence that the influx of glutamine into pyrimidine synthesis mediated by pCAD and the inability of TOPBP1 to localize to forks directly lead to sensitivity to DHODH inhibition. However, it is also possible that cancer cell lines enhance flux of pyrimidine synthesis by additional or alternate mechanisms, such that a neat correlation is not found. While it is known that AKT2 is primarily responsible for modulation of glycolysis, it is not clear which isoform is involved in phosphorylation of TOPBP1. It would be interesting if different isoforms of AKT are involved in affecting different aspects of metabolism.

Resistance

Even if leflunomide proves to be the best drug for treating PTEN mutant tumors in terms of greatest efficacy and least toxicity, it is likely that the cancer will eventually evolve resistance. The strategy that has been proposed in the field to combat resistance is the use of combinatorial therapies, to block multiple pathways and shut down the tumor before it is able to select for resistant clones. It is therefore important to discuss the combination therapies we have tried thus far.

First, brequinar and leflunomide did not have a synergistic or even additive effect in human PTEN mutant breast cancer cell lines. Perhaps we needed to use a higher dose of brequinar to see an effect, or perhaps double-targeting DHODH is fruitless. Second, it is interesting that the addition of a PI3K inhibitor to leflunomide not only did not enhance PTEN mutant sensitivity but seemed to work better in WT human breast cancer cells. This may be because PI3K is upstream of mTORC1 — if CAD isn't being phosphorylated due to the upstream block and glutamine is hence not being directed to pyrimidine

synthesis, it is possible that the sensitivity to leflunomide is no longer created in PTEN mutant cells. Additionally, AKT-mediated phosphorylation of TOPBP1 and CHK1 is central to the synthetic lethality observed in PTEN-deficient cells, and diminishing AKT signaling may prevent leflunomide-induced cell death. mTORC1 inhibition also did not enhance the effects of leflunomide, or vice versa. As with the PI3K inhibitor, this may be due to the obstruction of CAD phosphorylation and pyrimidine flux. This can also indicate redundancy in the pathway; if PTEN is regulating pyrimidine synthesis through mTORC1 downstream, blocking mTORC1 may not have an effect if a DHODH inhibitor is already applied.

Many of the results from this thesis will be published in Cancer Discovery. We co-submitted our paper with one from Dr. Alex Toker's group from Harvard, who found that breast cancer cells that were treated with the chemotherapeutic agent doxorubicin then become sensitive to leflunomide/A771726. In light of their results, it is interesting that doxorubicin enhanced PTEN WT but not mutant cell sensitivity to leflunomide. The metabolic signature genetically produced by PTEN loss, in particular pyrimidine influx, may be paralleled chemically by doxorubicin. If true, it would explain why doxorubicin had no added effect on PTEN mutant cells, since they are already dependent on pyrimidine synthesis. On the other hand, doxorubicin treatment of PTEN WT cells could stimulate pyrimidine flux to the approximate level of PTEN mutant cells, creating sensitivity to leflunomide.

In vitro, the chemotherapeutic agent paclitaxel did not affect the sensitivity to leflunomide, but leflunomide augmented the effect of paclitaxel in *Pten*$^{-/-}$ cells. Our subsequent *in vivo* experiment treated mice with paclitaxel after they were exposed to leflunomide, with no effect in part because leflunomide acted so well as a single agent. Additionally, perhaps we ought to have reversed the experiment: since the *in vitro* data showed leflunomide enhancing the effects of paclitaxel, it may be

worthwhile to pretreat tumors with paclitaxel and then add leflunomide to try to induce synergy in PTEN mutant cells. If the combination is ultimately only slightly beneficial, it may be worthwhile to forego paclitaxel in favor of increasing the dose of leflunomide instead; prior clinical evidence demonstrates the relatively fewer toxic side effects of leflunomide at normal doses, and at escalated doses may still be lower than the side effects of chemotherapy.

Additionally, it will be valuable to determine resistance mechanisms, either inherent or induced by DHODH inhibitors. We plan to address this by screening additional PTEN mutant cell lines and comparing genetic differences between sensitive and resistant lines. We also plan to treat sensitive lines with low doses of leflunomide for extensive periods of time in an attempt to stimulate resistance, and use the "before and after" to predict and eventually circumvent resistance mechanisms *in vivo*.

Additional future directions

From a broader perspective, we believe that additional metabolic changes induced upon PTEN loss present interesting lines of investigation. Preliminary data from our lab suggest that, compared to WT cells, *Pten*$^{-/-}$ cells increase serine and glycine synthesis from 3-phosphoglycerate. This could indicate the importance of single-carbon metabolism, perhaps in an effort to bring balance to purine and pyrimidines in PTEN-deficient cells. Pyrimidine metabolism was found to be upregulated to a greater extent than purine synthesis, but perhaps the cells attempt to normalize the difference through glucose redirection into serine and the folate cycle.

The screen of soluble metabolites pointed us in the direction of pyrimidine metabolism. We have not, however, explored insoluble metabolites. It is possible that there are alterations in fatty acid anabolism to help support heightened proliferation or for other purposes as yet undetermined. Heavy isotope labeling and extraction of insoluble metabolites will help us understand the role of lipids in PTEN mutant cells.

Our results also expose a very basic question: independently of DHODH inhibition, how are PTEN deficient cells increasing their number of replication forks? Future work into this question will include research into the coordination of origin firing and its determinants, including ATR as described above. Additionally, it will be important to know whether PTEN deficiency alters the recruitment of repair proteins to chromatin, both at endogenous levels and upon DHODH inhibition. The current literature on this subject is conflicted, but perhaps our model of primary MEFs will help elucidate mechanistic changes. ATR deficiency has been shown to impair localization of the repair protein FANCD2 to DNA, leading to chromosomal instability (Andreassen, D'Andrea et al. 2004). It will be interesting to measure FANCD2 foci in the setting of PTEN deficiency and DHODH inhibition, to see whether the ATR signaling defects we observed have additional downstream consequences. Perhaps the most interesting question in this realm of discussion is whether DHODH inhibition of PTEN mutant cells increases the overall probability of error in DNA replication. It is possible that the inability of cells in these conditions to adequately sustain nucleotide levels at the higher number of forks leads to more frequent mistakes during replication. Or, perhaps an imbalance of pyrimidines and purines at baseline conditions also increases the rate of error. We plan to examine RNA-seq data to determine whether there is an increase in the random distribution of point mutations in PTEN mutant cells, either with or without DHODH inhibition.

Overall, the work presented in this thesis has launched several lines of investigation, from the mechanistic to the clinical. Our *in vivo* studies thus far have been in triple negative breast cancer models, and it will be important to expand this to glioblastoma, prostate, and endometrial cancers which also have high frequency of PTEN mutations. Our *in vitro* studies on prostate and glioblastoma lines suggest a reasonable chance of success in these tumor types.

Significance

The findings of this thesis offer an understanding of the role of tumor suppression in metabolic signaling, and solidify the importance of metabolism in tumor development and therapeutic intervention. We have found a prospective targeted therapy for PTEN deficient tumors, with efficacy *in vitro* and *in vivo* in tumors derived from different tissues. Our results also open fascinating opportunities for further research into the consequences of PTEN deficiency.

Materials and Methods

Cell culture: MEFs and mouse breast tumor lines used the following media: DMEM (Corning mt10013cv) supplemented with 10% FBS (Atlanta Biologicals), 1% pen/strep (Fisher 30002ci) and 2mM L-glutamine (total 6mM) (Fisher MT25005CI). MDA-MB468, MDA-MB 231, Myc-CaP, and U87 used the following media: DMEM supplemented with 10% FBS and 1% pen/strep. HCC1419, HCC1187, HCC 1937, HCC 1806, BT549, ZR75-1, PC3, LNCAP, DBTRG, T-47D, HCC1954 used the following media: RPMI (Fisher 10040cv) supplemented with 10% FBS and 1% pen/strep. SUM149 and SUM159 used the following media: HAM's F-12 with 5% FBS, 1% pen/strep, .01mg/mL insulin, 500ng/mL hydrocortisone. CaP8 cells used the following media: DMEM with 10% FBS, 1% pen/strep, and 5μg/mL insulin (Sigma I9278). Neurospheres used the following media: stem cell media with 10ug/mL FGF (R&D Systems 233-FB-025), 20ug/mL EGF (Peprotech AF-100-15) and heparin. All cells were cultured in a 37°C incubator with humidity and 5% CO_2. Cell lines were obtained from ATCC (which authenticate cell lines using several methods including DNA fingerprinting), with the exception of MEFs, MCCL-278, and MCCL-357 which were produced in our lab from mice. Neurospheres were obtained from Dr. Raymund Yong, and prostate cancer organoids from Drs. Stuart Aaronson and Pamela Cheung. Cell lines were clear of mycoplasma as determined by the luminescence-based Lonza kit (LT07-418) within 6 months of their use. Cell lines were frozen in media containing 5-10% DMSO, in containers with isopropanol in the -80°C freezer prior to transfer to liquid nitrogen for long-term storage. Cell lines were further authenticated in 2015 by LabCorp using a short tandem repeat method.

Mouse Embryonic Fibroblasts: Embryos were harvested from pregnant B6.129S4 Pten flox/flox mice (from Jackson Laboratory) 15 days after setting up the cross. This timeline was used because the mice

typically do not actually mate until late that night; therefore, the embryos are collected effectively 14 days after the actual mating event. Head, limbs, liver, and other highly vascularized regions of the embryo were removed. The remaining trunk was minced using a scalpel in .25% trypsin, and resuspended in trypsin using a 5mL pipet. After 10 minutes of incubation at 37°C and 5% CO2, cells were further resuspended in trypsin with a 1mL pipet to generate a single-cell suspension. Cells were spun down and resuspended in fresh media before plating onto 10cm dishes. Cells were treated with an adenovirus with or without Cre recombinase (1:1000 of Vector Biolabs #1300 and #1045, respectively) as well as 4μg/mL polybrene in order to enhance infection efficiency. MEFs were studied passage 2 or later after infection to ensure proper Pten deletion (checked by western blot) as well as recovery from infection, and before passage 6 after infection while the MEFs were still viable.

Immunoblotting: Samples were lysed in 2x Laemelli sample buffer with mercaptoethanol and were boiled before separation by SDS-PAGE on Tris-Glycine gels (Invitrogen EC60352) at 100V. Wet-transfer to PVDF (Fisher ipvh00010) for 1.5h at 180mA was followed by blocking for 1 hour in 10% nonfat milk (Fisher M-0841) in TBST. Membranes were incubated in primary antibody overnight at 4°C, and washed with TBST prior to addition of secondary antibody (Fisher 31432, 31460) for 1 hour at room temperature. Blots were developed using ECL (Fisher 34080) and autoradiography film (Denville E3018). Antibodies: PTEN 6H2.1 (Millipore 04-035), DHODH (Protein Tech 14877-1-AP), vinculin (Sigma V9131), actin (Sigma A4700), pCHK1 (Cell Signaling 2341), p-AKT (S473) (Cell Signaling 3787), CHK1 G-4 (Santa Cruz sc-8408), pCAD (Cell Signaling 12662), CAD (Cell Signaling 11933), cleaved caspase 3 (Cell Signaling 9664), GADD153 (Santa Cruz sc-575), CREB-2 (Santa Cruz sc-200) .

Microarray: RNA from cell lines was analyzed using the Affymetrix® GeneChips and the procedure dictated by The Ambion® Whole Transcript (WT) Expression Array from Applied Biosystems. 250ng RNA per sample was used for poly-A controls and first and second strand cDNA synthesis, followed by cRNA synthesis and purification. Second cycle cDNA was synthesized and purified, and quantity was assessed with a nanodrop. Samples were sent to Applied Biosystems for analysis. Results were imported into R for quality control (including consistency of probe hybridization and signal intensity) and normalization using the affymetrix package.

Cluster analysis: Microarray data from cell lines were uploaded to and analyzed by the Broad Institute's Morpheus software.

Principal Component Analysis: PCA on MEFs was performed using the online program ClustVis (Metsalu and Vilo 2015) or on Matlab.

Proliferation assay: 1500 cells per well (mouse cells) or 3000 cells per well (human cells) were plated in 96 well plates (Corning 720089). Growth rates were determined using the phase-confluency readings on an IncuCyte ZOOM (Essen Biosciences) on live cells over time. A 4x objective was used in the instrument, and images were either collected once every 24h using the scan-on-demand feature or once every 6h using the scheduled scan feature. Unique processing definitions were created for different cell lines to train the program as accurately as possible to recognize cell vs. non-cell in each cell line.

Crystal violet assay: 3000 cells per well were plated into 48-well plates, one plate per time point. For each time point, wells were aspirated and washed with PBS, after which 300µL .05% crystal violet (in formalin, diluted 1:10 with PBS) was added. Cells were incubated 20-30 min at room temperature, and then washed 3 times with PBS. 500µL 10% acetic acid was added to each well, and put on a plate shaker for 20min-1hr at 400rpm until dissolved. Absorbance was read on a plate reader at 590nm wavelength.

Immunofluorescence: Cells were plated on fibronectin-coated cover slips in media. For detecting replication forks: following a 45min EdU pulse, cover slip-attached cells were fixed (4% paraformaldehyde for 15min room temperature), permeabilized and blocked (10% goat serum/PBS/0.1% Triton X-100), and detected after azide conjugation to EdU. For detecting gamma-H2AX or TOPBP1: following the above fixation and permeabilization/blocking protocols, cells were incubated with primary antibody (Upstate Cell Signaling and Bethyl A300-111A-M, respectively) overnight at 4°C (in 10% goat serum/PBS) and with secondary antibody (in PBS) for 2 hours at room temperature. Cells were washed with PBS in between each step, mounted on slides with prolong anti-fade with DAPI, allowed to dry overnight, and sealed with clear nail polish. Images were taken using a Zeiss LSM880 Airyscan confocal microscope at 63X, and foci number and colocalization was quantified with Image J using “colocalization” and “analyze particles” plugins.

EdU detection: Instructions for the EdU cell proliferation Kit (Millipore 17-10525) were followed: Cells were fixed (4% paraformaldehyde for 15min room temperature) and permeabilized (0.5% Triton X-100 in PBS for 20 min) following a 45min EdU pulse on live cells. The click chemistry reaction to add a fluorescent tag included an azide dye, catalyst, and buffer solutions, and cells were incubated for 30min.

Cells were washed and fluorescence was measured on a Guava® flow cytometer or by immunofluorescence.

Cell death: Instructions for the FlowCellect™ Annexin Red Kit (Millipore FCCH100108) were followed: both floating and adherent cells were collected, and resuspended in buffer. Cells were incubated in 1:200 Annexin V for 15min in a 37°C CO_2 incubator. Following washes, cells were resuspended in buffer and 1:200 7AAD was added for 5 min at room temperature in the dark. Fluorescence was measured on a Guava® flow cytometer.

Cell cycle Analysis: Instructions for the FlowCellect™ Bivariate Cell Cycle Kit (Millipore FCCH025102) were followed: prior to collection, cells were incubated with 1:2000 BrdU in culture (BrdU was pulsed for 18hrs). Cells were then fixed and permeabilized on ice, and DNA was denatured with DNaseI. Cells were incubated with Anti-BrdU direct conjugate to Alexa Fluor 488 for one hour in the dark followed by propidium iodide and RNase for 30min at room temperature in the dark. Fluorescence was measured on a Guava® flow cytometer.

Senescence assay: Cells were washed, fixed, and stained with β-gal staining solution (Cell Signaling) overnight in the dark. DAPI was added and cells were covered with 70% glycerol. Pictures were taken on a microscope and quantified with ImageJ.

Seahorse Analysis: A Seahorse XF (Agilent) was used to determine the oxygen consumption and extracellular acidification rates. Cells were seeded at 12.5, 25, or 50K cells per well in 100µL volume in

the Seahorse cartridge (well size equivalent to 96 well plate well). 5 hours later, 150µL pH-adjusted (to 7.4) DMEM XF Seahorse media was added to get a total volume of 250µL. 1mL of calibrant was added to an additional cartridge and warmed at 37°C in a non-CO2 incubator. The following day, this cartridge was used to calibrate the machine. Cells were washed and 550µL media was put in each well and incubated for 30min. 10µM oligomycin (55µL), 30µM FCCP (61µL), and 10µM rotenone (68µL) (Seahorse XF kit, Agilent) were injected into cartridge wells (volume reflects taking into account the additional volume added each time, therefore keeping concentration precise). Controls for establishing baseline were used. Plate was inserted into the machine for readings.

ROS: 1mL of 2.5µM DCFDA in PBS was added to cells and incubated for 30 min at 37°C protected from light. Cells were washed and collected in PBS for flow cytometry.

Mitochondrial ROS: A 5mM stock of MitoSOX™ reagent was made in DMSO. 1mL of 2.5µM (Mukhopadhyay, Rajesh et al. 2007) reagent in HBSS buffer was added to cells and incubated for 15min at 37°C protected from light. Cells were washed and collected in buffer for flow cytometry.

Metabolite labeling: For glutamine flux, media without glutamine was supplemented with ^{13}C glutamine (fully labeled) or ^{15}N glutamine (amide labeled) (Cambridge Isotope Labs). For glucose flux, media without added glucose was supplemented with ^{13}C glucose (fully labeled) (Cambridge Isotope Labs). Cells were plated in 10cm dishes; WT and $Pten^{-/-}$ MEFs were plated at slightly different confluencies (1:.8) to achieve equal confluency the day of the extraction and were grown in normal media (control plates were counted day-of experiment to ensure equal cell numbers). 1 hour prior to

metabolite extraction, media was aspirated and replaced with heavy isotope-labeled media for flux experiments.

Metabolic extraction: Metabolites were collected as previously described (Yuan, Breitkopf et al. 2012): Media was aspirated from plates, and 2.5mL 80% methanol (kept at -80°C) was added. Plates were incubated at 80°C for 20 minutes, after which cells were scraped into tubes and centrifuged to pellet insoluble cellular material. The soluble supernatant was saved. 2 more extractions on the insoluble pellet were performed with 500µL 80% methanol, and all extractions were pooled. Extractions were dried in a speed-vac and frozen at -80°C until analysis. All steps of the extraction were kept cold on dry ice.

Targeted Mass Spectrometry: Mass Spec was performed by the core facility at Beth Israel Deaconess Medical Center. Samples were re-suspended using 20 µL HPLC grade water for mass spectrometry. 5-7 µL were injected and analyzed using a hybrid 5500 QTRAP triple quadrupole mass spectrometer (AB/SCIEX) coupled to a Prominence UFLC HPLC system (Shimadzu) via selected reaction monitoring (SRM) of a total of 259 endogenous water soluble metabolites for steady-state analyses of samples. Some metabolites were targeted in both positive and negative ion mode for a total of 294 SRM 3 transitions using positive/negative ion polarity switching. ESI voltage was +4900V in positive ion mode and –4500V in negative ion mode. The dwell time was 3 ms per SRM transition and the total cycle time was 1.55 seconds. Approximately 10-14 data points were acquired per detected metabolite. Samples were delivered to the mass spectrometer via hydrophilic interaction chromatography (HILIC) using a 4.6 mm i.d x 10 cm Amide XBridge column (Waters) at 400 µL/min. Gradients were run starting from 85% buffer B (HPLC grade acetonitrile) to 42% B from 0-5 minutes; 42% B to 0% B from 5-16 minutes; 0% B

was held from 16-24 minutes; 0% B to 85% B from 24-25 minutes; 85% B was held for 7 minutes to re-equilibrate the column. Buffer A was comprised of 20 mM ammonium hydroxide/20 mM ammonium acetate (pH=9.0) in 95:5 water:acetonitrile. Peak areas from the total ion current for each metabolite SRM transition were integrated using MultiQuant v2.1 software (AB/SCIEX). ~150 SRM transitions were set up for 13C glutamine and 15N glutamine labeled metabolites in addition to unlabeled metabolites. Integrated Molecular Pathway Analysis (IMPaLA) was used to analyze metabolic pathways (Kamburov, Cavill et al. 2011). For cell-labeling experiments, the concentration of isotope-labeled metabolite = [labeled metabolite amount]/ [total metabolite amount] for each metabolite.

Gene Set Enrichment Analysis: Microarray data from Pten WT and KO MEFs (4 each) were analyzed using the GSEA program by the Broad Institute (Mootha, Lindgren et al. 2003, Subramanian, Tamayo et al. 2005).

Drug response assays: Cells were plated in 96-well plates at a density of 1500 or 3000 cells per well. Leflunomide (Sigma PHR1378-1G), A771726 (Sigma SML0936), mercaptopurine (Sigma 852678), brequinar (Sigma SML0113), 5-fluorouracil (Millipore 343922), rad001 and GDC0941(Stand Up to Cancer PI3K Dream Team), carboplatin (Selleckchem S1215), paclitaxel (Sigma T7402), carboplatin (Sigma 44583-1MG) and CB-839 (MedChemexpress HY-12248) were dissolved in DMSO. Sensitivity was determined by a dose-response titration for each cell line, with an equivalent amount of DMSO in each well: 300µL media with drug was added to one column of wells, and 150µL media with equivalent DMSO was added to remaining wells. Serial dilutions of 150µL resulted in a gradient with half the drug concentration as the previous column while maintaining the same amount of DMSO. GI50 was defined as the drug concentration required to achieve 50% of maximal growth in the cell line, and was calculated

by linear interpolation adapted from the *Nature* analysis of the NCI60 panel (Shoemaker 2006): the maximum growth confluence for a cell line prior to growth plateau was divided by 2 to obtain the 50% confluence value. A linear regression curve was calculated using drug concentrations as x-values and confluence as y-values for points surrounding the 50% value. Linear interpolation using the regression line yielded the GI50 concentration. For cell death assays, DRAQ7™ (Cell Signaling 7406S) was added to the media at a 1:200 dilution and red fluorescence was measured in addition to phase in live-cell imaging to measure accumulation of dead cells. For DRAQ7 readings, the number of dead cells was normalized to confluency and background red signal. An IncuCyte ZOOM was used to measure confluency and fluorescence.

Mammospheres: Cells were grown in serum-free DMEM or RPMI with B-27 supplement and rEGF. Cells were plated in non-adherent plates, and pictures covering the whole well were taken 5 days after treatment. Dense clusters >.05mm in diameter were counted as true tumor spheres. Spheres were measured on ImageJ and quantified.

Orotate Rescue: Orotate (Sigma O2750) was dissolved in DMSO. Cells were plated at fixed concentration leflunomide with increasing concentrations of orotate, keeping DMSO constant in all wells.

Uridine Rescue: Uridine (Sigma U 3750) was dissolved in media. Cells were plated at fixed concentration leflunomide with increasing concentrations of uridine, keeping DMSO constant in all wells.

RNA interference: siRNA for DHODH was purchased from Qiagen. Cells were transfected using lipofectamine (Invitrogen 11668-019): 250µL Optimem with 5µL siRNA at 20µM and 250µL Optimem with 5µL lipfectamine were incubated at room temperature for 5 minutes and then mixed and left to sit at room temperature for approximately 10min. Media on cells was replaced with 500µL antibiotic-free media, and the Optimem solution was added drop-wise. After 7 hours, the cells were switched to regular media, and knockdown was confirmed at 48 hours via western blot. Scrambled siRNA was used as a control.

Antioxidant rescue: N-acetyl-cysteine (Sigma A7250-10G) was dissolved in DMSO. Cells were plated at fixed concentration leflunomide with increasing concentrations of N-acetyl-cysteine, keeping DMSO constant in all wells.

Xenografts: 6-week old female nu/nu mice were engrafted orthotopically with either 5 million SUM149, 5 million MDAMB 468-luciferase, 1 million MCCL-357, or .75million MCCL-278 cells. Mice with PDX implants at passage 2-3 were obtained from Jackson Labs (model TM00090: breast metaplasmic carcinoma, primary malignancy, deficiency in PTEN greater than any other gene tested based on RNAseq and second most based on copy number analysis). Mice were treated by oral gavage with 100mg/kg leflunomide or vehicle (1% carboxymethylcelluose in water). Tumor size was measured by calipers (modified ellipsoid formula = ½(length*width2)) or luminescence, which was quantified as photons/second/cm2/steradian and normalized to baseline. Mice were treated orally as is done clinically; leflunomide binds tightly to serum proteins and has a long half-life (about 2 weeks), precluding daily treatments for the duration of the experiment (Breedveld and Dayer 2000, Rozman 2002). Paclitaxel was dissolved in 160µL 1:1 ethanol to Crempohor EL and diluted in PBS; 200L per mouse was

injected intraperitoneal. Vehicle-treated mice in this experiment were given both ethanol/Cremophor/PBS and 1% carboxymethylcellulose. Mice were from Jackson Laboratory and were 20-25g. Animal experiments were approved by an Institutional Animal Care and Use Committee.

Neurosphere sensitivity assay: Neurospheres were disrupted by manual pipetting until single cell suspension was achieved, and 10,000cells/well were plated in low-attachment 6-well plates (Fisher 3471). After 5 days, neurosphere formation was counted; pictures covering the whole well were taken 5 days after treatment. Dense clusters >.05mm in diameter were counted as true tumor spheres. Spheres were measured on ImageJ and quantified.

Gamma-H2AX measurement: Instructions for the FlowCellect™ Cell Cycle Checkpoint H2A.X DNA Damage Kit (Millipore FCCH12542) were followed: cells were fixed and permeabilized, followed by staining with an anti-phospho-H2A.X antibody and propidium iodide. For co-staining with RPA, an additional step was performed during which cells were incubated with an RPA antibody (Abcam ab79398) for 1 hour and secondary antibody for 1 hour. (Propidium iodide was not used in this setting.) Fluorescence was measured on a Guava® flow cytometer.

pTOPBP1 measurement: Cells were fixed and permeabilized, followed by incubation with primary antibody (Abgent AP3774a) for 2 hours at room temperature and secondary antibody for 2 hours at room temperature. Fluorescence was measured on a Guava® flow cytometer.

Transfection: Plasmids were electroporated into cells using an Amaxa Nucleofector™ 2b (Lonza) and Cell Line Nucleofector® Kit V (Lonza VCA-1003). TOPBP1 WT and mutant plasmids were graciously supplied by Dr. Weei-Chin Lin. An mcherry plasmid was kindly given to us by Dr. Papapetrou and was co-transfected to determine transfection efficiency and to gate transfected cells for flow cytometry experiments.

Karyotyping: Chromosomal analysis was done by Dr. Murty Vundavalli at Columbia University as follows: Mouse PTEN$^{-/-}$ and PTEN WT cells were sub-cultured and the drug was added at the indicated concentrations 24h after sub-culturing. The cells were processed for metaphases preparations by standard protocols after 48h and 72h of drug exposure with the addition of colcemid for the last 2hr. A total of 100 metaphases were analyzed from replicate experiments to identify chromatid- and chromosome-type aberrations such as chromatid and chromosome breaks, multi-radial chromosomes, extensive breakage resulting in pulverization. Chromatid and chromosome breaks were considered as a single break, multi-radial chromosomes were considered as 3 breaks in assessing the frequency of abnormal metaphases and chromosome breaks. However, extensive breakage resulting in pulverization in rare metaphases was not considered in calculating the frequency of breaks. Experiment was repeated twice.

Statistical Analysis: ANOVA or student's *t*-tests were used to test means between groups. Correction for multiple comparisons was added where needed. Analysis was done using GraphPad Prism 6 or Microsoft Excel. Data are shown as means $\pm$ SD, except for mouse experiments which are shown as $\pm$ SEM.

References

Alessi, D. R., S. R. James, C. P. Downes, A. B. Holmes, P. R. J. Gaffney, C. B. Reese and P. Cohen (1997). "Characterization of a 3-phosphoinositide-dependent protein kinase which phosphorylates and activates protein kinase Bα." Current Biology **7**(4): 261-269.

Alimonti, A., C. Nardella, Z. Chen, J. G. Clohessy, A. Carracedo, L. C. Trotman, K. Cheng, S. Varmeh, S. C. Kozma, G. Thomas, E. Rosivatz, R. Woscholski, F. Cognetti, H. I. Scher and P. P. Pandolfi "A novel type of cellular senescence that can be enhanced in mouse models and human tumor xenografts to suppress prostate tumorigenesis." The Journal of Clinical Investigation **120**(3): 681-693.

Alt, J. R., J. L. Cleveland, M. Hannink and J. A. Diehl (2000). "Phosphorylation-dependent regulation of cyclin D1 nuclear export and cyclin D1–dependent cellular transformation." Genes & Development **14**(24): 3102-3114.

Ames, B. N., M. K. Shigenaga and T. M. Hagen (1993). "Oxidants, antioxidants, and the degenerative diseases of aging." Proceedings of the National Academy of Sciences **90**(17): 7915-7922.

Andreassen, P. R., A. D. D'Andrea and T. Taniguchi (2004). "ATR couples FANCD2 monoubiquitination to the DNA-damage response." Genes & Development **18**(16): 1958-1963.

ANITA, S. C., A. Finnegan, X. Jiang, H. Gebel, H. N. Sankary, P. Foster and J. W. Williams (1993). "LEFLUNOMIDE, A NOVEL IMMUNOSUPPRESSIVE AGENT: THE MECHANISM OF INHIBITION OF T CELL PROLIFERATION." Transplantation **55**(6): 1361-1366.

Backer, J. M., M. G. Myers Jr, S. E. Shoelson, D. J. Chin, X. J. Sun, M. Miralpeix, P. Hu, B. Margolis, E. Y. Skolnik and J. Schlessinger (1992). "Phosphatidylinositol 3'-kinase is activated by association with IRS-1 during insulin stimulation." The EMBO journal **11**(9): 3469.

Bartek, J. and J. Lukas (2003). "Chk1 and Chk2 kinases in checkpoint control and cancer." Cancer Cell **3**(5): 421-429.

Bartlett, R. R. and R. Schleyerbach (1985). "Immunopharmacological profile of a novel isoxazol derivative, HWA 486, with potential antirheumatic activity—I. Disease modifying action on adjuvant arthritis of the rat." International journal of immunopharmacology **7**(1): 7-18.

Bassi, C., J. Ho, T. Srikumar, R. Dowling, C. Gorrini, S. Miller, T. Mak, B. Neel, B. Raught and V. Stambolic (2013). "Nuclear PTEN controls DNA repair and sensitivity to genotoxic stress." Science **341**(6144): 395-399.

Baysal, B. E., R. E. Ferrell, J. E. Willett-Brozick, E. C. Lawrence, D. Myssiorek, A. Bosch, A. v. d. Mey, P. E. M. Taschner, W. S. Rubinstein, E. N. Myers, C. W. Richard , C. J. Cornelisse, P. Devilee and B. Devlin (2000). Science **287**(5454): 848-851.

Ben-Sahra, I., J. J. Howell, J. M. Asara and B. D. Manning (2013). "Stimulation of de novo pyrimidine synthesis by growth signaling through mTOR and S6K1." Science **339**(6125): 1323-1328.

Berwick, D. C., I. Hers, K. J. Heesom, S. K. Moule and J. M. Tavaré (2002). "The Identification of ATP-citrate Lyase as a Protein Kinase B (Akt) Substrate in Primary Adipocytes." Journal of Biological Chemistry **277**(37): 33895-33900.

Bester, Assaf C., M. Roniger, Yifat S. Oren, Michael M. Im, D. Sarni, M. Chaoat, A. Bensimon, G. Zamir, Donna S. Shewach and B. Kerem (2011). "Nucleotide Deficiency Promotes Genomic Instability in Early Stages of Cancer Development." Cell **145**(3): 435-446.

Breedveld, F. and J. Dayer (2000). "Leflunomide: mode of action in the treatment of rheumatoid arthritis." Annals of the Rheumatic Diseases **59**(11): 841-849.

Bultman, S. J. (2016). "Interplay between diet, gut microbiota, epigenetic events, and colorectal cancer." Molecular Nutrition & Food Research: n/a-n/a.

Burnett, P. E., R. K. Barrow, N. A. Cohen, S. H. Snyder and D. M. Sabatini (1998). "RAFT1 phosphorylation of the translational regulators p70 S6 kinase and 4E-BP1." Proceedings of the National Academy of Sciences **95**(4): 1432-1437.

Bush, N. A. O., S. M. Chang and M. S. Berger (2016). "Current and future strategies for treatment of glioma." Neurosurgical Review: 1-14.

Chang, L., H. Kamata, G. Solinas, J. L. Luo, S. Maeda, K. Venuprasad, Y. C. Liu and M. Karin (2006). "The E3 ubiquitin ligase itch couples JNK activation to TNFalpha-induced cell death by inducing c-FLIP(L) turnover." Cell **124**.

Charette, M. and M. W. Gray (2000). "Pseudouridine in RNA: what, where, how, and why." IUBMB life **49**(5): 341-351.

Chen, Z., L. C. Trotman, D. Shaffer, H.-K. Lin, Z. A. Dotan, M. Niki, J. A. Koutcher, H. I. Scher, T. Ludwig, W. Gerald, C. Cordon-Cardo and P. Paolo Pandolfi (2005). "Crucial role of p53-dependent cellular senescence in suppression of Pten-deficient tumorigenesis." Nature **436**(7051): 725-730.

Cherwinski, H. M., R. G. Cohn, P. Cheung, D. J. Webster, Y. Z. Xu, J. P. Caulfield, J. M. Young, G. Nakano and J. T. Ransom (1995). "The immunosuppressant leflunomide inhibits lymphocyte proliferation by inhibiting pyrimidine biosynthesis." Journal of Pharmacology and Experimental Therapeutics **275**(2): 1043-1049.

Cho, S. H., C. D. Toouli, G. H. Fujii, C. Crain and D. Parry (2005). "Chk1 is Essential for Tumor Cell Viability Following Activation of the Replication Checkpoint." Cell Cycle **4**(1): 131-139.

Christofk, H. R., M. G. Vander Heiden, M. H. Harris, A. Ramanathan, R. E. Gerszten, R. Wei, M. D. Fleming, S. L. Schreiber and L. C. Cantley (2008). "The M2 splice isoform of pyruvate kinase is important for cancer metabolism and tumour growth." Nature **452**(7184): 230-233.

Coleman, P., D. Suttle and G. Stark (1977). "Purification from hamster cells of the multifunctional protein that initiates de novo synthesis of pyrimidine nucleotides." Journal of Biological Chemistry **252**(18): 6379-6385.

Cory, J. G. and A. H. Cory (2006). "Critical roles of glutamine as nitrogen donors in purine and pyrimidine nucleotide synthesis: asparaginase treatment in childhood acute lymphoblastic leukemia." In vivo **20**(5): 587-589.

Csibi, A., S.-M. Fendt, C. Li, G. Poulogiannis, Andrew Y. Choo, Douglas J. Chapski, Seung M. Jeong, J. M. Dempsey, A. Parkhitko, T. Morrison, E. P. Henske, Marcia C. Haigis, Lewis C. Cantley, G. Stephanopoulos, J. Yu and J. Blenis (2013). "The mTORC1 Pathway Stimulates Glutamine Metabolism and Cell Proliferation by Repressing SIRT4." Cell **153**(4): 840-854.

Dang, L., D. W. White, S. Gross, B. D. Bennett, M. A. Bittinger, E. M. Driggers, V. R. Fantin, H. G. Jang, S. Jin, M. C. Keenan, K. M. Marks, R. M. Prins, P. S. Ward, K. E. Yen, L. M. Liau, J. D. Rabinowitz, L. C. Cantley, C. B. Thompson, M. G. Vander Heiden and S. M. Su (2009). "Cancer-associated IDH1 mutations produce 2-hydroxyglutarate." Nature **462**(7274): 739-744.

Das, S., J. E. Dixon and W. Cho (2003). "Membrane-binding and activation mechanism of PTEN." Proceedings of the National Academy of Sciences **100**(13): 7491-7496.

Datta, S. R., H. Dudek, X. Tao, S. Masters, H. Fu, Y. Gotoh and M. E. Greenberg (1997). "Akt Phosphorylation of BAD Couples Survival Signals to the Cell-Intrinsic Death Machinery." Cell **91**(2): 231-241.

Datta, S. R., A. Katsov, L. Hu, A. Petros, S. W. Fesik, M. B. Yaffe and M. E. Greenberg (2000). "14-3-3 Proteins and Survival Kinases Cooperate to Inactivate BAD by BH3 Domain Phosphorylation." Molecular Cell **6**(1): 41-51.

DeBerardinis, R. J. and T. Cheng (2010). "Q's next: the diverse functions of glutamine in metabolism, cell biology and cancer." Oncogene **29**(3): 313-324.

DeBerardinis, R. J., J. J. Lum, G. Hatzivassiliou and C. B. Thompson (2008). "The Biology of Cancer: Metabolic Reprogramming Fuels Cell Growth and Proliferation." Cell Metabolism **7**(1): 11-20.

DeBerardinis, R. J., A. Mancuso, E. Daikhin, I. Nissim, M. Yudkoff, S. Wehrli and C. B. Thompson (2007). "Beyond aerobic glycolysis: Transformed cells can engage in glutamine metabolism that exceeds the requirement for protein and nucleotide synthesis." Proceedings of the National Academy of Sciences **104**(49): 19345-19350.

Diehl, J. A., M. Cheng, M. F. Roussel and C. J. Sherr (1998). "Glycogen synthase kinase-3β regulates cyclin D1 proteolysis and subcellular localization." Genes & Development **12**(22): 3499-3511.

Dolado, I. and A. R. Nebreda (2008). "AKT and Oxidative Stress Team Up to Kill Cancer Cells." Cancer Cell **14**(6): 427-429.

Dos, D. S., S. M. Ali, D.-H. Kim, D. A. Guertin, R. R. Latek, H. Erdjument-Bromage, P. Tempst and D. M. Sabatini (2004). "Rictor, a Novel Binding Partner of mTOR, Defines a Rapamycin-Insensitive and Raptor-Independent Pathway that Regulates the Cytoskeleton." Current Biology **14**(14): 1296-1302.

Dourdin, N., B. Schade, R. Lesurf, M. Hallett, R. J. Munn, R. D. Cardiff and W. J. Muller (2008). "Phosphatase and Tensin Homologue Deleted on Chromosome 10 Deficiency Accelerates Tumor Induction in a Mouse Model of ErbB-2 Mammary Tumorigenesis." Cancer Research **68**(7): 2122-2131.

Elledge, S. J. (1996). "Cell Cycle Checkpoints: Preventing an Identity Crisis." Science **274**(5293): 1664-1672.

Elstrom, R. L., D. E. Bauer, M. Buzzai, R. Karnauskas, M. H. Harris, D. R. Plas, H. Zhuang, R. M. Cinalli, A. Alavi and C. M. Rudin (2004). "Akt stimulates aerobic glycolysis in cancer cells." Cancer research **64**(11): 3892-3899.

Farber , S., L. K. Diamond , R. D. Mercer , R. F. J. Sylvester and J. A. Wolff (1948). "Temporary Remissions in Acute Leukemia in Children Produced by Folic Acid Antagonist, 4-Aminopteroyl-Glutamic Acid (Aminopterin)." New England Journal of Medicine **238**(23): 787-793.

Fendt, S.-M., J. M. Buescher, F. Rudroff, P. Picotti, N. Zamboni and U. Sauer (2010). "Tradeoff between enzyme and metabolite efficiency maintains metabolic homeostasis upon perturbations in enzyme capacity." Molecular Systems Biology **6**: 356-356.

Feng, J., J. Park, P. Cron, D. Hess and B. A. Hemmings (2004). "Identification of a PKB/Akt Hydrophobic Motif Ser-473 Kinase as DNA-dependent Protein Kinase." Journal of Biological Chemistry **279**(39): 41189-41196.

Figueroa, M. E., O. Abdel-Wahab, C. Lu, P. S. Ward, J. Patel, A. Shih, Y. Li, N. Bhagwat, A. Vasanthakumar, H. F. Fernandez, M. S. Tallman, Z. Sun, K. Wolniak, J. K. Peeters, W. Liu, S. E. Choe, V. R. Fantin, E. Paietta, B. Löwenberg, J. D. Licht, L. A. Godley, R. Delwel, P. J. M. Valk, C. B. Thompson, R. L. Levine and A. Melnick (2010). "Leukemic IDH1 and IDH2 Mutations Result in a Hypermethylation Phenotype, Disrupt TET2 Function, and Impair Hematopoietic Differentiation." Cancer Cell **18**(6): 553-567.

Fine, B., C. Hodakoski, S. Koujak, T. Su, L. H. Saal, M. Maurer, B. Hopkins, M. Keniry, M. L. Sulis, S. Mense, H. Hibshoosh and R. Parsons (2009). "Activation of the PI3K Pathway in Cancer Through Inhibition of PTEN by Exchange Factor P-REX2a." Science **325**(5945): 1261-1265.

Fraser, M., H. Zhao, K. R. Luoto, C. Lundin, C. Coackley, N. Chan, A. M. Joshua, T. A. Bismar, A. Evans, T. Helleday and R. G. Bristow (2012). Clinical Cancer Research **18**(4): 1015-1027.

Freedman, V. H. and S.-i. Shin "Cellular tumorigenicity in nude mice: Correlation with cell growth in semi-solid medium." Cell **3**(4): 355-359.

Freeman, D. J., A. G. Li, G. Wei, H.-H. Li, N. Kertesz, R. Lesche, A. D. Whale, H. Martinez-Diaz, N. Rozengurt, R. D. Cardiff, X. Liu and H. Wu (2003). "PTEN tumor suppressor regulates p53 protein levels and activity through phosphatase-dependent and -independent mechanisms." Cancer Cell **3**(2): 117-130.

Furnari, F. B., H.-J. S. Huang and W. K. Cavenee (1998). Cancer Research **58**(22): 5002-5008.

Gaglio, D., C. M. Metallo, P. A. Gameiro, K. Hiller, L. S. Danna, C. Balestrieri, L. Alberghina, G. Stephanopoulos and F. Chiaradonna (2011). "Oncogenic K-Ras decouples glucose and glutamine metabolism to support cancer cell growth." Molecular systems biology **7**(1): 523.

Garcia-Cao, I., Min S. Song, Robin M. Hobbs, G. Laurent, C. Giorgi, Vincent C. J. de Boer, D. Anastasiou, K. Ito, Atsuo T. Sasaki, L. Rameh, A. Carracedo, Matthew G. Vander Heiden, Lewis C. Cantley, P. Pinton, Marcia C. Haigis and Pier P. Pandolfi (2012). "Systemic Elevation of PTEN Induces a Tumor-Suppressive Metabolic State." Cell **149**(1): 49-62.

Gatei, M., K. Sloper, C. Sörensen, R. Syljuäsen, J. Falck, K. Hobson, K. Savage, J. Lukas, B. B. Zhou, J. Bartek and K. K. Khanna (2003). "Ataxia-telangiectasia-mutated (ATM) and NBS1-dependent phosphorylation of Chk1 on Ser-317 in response to ionizing radiation." Journal of Biological Chemistry **278**(17): 14806-14811.

Goodwin, P. J., K. I. Pritchard, M. Ennis, M. Clemons, M. Graham and I. G. Fantus (2008). "Insulin-Lowering Effects of Metformin in Women with Early Breast Cancer." Clinical Breast Cancer **8**(6): 501-505.

Greene, S., K. Watanabe, J. Braatz-Trulson and L. Lou (1995). "Inhibition of dihydroorotate dehydrogenase by the immunosuppressive agent leflunomide." Biochemical Pharmacology **50**(6): 861-867.

Grimshaw, M. J., L. Cooper, K. Papazisis, J. A. Coleman, H. R. Bohnenkamp, L. Chiapero-Stanke, J. Taylor-Papadimitriou and J. M. Burchell (2008). "Mammosphere culture of metastatic breast cancer cells enriches for tumorigenic breast cancer cells." Breast Cancer Research **10**(3): R52.

Gross, M. I., S. D. Demo, J. B. Dennison, L. Chen, T. Chernov-Rogan, B. Goyal, J. R. Janes, G. J. Laidig, E. R. Lewis and J. Li (2014). "Antitumor activity of the glutaminase inhibitor CB-839 in triple-negative breast cancer." Molecular cancer therapeutics **13**(4): 890-901.

Gupta, A., Q. Yang, R. K. Pandita, C. R. Hunt, T. Xiang, S. Misri, S. Zeng, J. Pagan, J. Jeffery, J. Puc, R. Kumar, Z. Feng, S. N. Powell, A. Bhat, T. Yaguchi, R. Wadhwa, S. C. Kaul, R. Parsons, K. K. Khanna and T. K. Pandita (2009). "Cell cycle checkpoint defects contribute to genomic instability in PTEN deficient cells independent of DNA DSB repair." Cell Cycle **8**(14): 2198-2210.

Haar, E. V., S.-i. Lee, S. Bandhakavi, T. J. Griffin and D.-H. Kim (2007). "Insulin signalling to mTOR mediated by the Akt/PKB substrate PRAS40." Nat Cell Biol **9**(3): 316-323.

Hail, N., P. Chen and L. R. Bushman (2010). "Teriflunomide (leflunomide) promotes cytostatic, antioxidant, and apoptotic effects in transformed prostate epithelial cells: evidence supporting a role for teriflunomide in prostate cancer chemoprevention." Neoplasia **12**(6): 464-475.

Hanahan, D. and R. A. Weinberg (2000). "The Hallmarks of Cancer." Cell **100**(1): 57-70.

Hanahan, D. and Robert A. Weinberg (2011). "Hallmarks of Cancer: The Next Generation." Cell **144**(5): 646-674.

Hancock, J. T., R. Desikan and S. J. Neill (2001). "Role of reactive oxygen species in cell signalling pathways." Biochemical Society Transactions **29**(2): 345-349.

Hara, K., Y. Maruki, X. Long, K.-i. Yoshino, N. Oshiro, S. Hidayat, C. Tokunaga, J. Avruch and K. Yonezawa (2002). "Raptor, a Binding Partner of Target of Rapamycin (TOR), Mediates TOR Action." Cell **110**(2): 177-189.

He, J., X. Kang, Y. Yin, K. C. Chao and W. H. Shen (2015). "PTEN regulates DNA replication progression and stalled fork recovery." Nature communications **6**.

Hodakoski, C., B. D. Hopkins, D. Barrows, S. M. Mense, M. Keniry, K. E. Anderson, P. A. Kern, P. T. Hawkins, L. R. Stephens and R. Parsons (2014). "Regulation of PTEN inhibition by the pleckstrin homology domain of P-REX2 during insulin signaling and glucose homeostasis." Proceedings of the National Academy of Sciences **111**(1): 155-160.

Hu, H., A. Juvekar, Costas A. Lyssiotis, Evan C. Lien, John G. Albeck, D. Oh, G. Varma, Yin P. Hung, S. Ullas, J. Lauring, P. Seth, Mark R. Lundquist, Dean R. Tolan, Aaron K. Grant, Daniel J. Needleman, John M. Asara, Lewis C. Cantley and Gerburg M. Wulf (2016). "Phosphoinositide 3-Kinase Regulates Glycolysis through Mobilization of Aldolase from the Actin Cytoskeleton." Cell **164**(3): 433-446.

Huang, H., J. C. Cheville, Y. Pan, P. C. Roche, L. J. Schmidt and D. J. Tindall (2001). "PTEN induces chemosensitivity in PTEN-mutated prostate cancer cells by suppression of Bcl-2 expression." Journal of Biological Chemistry **276**(42): 38830-38836.

Hutchings, B., J. Mowat, J. Oleson, E. Stokstad, J. Boothe, C. Waller, R. Angier, J. Semb and Y. SubbaRow (1947). "Pteroylaspartic acid, an antagonist for pteroylglutamic acid." J. biol. Chem **170**: 323.

Inoki, K., Y. Li, T. Zhu, J. Wu and K.-L. Guan (2002). "TSC2 is phosphorylated and inhibited by Akt and suppresses mTOR signalling." Nat Cell Biol **4**(9): 648-657.

Jiao, J., S. Wang, R. Qiao, I. Vivanco, P. A. Watson, C. L. Sawyers and H. Wu (2007). "Murine Cell Lines Derived from Pten Null Prostate Cancer Show the Critical Role of PTEN in Hormone Refractory Prostate Cancer Development." Cancer Research **67**(13): 6083-6091.

Kamburov, A., R. Cavill, T. M. Ebbels, R. Herwig and H. C. Keun (2011). "Integrated pathway-level analysis of transcriptomics and metabolomics data with IMPaLA." Bioinformatics **27**(20): 2917-2918.

Kandel, E. S., J. Skeen, N. Majewski, A. Di Cristofano, P. P. Pandolfi, C. S. Feliciano, A. Gartel and N. Hay (2002). "Activation of Akt/Protein Kinase B Overcomes a G2/M Cell Cycle Checkpoint Induced by DNA Damage." Molecular and Cellular Biology **22**(22): 7831-7841.

Keniry, M. and R. Parsons (2008). "The role of PTEN signaling perturbations in cancer and in targeted therapy." Oncogene **27**(41): 5477-5485.

Kim, D.-H., D. D. Sarbassov, S. M. Ali, J. E. King, R. R. Latek, H. Erdjument-Bromage, P. Tempst and D. M. Sabatini (2002). "mTOR Interacts with Raptor to Form a Nutrient-Sensitive Complex that Signals to the Cell Growth Machinery." Cell **110**(2): 163-175.

Kim, M. Y., T. Zhang and W. L. Kraus (2005). "Poly(ADP-ribosyl)ation by PARP-1: `PAR-laying' NAD+ into a nuclear signal." Genes & Development **19**(17): 1951-1967.

King, F. W., J. Skeen, N. Hay and E. Shtivelman (2004). "Inhibition of Chk1 by activated PKB/Akt." Cell Cycle **3**(5): 632-635.

Klil-Drori, A. J., L. Azoulay and M. N. Pollak (2016). "Cancer, obesity, diabetes, and antidiabetic drugs: is the fog clearing?" Nat Rev Clin Oncol **advance online publication**.

Klinghoffer, R. A., B. Duckworth, M. Valius, L. Cantley and A. Kazlauskas (1996). "Platelet-derived growth factor-dependent activation of phosphatidylinositol 3-kinase is regulated by receptor binding of SH2-domain-containing proteins which influence Ras activity." Molecular and Cellular Biology **16**(10): 5905-5914.

Kohn, A. D., S. A. Summers, M. J. Birnbaum and R. A. Roth (1996). "Expression of a Constitutively Active Akt Ser/Thr Kinase in 3T3-L1 Adipocytes Stimulates Glucose Uptake and Glucose Transporter 4 Translocation." Journal of Biological Chemistry **271**(49): 31372-31378.

Koppenol, W. H., P. L. Bounds and C. V. Dang (2011). "Otto Warburg's contributions to current concepts of cancer metabolism." Nat Rev Cancer **11**(5): 325-337.

Kumagai, A., J. Lee, H. Y. Yoo and W. G. Dunphy (2006). "TopBP1 activates the ATR-ATRIP complex." Cell **124**(5): 943-955.

Kushner, J. A., L. Simpson, L. M. Wartschow, S. Guo, M. M. Rankin, R. Parsons and M. F. White (2005). "Phosphatase and Tensin Homolog Regulation of Islet Growth and Glucose Homeostasis." Journal of Biological Chemistry **280**(47): 39388-39393.

Lawrence, M. S., P. Stojanov, C. H. Mermel, J. T. Robinson, L. A. Garraway, T. R. Golub, M. Meyerson, S. B. Gabriel, E. S. Lander and G. Getz (2014). "Discovery and saturation analysis of cancer genes across 21 tumour types." Nature **505**(7484): 495-501.

Lee, J. and P. F. Pilch (1994). "The insulin receptor: structure, function, and signaling." American Journal of Physiology - Cell Physiology **266**(2): C319-C334.

Leger, D., B. Liagre and J. Beneytout (2006). "Low dose leflunomide activates PI3K/Akt signalling in erythroleukemia cells and reduces apoptosis induced by anticancer agents." Apoptosis **11**(10): 1747-1760.

Li, G., G. W. Robinson, R. Lesche, H. Martinez-Diaz, Z. Jiang, N. Rozengurt, K.-U. Wagner, D.-C. Wu, T. F. Lane, X. Liu, L. Hennighausen and H. Wu (2002). "Conditional loss of PTEN leads to precocious development and neoplasia in the mammary gland." Development **129**(17): 4159-4170.

Li, J., C. Yen, D. Liaw, K. Podsypanina, S. Bose, S. I. Wang, J. Puc, C. Miliaresis, L. Rodgers, R. McCombie, S. H. Bigner, B. C. Giovanella, M. Ittmann, B. Tycko, H. Hibshoosh, M. H. Wigler and R. Parsons (1997). "PTEN, a Putative Protein Tyrosine Phosphatase Gene Mutated in Human Brain, Breast, and Prostate Cancer." Science **275**(5308): 1943-1947.

Liaw, D., D. J. Marsh, J. Li, P. L. M. Dahia, S. I. Wang, Z. Zheng, S. Bose, K. M. Call, H. C. Tsou, M. Peacoke, C. Eng and R. Parsons (1997). "Germline mutations of the PTEN gene in Cowden disease, an inherited breast and thyroid cancer syndrome." Nat Genet **16**(1): 64-67.

Linder-Horowitz, M., W. E. Knox and H. P. Morris (1969). "Glutaminase Activities and Growth Rates of Rat Hepatomas." Cancer Research **29**(6): 1195-1199.

Liu, K., J. D. Graves, J. D. Scott, R. Li and W.-C. Lin (2013). "Akt switches TopBP1 function from checkpoint activation to transcriptional regulation through phosphoserine binding-mediated oligomerization." Molecular and cellular biology **33**(23): 4685-4700.

Liu, K., J. C. Paik, B. Wang, F. T. Lin and W. C. Lin (2006). "Regulation of TopBP1 oligomerization by Akt/PKB for cell survival." The EMBO journal **25**(20): 4795-4807.

Liu, Q., S. Guntuku, X.-S. Cui, S. Matsuoka, D. Cortez, K. Tamai, G. Luo, S. Carattini-Rivera, F. DeMayo and A. Bradley (2000). "Chk1 is an essential kinase that is regulated by Atr and required for the G2/M DNA damage checkpoint." Genes & development **14**(12): 1448-1459.

Locasale, J. W. (2013). "Serine, glycine and one-carbon units: cancer metabolism in full circle." Nat Rev Cancer **13**(8): 572-583.

Locasale, J. W., A. R. Grassian, T. Melman, C. A. Lyssiotis, K. R. Mattaini, A. J. Bass, G. Heffron, C. M. Metallo, T. Muranen, H. Sharfi, A. T. Sasaki, D. Anastasiou, E. Mullarky, N. I. Vokes, M. Sasaki, R. Beroukhim, G. Stephanopoulos, A. H. Ligon, M. Meyerson, A. L. Richardson, L. Chin, G. Wagner, J. M. Asara, J. S. Brugge, L. C. Cantley and M. G. Vander Heiden (2011). "Phosphoglycerate dehydrogenase diverts glycolytic flux and contributes to oncogenesis." Nat Genet **43**(9): 869-874.

Lodish, H., A. Berk, S. L. Zipursky, P. Matsudaira, D. Baltimore and J. Darnell (2000). "Proto-oncogenes and tumor-suppressor genes."

Loewith, R., E. Jacinto, S. Wullschleger, A. Lorberg, J. L. Crespo, D. Bonenfant, W. Oppliger, P. Jenoe and M. N. Hall (2002). "Two TOR Complexes, Only One of which Is Rapamycin Sensitive, Have Distinct Roles in Cell Growth Control." Molecular Cell **10**(3): 457-468.

Maehama, T. and J. E. Dixon (1998). "The tumor suppressor, PTEN/MMAC1, dephosphorylates the lipid second messenger, phosphatidylinositol 3, 4, 5-trisphosphate." Journal of Biological Chemistry **273**(22): 13375-13378.

Manning, B. D., A. R. Tee, M. N. Logsdon, J. Blenis and L. C. Cantley (2002). "Identification of the Tuberous Sclerosis Complex-2 Tumor Suppressor Gene Product Tuberin as a Target of the Phosphoinositide 3-Kinase/Akt Pathway." Molecular Cell **10**(1): 151-162.

Martin, S. A. and T. Ouchi (2008). "Cellular commitment to reentry into the cell cycle after stalled DNA is determined by site-specific phosphorylation of Chk1 and PTEN." Molecular cancer therapeutics **7**(8): 2509-2516.

Mayo, L. D. and D. B. Donner (2001). "A phosphatidylinositol 3-kinase/Akt pathway promotes translocation of Mdm2 from the cytoplasm to the nucleus." Proceedings of the National Academy of Sciences of the United States of America **98**(20): 11598-11603.

McLean, J. E., E. A. Neidhardt, T. H. Grossman and L. Hedstrom (2001). "Multiple inhibitor analysis of the brequinar and leflunomide binding sites on human dihydroorotate dehydrogenase." Biochemistry **40**(7): 2194-2200.

Mendes-Pereira, A. M., S. A. Martin, R. Brough, A. McCarthy, J. R. Taylor, J. S. Kim, T. Waldman, C. J. Lord and A. Ashworth (2009). "Synthetic lethal targeting of PTEN mutant cells with PARP inhibitors." EMBO molecular medicine **1**(6-7): 315-322.

Meng, F., R. Henson, H. Wehbe–Janek, K. Ghoshal, S. T. Jacob and T. Patel (2007). "MicroRNA-21 Regulates Expression of the PTEN Tumor Suppressor Gene in Human Hepatocellular Cancer." Gastroenterology **133**(2): 647-658.

Mense, S. M., D. Barrows, C. Hodakoski, N. Steinbach, D. Schoenfeld, W. Su, B. D. Hopkins, T. Su, B. Fine and H. Hibshoosh (2015). "PTEN inhibits PREX2-catalyzed activation of RAC1 to restrain tumor cell invasion." Sci. Signal. **8**(370): ra32-ra32.

Metsalu, T. and J. Vilo (2015). "ClustVis: a web tool for visualizing clustering of multivariate data using Principal Component Analysis and heatmap." Nucleic Acids Research **43**(W1): W566-W570.

Minotti, G., P. Menna, E. Salvatorelli, G. Cairo and L. Gianni (2004). "Anthracyclines: molecular advances and pharmacologic developments in antitumor activity and cardiotoxicity." Pharmacological reviews **56**(2): 185-229.

Moasser, M. M. (2007). "The oncogene HER2: its signaling and transforming functions and its role in human cancer pathogenesis." Oncogene **26**(45): 6469-6487.

Mone, A. P. and J. C. Byrd (2004). Leflunomide Inhibits Proliferation of Neoplastic B-Cell Lines and Induces Apoptosis in Primary CLL Cells. ASH Annual Meeting Abstracts.

Mootha, V. K., C. M. Lindgren, K.-F. Eriksson, A. Subramanian, S. Sihag, J. Lehar, P. Puigserver, E. Carlsson, M. Ridderstrale, E. Laurila, N. Houstis, M. J. Daly, N. Patterson, J. P. Mesirov, T. R. Golub, P. Tamayo, B. Spiegelman, E. S. Lander, J. N. Hirschhorn, D. Altshuler and L. C. Groop (2003). "PGC-1[alpha]-responsive genes involved in oxidative phosphorylation are coordinately downregulated in human diabetes." Nat Genet **34**(3): 267-273.

Mouw, J. K., Y. Yui, L. Damiano, R. O. Bainer, J. N. Lakins, I. Acerbi, G. Ou, A. C. Wijekoon, K. R. Levental, P. M. Gilbert, Y.-Y. Chen and V. M. Weaver (2014). "Tissue mechanics modulate microRNA-dependent PTEN expression to regulate malignant progression." Nature medicine **20**(4): 360-367.

Mukherjee, S. (2010). The emperor of all maladies: a biography of cancer, Simon and Schuster.

Mukhopadhyay, P., M. Rajesh, G. Hasko, B. J. Hawkins, M. Madesh and P. Pacher (2007). "Simultaneous detection of apoptosis and mitochondrial superoxide production in live cells by flow cytometry and confocal microscopy." Nat. Protocols **2**(9): 2295-2301.

Mullen, A. R., W. W. Wheaton, E. S. Jin, P.-H. Chen, L. B. Sullivan, T. Cheng, Y. Yang, W. M. Linehan, N. S. Chandel and R. J. DeBerardinis (2012). "Reductive carboxylation supports growth in tumour cells with defective mitochondria." Nature **481**(7381): 385-388.

Munier-Lehmann, H. l. n., P.-O. Vidalain, F. d. r. Tangy and Y. L. Janin (2013). "On dihydroorotate dehydrogenases and their inhibitors and uses." Journal of medicinal chemistry **56**(8): 3148-3167.

Myers, M. P., I. Pass, I. H. Batty, J. Van der Kaay, J. P. Stolarov, B. A. Hemmings, M. H. Wigler, C. P. Downes and N. K. Tonks (1998). "The lipid phosphatase activity of PTEN is critical for its tumor supressor function." Proceedings of the National Academy of Sciences **95**(23): 13513-13518.

Myers, M. P., J. P. Stolarov, C. Eng, J. Li, S. I. Wang, M. H. Wigler, R. Parsons and N. K. Tonks (1997). "P-TEN, the tumor suppressor from human chromosome 10q23, is a dual-specificity phosphatase." Proceedings of the National Academy of Sciences of the United States of America **94**(17): 9052-9057.

Nelson, D. L., A. L. Lehninger and M. M. Cox (2008). Lehninger principles of biochemistry, Macmillan.

Neshat, M. S., I. K. Mellinghoff, C. Tran, B. Stiles, G. Thomas, R. Petersen, P. Frost, J. J. Gibbons, H. Wu and C. L. Sawyers (2001). "Enhanced sensitivity of PTEN-deficient tumors to inhibition of FRAP/mTOR." Proceedings of the National Academy of Sciences **98**(18): 10314-10319.

Newsholme, E. A., B. Crabtree and M. S. M. Ardawi (1985). "The role of high rates of glycolysis and glutamine utilization in rapidly dividing cells." Bioscience Reports **5**(5): 393-400.

Nicklin, P., P. Bergman, B. Zhang, E. Triantafellow, H. Wang, B. Nyfeler, H. Yang, M. Hild, C. Kung, C. Wilson, V. E. Myer, J. P. MacKeigan, J. A. Porter, Y. K. Wang, L. C. Cantley, P. M. Finan and L. O. Murphy (2009). "Bidirectional Transport of Amino Acids Regulates mTOR and Autophagy." Cell **136**(3): 521-534.

Nogueira, V., Y. Park, C.-C. Chen, P.-Z. Xu, M.-L. Chen, I. Tonic, T. Unterman and N. Hay (2008). "Akt determines replicative senescence and oxidative or oncogenic premature senescence and sensitizes cells to oxidative apoptosis." Cancer cell **14**(6): 458-470.

Novo, E. and M. Parola (2008). "Redox mechanisms in hepatic chronic wound healing and fibrogenesis." Fibrogenesis & Tissue Repair **1**(1): 1-58.

Okumura, K., M. Mendoza, R. M. Bachoo, R. A. DePinho, W. K. Cavenee and F. B. Furnari (2006). "PCAF Modulates PTEN Activity." Journal of Biological Chemistry **281**(36): 26562-26568.

Ortega-Molina, A., A. Efeyan, E. Lopez-Guadamillas, M. Muñoz-Martin, G. Gómez-López, M. Cañamero, F. Mulero, J. Pastor, S. Martinez, E. Romanos, M. Mar Gonzalez-Barroso, E. Rial, Angela M. Valverde, James R. Bischoff and M. Serrano (2012). "Pten Positively Regulates Brown Adipose Function, Energy Expenditure, and Longevity." Cell Metabolism **15**(3): 382-394.

Oslowski, C. M. and F. Urano (2011). "Measuring ER stress and the unfolded protein response using mammalian tissue culture system." Methods in enzymology **490**: 71-92.

Pal, A., T. M. Barber, M. Van de Bunt, S. A. Rudge, Q. Zhang, K. L. Lachlan, N. S. Cooper, H. Linden, J. C. Levy, M. J. O. Wakelam, L. Walker, F. Karpe and A. L. Gloyn (2012). "PTEN Mutations as a Cause of Constitutive Insulin Sensitivity and Obesity." New England Journal of Medicine **367**(11): 1002-1011.

Papa, V., V. Pezzino, A. Costantino, A. Belfiore, D. Giuffrida, L. Frittitta, G. B. Vannelli, R. Brand, I. D. Goldfine and R. Vigneri (1990). "Elevated insulin receptor content in human breast cancer." Journal of Clinical Investigation **86**(5): 1503-1510.

Parlo, R. A. and P. S. Coleman (1984). "Enhanced rate of citrate export from cholesterol-rich hepatoma mitochondria. The truncated Krebs cycle and other metabolic ramifications of mitochondrial membrane cholesterol." Journal of Biological Chemistry **259**(16): 9997-10003.

Peso, L. d., M. González-García, C. Page, R. Herrera and G. Nuñez (1997). "Interleukin-3-Induced Phosphorylation of BAD Through the Protein Kinase Akt." Science **278**(5338): 687-689.

Peters, G. J., G. Schwartsmann, J. C. Nadal, E. J. Laurensse, C. J. van Groeningen, W. J. F. van der Vijgh and H. M. Pinedo (1990). Cancer Research **50**(15): 4644-4649.

Planchon, S. M., K. A. Waite and C. Eng (2008). "The nuclear affairs of PTEN." Journal of Cell Science **121**(3): 249-253.

Podsypanina, K., L. H. Ellenson, A. Nemes, J. Gu, M. Tamura, K. M. Yamada, C. Cordon-Cardo, G. Catoretti, P. E. Fisher and R. Parsons (1999). "Mutation of Pten/Mmac1 in mice causes neoplasia in multiple organ systems." Proceedings of the National Academy of Sciences **96**(4): 1563-1568.

Podsypanina, K., R. T. Lee, C. Politis, I. Hennessy, A. Crane, J. Puc, M. Neshat, H. Wang, L. Yang and J. Gibbons (2001). "An inhibitor of mTOR reduces neoplasia and normalizes p70/S6 kinase activity in Pten+/− mice." Proceedings of the National Academy of Sciences **98**(18): 10320-10325.

Puc, J., M. Keniry, H. S. Li, T. K. Pandita, A. D. Choudhury, L. Memeo, M. Mansukhani, V. V. Murty, Z. Gaciong and S. E. Meek (2005). "Lack of PTEN sequesters CHK1 and initiates genetic instability." Cancer cell **7**(2): 193-204.

Puc, J. and R. Parsons (2005). "PTEN loss inhibits CHK1 to cause double stranded-DNA breaks in cells." Cell Cycle **4**(7): 927-929.

Quinn, R., M. Basanta-Sanchez, R. E. Rose and D. Fabris (2013). "Direct infusion analysis of nucleotide mixtures of very similar or identical elemental composition." Journal of mass spectrometry : JMS **48**(6): 703-712.

Ralph, S. J., S. Rodríguez-Enríquez, J. Neuzil, E. Saavedra and R. Moreno-Sánchez (2010). "The causes of cancer revisited: “Mitochondrial malignancy” and ROS-induced oncogenic transformation – Why mitochondria are targets for cancer therapy." Molecular Aspects of Medicine **31**(2): 145-170.

Raught, B., F. Peiretti, A.-C. Gingras, M. Livingstone, D. Shahbazian, G. L. Mayeur, R. D. Polakiewicz, N. Sonenberg and J. W. B. Hershey (2004). "Phosphorylation of eucaryotic translation initiation factor 4B Ser422 is modulated by S6 kinases." The EMBO Journal **23**(8): 1761-1769.

Reitzer, L. J., B. M. Wice and D. Kennell (1979). "Evidence that glutamine, not sugar, is the major energy source for cultured HeLa cells." Journal of Biological Chemistry **254**(8): 2669-2676.

Rowinsky, M., Eric K (1997). "The development and clinical utility of the taxane class of antimicrotubule chemotherapy agents." Annual review of medicine **48**(1): 353-374.

Rozman, B. (2002). "Clinical pharmacokinetics of leflunomide." Clinical pharmacokinetics **41**(6): 421-430.

Rückemann, K., L. D. Fairbanks, E. A. Carrey, C. M. Hawrylowicz, D. F. Richards, B. Kirschbaum and H. A. Simmonds (1998). "Leflunomide Inhibits Pyrimidine de Novo Synthesis in Mitogen-stimulated T-lymphocytes from Healthy Humans." Journal of Biological Chemistry **273**(34): 21682-21691.

Salser, J. S., D. J. Hutchison and M. E. Balis (1960). "Studies on the Mechanism of Action of 6-Mercaptopurine in Cell-free Preparations." Journal of Biological Chemistry **235**(2): 429-432.

Samuels, Y. and K. Ericson (2006). "Oncogenic PI3K and its role in cancer." Current opinion in oncology **18**(1): 77-82.

Sano, R. and J. C. Reed (2013). "ER stress-induced cell death mechanisms." Biochimica et Biophysica Acta (BBA) - Molecular Cell Research **1833**(12): 3460-3470.

Sarbassov, D. D., D. A. Guertin, S. M. Ali and D. M. Sabatini (2005). "Phosphorylation and Regulation of Akt/PKB by the Rictor-mTOR Complex." Science **307**(5712): 1098-1101.

Sauter, G., T. Maeda, F. M. Waldman, R. L. Davis and B. G. Feuerstein (1996). "Patterns of epidermal growth factor receptor amplification in malignant gliomas." The American Journal of Pathology **148**(4): 1047-1053.

Sawamukai, N., K. Saito, K. Yamaoka, S. Nakayamada, C. Ra and Y. Tanaka (2007). "Leflunomide Inhibits PDK1/Akt Pathway and Induces Apoptosis of Human Mast Cells." The Journal of Immunology **179**(10): 6479-6484.

Segal-Bendirdjian, E., D. Coulaud, B. P. Roques and J.-B. Le Pecq (1988). "Selective Loss of Mitochondrial DNA after Treatment of Cells with Ditercalinium (NSC 335153), an Antitumor Bis-intercalating Agent." Cancer Research **48**(17): 4982-4992.

Serunian, L. A., K. R. Auger, T. M. Roberts and L. C. Cantley (1990). "Production of novel polyphosphoinositides in vivo is linked to cell transformation by polyomavirus middle T antigen." Journal of virology **64**(10): 4718-4725.

Sharma, P. (2016). "Biology and Management of Patients With Triple-Negative Breast Cancer." The Oncologist: theoncologist. 2016-0067.

Shaw, F. L., H. Harrison, K. Spence, M. P. Ablett, B. M. Simões, G. Farnie and R. B. Clarke (2012). "A Detailed Mammosphere Assay Protocol for the Quantification of Breast Stem Cell Activity." Journal of Mammary Gland Biology and Neoplasia **17**(2): 111-117.

Shechter, D., V. Costanzo and J. Gautier (2004). "ATR and ATM regulate the timing of DNA replication origin firing." Nat Cell Biol **6**(7): 648-655.

Shen-Li, H., S. Koujak, M. Szablocs and R. Parsons (2010). "Reduction of Pten dose leads to neoplastic development in multiple organs of Pten(shRNA) mice." Cancer Biology & Therapy **10**(11): 1194-1200.

Shen, W. H., A. S. Balajee, J. Wang, H. Wu, C. Eng, P. P. Pandolfi and Y. Yin (2007). "Essential role for nuclear PTEN in maintaining chromosomal integrity." Cell **128**(1): 157-170.

Shen, Z., S. Huang, M. Fang and X. Wang (2011). ENTPD5, an endoplasmic reticulum UDPase, alleviates ER stress induced by protein overloading in AKT-activated cancer cells. Cold Spring Harbor symposia on quantitative biology, Cold Spring Harbor Laboratory Press.

Shim, H., Y. S. Chun, B. C. Lewis and C. V. Dang (1998). "A unique glucose-dependent apoptotic pathway induced by c-Myc." Proceedings of the National Academy of Sciences **95**(4): 1511-1516.

Shim, H., C. Dolde, B. C. Lewis, C.-S. Wu, G. Dang, R. A. Jungmann, R. Dalla-Favera and C. V. Dang (1997). "c-Myc transactivation of LDH-A: Implications for tumor metabolism and growth." Proceedings of the National Academy of Sciences **94**(13): 6658-6663.

Shoemaker, R. H. (2006). "The NCI60 human tumour cell line anticancer drug screen." Nat Rev Cancer **6**(10): 813-823.

Shtivelman, E., J. Sussman and D. Stokoe (2002). "A role for PI 3-kinase and PKB activity in the G2/M phase of the cell cycle." Current Biology **12**(11): 919-924.

Siegel, R. L., K. D. Miller and A. Jemal (2016). "Cancer statistics, 2016." CA: A Cancer Journal For Clinicians **66**(1): 7-30.

Siemasko, K. F., A. S. Chong, J. W. Williams, E. G. Bremer and A. Finnegan (1996). "REGULATION OF B CELL FUNCTION BY THE IMMUNOSUPPRESSIVE AGENT LEFLUNOMIDE1." Transplantation **61**(4): 635-642.

Stamato, T. D. and D. Patterson (1979). "Biochemical genetic analysis of pyrimidine biosynthesis in mammalian cells. II. Isolation and characterization of a mutant of Chinese hamster ovary cells with defective dihydroorotate dehydrogenase (EC 1.3. 3.1) activity." Journal of cellular physiology **98**(3): 459-468.

Stambolic, V., D. MacPherson, D. Sas, Y. Lin, B. Snow, Y. Jang, S. Benchimol and T. W. Mak (2001). "Regulation of PTEN Transcription by p53." Molecular Cell **8**(2): 317-325.

Stambolic, V., A. Suzuki, J. L. De La Pompa, G. M. Brothers, C. Mirtsos, T. Sasaki, J. Ruland, J. M. Penninger, D. P. Siderovski and T. W. Mak (1998). "Negative regulation of PKB/Akt-dependent cell survival by the tumor suppressor PTEN." Cell **95**(1): 29-39.

Statz, C. M., S. E. Patterson and S. M. Mockus (2016). "mTOR Inhibitors in Castration-Resistant Prostate Cancer: A Systematic Review." Targeted Oncology: 1-13.

Steck, P. A., M. A. Pershouse, S. A. Jasser, W. K. A. Yung, H. Lin, A. H. Ligon, L. A. Langford, M. L. Baumgard, T. Hattier, T. Davis, C. Frye, R. Hu, B. Swedlund, D. H. R. Teng and S. V. Tavtigian (1997). "Identification of a candidate tumour suppressor gene, MMAC1, at chromosome 10q23.3 that is mutated in multiple advanced cancers." Nat Genet **15**(4): 356-362.

Stemke-Hale, K., A. M. Gonzalez-Angulo, A. Lluch, R. M. Neve, W.-L. Kuo, M. Davies, M. Carey, Z. Hu, Y. Guan and A. Sahin (2008). "An integrative genomic and proteomic analysis of PIK3CA, PTEN, and AKT mutations in breast cancer." Cancer research **68**(15): 6084-6091.

Stephens, L., K. Anderson, D. Stokoe, H. Erdjument-Bromage, G. F. Painter, A. B. Holmes, P. R. J. Gaffney, C. B. Reese, F. McCormick, P. Tempst, J. Coadwell and P. T. Hawkins (1998). "Protein Kinase B Kinases That Mediate Phosphatidylinositol 3,4,5-Trisphosphate-Dependent Activation of Protein Kinase B." Science **279**(5351): 710-714.

Stratikopoulos, E. E., M. Dendy, M. Szabolcs, A. J. Khaykin, C. Lefebvre, M.-M. Zhou and R. Parsons (2015). "Kinase and BET inhibitors together clamp inhibition of PI3K signaling and overcome resistance to therapy." Cancer cell **27**(6): 837-851.

Subramanian, A., P. Tamayo, V. K. Mootha, S. Mukherjee, B. L. Ebert, M. A. Gillette, A. Paulovich, S. L. Pomeroy, T. R. Golub, E. S. Lander and J. P. Mesirov (2005). "Gene set enrichment analysis: A knowledge-based approach for interpreting genome-wide expression profiles." Proceedings of the National Academy of Sciences **102**(43): 15545-15550.

Sul, H. S., M.-J. Latasa, Y. Moon and K.-H. Kim (2000). "Regulation of the Fatty Acid Synthase Promoter by Insulin." The Journal of Nutrition **130**(2): 315.

Surova, O. and B. Zhivotovsky (2013). "Various modes of cell death induced by DNA damage." Oncogene **32**(33): 3789-3797.

Sykes, David B., Youmna S. Kfoury, François E. Mercier, Mathias J. Wawer, Jason M. Law, Mark K. Haynes, Timothy A. Lewis, A. Schajnovitz, E. Jain, D. Lee, H. Meyer, Kerry A. Pierce, Nicola J. Tolliday, A. Waller, Steven J. Ferrara, Ashley L. Eheim, D. Stoeckigt, Katrina L. Maxcy, Julien M. Cobert, J. Bachand, Brian A. Szekely, S. Mukherjee, Larry A. Sklar, Joanne D. Kotz, Clary B. Clish, Ruslan I. Sadreyev, Paul A. Clemons, A. Janzer, Stuart L. Schreiber and David T. Scadden "Inhibition of Dihydroorotate Dehydrogenase Overcomes Differentiation Blockade in Acute Myeloid Leukemia." Cell **167**(1): 171-186.e115.

Tan, An S., James W. Baty, L.-F. Dong, A. Bezawork-Geleta, B. Endaya, J. Goodwin, M. Bajzikova, J. Kovarova, M. Peterka, B. Yan, Elham A. Pesdar, M. Sobol, A. Filimonenko, S. Stuart, M. Vondrusova, K. Kluckova, K. Sachaphibulkij, J. Rohlena, P. Hozak, J. Truksa, D. Eccles, L. M. Haupt, L. R. Griffiths, J. Neuzil and Michael V. Berridge (2015). "Mitochondrial Genome Acquisition Restores Respiratory Function and Tumorigenic Potential of Cancer Cells without Mitochondrial DNA." Cell Metabolism **21**(1): 81-94.

Tay, B., R. M. Lilley, A. Murray and M. Atkinson (1969). "Inhibition of phosphoribosyl pyrophosphate amidotransferase from Ehrlich ascites-tumour cells by thiopurine nucleotides." Biochemical pharmacology **18**(4): 936-938.

Tibbetts, R. S., D. Cortez, K. M. Brumbaugh, R. Scully, D. Livingston, S. J. Elledge and R. T. Abraham (2000). "Functional interactions between BRCA1 and the checkpoint kinase ATR during genotoxic stress." Genes & development **14**(23): 2989-3002.

Tokudome, T., A. Sasaki, M. Tsuji, Y. Udaka, H. Oyamada, H. Tsuchiya and K. Oguchi (2015). "Reduced PTEN expression and overexpression of miR-17-5p,-19a-3p,-19b-3p,-21-5p,-130b-3p,-221-3p and-222-3p by glioblastoma stem-like cells following irradiation." Oncology letters **10**(4): 2269-2272.

Toledo, Luis I., M. Altmeyer, M.-B. Rask, C. Lukas, Dorthe H. Larsen, Lou K. Povlsen, S. Bekker-Jensen, N. Mailand, J. Bartek and J. Lukas (2013). "ATR Prohibits Replication Catastrophe by Preventing Global Exhaustion of RPA." Cell **155**(5): 1088-1103.

Torres, J. and R. Pulido (2001). "The Tumor Suppressor PTEN Is Phosphorylated by the Protein Kinase CK2 at Its C Terminus: IMPLICATIONS FOR PTEN STABILITY TO PROTEASOME-MEDIATED DEGRADATION." Journal of Biological Chemistry **276**(2): 993-998.

Torres, J., J. Rodriguez, M. P. Myers, M. Valiente, J. D. Graves, N. K. Tonks and R. Pulido (2003). "Phosphorylation-regulated Cleavage of the Tumor Suppressor PTEN by Caspase-3: IMPLICATIONS FOR THE CONTROL OF PROTEIN STABILITY AND PTEN-PROTEIN INTERACTIONS." Journal of Biological Chemistry **278**(33): 30652-30660.

Trotman, L. C., M. Niki, Z. A. Dotan, J. A. Koutcher, A. Di Cristofano, A. Xiao, A. S. Khoo, P. Roy-Burman, N. M. Greenberg, T. V. Dyke, C. Cordon-Cardo and P. P. Pandolfi (2003). "Pten Dose Dictates Cancer Progression in the Prostate." PLoS Biology **1**(3): e59.

Trotman, L. C., X. Wang, A. Alimonti, Z. Chen, J. Teruya-Feldstein, H. Yang, N. P. Pavletich, B. S. Carver, C. Cordon-Cardo, H. Erdjument-Bromage, P. Tempst, S.-G. Chi, H.-J. Kim, T. Misteli, X. Jiang and P. P. Pandolfi (2007). "Ubiquitination Regulates PTEN Nuclear Import and Tumor Suppression." Cell **128**(1): 141-156.

Van de Sande, T., E. De Schrijver, W. Heyns, G. Verhoeven and J. V. Swinnen (2002). "Role of the Phosphatidylinositol 3'-Kinase/PTEN/Akt Kinase Pathway in the Overexpression of Fatty Acid Synthase in LNCaP Prostate Cancer Cells." Cancer Research **62**(3): 642-646.

Vanhaesebroeck, B. and M. D. Waterfield (1999). "Signaling by Distinct Classes of Phosphoinositide 3-Kinases." Experimental Cell Research **253**(1): 239-254.

Vazquez, F., S. Ramaswamy, N. Nakamura and W. R. Sellers (2000). "Phosphorylation of the PTEN Tail Regulates Protein Stability and Function." Molecular and Cellular Biology **20**(14): 5010-5018.

Wang, G., Y. Li, P. Wang, H. Liang, M. Cui, M. Zhu, L. Guo, Q. Su, Y. Sun and M. A. McNutt (2015). "PTEN regulates RPA1 and protects DNA replication forks." Cell Research **25**(11): 1189-1204.

Wang, X., L. C. Trotman, T. Koppie, A. Alimonti, Z. Chen, Z. Gao, J. Wang, H. Erdjument-Bromage, P. Tempst, C. Cordon-Cardo, P. P. Pandolfi and X. Jiang (2007). "NEDD4-1 Is a Proto-Oncogenic Ubiquitin Ligase for PTEN." Cell **128**(1): 129-139.

Warburg, O., F. Wind and E. Negelein (1927). "The metabolism of tumors in the body." The Journal of general physiology **8**(6): 519-530.

Ward, Patrick S. and Craig B. Thompson (2012). "Metabolic Reprogramming: A Cancer Hallmark Even Warburg Did Not Anticipate." Cancer Cell **21**(3): 297-308.

Weng, L.-P., J. L. Brown and C. Eng (2001). "PTEN coordinates G1 arrest by down-regulating cyclin D1 via its protein phosphatase activity and up-regulating p27 via its lipid phosphatase activity in a breast cancer model." Human Molecular Genetics **10**(6): 599-604.

White, R. M., J. Cech, S. Ratanasirintrawoot, C. Y. Lin, P. B. Rahl, C. J. Burke, E. Langdon, M. L. Tomlinson, J. Mosher and C. Kaufman (2011). "DHODH modulates transcriptional elongation in the neural crest and melanoma." Nature **471**(7339): 518-522.

Whiteman, D. C., X.-P. Zhou, M. C. Cummings, S. Pavey, N. K. Hayward and C. Eng (2002). "Nuclear PTEN expression and clinicopathologic features in a population-based series of primary cutaneous melanoma." International Journal of Cancer **99**(1): 63-67.

Wiencke, J. K., S. Zheng, N. Jelluma, T. Tihan, S. Vandenberg, T. Tamgüney, R. Baumber, R. Parsons, K. R. Lamborn, M. S. Berger, M. R. Wrensch, D. A. Haas-Kogan and D. Stokoe (2007). "Methylation of the PTEN promoter defines low-grade gliomas and secondary glioblastoma." Neuro-Oncology **9**(3): 271-279.

Wise, D. R., R. J. DeBerardinis, A. Mancuso, N. Sayed, X.-Y. Zhang, H. K. Pfeiffer, I. Nissim, E. Daikhin, M. Yudkoff, S. B. McMahon and C. B. Thompson (2008). "Myc regulates a transcriptional program that stimulates mitochondrial glutaminolysis and leads to glutamine addiction." Proceedings of the National Academy of Sciences **105**(48): 18782-18787.

Wong, J., P. Kim, J. Peacock, T. Yau, A.-F. Mui, S. Chung, V. Sossi, D. Doudet, D. Green, T. Ruth, P. R, V. CB and O. CJ (2007). "Pten (phosphatase and tensin homologue gene) haploinsufficiency promotes insulin hypersensitivity." Diabetologia **50**(2): 395-403.

Xu, C., B. Bailly-Maitre and J. C. Reed (2005). "Endoplasmic reticulum stress: cell life and death decisions." The Journal of Clinical Investigation **115**(10): 2656-2664.

Yang, Y., N. Shao, G. Luo, L. Li, L. Zheng, P. Nilsson-Ehle and N. Xu (2010). "Mutations of PTEN gene in gliomas correlate to tumor differentiation and short-term survival rate." Anticancer research **30**(3): 981-985.

Yarbro, J. W. (1992). Mechanism of action of hydroxyurea.

Yoshida, M., A. Hoshi and K. KURETANI (1980). "The difference in mechanism of action of 5-fluorouracil and its nucleosides in L5178Y cells." Journal of pharmacobio-dynamics **3**(8): 374-379.

Yuan, M., S. B. Breitkopf, X. Yang and J. M. Asara (2012). "A positive/negative ion-switching, targeted mass spectrometry-based metabolomics platform for bodily fluids, cells, and fresh and fixed tissue." Nature protocols **7**(5): 872-881.

Yue, S., J. Li, S.-Y. Lee, H. J. Lee, T. Shao, B. Song, L. Cheng, T. A. Masterson, X. Liu and T. L. Ratliff (2014). "Cholesteryl ester accumulation induced by PTEN loss and PI3K/AKT activation underlies human prostate cancer aggressiveness." Cell metabolism **19**(3): 393-406.

Yun, J., C. Rago, I. Cheong, R. Pagliarini, P. Angenendt, H. Rajagopalan, K. Schmidt, J. K. V. Willson, S. Markowitz, S. Zhou, L. A. Diaz, V. E. Velculescu, C. Lengauer, K. W. Kinzler, B. Vogelstein and N. Papadopoulos (2009). Science **325**(5947): 1555-1559.

Yuneva, M., N. Zamboni, P. Oefner, R. Sachidanandam and Y. Lazebnik (2007). "Deficiency in glutamine but not glucose induces MYC-dependent apoptosis in human cells." The Journal of Cell Biology **178**(1): 93-105.

Zanssen, S. and E. A. Schon (2005). "Mitochondrial DNA Mutations in Cancer." PLoS Medicine **2**(11): e401.

Zhang, X., N. Tang, T. J. Hadden and A. K. Rishi (2011). "Akt, FoxO and regulation of apoptosis." Biochimica et Biophysica Acta (BBA) - Molecular Cell Research **1813**(11): 1978-1986.

Zhao, H. and H. Piwnica-Worms (2001). "ATR-Mediated Checkpoint Pathways Regulate Phosphorylation and Activation of Human Chk1." Molecular and Cellular Biology **21**(13): 4129-4139.

Zhao, H., J. L. Watkins and H. Piwnica-Worms (2002). "Disruption of the checkpoint kinase 1/cell division cycle 25A pathway abrogates ionizing radiation-induced S and G(2) checkpoints." Proceedings of the National Academy of Sciences of the United States of America **99**(23): 14795-14800.

Zhou, B. P., Y. Liao, W. Xia, B. Spohn, M.-H. Lee and M.-C. Hung (2001). "Cytoplasmic localization of p21Cip1/WAF1 by Akt-induced phosphorylation in HER-2/neu-overexpressing cells." Nat Cell Biol **3**(3): 245-252.

Zhou, B. P., Y. Liao, W. Xia, Y. Zou, B. Spohn and M.-C. Hung (2001). "HER-2/neu induces p53 ubiquitination via Akt-mediated MDM2 phosphorylation." Nat Cell Biol **3**(11): 973-982.

Zhu, Y., P. Hoell, B. Ahlemeyer, U. Sure, H. Bertalanffy and J. Krieglstein (2007). "Implication of PTEN in production of reactive oxygen species and neuronal death in in vitro models of stroke and Parkinson's disease." Neurochemistry International **50**(3): 507-516.

Zou, L. and S. J. Elledge (2003). "Sensing DNA damage through ATRIP recognition of RPA-ssDNA complexes." Science **300**(5625): 1542-1548.